The effect of epigenetic therapies on Glioblastoma Multiforme cancer stem cells

Bnar Paula Abdul Kader

MSc.

Submitted in the fulfilment of the requirements for the Degree in the Doctor of Philosophy

Institute of Cancer Sciences

College of Medical, Veterinary and Life Science

University of Glasgow

28 August 2022

Abstract

Glioblastoma Multiforme (GBM) is one of the most aggressive types of brain tumour; it is hard to treat with conventional therapy and often shows tumour regrowth after surgical removal. Recent studies have indicated the presence of cancer stem cells in GBM tumours, which are more resistant to therapy and driver of tumour recurrence after treatment. Here, we investigate the effect of several epigenetic inhibitors on two GBM stem cell lines, G7 and E2. Cells were not sensitive to the BET inhibitor OTX015, but the EZH2 inhibitors EPZ6438, UNC1999 and GSK343 all significantly reduced colony formation. The three EZH2 inhibitors induced expression of senescence-associated ß-galactosidase, sensitised both cell lines to the alkylating agent temozolomide, and sensitised the E2 cell line to radiation. RNA-seq analysis following treatment with EZH2 inhibitors revealed a significant induction of genes related to neurogenesis and neuronal function, particular in the G7 cell line.

ChIP-seq analysis of the epigenetic changes following EZH2 treatment was used to identify genes that were both upregulated and showed a decrease in histone H3 lysine 27 tri-methylation, which is the epigenetic mark deposited by EZH2. Several regulatory factors were identified that are potential candidates for driving the neuronal differentiation of the cancer stem cells. One of these candidates is the transcription factor PAX2, which is upregulated in both G7 and E2 cells. PAX2 is essential for the correct development of the inner ear and the eye, and is known to regulate expression of the neural transcription factors NEUROG1, NEUROD1 and ATOH1.

Based on these data, it is hypothesise that the EZH2 inhibitors reduce GBM stem cell proliferation by inducing neuronal differentiation of the cancer stem cells, in addition to causing therapy induced senescence. Further work is required to investigate whether the candidate regulatory genes that were identified, including PAX2, do indeed play a role in driving this differentiation. Sensitisation of the GBM stem cells to temozolomide and radiation is a promising line of enquiry for further investigation into improving treatments for GBM.

Acknowledgments

I would like to begin by thanking my supervisor Dr.Katherine West for her help and guidance during my research project. I'm also grateful to my second supervisor Dr.Andrew Hamilton for his support and advice for this project.

Especial thanks to members of Dr.Katherine West group (Sylvia Garza, Sarah El-messeiry and Abdulmajeed Al-Sindi) for their help with qPCR, cell culture, clonogenic assay and Cell- Titer Glo assay. I'm also thankful to members of Dr.Adam West group (Rio Hermantara and Valentine Jeantet) for giving me advice and help.

I'm grateful to Glasgow polyomics members for their help in quantifying ChIP DNA samples using Qubit quantification. I'm also thankful to Professor Anthony Chalmers group for providing GBM cell lines frozen vials and for their advice on how to grow cell lines.

Finally I would like to thank my family for their support and encouragement throughout my research project.

Author's Declaration

I declare that the work presented is my own, unless stated otherwise. This thesis has not been submitted for consideration for another degree.

Bnar Paula Abdul Kader

Contents

List of Figures

List of Tables

Abbreviations

ABC	ATP binding cassette
ADGRB1	Adhesion molecule G protein coupled with receptor B1
AIC	5- aminoamidazole -4-carboxamide
APC	Adenomatous polyposis coli
BET	Bromodomain and extra terminal domain
bFGF	Basic fibroblast growth factor
bHLH	Basic helix loop helix
BMI1	B lymphoma Mo-MLV insertion region1
CBX	Chromobox homolog
CDKI	Cyclin dependent kinase inhibitor
ChIP-seq	ChIP sequencing
CK1	Casein kinase 1
CSC	Cancer stem cell
DEG	Differentially expressed gene
DMR	Dose modifying ratio
DMSO	Dimethyl sulfoxide
DZNep	3-deazaneplanocin A
EED	Embryonic ectoderm development
EGF	Epidermal growth factor
EGFR	Epidermal growth factor receptor
EMT	Epithelial-mesenchymal transition
EPZ6438	Tazemetostat
ES	Enrichment score
EZH2	Enhancer of zeste homolog 2
FBS	Fetal bovine serum
FDR	False discovery rate
GBM	Glioblastoma Multiforme
GO	Gene ontology
GSC	Glioblastoma stem cell
GSEA	Gene set enrichment analysis
GSK3	Glycogen synthase kinase3
H3K27me3	Trimethylation of Histone 3 on lysine 27
H3K4me3	Trimethylation of Histone 3 on lysine 4
HBSS	Hank’s Balanced salt solution
HPH	Human polyhomeotic homolog
LRP5/6	Low density lipoprotein receptor related protein 5/6
MGMT	O6-Methylquanine-DNA Methyltransferase
MMR	Mismatch repair

MTIC	Methyl triazeno imidazole carboxamide
NES	Normalised enrichment score
NOM	Nominal
NSC	Neural stem cell
OxPhos	Oxidative phosphorylation
PCA	Principal component analysis
PcG	Polycomb group
PDGFR	Platelet derived growth factor receptor
PEST	Proline serine threonine
PHC	Polyhomeotic homolog
PRC	Polycomb repressive complex
PTEN	Phosphatase and tensin homolog
RB	Retinoblastoma protein
RBAP46/48	Retinoblastoma suppressor associated proteins 46/48
RING1A/B	Ring finger protein1 A/B
RNA-seq	RNA sequencing
SAM	S-Adenosyl-L-Methionine
SASP	senescence-associated seescretory phenotype
SUZ12	Suppressor of zeste 12
TCF/LEF1	T cell factor/lymphoid enhancer factor-1
TMZ	Temozolomide
TSS	Transcription start site
VEGF	Vascular endothelial growth factor

Chapter 1 Introduction

1.1 Introduction

Malignant brain tumours account for approximately 2% of cancers, with gliomas making up 86% of those (McKinney, 2004). Based on the WHO grading system, gliomas are divided into low grade (grades I and II) and high grade (grades III and IV). Low grade gliomas have low proliferative potential and have good prognosis, while high grade gliomas have histological evidence of malignancy and tend to have a poorer prognosis (Louis *et al.*, 2007).

Glioblastoma multiforme (GBM) is a subtype of glioma that is thought to arise from glial or neural stem cells (NSCs) and is graded IV on the basis of more advanced malignancy features, which include necrosis and vascular invasion (Zong, Verhaak and Canoll, 2012). GBM is characterised by being highly proliferative and infiltrative in nature, which makes surgical resection of the tumour challenging and hard to cure. The median survival of patient with GBM is approximately 1 year due to resistance to conventional therapy (Villano, Seery and Bressler, 2009; Alcantara Llaguno and Parada, 2016). It has been established that pathological diagnosis cannot predict clinical outcome, due to molecular heterogeneity among GBM cells (Veliz *et al.*, 2015).

1.2 GBM classification and characteristics

GBM considered the most lethal type of brain tumour, and it shows heterogeneity at the genomic, transcriptional and cytopathological levels. Under the microscope regions of microvascular proliferation, pleomorphic nuclei and cell and pseudopalisading necrosis can be seen. One of the features of malignant glioma is existence of area of pseudopalisading cells that surrounds necrotic foci. It is been reported the existence of hypoxic and necrotic regions within astrocytoma. This result in tumour cells to migrate away from hypoxic region thus indicating the existence of pseudpalisades (Rong *et al.*, 2006).

GBM can be divided into two subtypes based on clinical presentation. Primary GBM arises without a precursor of lower grade disease and without any prior

clinical symptoms. Primary GBM is also considered to be derived from cells with stem like properties such as glial precursor cells or NSCs. Secondary GBM arises from the progression of lower grade astrocytoma. Histologically, primary and secondary GBMs are very similar, and prognosis is the same between the two subtypes (Parsons *et al.*, 2008)

Primary and secondary glioma can often be distinguished by their genomic and transcriptional profiles (Furnari *et al.*, 2007). For example, mutation of PTEN and amplification of epidermal growth factor receptor (EGFR) are most commonly found in primary GBM, while mutation in TP53 is frequently seen in secondary GBMs. However, these modifications alone are not sufficient to differentiate between the two subtypes of GBMs (Parsons *et al.*, 2008). It was found that *IDH1* mutant GBM is more sensitive to radiochemotherapy than *IDH1* wild type GBM, and mutant *IDH1* is correlated with higher survival in patients (Tran *et al.*, 2014). Mutation in *IDH1* and *IDH2* can lead to a loss of normal catalytic activity and abnormal production of 2 hydroxyglutarate (2-HG), which is similar in structure to α-ketoglutarate (α-KG) and acts as an antagonist to α-KG. 2-HG is an inhibitor α-KG - dependent dioxygenases, which includes inhibition of the ten eleven translocation (TET) family of 5-methylcytosine hydroxylases, and lysine histone demethylases (Yang *et al.*, 2012). Thus, 2-HG induces a range of metabolic and epigenetic reprogramming steps that affect tumour growth and development (Huang, 2019).

GBM can also be classified into four subtypes based on genomic profiling of human samples, which include classical, neural, mesenchymal and proneural. Genetic lesions in GBM typically lead to activation of signalling pathways downstream of tyrosine kinase receptors such as platelet derived growth factor receptor (PDGFR) and epidermal growth factor receptor (EGFR), either through oncogene activation and/or inactivation of tumour suppressors such as PTEN (Figure 1-1) (Holland, 2000).Classical GBM is characterised by amplification of *EGFR* and lack of *CDKN2A* and *PTEN*. Neural GBM expresses genes involved with neuron projection and axons, along with expression of high levels of neuron markers. Mesenchymal GBM is typified by *NF1* deletion, *TP53* and *PTEN* mutation, *CDKN2A* loss and epithelial-mesenchymal transition (EMT) marker expression. Proneural GBM is associated with genetic lesions in *IDH1* and *PDGFRA*, loss of *PTEN* and *TP53,* and also loss of *CDKN2A* (Clarke *et al.*, 2013).

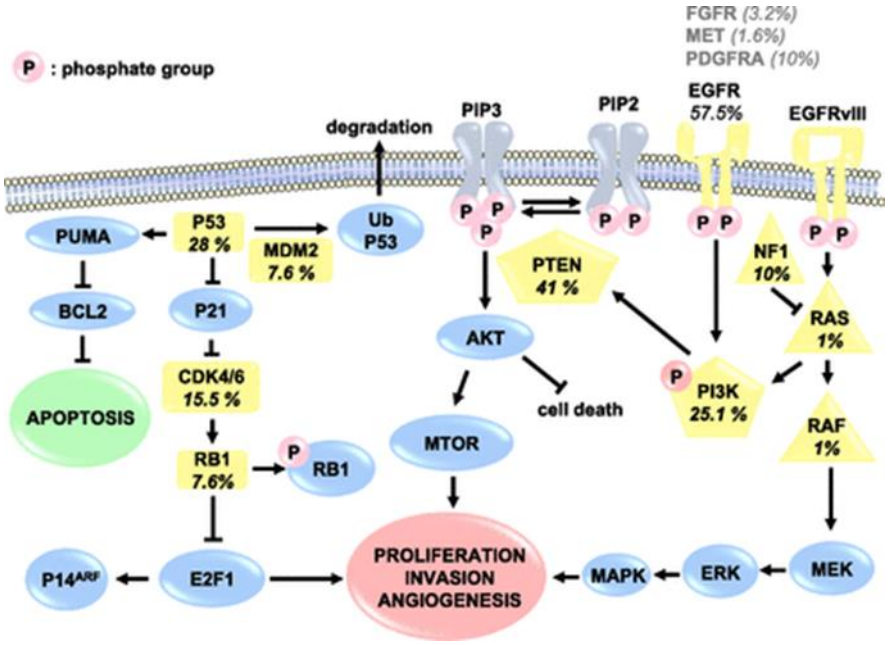

Figure 1-1 An illustration of EGFR, Retinoblastoma protein and P53 known as canonical gliomagenesis mediators that is crucial for signalling in tumour cells.

The promotion of angiogenesis proliferation and invasion is usually mediated by EGFR that is either mutated or amplified. The inactivation of Retinoblastoma protein (RB), a tumour suppresser gene, leads to transcription of E2F1 thus activating cell cycle. In GBM, mutation of P53 also leads to inhibition of apoptosis "Figure taken from (Shergalis *et al.*, 2018)".

Recent findings proposed that GBM can have either proneural or mesenchymal features while the other two types (classical and neural) intersect with either proneural or mesenchymal features. GBMs with proneural properties express neuronal markers and often have mutated *IDH1* that is a feature of secondary GBM. Mesenchymal GBM tends to be more aggressive and expresses more stem cell markers. The other types can go through the EMT and acquire mesenchymal features (Verhaak *et al.*, 2010). Targeting the mesenchymal transition and forcing the cells to convert to proneural might increase a patient's survival rate since tumours with mesenchymal characteristics are more aggressive and show the worst prognosis.

1.3 Cancer stem cell hypothesis

Current literature indicates that many cancers contain a small population of cells responsible for tumour initiation and maintenance known as cancer stem cells (CSCs). These stem like cells express the same markers as normal stem cells, with the ability to self renewal (Figure 1-2) and also to form daughter cells that are phenotypically different from mother cells (Yuan *et al.*, 2004). The growth of these cells tends to be in a conserved hierarchy, with slow cycling stem cells generating progenitor cells that in turn generate differentiated cells. This model suggests that tumour cells exhibit heterogeneity, in which cancer stem cells are at the top of hierarchy followed by more differentiated cancer cells at lower hierarchical order. These differentiated cells are fast growing cells that comprise vast majority of the tumour's volume. The differentiated cells lack the ability to self renew and regrow new tumours (Lan *et al.*, 2017).

One of the key features of CSCs is self renewal, which allows cells to go through unlimited cell division and ensures expansion of the tumour. Along with persistent proliferation, CSCs are also characterised by their ability to differentiate down multiple lineages. CSCs can either divide into two identical daughter (stem or progenitor) cells in a process known as symmetrical division or can divide into one stem cell and one progenitor/differentiated cell, known as asymmetrical division (Morrison and Kimble 2006). CSCs that are capable of forming tumours in a xenograft model are known as tumour initiating cells. The failure of current treatment to target these CSCs population might be associated with the recurrence, invasiveness and metastasis of the tumour (Frank, Schatton and Frank, 2010).

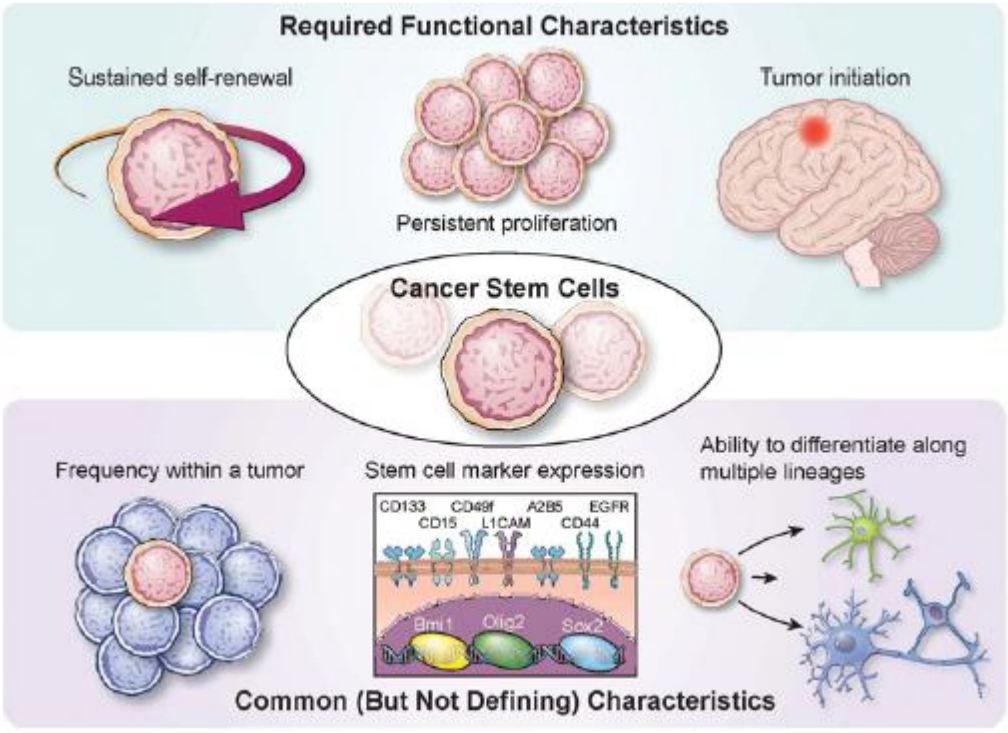

Figure 1-2 Evidence indicated the existence of small population of cells responsible for tumour initiation and maintenance known as CSCs.

These cells are characterised by sustained self renewal and sustained proliferation. They also share the same features as normal stem cells such as expression of stem cell markers and the ability to differentiate. Unlike differentiated cancer cells, CSCs shows resistance to the treatment resulting in recurrence of the disease after exposure to conventional cancer therapy "Figure taken from (Lathia *et al.*, 2015)".

1.4 The CSC origin

Knowing the origin of CSCs might help in developing suitable and effective treatment strategies. Bonnet *et al*. proposed the concept of CSCs, and his group observed that malignant cells have self renewal ability that resembles that of normal stem cells within the same organ. They proposed that a small group of cells possess the ability to form tumour (Bonnet and Dick, 1997). Another published study indicated that both stem cells and differentiated cells can become cancer cells(Bachoo *et al.*, 2002). In this study they found that NSCs and mature astrocytes can become immortal cells after serial passaging. The loss of tumour suppressor genes *p16* and *p19* and activation of EGFR promotes astrocytic dedifferentiation (Bachoo *et al.*, 2002). There are two theories that explain the origin of CSCs; the first one indicates that normal stem cells can undergo mutation and transform into CSCs. The second theory implies that CSCs

behave like stem cells and can arise from any cells that have some stem cells characteristics (Figure 1-3). Mutation in stem cells, progenitor cells or even differentiated cells can lead to CSCs that contributes to tumour development. This model indicates that differentiated cells might lose their properties and gain self renewal capacity. CSCs can arise from mutation of genes of normal stem cells, but in some cases progenitor cells may undergo mutation resulting in reacquired self renewal ability (Sell, 2010).

Embryonic stem cells are characterised by pluripotency, which gives the cells the capacity to generate any type of cells. This pluripotency in embryonic stem cells is promoted by maintaining proliferation and self renewal capacity, which allows the cells to self renew continuously when growing *in vitro*. Recent reports suggest that these specific characteristics of embryonic cells are expressed in various types of cancer, indicating that these shared characteristics might help in identifying new approaches in cancer therapy (Kim and Orkin, 2011).

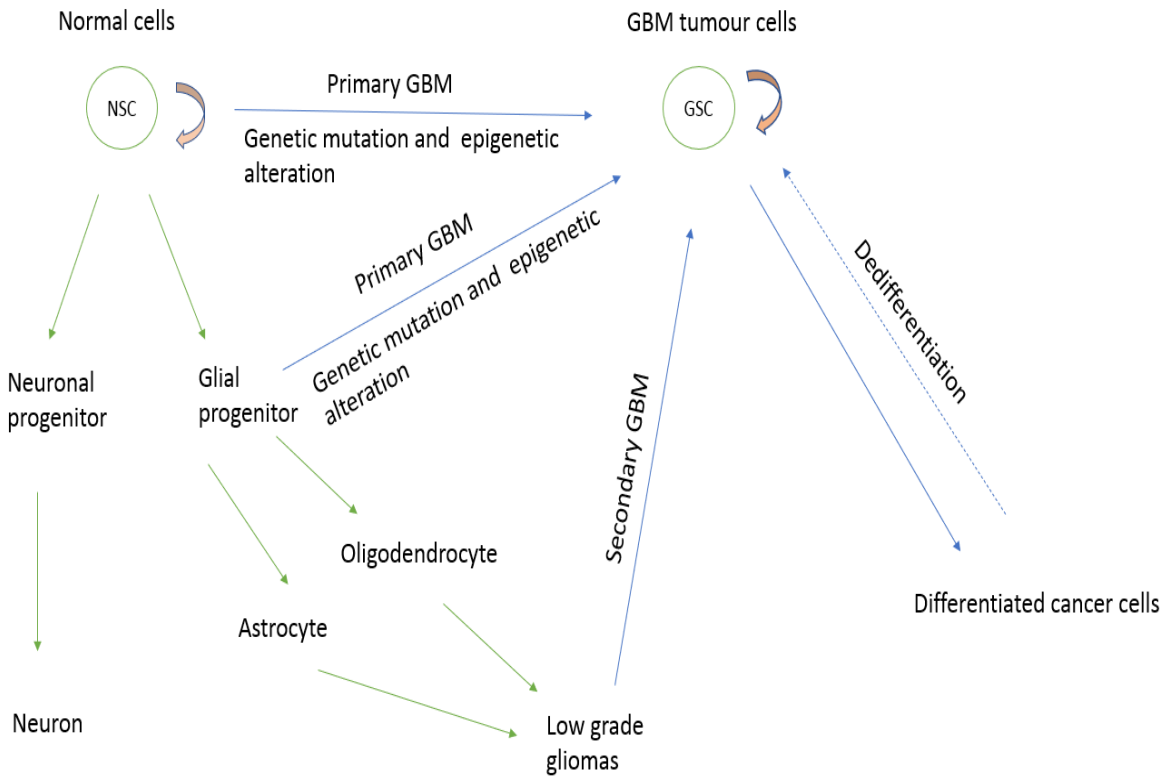

Figure 1-3 This figure shows the origin of GBM stem cells (GSC)s.

Primary GBM thought to be developed from genetic and epigenetic dysregulation that occur in NSCs or glial progenitor cells while secondary GBM is derived from low grade gliomas. In GBM, GSCs can retain stemness and thought to be at the top of hierarchy that forms heterogeneous tumour. Some of the GBM differentiated cells shows resistance to conventional therapy and dedifferentiate into GSCs resulting in tumour relapse (original figure).

1.5 Existence of CSC population in GBM

Increasing evidence indicates the existence of a small population of stem like cells known as GSCs in GBM tumours that play a significant role in resistance to conventional therapy and recurrence of disease after treatment (Bao *et al.*, 2006). GBM cells that are taken from patients showed the ability to form spheres when grown in media containing growth factors, including epidermal growth factor (EGF) and basic fibroblast growth factor (bFGF), similar to the *in vitro* conditions in which NSCs are grown (Kondo, Setoguchi and Taga, 2004).

Recent hypotheses indicate that the origin of GSCs might come from genetic mutation and epigenetic alteration of NSCs.

In the brain, NSCs can differentiate into progenitor cells (neuronal or glial), neuronal progenitor cells differentiate into neurons, while glial progenitor cells can differentiate into astrocytes, ependymal cells or oligodendrocytes. Brain tumours can develop as a result of transformation of NSCs into CSCs. Similarly, glial progenitor cells and differentiated cells such as astrocytes , oligodendrocytes, ependyma cells and neurons also have the potential to undergo abnormal transformation into CSCs and develop malignant tumours (Safa *et al.*, 2015).

1.6 GSCs microenvironment

GSCs arise in a stem cell niche in which angiogenesis and stemness is influenced by the microenvironment. One study suggested that necrosis can be found in hyperproliferating areas where there is a high level of stem cell antigens. Necrotic areas develop in the centre which makes GSCs form a ring outside the proliferating areas (Schiffer *et al.*, 2014). GSCs are often located in perivascular niches and can manipulate their microenvironment both through secretion of vascular endothelial growth factor (VEGF) and through differentiation into pericytes themselves. TGFβ released by endothelial cells induces differentiation of GSCs into vascular pericytes, which support blood vessel structure and function thus promoting vascularisation and tumour growth. Evidence suggests that since GSCs have similar characteristics as NSCs they can act as pericytes progenitors. These GBM pericytes express the same markers as normal brain vascular pericytes. *In vivo* models showed the ability of these GSCs to promote vasculature formation to support tumour growth without relying on surrounding normal pericytes (Sena *et al.*, 2018; Cheng *et al.*, 2013a).

1.7 GBM and stem cell markers

Several studies focus on identifying reliable CSC markers for isolation of GBM stem cells within tumour. Due to the lack of decisive markers it is hard to distinguish CSCs from the rest of non stem cell population. In somatic cells, the expression of transcription factors that induce pluripotency in stem cells. Overexpression of these embryonic transcription factors can be seen in tumour cells due to the similarities between embryonic stem cells and CSCs. Thus, transcription factors play key role in regulating growth in CSCs. Markers such as *CD15* and *CD133* were used in combination with other markers such as *OCT4*, *SOX2* and *NESTIN* which were found to be successful in identification of GSC population *in vivo* and *in vitro*. These markers were selected for identifying new GSCs that showed high level of tumour engraftment and are more invasive phenotypically.This population of CSCs were shown to be more resistant to conventional therapy than bulk differentiated cells (Auffinger *et al.*, 2014). Brescia *et al.* suggested that *CD133* is important for maintaining the GSC population. qRT-PCR analysis showed differences in mRNA expression of *CD133* taken from different GBM samples. Flow cytometric analysis indicated that in neurospheres not all GBM cells are expressing the same level of CD133, in fact there are populations of cells who lack the expression of CD133 (Brescia *et al.*, 2013). Another *in vitro* study showed that CD133+ GBM cells are more resistant to conventional therapy. The same study also indicated that GSCs population is still highly tumourgeneic despite the variation in CD133 expression (Liu *et al.*, 2006).These results indicate that GBM tumours are heterogeneous and there is not a single marker for all GSC populations. A recent study demonstrated that from a single GBM tumour a mixed population of cells can be found based on expression of markers CD133 and CD44. The cells were sorted using FACS into four groups: CD133+ CD44+, CD133- CD44-, CD133+CD44-and CD133-CD44+ (Brown *et al.*, 2017).

CSCs markers are also found to be useful in identifying different subtypes of GBM. One *in vitro* study indicated the existence of two main subtypes of GBM, mesenchymal and proneural (Denysenko *et al.*, 2014). High expression of the CD133 marker indicated proneural properties, while low CD133 expression showed mesenchymal characteristics *in vitro*. Cell lines that have mesenchymal properties showed high resistance to hydroxyurea treatment (Denysenko *et al.*,

2014). In general, most GSCs were found to express CD133 while some of them expressed CD44 instead of CD133. Mesenchymal GSCs express CD44 while proneural GSCs are express CD133 (Nakano, 2015).

A number of transcription factors found to be activated in GSCs are involved in tumour maintenance through self renewal, stemness and proliferation. These transcription factors were found to be expressed at higher levels in GSCs and are involved in several pathways that contribute to therapeutic resistance (Auffinger *et al.*, 2014). OCT4, a transcription factor belonging to the POU family, is found to be expressed in mammalian embryonic cells at early development. The activity of OCT4 was found to induce pluripotency and proliferation in germ cells and embryo cells (Nichols *et al.*, 1998). OCT4 can work alone or in cooperation with other transcription factors by recruiting chromatin remodelers that are involved in regulating the expression of specific target genes. Therefore, OCT4 has a key role as developmental regulator that is involved in reprogramming somatic cells (Jerabek *et al.*, 2014). An experimental model of rat glioma cells showed decreased level of *Oct4* resulted in reduction of proliferation and colony formation (Du *et al.*, 2009).

Regulation of gene expression by the transcription factor SOX2 is found to be associated with CSCs as well as differentiated cancer cells (Berezovsky *et al.*, 2014). In normal cells, SOX2 is expressed by stem cells and is thought promote stem cell proliferation. SOX2 was found to play a role in maintaining the characteristics of neural progenitor cells and inhibiting differentiation (Graham *et al.*, 2003). High levels of SOX2 were found to be correlated with basal like breast cancer (Rodriguez-Pinilla *et al.*, 2007). Recent work revealed that downregulation of SOX2 can decrease the chemoresistance of GSCs. Encouraging results demonstrated that silencing SOX2 through miRNA 145 might be a promising therapeutic approach (Garros-Regulez *et al.*, 2016). In glioma cells, SOX2 was found to maintain proliferation. Knocking down *SOX2* expression using a retroviral victor expressing miRNA that is engineered for targeting *SOX2* mRNA can reduce tumourigenicity and reduce proliferation capacity of the cells (Gangemi *et al.*, 2009).

In vitro analysis showed the expression level of the transcription factor *Nanog* was higher in stem cells and lower in differentiated cells.The elevated level of

Nanog was associated with clonal expansion and maintaining the level of OCT4 in embryonic stem cells (Chambers *et al.*, 2003). Furthermore, the maintenance of brain tumour stem cells was found to be associated with high level of *Nanog* expression. In a GBM xenograft model, the inhibition of Nanog expression led to decreases in pluripotency, proliferation, invasiveness and migration in tumour cells (Higgins *et al.*, 2013). Expression of Nanog can also promote EMT, which allows the tumour cells to migrate to other organs and form metastatic tumours (Wang *et al.*, 2014).

OLIG2, a member of the basic helix loop helix (bHLH) family of transcription factors, is universally expressed in the central nervous system (Kosty *et al.*, 2017). OLIG2 has a critical role in proliferation of glial progenitor cells, and is found to be expressed at higher levels in gliomas. Deletion of OLIG2 in animal models with the proneural subtype of GBM inhibits tumour growth resulting in a phenotypic shift from oligodendrocyte to astrocyte with upregulation of EGFR and downregulation of PDGFR (Kosty *et al.*, 2017). Immunohistochemical analysis of patient samples showed that the number of GBM cells with positive Olig2 was higher in secondary GBM when compared to primary GBM, in recurrent GBMs there were also high level of Olig2 expression (Trépant *et al.*, 2015) .OLIG2 has a role in activating cell proliferation through regulating growth receptors such as EGFR and PDGFR and controls plasticity in glioma cells. OLIG2 inhibition makes tumour cells sensitive to EGFR inhibitors, and expression of OLIG2 is also essential for maintaining tumour propagation in proneural subtype of GBM (Lu *et al.*, 2016). In NSCs, OLIG2 has a role in initiating oligodendrocyte differentiation (Zhou and Anderson, 2002).

The level of NESTIN, a type IV intermediate filament, is found to change the properties of stem cells. During embryonic development, NESTIN is expressed in cells that show migration and proliferation capacity. In GBM cell lines, data indicates that NESTIN downregulation leads to a reduction in sphere formation and a reduction in tumour size *in vivo* models (Matsuda *et al.*, 2015). One study showed that NESTIN expression is regulated by γ secretase in glioma stem cells, which has a role in activating notch signalling pathways and stemness of cells (Jin *et al.*, 2013). Western blot analysis also revealed the potential role of OCT4 in regulating the expression of NESTIN and GFAP, as downregulation of OCT4 in

glioma cell lines led to downregulation of NESTIN and upregulation of GFAP and vice versa (Du *et al.*, 2009)

Suva *et al.* proposed that four types of transcription factors (SOX2, OLIG2, SALL2 and POU3F2) were found to be important for GSCs proliferation. This study showed that expression of these transcription factors is important for maintenance of GSC population in GBM tumour. GBM cells expressing these markers are reprogramed into CSCs (Suvà *et al.*, 2014). GBM cells also showed upregulation of transcription factors including SOX2 and FOXG1; upregulation of these transcription factors can cause the cells to dedifferentiate into stem cells and limit astrocyte differentiation (Bulstrode *et al.*, 2017). These data indicate that shifting of differentiated cancer cell into a non differentiated state that is controlled by epigenetic regulators. Prohibiting the dedifferentiation of cancer cell could be a new therapeutic approach, if there was a better understanding of mechanism underlying epigenetic regulatory involvement in the reprogramming of differentiated cells into CSCs.

Stem cell markers	Function	Pathways involved in GBM cells	References
OCT4 and SOX2	Pluripotency stem cell marker	Downregulation of miRNAs include miR-148a SOX2 also Induce plasticity by downregulation of Wnt pathways and upregulation of cytokine pathways	(Lopez-Bertoni *et al.*, 2015) (Berezovsky *et al.*, 2014)
NANOG	Increase stemness in GBM	Involved in hedgehog GLI signalling pathways required for GBM growth	(Zbinden *et al.*, 2010)
OLIG2	Reprogramming into stem like properties	Regulating linage restriction pathways essential for proliferation	(Ligon *et al.*, 2007)

Table 1-1 Common transcription factors that are expressed in GBM cells and are thought to have a role in cancer cell plasticity.

1.8 GBM and CSC resistance

It is reported that CSCs are responsible for resistance and regrowth of tumour after treatment. There are different mechanisms that makes GSCs resistant to conventional therapy such as overexpression of O6-Methylquanine-DNA

Methyltransferase (MGMT) which is DNA repair gene that makes differentiated cancer cells undergoes dedifferentiation to CSCs. These cells acquire the stemness properties and are mediated by several pathways that maintains reprograming of tumour cells (Dahan *et al.*, 2014). The effect of radiation and chemotherapy usually depends on the rate of cell proliferation, which makes differentiated cancer cells more sensitive than normal cells. Cancer cells that are in slow growth state have a significant role in tumour recurrence. RNA-seq analysis showed that high number GBM cells that have low proliferative rate also have high expression of stem related genes (Sen *et al.*, 2018).

CSCs have a major role in tumour recurrence after treatment with radiation as a result of innate resistance such as developing antioxidant and high DNA repair capabilities. One experiment showed that exposing glioma stem cells to radiation can leads to radioresistance not only through intrinsic resistance but also by developing adaptive mechanism as a result of repeated radiation. (Otsuka *et al.*, 2018). CSCs can acquire resistant mechanisms and become radioresistant. *In vitro* study showed that brain tumour cells enriched with CD15+/CD133- have increased stem gene expression and self renewal ability after treatment with chemorediotherpay (Qazi *et al.*, 2016). Developing an effective therapy that can cross the blood-brain barrier and target slow growing CSCs can be challenging.

1.9 Cancer cell quiescence

The ability of cells to go through reversable G0 phase to avoid re-entering the cell cycle in response to physiological stimuli is known as cell quiescence. Quiescent cells are characterised by being in a state of dormancy but still retain their proliferation capacity. This phenomenon can be particularly observed in stem cells in which cells enter a quiescence state to preserve their ability of self renewal and avoid genetic alteration resulted from repeated division (Gulaia *et al.*, 2018).

Cell quiescence is usually controlled by signalling pathways, the signalling molecules that are involved in regulating stem cell quiescence include p21, p27, p53, RB proteins and some miRNAs (Cheung and Rando, 2013). Some evidence suggests that CSCs populations are relatively quiescent which ensures long term

survival against environmental stress. It was also reported that some tumour cells can enter state of dormancy that allows cells to maintain non proliferative quiescent stage, that can lead to tumour relapse and progression when these dormant cell are exposed to conventional therapy (Wang and Lin, 2013).

In GBM, a population of CSCs were identified by expressing transgenes that are specific for quiescent NSCs. After treatment with chemotherapy, these cells were able to produce cancer cells and maintain tumour regrowth (Chen *et al.*, 2012b). RNA-seq analysis of GBM tumour cells also indicated the heterogeneity among tumour cells and that a population of these cells harbours markers that are associated with quiescent characteristics and showed stemness signatures. This quiescent state is considered an important factor that contributes to the resistance against the conventional therapy by protecting CSCs population from antiproliferative agents (Patel *et al.*, 2014).

1.10 Experimental methods for characterisation of CSCs populations

Various experiments are conducted to assess the features of CSCs both *in vivo* and *in vitro*. Neurosphere assay was able to evaluate self renewal and proliferation capacity but was unable to assess tumour hierarchy. *In vivo* transplantation to form tumour might be essential to indicate the presence of the CSC population (Lathia *et al.*, 2015). The expression of markers is not sufficient for identifying CSCs population. Various *in vitro* and *in vivo* methods have been used to assess the properties of stem cells. For *in vitro* evaluation, limiting dilution assay and sphere formation assay are used for assessment of self renewal and proliferation capacity. CSCs also exhibits clonal characteristics in which they possess the ability to grow in serum free media forming clonal tumourspheres. Based on Hoechst dye staining method, CSCs are isolated depending on their dye efflux. Cells that show stem cells characteristics exhibited the lowest amount of dye and had the highest rate of dye efflux. CSCs were also identified based on ATP binding cassette (ABC) transporter' overexpression, which is associated with chemoresistance and tumour progression (Richard *et al.*, 2013). Lastly, *in vivo* ability of CSCs for limiting

dilution makes these cells able to form heterogeneous tumour after serial transplantations into mice models (Bandhavkar, 2016).

1.11 Epigenetic alteration in GBM

In mammals, epigenetic modifications are important for regulating expression of genes involved in cell growth and maintenance. Disruption of this epigenetic machinery is one of the hallmarks of cancer that can lead to abnormal cellular growth and development of malignant tumour (Sharma, Kelly and Jones, 2010). H2A, H2B,H3 and H4 are the core histone proteins that undergo post translation modifications which include methylation, acetylation, ubiquitylation and phosphorylation. Among these modifications, methylation of lysine 27(K27) and lysine 4 (K4) are of certain interest due to their key role in developmental process (Ringrose and Paro, 2004).

It is believed that accumulation of genetic mutation and epigenetic dysregulation can lead to cancer development and progression, and alteration of epigenetics in tumour suppresser genes and oncogenes have a critical role in GBM development. Epigenetic changes such as microRNA dysregulation, aberrant DNA methylation and chromatin remodelling have been closely associated with the GBM development (Figure 1-4). Genes and enzymes that are involved in regulation of these modification are considered new targets for treating cancer. According to Lathia *et al*. epigenetic alterations can play an important role in resistance, suggesting that tumour contain subpopulation of cells known as CSCs that are drug tolerant. Epigenetic targeted therapy might reverse epigenetic abnormalities and sensitise these cells to conventional therapy (Lathia *et al.*, 2015).

Epigenetic modifications have an effect on transcription factor binding affinities that is present in all genome region. It was found that these changes have a role in transcribing genes. Recent literature showed various location that indicates correlation between epigenetic modification and transcription factors. Analysis revealed that some histone modifications such as H3K4me3 was found near

transcription start site (TSS) while some other histone modifications such as H3K4me1 was found far from TSS (Liu, Jin and Zhou, 2015).

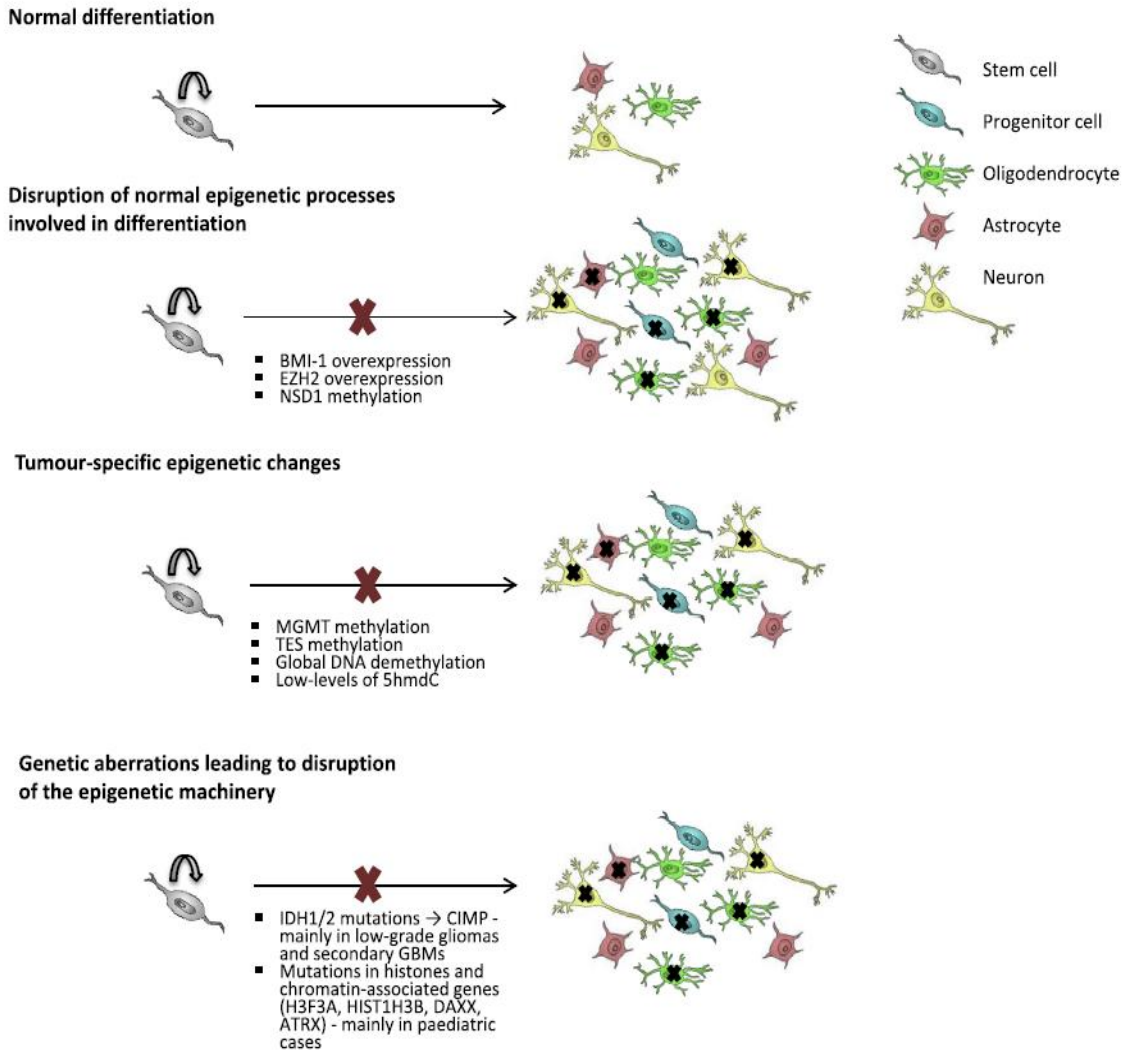

Figure 1-4 Different type of routes that contribute with the disruption of epigenetic machinery,

Altered epigenetic mechanism affects cellular hierarchy that is involved in normal differentiation of neural cells "Figure taken from (Carén, Pollard and Beck, 2013)".

Deregulation of epigenetic mechanisms can impact on neoplastic transformation, cell state and identity. Epigenetic regulation mechanisms include non-coding RNA, DNA methylation and histone modification. These mechanisms control transcription by regulating the accessibility of transcription factors to DNA and the efficiency of transcription. In GBM, epigenetic mechanisms have attracted attention as diagnostic biomarkers, in developing therapy and predicting

responsiveness to treatment. Trimethylation of H3K27 and H3K9 are known to have roles in repressing transcription. In NSCs, H3K27me3 is considered to be a key epigenetic change and aberrant alteration is often found to be associated with GBM (Mack *et al.*, 2016).

1.12 The role Polycomb group proteins in GBM

1.12.1 Polycomb group proteins

Post translational modification of histone proteins plays a critical role in gene regulation. Many studies have investigated the effect of epigenetic modifications on CSCs, as they can lead to upregulation of oncogenes or repression of tumour suppressors and can cause tumour heterogeneity in many types of cancer. One of these modifications is methylation of arginine and lysine residues, which are catalysed by histone methyl transferase enzymes (Weber and Henikoff, 2014). The addition of a methyl group to a histone tale can activate or repress target genes depending on exactly which amino acid residue is modified (Chi, Allis and Wang, 2010).

Polycomb group (PcG) proteins were first discovered in *Drosophila melanogaster* as epigenetic regulators that control gene expression through catalysing histone post translation modifications (Chi, Allis and Wang,2010). PcG proteins are epigenetic regulators that is crucial for maintaining stem cells. PcG proteins have been associated with different types of cancer. The two classes of polycomb group proteins, polycomb repressive complex 1 (PRC1) and polycomb repressive complex 2 (PRC2) are involved in gene silencing (Sauvageau and Sauvageau, 2010). The two types of PRC are found to be linked to many forms of tumours resulting in transcriptional silencing of tumour suppressor genes. These epigenetic dysregulation are involved in changing cellular pathways, thereby increasing proliferation capacity of tumour cells. In mammals, PRC2 consists of four functional core subunits, enhancer of zeste homolog 2 (EZH2) with histone methyl transferase activity, embryonic ectoderm development (EED), suppressor of zeste 12 (SUZ12) and retinoblastoma suppressor associated proteins 46/48 (RBAP46/48) (Richly, Aloia and Di Croce, 2011).The core subunits of PRC1

consists of B lymphoma Mo-MLV insertion region1 (BMI1), ring finger protein1 A/B (RING1A/B), human polyhomeotic homolog (HPH), chromobox homolog (CBX) and polyhomeotic homolog (PHC).

The expression of PRC2 components can be controlled by c-MYC and E2F that maintains self renewal and proliferation. In embryonic stem cells, c-MYC maintains pluripotency by direct transcriptional upregulation of PRC2 subunits. c-MYC is a transcription factor that is belong to MYC family proteins and is highly expressed in cancer cells resulting in rapid cell division and suppression of gene with antiproliferative effect (Miller *et al.*, 2012). Inhibition of c-MYC can affect transcriptional response of cells to hypoxia, this finding was also enabled to distinguish proneural from other GBM subtypes based on genes whose expression altered by c-MYC inhibition (Mongiardi *et al.*, 2016). Upregulation of c-MYC leads to over expression of miR-29c and REV3L induction which subsequently facilitate the mechanism of resistance to alkylating agent temozolomide (TMZ). Disrupting the signalling pathway of c-Myc/miR-29c/REV3L might make GBM cells more sensitive to conventional treatment (Luo *et al.*, 2015a). PRC2 also found to repress a subset of genes during embryonic development to maintain pluripotency (Lee *et al.*, 2006).

Polycomb repressive complexes (PRC1 and PRC2) play a critical role in silencing target genes through histone modification (Figure 1-5) (Chittock *et al.*, 2017). The two polycomb group can work together or separate from one another. PRC2 has been linked with tumourgenesis through recruiting DNA methyltransferases and silencing tumour suppresser p21. EZH2, a member of the PRC2 complex, inhibits gene expression through trimethylation of lysine 27 on H3 (Herviou *et al.*, 2016).

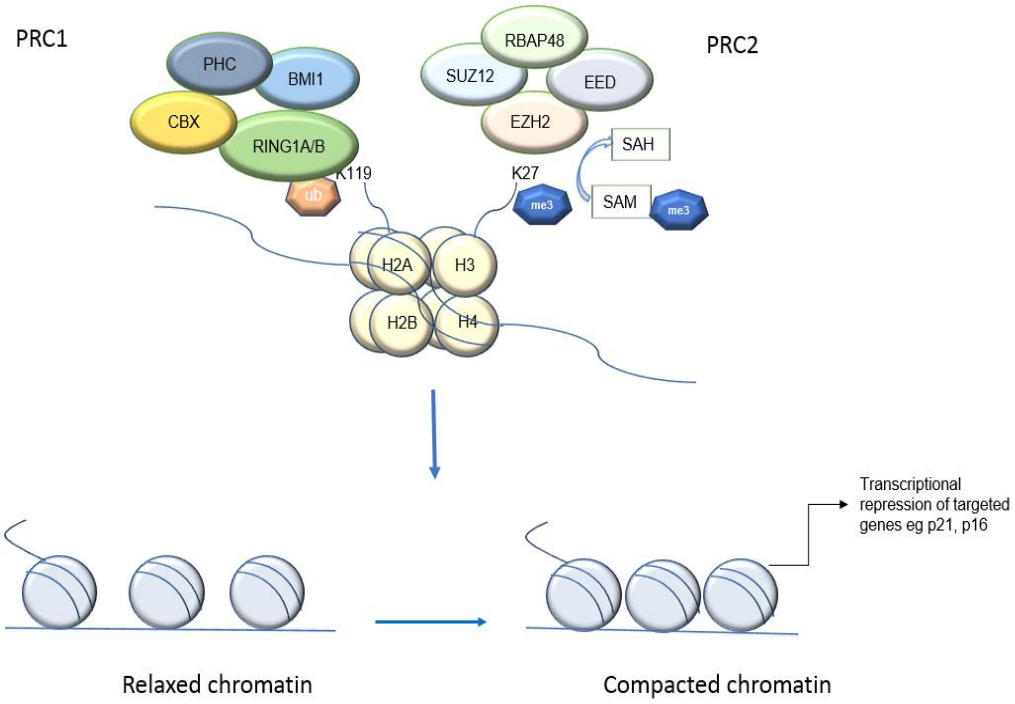

Figure 1-5 Role of PRC2 and PRC1 complexes on chromatin structure and gene expression. PRC2 trimethylates histone H3 at K27 that is recognised by PRC1 complex. The PRC1 complex monoubiquitinates histone H2A at K119, both complexes work together to repress transcription of targeted genes (original figure).

Existing evidence shows that PRC2 can recruit PRC1 though the PHC subunit, and the two complexes can work together to mediate chromatin compaction and gene silencing (Veazey, Muller and Golding, 2013). The SET domain (with histone methyl transferase activity) of EZH2 catalyses trimethylation of histone (H3) at Lysine 27 (K27). The CBX protein subunit of the PRC1 component recognises trimethylation of H3K27 and recruits the PRC1 complex. BMI1 interacts with RING1B enhancing the activity of E3 ligase. The enzymatic activity E3 ligase of RING1B catalyses monoubiquitination of H2A at lysine 119 mediating chromatin compaction and repressing transcription of the targeted genes (Wu *et al.*, 2013).

1.12.2 PRC role in cell cycle dysregulation

PcG proteins contribute to the repression of INK4b-ARF-INK4a transcription that encodes p14, p15 and p16 proteins. These proteins regulate signalling pathways that protect the cell from uncontrolled cell division or proliferation by promoting apoptosis or senescence (Gil and Peters 2006). p16 and p15 are cyclin dependent kinase inhibitors (CDKI), p16 prevents the transition of cell from G1 phase to S phase. p16 binds to CDK4/6 and prevents phosphorylation of RB, which binds to E2F preventing transcription of its targeted genes that are critical in G1 phase to S phase transition. p14 promotes apoptosis by arresting cell cycle progression in G1 phase and G2 phase. p14 inhibits MDM2 thus activating p53 pathway, MDM2 induces transcriptional repression of p53 and also mediates degradation of proteasome (Gil and Peters, 2006).

Over expression of EZH2 has been linked with silencing of differential genes and tumour suppresser genes which contributes with self renewal and uncontrolled cell division in cancer. A member of RB known as pRb2/p130 binds with HDAC1 resulting in gene silencing, EZH2 competes with HDAC1 for binding to pRb2/p130 leading to cell cycle progression (Tonini *et al.*, 2004). In B cell acute lymphoblastic Leukemia, overexpression of EZH2 inhibits p21, p53 and phosphatase and tensin homolog (PTEN) resulting in reduction of apoptosis and cell cycle progression (Chen *et al.*, 2012a). EZH2 overexpression is also involved with DAB2IP silencing. DAB2IP is a Ras GTPase-activating protein and tumour necrosis factor that is associated with JNK signalling pathways promoting apoptosis.In various types pf cancer, downregulation of DAB2IP by EZH2 dependent repression is linked with poor prognosis and metastasis (Chen, Tu and Hsieh, 2005).

1.12.3 Role of EZH2 in cancer cells

Recent studies indicates that EZH2 mutation or overexpression have been detected in many types of cancer, including GBM, and are associated with maintaining pluripotency of CSCs (Richly, Aloia and Di Croce, 2011). In human, EZH2 consists of several domains (Figure 1-6). One of the domain is SET domain at C- terminus which is required for histone methyltransferase maintenance. Other domains interact with PRC2 components and include; WDB domain binding region for EED, SANT domains involved in chromatin remodelling, CXC cysteine rich domain and Domain I and II that are binding domains for PHF1 and SUZ12, respectively (Margueron and Reinberg, 2011). Domains I and II are known as domain for protein interaction and is required for assembly and maintenance PRC2 complex.

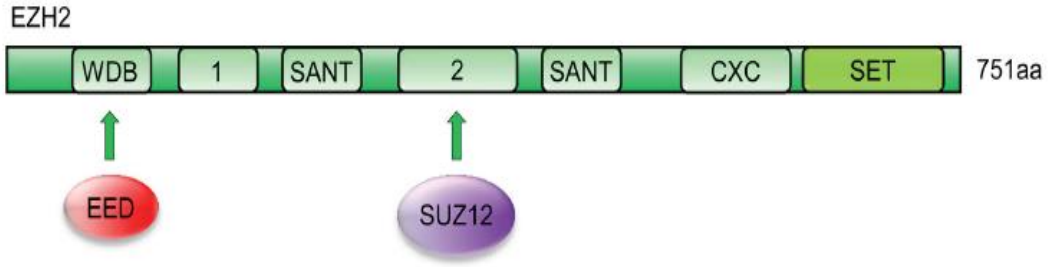

Figure 1-6 The organisation and interaction of human EZH2 domains.

WBD and domain 2 serve as binding site for PRC2 components which include EED and SUZ12 respectively. The C-terminal SET domain is require for histone methyltransferase activity "Figure adapted from (Wen *et al.*, 2017)".

In human, the EZH2 gene is located on chromosome 7q35 with 746 amino acid residues. EZH2 is typically found in nucleus but it can also be located in the cytoplasm (Su *et al.*, 2005). In order for EZH2 to obtain histone methyltransferase activity it has to interact with other PRC2 subunits EED and SUZ12 to form a complex (Cao and Zhang, 2004). Besides methylation of H3K27, EZH2 found to be involved in other modifications such as ubiquitination and phosphorylation (Figure 1-7) (Han Li and Chen, 2015). EZH2 also methylates non histone proteins through PRC2 mediated gene repression, such as direct methylation of GATA4 at lysine 299 (He et al., 2012). EZH2 can have an activating role that is independent from PRC2 (not part of the complex) through direct methylation of STAT3. Reports showed that AKT signalling plays an

important role in interaction of EZH2-STAT3. AKT phosphorylates EZH2 at serine residue 21 which in turn binds to and methylates STAT3. That leads to activation of STAT3 which contributes to GBM tumour progression (Kim *et al.*, 2013).

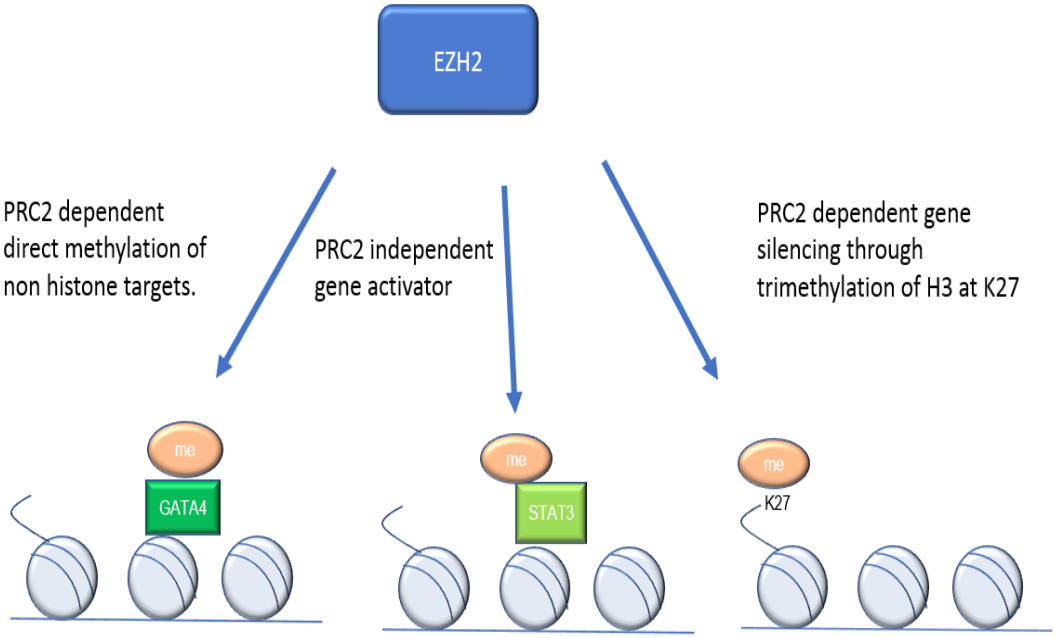

Figure 1-7 Mechanism action of EZH2 in activation and repression of targeted genes.

EZH2 acts as epigenetic silencer of targeted genes as a part of PRC2 recruited subunits. While EZH2 directly methylates non histone target mediated through dependent manner. EZh2 also works independently from PRC2 recruitment as gene activator (original figure).

EZH2 has been found to play a role in tumour initiation and its maintenance. Recent *in vitro* study using RNA interference indicated that EZH2 downregulation results in G1/S phase cell cycle arrest and apoptosis (Fan *et al.*, 2014). EZH2 has another homologue called EZH1, both members of EZH are involved with PRC2 complex although their end products seem to have different function. It is indicated that EZH2 contributes more to di and tri methylation of H3K27 compared to EZH1 that has lower methyltransferase activity (Margueron *et al.*, 2008).

The overexpression of EZH2 is dependent on the type of GBM. The two GBM subtypes proneural and mesenchymal are found to be unevenly distributed in a

tumour based on GSCs interaction with microenvironment(Jin *et al.*, 2017). Cells with a proneural profile are usually found in vascular regions, while cells with a mesenchymal profile are typically located in hypoxic regions. The proneural GSCs express high level of EZH2 while the mesenchymal GSCs show high level of BMI1 protein. The heterogeneous nature of cell phenotypes within an individual tumour indicates that the combined therapy BMI1 and EZH2 inhibitors might be effective in GBM with proneural and mesenchymal characteristics(Jin *et al.*, 2017).

The MYC proteins are transcription factors that are usually mutated and amplified in most tumours. New evidence indicated that MYC not only controls gene expression but also as act as a regulator of miRNA expression (Dang, 2012). In most tumour cells, the expression of miRNAs is repressed by MYC resulting in cell proliferation and impairment of cell cycle arrest (Lu *et al.*, 2005). MYC was also found to regulate the expression of EZH2 through repression of miR-26a and miR-26b (Sander, Bullinger and Wirth,2009).

Data showed that nuclear EZH2 is involved in reprograming GBM cells which help their adaptation to microenvironment (Natsume *et al.*, 2013). EZH2 is highly expressed in GBM cells compared to other lower grade. Inhibition of EZH2 expression led to a decrease in proliferation of glioma stem like cells (Orzan *et al.*, 2011). Lee *et al*. demonstrated the repression of BMPR1B expression that blocks differentiation and enhances tumourgenicity in GBM tumour cells. They found that knockdown of EZH2 increased the level of BMPR1B and that the CpG nucleotide BMPR1B promoter was less methylated, which indicates the role of EZH2 transcriptional repression mediated by PRC2 in BMP signalling pathway (Lee *et al.*, 2008). Targeting EZH2 in GBM cells might strongly impair CSCs capacity for self renewal and tumour initiation (Suvà *et al.*, 2009) .

In paediatric GBM, mutation of H3F3A that encodes H3.3 leads to decreasing the level of H3K27me3 without affecting the expression of EZH2 (Venneti *et al.*, 2013). The H3F3A mutations result in substitution of amino acids at two site on the histone tail:G34R/G34V and K27M (Schwartzentruber *et al.*, 2012). Mutation of G34 and K27 in H3F3A results in trimethylation of H3K36 which is involved in active transcription. This causes upregulating of MYCN which is a potent gene involved in tumourgenesis in paediatric GBM (Bjerke *et al.*, 2013). In paediatric

high-grade glioma, it was found that DNA hypomethylation and reduced level of H3K27me3 are associated with activation of gene expression in cells carrying the K27M mutant of histone H3.3 (Bender *et al.*, 2013).

1.12.4 Role of BMI1 in cancer

PRC1 represses gene transcription though monoubiquitylation of H2AK119. One of the PRC1 subunits BMI1 has been shown to contribute to tumour development in various types of cancer. A recent study showed that upregulation of BMI1 leads to progression and aggressiveness of tumour in biliary tract cancer (Mayr *et al.*, 2016). Studies showed that PRC1 binds to H3K27me3 and H2AK119ub1 and thus works with the PRC2 complex to mediate chromatin compaction (Francis, Kingston and Woodcock, 2004). BMI1 consists of three functional regions: the central helix turn helix (HTH) domain that binds to DNA, the RING domain that has a role in DNA damage repair and the C- terminal region known as the proline serine threonine (PEST) rich domain that is involved in protein degradation. The RING domain allows BMI1 to form a complex with RING1 A/B, which comprises a E3 ubiquitine ligase that upregulates the activity of monoubiquitination of H2A. The HTH domain is involved in protein-protein interactions and it serves as binding region for polyhomeotic proteins (PHC1, PHC2 and PHC3). Both HTH and RING domains were found to prevent cellular senescence (Gray *et al.*, 2016). Downregulation of BMI1 is found to upregulate expression of $p16^{INK4a}$ and $p19^{ARF}$, genes which are involved in pathways that regulates apoptosis and senescence (López-Arribillaga *et al.*, 2015). In GBM cells, *in vitro* observations revealed that knocking down BMI1 resulted in increased expression of transcripts involved in neurogenesis.

It was also reported that BMI1 prevents GBM cells from undergoing cell cycle arrest and apoptosis. ChIP assay revealed that $P21^{Cip}$ is a direct target of BMI1. The expression of *FOXOA3*, which induces apoptosis, was also upregulated following knocking down of BMI1 (Abdouh *et al.*, 2009). *In vivo* experiments revealed that *Bmi-1* directly represses the expression of *p21* in NSCs. Knocking down *Bmi-1* in a mouse model resulted in elevated expression of *p21* that inhibits phosphorylation of RB (Fasano *et al.*, 2007). There is evidence that BMI1

is expressed at higher levels in GBM cells which is essential for maintaining self renewal capacity in cells through downregulation of *P21* (Abdouh *et al.*, 2009).

1.12.5 Polycomb group proteins and microRNAs

Several non-coding RNAs are associated with PRC complex recruitment. Micro RNA (miRNA) is short non-coding RNAs that have a role in post transcriptional regulation of genes. miRNAs have been found play a key role in the pathogenesis of GBM, and are involved in regulation of cell cycle, apoptosis, angiogenesis, invasion and cell proliferation (Luo *et al.*, 2015b). In GBM, the enzymatic activity of EZH2 inhibits miR-26a-5p that regulates EZH2 transcription, suggesting a negative feedback loop between EZH2 and miR-26a-3p (Sharma *et al.*, 2016). Overexpression of miRNA 873 reduces invasion, cell proliferation and migration in GBM. It was found that miRNA 873 involved in inhibition of IGF2BPI expression that plays a role in stabilizing mRNA transcripts of genes that are involved in GBM progression (Wang *et al.*, 2015). The evidence of regulatory changes between miRNA and PRC are seen in GBM, upregulation of miR-128 inhibits PRC subunits BMI1 and SUZ12 as well as cell proliferation (Peruzzi *et al.*, 2013; Dawson and Kouzarides, 2012).

1.13 Tumour cell heterogeneity and plasticity

1.13.1 Tumour cell heterogeneity

During tumour development, changes in epigenetic regulators can cause cellular reprograming which leads to uncontrolled cell division. In cancer cells, sub-clonal mutations in epigenetic mechanisms can result in tumour heterogeneity through promoting changes in signalling of microenvironment (Dawson and Kouzarides, 2012). There are two general models that explain heterogeneity in solid tumours. The first model suggest that all cancer cells have a low proliferating capacity in which they behave as CSCs in a clonogenic assay and have the ability to form new tumours *in vivo*. The second model indicates that only small subset of cells has the capacity to proliferate extensively and

form tumour known as CSCs, the rest of the cells are depleted of that ability. The existing treatments are based largely on the first model, but the failure of these treatments to ultimately cure cancer might indicate that the second model might be more accurate (Reya *et al.*, 2001). It has been proposed that the intertumoural heterogeneity in GBM might depend on the origin of the cells as well as genetic mutation and epigenetic alteration. Based on the level of gene expression, the fragments of the tumour taken from the same GBM patient can be categorised into different GBM subtypes (Sottoriva *et al.*, 2013).

Single cell RNA-seq analysis highlighted the hierarchical modelling and intratumoural heterogeneity in GBM tumour cells (Couturier *et al.*, 2020; Patel *et al.*, 2014). Interestingly, Single cell RNA-seq analysis revealed diversity in oncogenic signalling in relation with transcriptional program in five primary GBMs. Individual cells shows characteristics of different GBM subtypes that indicates heterogeneity mixture within single tumour. Regardless of the predominant subtype of the tumour, few cells had proneural characteristics in all tumours (Patel *et al.*, 2014). PRC2 mediated H3K27me3 controls the expression of miR-1275 that regulates cell differentiation indicating the role of PRC2 and miRNA in GBM tumour heterogeneity (Katsushima *et al.*, 2012).

1.13.2 EZH2 and tumour cell plasticity

In embryonic stem cells, genes are characterised by a bivalent domain structure which is important for maintaining plasticity of the cells and regulating the expression of many important genes during development (Figure 1-8). A bivalent domain consists of repressive H3K27me3 and active H3K4me3. Genes lose their bivalent structure during differentiation process, as active or repressive monovalent domains are established (Sharma, Kelly and Jones, 2010). For example, bivalent domains disappears when embryonic stem cells differentiate into NSCs. However, there is emerging evidence that the resolution of bivalent domains can be reversed, allowing plasticity in gene expression and cell phenotype. Epigenetic alterations play a part in cellular plasticity through induction of dysfunction in DNA repair genes or silencing tumour suppressor genes (Easwaran, Tsai and Baylin, 2014). PRC2 plays a key role in this plasticity,

and may act as a driver of dedifferentiation in cancer cells. It has been reported that the mechanism of PRC2 mediated H3K27me3 regulates the interconnection between GSCs and GBM differentiated cells, leading to tumour heterogeneity (Natsume *et al.*, 2013).

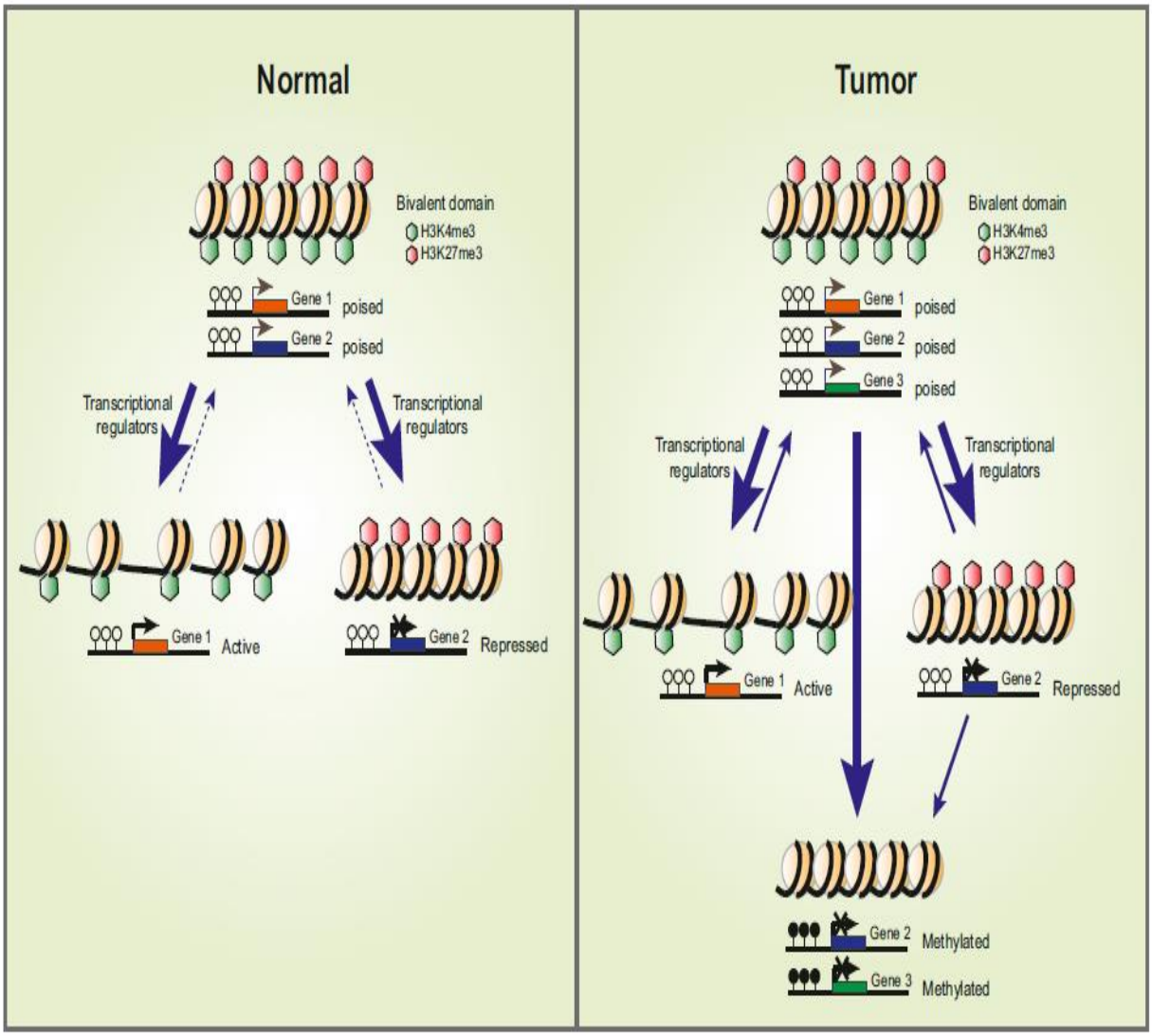

Figure 1-8 Bivalent domains in normal and tumour cells.

In normal cells, bivalent domains are converted to monovalent domains during differentiation to either active H3K4me3 resulting in transcription, or repressive H3K27me3 leading to silencing of certain genes. In tumour, cells might undergo dedifferentiation as a result of bivalent domain being recreated. This bivalency of genes has vital role in cancer cell plasticity "Figure taken from (Easwaran, Tsai and Baylin, 2014)".

The interconversion between GSCs and differentiated cells is associated with loss or gain of developmental or pluripotent genes mediated by activity of H3K27me3. EZH2 knockdown disrupts this interconversion. In GBM tumours, the level of EZH2 is higher in blood vessel areas, indicating the involvement of EZH2 in reprograming cells in response to the surrounding environment into more invasive forms (Kondo *et al.*, 2014).

1.14 Therapeutic resistance

Typical treatments for GBM include surgery followed by radiation and chemotherapy. However, the 5 year survival rate is still very poor. Previous studies indicate that GSCs cells are resistant to current therapy, which makes GBM difficult to treat (Auffinger *et al.*, 2014; Alves *et al.*, 2021). Radiation therapy causes the cell to go through apoptosis as a result of double strand breaks which leads to severe damage of DNA. EGFRvIII, a constitutively active mutant form of EGFR, mediates resistance to radiotherapy by upregulating the repair pathways for DNA double strand breaks (Carlsson, Brothers and Wahlestedt, 2014).

Therapeutic efficacy and resistance are complicated by intra and inter tumour heterogeneity. For example, isolated clones from fresh GBM tumour showed that the response of each clone to cancer therapy is different (Meyer *et al.*, 2015). Transcriptional profiling that was calculated using GBM subtype score showed clones that are sensitive to TMZ had higher score in classical and proneural and lower score in mesenchymal compared to resistant clones (Meyer *et al.*, 2015).

1.15 Mechanism of resistance to TMZ

Standard treatment for GBM include surgical removal of tumour followed by radiation and chemotherapy (Stupp et al., 2005). TMZ is an alkylating agent that is given orally to patients and it is considered the drug of choice for treatment of GBM. It has been indicated that about half of patients have a little or no

response to the treatment due to a population of cells within tumour that show resistance to TMZ (Perazzoli *et al.*, 2015).

Following oral administration of TMZ, the prodrug is absorbed in the small intestine and then penetrates blood-brain barrier. It then converts via hydrolysis into methyl triazeno imidazole carboxamide (MTIC) which is an aqueous solution and potent agent. MTIC transforms to 5- aminoamidazole -4-carboxamide (AIC) that adds a methyl group to nucleotides, especially to guanine bases, that leads to double strand breaks and cell death (Wesolowski, Rajdev and Mukherji, 2010; Villano, Seery and Bressler, 2009). Alkylation of guanine that results in O6 methyl guanine lesion can be repaired by the protein MGMT. MGMT acts as suicide protein by transmitting methyl group to its own residue leading to degradation (Figure 1-9). Cells with high levels of MGMT usually show resistance to TMZ (Lee, 2016). MGMT silencing through DNA methylation of the promotor region is associated with increased sensitivity to TMZ in GBM patients (Hegi *et al.*, 2005).

Other mechanisms of resistance to TMZ have been found. For example, in one investigation that was conducted on primary and recurrent GBM, it was found in patient with recurrent disease that MGMT promotor methylation status did not change, but there were lower levels of mismatch repair (MMR) proteins (MLH1, MSH2, MSH6 and PMS2) (Felsberg *et al.*, 2011). There is also evidence that suggests the role of TMZ in conversion of non GSC into GSC. TMZ induces hypoxic responses as well as regulating chemoresistance gene expression in new GSCs (Deheeger, Lesniak and Ahmed, 2014).

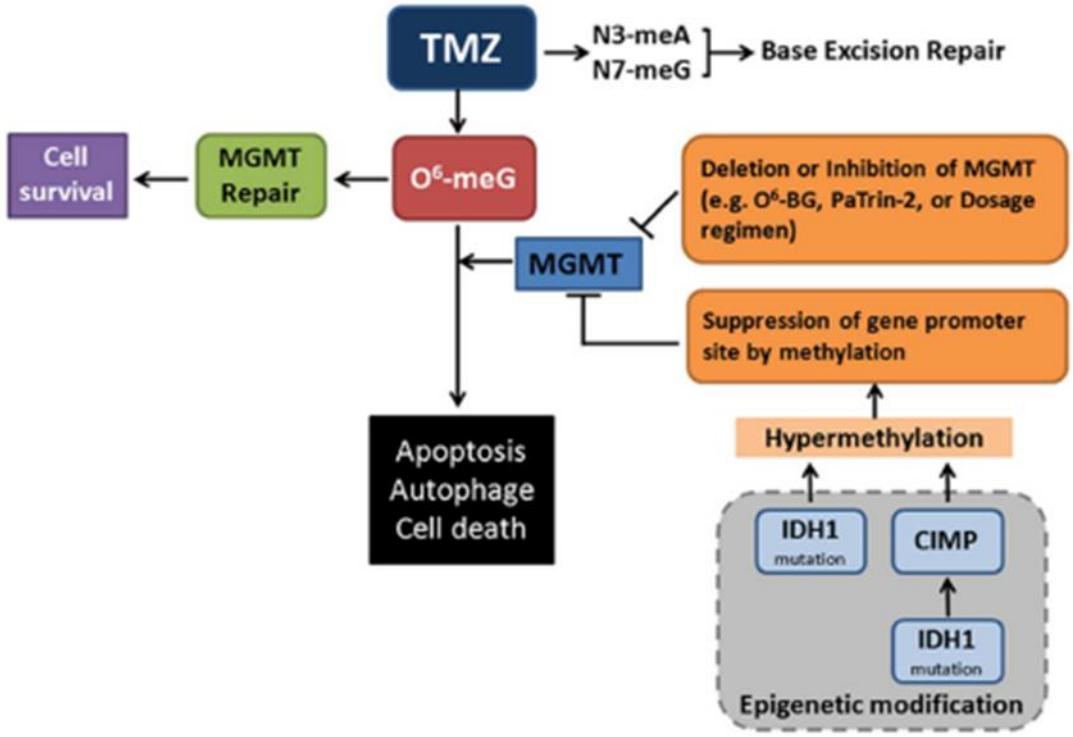

Figure 1-9 Mechanism action of TMZ in GBM cells.

TMZ forms lesion in DNA which include O6-methylguanine(O6-meG), N7-methylguanine (N7-meG) and N3-methyladenine (N3-meA). MGMT removes methyl group from O6-meG thus by restoring guanine to its normal state. MGMT function can be impaired by O6-4-bromothenyl guanine (PaTrin-2) and O6 -benzylguanine (O6-BG) inhibitors. Mutation of IDH1 can form CpG island methylator phenotype (CIMP) resulting in hypermethylation of MGMT leading to DNA double strand break and cell death. N3-meA and N7-meG lesions are usually repaired by Base excision repair pathway "Figure taken from (Sze *et al.*, 2013)".

1.16 Epigenetic targeting of the GSC population

Current therapy focuses largely on targeting bulk tumour cells lead to shrinkage of the tumour. Therapies that are more specific against CSCs might be more effective, so the tumour loses the ability to maintain and regrowth (Figure 1-10). Epigenetic modifications are found to play vital role in GBM tumour development. These epigenetic alterations are considered a potential therapeutic targets because of their interactions with the biological characteristics of GBM (Gusyatiner and Hegi, 2018). The brain is protected by the blood-brain barrier that is highly selective and prohibits entering larger molecules, so finding suitable treatment that are highly specific and can cross blood -brain barrier can be difficult.

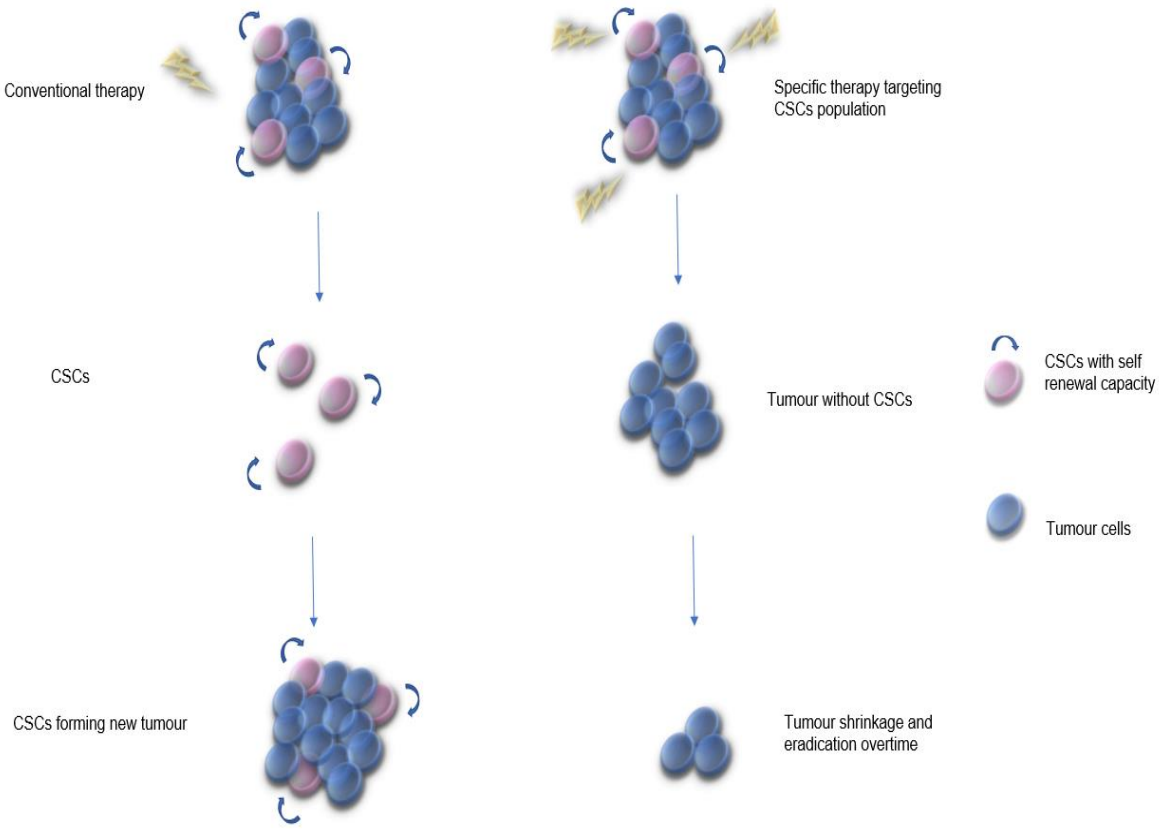

Figure 1-10 CSCs hypothesis and treatments that target tumour cells.

Conventional therapy usually targets bulk differentiated cells leaving CSCs that leads to tumour relapse. Current literature focus on eradication of CSCs population , with the absence of CSCs tumour losses the ability to sustain itself leading tumour eradication (original figure).

Several epigenetic drugs have been used to reverse the epigenetic reprograming of tumour cells. However, these drugs lack selective specificity on genomic basis and may cause toxicity. Bromodomain and extra terminal domain (BET) family proteins, act as repressors or activators of gene expression by binding to acetylated lysine residues on histones. Members of the BET family such as BRD2 and BRD4 have been linked with GBM pathogenesis. Inhibiting BET proteins reduces cell proliferation in GBM, which make them a potential target for epigenetic therapy (Pastori *et al.*, 2014). BET bromodomain inhibitors have shown efficacy in treatment of GBM cells that are resistant to TMZ. OTXO15, a novel BRD inhibitors displayed a significant therapeutic effect in GBM xenograft model, both alone or in combination with TMZ (Berenguer-Daizé *et al.*, 2016).

One research showed that inhibition of BET in lymphoma and leukaemia cells can selectively downregulate the level of MYC resulting in P21 reactivation, G1 arrest and cell death (Mertz *et al.*, 2011).

The effect of JQ1, another BET inhibitor, was tested on GBM cells. Treatment with JQ1 had significantly altered the expression of a number of genes that contribute to the pathogenesis of GBM such as $p21^{CIP1/WAF1}$, c-Myc, Bcl-xL, Bcl-2 and hTERT(Cheng *et al.*, 2013b). New evidence suggested that the I-BET151 drug, which is also a BET inhibitor, causes cell cycle arrest resulting in inhibition of GBM cell proliferation (Pastori *et al.*, 2014). In glioma cells, it has been established that HDACi decreases the expression of proteins that have role in formation of the mitotic spindle, segregation of chromosomes and DNA repair mechanisms resulting in cell death (Cornago *et al.*, 2014) .

1.16.1 EZH2 inhibitors

Given the role of EZH2 in stem cell maintenance, it has attracted much attention as a potential target for tumour treatment. Recent investigation showed that treatment with small molecule 3-deazaneplanocin A (DZNep) that inhibits the level of S-adenosylhomocysteine hydrolase was found to be associated with suppression of tumour growth in various types of cancer (Glazer *et al.*, 1986). DZNep is a commonly used EZH2 inhibitor that downregulates the level of EZH2 protein effectively. The inhibition of S-adenosylhomocysteine hydrolase leads to S- adenosylhomocysteine accumulation in the cell that reduces methylation of H3K27. Although DZNep suppressed proliferation and stemness in CSCs, it was found to be non specific for EZH2 inhibition and toxic in animal models (Miranda *et al.*, 2009). DZNep is also found to inhibit other PRC2 subunits including SUZ12 and EED. Recent approaches focus on developing compounds that are highly selective toward inhibition of EZH2 to avoid interfering with non tumourigenic pathways, Research groups are examining agents that are more specific to the inhibition of histone methyl transferases. These new compounds include S-adenosyl methionine (SAM) competitive inhibitors that compete with SAM methyl donor for binding site without targeting other PRC2 subunits. There are several types of histone methyl transferases and each one has different structure of methyl donor pocket although they all share the same SAM methyl donor to add methyl groups to histones. This allows the

development of compounds that can target one type of histone methyl transferase (Miranda *et al.*, 2009).

Several inhibitors that are SAM competitive inhibitors have been reported to reduce the level of H3K27me3. These compounds demonstrated potent effect in CSCs via impairing PRC function (Wen *et al.*, 2017). These selective EZH2 inhibitors were developed in recent years which include EPZ005687, EPZ6438, E11, GSK343, GSK126 (Helin and Dhanak, 2013). These compounds were developed based on their potency against the SET domain of EZH2, which is binding site of SAM and histone H3 lysine K27 (Figure 1-11).

These inhibitors have similar structure with 2-pyridone core that blocks the site of binding pocket for SAM methyl donor(Fioravanti *et al.*, 2018). EPZ005687 inhibits trimethylation of H3K27 and exhibits more selectivity for EZH2, although it showed minimal pharmacokinetic effects. A second EZH2 inhibitor known as EPZ6438 was developed from EPZ005687 and optimised with higher potency and pharmacokinetic properties. EPZ6438 also known as Tazemetostat or E7438, displayed greater selectivity for EZH2 activity over EZH1 and is more potent than EPZ005687(Knutson *et al.*, 2013). Another potent inhibitor of EZH2 activity is GSK126, similar to EPZ6438 it is a SAM competitive inhibitor with high selectivity for inhibition of EZH2 over EZH1. Furthermore, GSK343 is also a highly selective SAM competitive that showed antitumor effects and is a structurally related to GSK126. GSK343 showed more potency in inhibition of EZH2 and in global reduction of H3K27 methylation (Verma *et al.*, 2012).

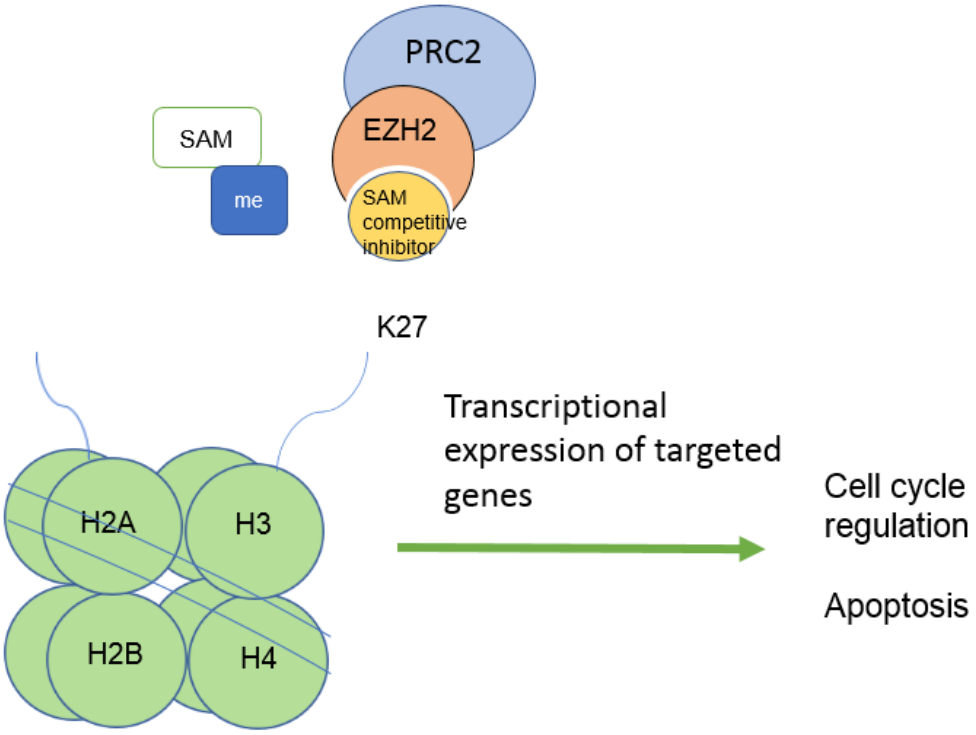

Figure 1-11 Mechanism action of SAM competitive inhibitors.

EZH2 trimethylates H3 at K27 by transferring methyl group from SAM methyl donor in PRC2 dependent manner. EZH2 inhibitors binds with EZH2 binding pocket competing with SAM methyl donor blocking methyl group transference (original figure).

In vivo studies have shown that EPZ6438 prolonged the survival of xenograft model by blocking medulloblastoma tumour growth. In this study, *in vitro* analysis showed reactivation of adhesion molecule G protein coupled with receptor B1(ADGRB1) that controls the expression of p53. Inhibition of H3K27me3 resulted in switching the chromatin into an active status and expression of BAI1 gene (Zhang *et al.*, 2020). Treatment with EPZ6438 was also found to reduce spheroid formation and invasion. Moreover, the level of polycomb subunits BMI1 and SUZ12 were reduced following treatment, and the level of Oct4 was also declined. EPZ6438 was also shown to activate apoptotic pathways through downregulation of PARP and upregulation of caspase 3 (Adhikary *et al.*, 2015). Additionally, EPZ6438 induces G1 arrest and increases the level of the cell cycle regulator p21 (Knutson *et al.*, 2014a).

Targeted genes	Regulation	Function	References
c-MYC	Upregulated	Oncogene expressed in many types of cancer	(Suvà *et al.*, 2009)
E-cadherin	Downregulated	Involved in cell adhesion	(Rosa *et al.*, 2016)
TIMP3	Downregulated	Metalloproteinase inhibitor	(Rosa *et al.*, 2016)
p21	Downregulated	Regulates cell cycle	(Yu *et al.*, 2017)
miR 26a 5p	Downregulated	Regulates EZH2 transcription	(Sharma *et al.*, 2016)
p16	Downregulated	Regulates cell cycle	(Zhang and Jiao, 2015)

Table 1-2 This table shows genes affected by the enzymatic activity of EZH2 in GBM cells.

Recent studies indicate that inhibition of EZH2 might lead to compensation by EZH1 activity (Margueron *et al.*, 2008; Shen *et al.*, 2008). Given the similarity between EZH2 and EZH1 in enzymatic activity and their interchangeability, a new compound known as UNC1999 was developed with dual inhibition for both EZH2 and EZH1 enzymatic activity. UNC1999 potently inhibited both wild and mutated Y641 of EZH2 or EZH1(Konze *et al.*, 2013) and used in combination with HDAC resulted in increased DNA damage and apoptosis in GBM tumour cells (Grinshtein *et al.*, 2016).The dual inhibition of EZH2 and EZH1 might have more effect on tumour cells than inhibition of EZH2 alone. However, the exact significant of EZH1 in cancer cells is not well understood, nor whether targeting both EZH2 and EZH1 can have a more toxic effect on cancer cells (Wen *et al.*,

2017). EPZ6438 was the first SAM competitive inhibitor to enter human clinical trials (Knutson *et al.*, 2014a; Morschhauser *et al.*, 2020), and has since been approved by the FDA for the treatment of follicular lymphoma and epithelial sarcoma under the brand name Tazverik.

1.17 Tumour angiogenesis and metastasis

Angiogenic pathway activation is a key part of metastasis and tumour invasion into other organs. When tumour cells start to move from primary site and invade other organs, cells obtain mesenchymal features and lose epithelial characteristics. This phenomenon known as EMT (Thiery, 2002; Mani *et al.*, 2008). Loss of tight junctions through silencing of adhesion molecules such as E-Cadherin (encoded by the CDH1 gene), and activating metalloproteinases enables the cancer cells to become more invasive and move through the extracellular matrix (Lombaerts *et al.*, 2006). In metastatic cancer, cell cycle inhibitory signals are supressed to promote anchorage independent growth. Cancer cell proliferation can also promoted by angiogenesis, in normal cells angiogenesis is controlled by a number of pro-angiogenic and anti-angiogenic factors, these factors have altered expression during tumour growth and invasion.

EZH2 act as gene silencer in a PRC2 dependent manner to silence anti-angiogenic and anti-metastatic genes. The enzymatic activity of EZH2 triggers suppression of the Ras inhibitor DAB2IP, which encodes for a Ras-GTPase- activating protein, and leads to decreased GTPase activity. In turn, this results in stimulation of the Ras-MEK-ERK pathway that phosphorylates EZH2. These events lead to phosphorylated EZH2 silencing miRNAs that are involved in inhibiting the expression of *EZH2* in positive feedback loop(Crea *et al.*, 2012). Some miRNAs are known to act as anti-metastatic factors; in GBM cells downregulation of miR-101 is associated with overexpression of EZH2 which increases metastases and angiogenesis (Smits *et al.*, 2010).

1.18 EZH2 and signalling pathways in cancer

There are a number of pathways in GBM cells that are associated with conventional therapeutic resistance. Genome wide analysis shows multiple dysregulations in cellular signalling pathways in GBM cells. Therefore, targeting these pathways with inhibitors might be successful in cancer treatment. Since tumour cells are heterogeneous, targeting several pathways might be more effective in eradicating GBM tumour. One of these pathways are WNT/B-catenin and Notch pathways are found to promote stemness in different types of cancer.

The WNT signalling pathway is recognised as one of the fundamental regulatory pathways that are involved in embryonic development as well as in self renewal proliferation and maintenance of stem cells in adult tissues. Dysregulation of the WNT signalling pathway has implicated in many forms of cancer, which leads to increase of self renewal and invasiveness of tumour cells (Logan and Nusse, 2004). WNT signalling pathway was also found to have a critical role in brain development, thus alteration of this signalling pathway was found to be associated with aggressiveness in GBM (Denysenko *et al.*, 2016). CSCs maintain tumour growth as well as invasiveness as the cells go through EMT. A similar process can be seen in GBM tumours making the cells go through glial-mesenchymal transition, which enhances migration and decreases apoptosis. Recent data demonstrated the relationship between WNT signalling pathways and EMT (Chang *et al.*, 2015). One study indicated that in tumour cells inhibiting related genes involved in WNT signalling pathway such as ß catenin reduces EMT (Cilibrasi *et al.*, 2017).

PRC1 and PRC2 complexes interacts with transcriptional regulators that are considered to have key role in signalling pathways such as WNT, NOTCH and HEDGHOG. The WNT signalling pathway is divided into two types, canonical which is ß catenin dependent, and non canonical that is ß catenin independent. In canonical signalling pathways, ß catenin is trapped by a complex consisting of casein kinase 1 (CK1), glycogen synthase kinase3 (GSK3), adenomatous polyposis coli (APC) and Axin (Figure 1-12). This complex degrades ß catenin through proteasomal ubiquitination (Stamos and Weis, 2013). The degradation complex is inhibited when WNT protein binds to low density lipoprotein receptor related

protein (LRP5/6) and frizzled (FZD) receptor. This leads to accumulation of ß catenin in cytoplasm, that moves into nucleus and binds to T cell factor/lymphoid enhancer factor-1 (TCF/LEF1) enabling activation of repressed genes (MacDonald, Tamai and He, 2009).

Evidence suggested the prevalence of genomic alteration in the canonical WNT signalling pathway and its association with increased tumourigenesis. It was found that the canonical WNT signalling pathway drives ß catenin into activation of specific genes and is linked to CSCs self renewal in many types of cancer (Wen *et al.*, 2020). Multiple data recently proposed that modification of histones might have a key role as epigenetic regulators in canonical WNT signalling pathway. Further studies indicate that EZH2 mediated H3K27me3 transcription repression of WNT signalling inhibitors leads to constitutive activation of canonical WNT signalling, that increases proliferation in tumour cells. This study showed the role of PRC complexes as epigenetic silencer in modulating canonical WNT signalling pathways that causes uncontrolled cell division in cancer (Chang *et al.*, 2015).

Recent studies indicated dysregulation of canonical WNT signalling pathways in relation to EZH2 overexpression. A positive correlation was found between levels of WNT ß catenin mRNA and the level of EZH2 mRNA expression (Chen, Zheng and Yang, 2016).

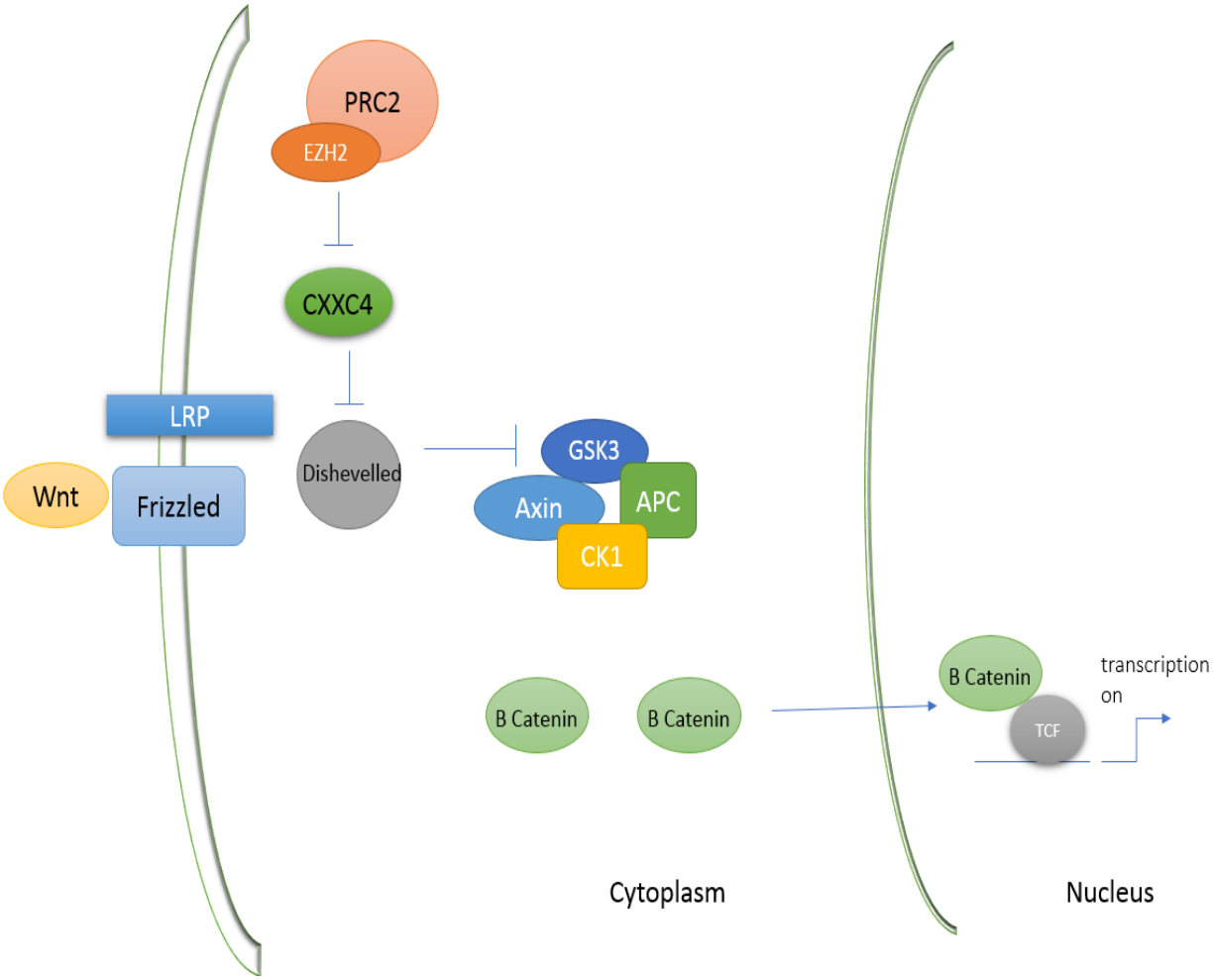

Figure 1-12 Epigenetic modification of canonical WNT signalling pathways in CSCs.

The activity of WNT β catenin pathways depends on multiple epigenetic regulators. The enzymatic activity of EZH2 targets contributes in accumulation of β catenin that is associated with self renewal in CSCs (original figure).

An elevated expression of EZH2 has been related to the increase in ß catenin accumulation in tumour cells. CXXC4 was identified as one of EZH2 targets that is known to inhibit dishevelled and stabilise the degradation complex of ß catenin (Lu *et al.*, 2013). Downregulation of CXXC4 that is associated with metastasis and poor prognosis was observed in many types of cancer (Kojima *et al.*, 2009). The epigenetic silencing of EZH2 was found to be contributing to the activation of canonical WNT signalling and promoting cell proliferation. EZH2 supresses the expression of WNT signalling inhibitors that are GSK3 and TP53 in PRC2 dependent manner(Chen, Zheng and Yang, 2016). These finding indicates

the role of EZH2 in repressing canonical WNT signalling inhibitors thus increasing the expression of its targeted genes. Furthermore, pharmacological inhibition of EZH2 was found to restore canonical WNT signalling pathway to its proper activity (Jiang *et al.*, 2008).

1.19 GBM cell lines

The most common GBM models that are used in research are U87, U251, T98G, and A172. These cell lines have been widely used for *in vitro* and *in vivo* studies, and are cultured in standard media that contains serum (De Vleeschouwer, 2017). However, it has been shown that culturing glioma-derived cells under serum-free conditions, similar to those used for NSCs, preserves tumour-initiating cells more effectively, and enriches for phenotypes that are more similar to those of the primary tumour .

G7 and E2 are two primary GBM cell lines that were obtained from freshly resurrected tumour specimens (Fael Al-Mayhani *et al.*, 2009). When grown under serum free neurosphere condition that promote stem cell maintenance, upregulation of stem cell markers SOX2, NESTIN and CD133 and downregulation of GFAP astrocytic marker was observed in both cell lines. Intracranial injection of these G7 and E2 GSCs generated highly invasive tumours in 100% of mice. However, injection of G7 cells grown under "differentiation conditions" that include serum led to the formation of non-invasive tumours, while E2 cells grown under differentiation conditions didn't form tumours in mice at all (Mannino *et al.*, 2014). G7 and E2 cell lines grown under stem cell conditions in 2D and 3D cultures also showed upregulation of markers such as SOX2 and NESTIN, showing that maintenance of stem cell phenotypes does not require neurosphere culture (Gomez-Roman *et al.*, 2017). In immunodeficient mice, tumours derived from 2D and 3D cultured G7 exhibited similar histopathological characteristics to GBM tumours, including high rates of mitosis and, proliferation and white matter infiltration. Tumours derived from E2 cells grown under 2D and 3D culture displayed upregulation of Ki67 proliferative marker and high invasiveness (Gomez-Roman *et al.*, 2017). Thus, 2D culture of G7 and E2 cells under stem cell conditions maintains their tumorigenic potential .

1.20 Rationale

In recent decades, accumulating evidence has supported the hypothesis that CSCs play a key role in many tumours, including GBM (Yu *et al.*, 2012; Batlle and Clevers, 2017). These CSC subpopulations have properties similar to stem cells in terms of self renewal, proliferation and ability to differentiate.

Several authors have attributed tumour progression and relapse following therapy to the existence of a population of radio-resistant GSCs (Alves *et al.*, 2021; Lathia *et al.*, 2015; Prager *et al.*, 2020). Intra and inter- tumour heterogeneity also leads to varying responses to conventional treatment and development of resistance. The failure of conventional therapy to target the GSC populations and to deal with tumour heterogeneity means there is an urgent need for further research to develop an effective treatment.

The role of epigenetic regulators in normal and cancer cells has been widely studied, and upregulation of PRC1 and/or PRC2 components, which act via H3K27me3, has been linked to GBM progression (Zhang *et al.*, 2015) . Several SAM competitive inhibitors have been synthesised to target enzymatic activity of EZH2, and one of them, EPZ6438, has been approved for clinical treatment of certain cancers in the USA. There is also considerable interest in combining epigenetic inhibitors with chemo-, radio- or immuno-therapies in order to improve sensitivity and specificity towards cancer cells (Feng and De Carvalho, 2022).

As explained earlier, many studies have examined the effects of EZH2 inhibitors on GBM *in vitro* and *in vivo*, and the changes in expression of various well known cancer-related genes have been reported. However, there have been no efforts to explore the effects of these inhibitors on the transcriptome as a whole, so a detailed understanding of the mechanisms of action of these drugs is unknown . Furthermore, although these inhibitors are predicted to affect the histone modification H3K27me3, there are no reports of their effects on H3K27me3 across the genome.

This study focuses on investigating three SAM competitive inhibitors: EPZ6438, UNC1999 and GSK343. The main aim is to investigate the mechanisms that contribute to their antitumour activity in GBM tumour cells by determining the underlying transcriptomic and epigenomic changes that occur in GBM stem cell lines before and after treatment with these EZH2 inhibitors. By using three different EZH2 inhibitors and two GBM stem cell lines, the aim is to identify responses, genes and pathways that are common to all experiments. This robust approach should highlight core mechanisms involved in the response to EZH2 inhibitors that will be applicable to future studies and can guide the development of improved therapeutic approaches.

1.21 Aims and objectives

1.21.1 Aims

1. To investigate whether GSCs are sensitive to various epigenetic inhibitors, particular those that act via the PRC1 and PRC2 complexes.

2. To investigate the mechanism of action of these inhibitors. This study uses two GBM stem cell lines, termed G7 and E2 (Gomez-Roman *et al.*, 2017), which were a kind gift from Prof. Chalmers.

1.21.2 Objectives

1. How do culture conditions affect gene expression in the two GBM stem cell lines? Previous studies have shown that culturing under "stem cell" conditions can preserve the stem cell characteristics of GBM lines. The first objective was to investigate the effect of culture conditions on the expression of various stem cell marker genes, thus ensuring that the most appropriate conditions were used for subsequent experiments.

2. What are the missense mutations in G7 and E2 cells that might be driving their cancer phenotype? The response of G7 and E2 cells to epigenetic inhibitors could be influenced by their genetic makeup. RNA-seq data from subsequent objectives was used to identify coding changes in cancer driver genes.

3. Are G7 and E2 cells sensitive to epigenetic inhibitors? The epigenetic drugs tested were the BET inhibitor OTX015, the BMI1 inhibitor PTC209 and the EZH2 inhibitors EPZ6438, UNC1999 and GSK343. Cell survival was assayed, as was induction of apoptosis and expression of a senescence-related marker gene. Based on these data, the decision was taken to focus on the three EZH2 inhibitors in subsequent experiments.

4. Do the epigenetic inhibitors sensitise G7 and E2 cells to the standard DNA damaging agents used in the clinic, TMZ and radiation?

5. What are the molecular mechanisms by which EZH2 inhibitors reduce cell proliferation? RNA-seq analysis was performed to investigate the gene expression changes following EZH2 inhibitor treatment of the cells.

6. How does the EZH2 inhibitor EPZ6438 change the epigenetic profile of G7 and E2 cells, and what are the direct targets of EZH2 that might be driving the observed cellular phenotypes?

Chapter 2 Material and methods

2.1 Cell culture

2.1.1 GBM cell lines

Frozen vials of G7 and E2 cells were collected from Professor Anthony Chalmers Laboratory. Cells in frozen vials were partially thawed at 37ºC, transferred drop by drop into 15 ml tubes containing 8 ml of pre-warmed media with supplements (described below). The tubes containing cell and media was centrifuged for 5 minutes at 2000 rpm, the pellet was resuspended in residual media. 10 ml of media was added into the 15 ml tube containing the cell suspension by pipetting up and down several times. Then the 10 ml of media with cells was transferred into T75 flask with vented cap (Corning). Cells are grown as monolayer and incubated in a 37ºC incubator at 5% CO_2 until reached 90% confluency.

2.1.2 Culturing of GSCs and differentiated cell populations

CSCs were grown in stem cells condition in AdDMEM/F12 medium supplemented with 20 ng/ml.epidermal growth factor (EGF), 10 ng/ml basic fibroblast growth factors (bFGF),1% B27, 0.5% N2, 4 ng/µl.Heparin, and L-Glutamine. CSCs were seeded onto Matrigel coated Flasks or plates. Matrigel was diluted in AdDMEM/F12 medium with no supplements in 1:40 dilution . Differentiated (bulk) cancer cells were maintained in MEM medium with 10% fetal bovine serum (FBS) and 1% L-Glutamine.

2.1.3 Growth of GSCs and differentiated cells.

Both CSCs and differentiated cancer cells were grown as adherent monolayers in T75 flasks with vented cap, with 12-14 ml of CSCs or differentiated cancer cell media. Cells were incubated in 37^{O}C with 5% CO2.

When cells reached 80-90% confluency, serial passaging of cells was performed. The media was aspirated off from the flask and the cells were washed twice with phosphate buffer saline (PBS, Gibco), Accutase was used to dissociate cells from the flasks, cells were incubated with 2 ml Accutase for 5 minutes to allow cells to detach then 3 ml of pre-warmed media was added to the flask and pipetted up and down several times. Then cell suspension was seeded into new flasks with 12-14 ml pre-warmed media.

Reagents	Supplier	Catalogue number
Hu EGF (1mg)	Invitrogen	PHG0313
Hu bFGF (1mg)	Invitrogen	PHG0263
Matrigel (10 ml)	BD	354230
B27 Supplement (10 ml)	Invitrogen	17504-044
N2 Supplement (5 ml)	Invitrogen	17502-048
Pen/Strep (100 ml)	Invitrogen	15140122
AdDMEM/F12 (10 x 500 ml)	Invitrogen	12634028
Accutase (100 ml)	Invitrogen	A11105-01
MEM (500 ml)	Invitrogen	10370047
Heparin (50 mg)	Sigma	H3393-10KU

Table 2-1 List or reagents used in GBM cell culture.

2.1.4 Cryopreservation of cells

Cells were detached from flasks and centrifuged for 5 minutes at 1200 rpm. The pellet were resuspended in culture media (with no supplements) containing 10% dimethyl sulfoxide (DMSO), then cryovials containing 1 ml of cell suspension were stored in - 80^{O}C freezer.The next day cryovials were transferred into liquid nitrogen for long term storage.

2.1.5 Cell counting

Cells were detached after incubation with 2 ml of Accutase, 3 ml of media was added into cell suspension. Number of viable cells were counted using Trypan blue and haemocytometer slides . The mean of cells counted from four corner of haemocytometer's squares and divided by 4. The total number of cells/ml was calculated using the equation: total cells counted x dilution factor x 10000 cells/ml.

2.2 RNA isolation and qRT-PCR

2.2.1 RNA extraction

RNA was collected from 3 different passages of stem and differentiated conditions for both G7 and E2 cells. Cells were seeded at 600000 in 10 cm dishes. Cells were scraped after adding 600 µl of RLT lysis buffer and transferred to 1 ml tubes. 70% ethanol was added into lysate (1:1 ratio) and mixed by pipetting up and down. 700 µl sample was transferred into RNeasy mini spin column, centrifuged at 1200 rpm for 1 minute, the flow though was discarded. 700 µl of RW1 was added then centrifuged at 1200 rpm for 1 minute, 500 µl of RPE was added twice into the columns and centrifuged each time for 1 minute at 1200 rpm, after that the flow through was discarded. The RNeasy mini spin column was placed into new 1.5 ml tube, 50 µl of RNase free water was added directly into the spine column membrane. Then centrifuged for 1 minute at 1200 rpm.

For RNA isolation, RNeasy® Mini kit (Qiagen) was used following manufacturer's instruction.

Reagents	Supplier	Catalogue number
RNeasy® Mini kit	Qiagen	74104
RLT lysis buffer	Qiagen	79216

Table 2-2 Reagents with supplier and catalogue number

2.2.2 cDNA synthesis

After total RNA extraction, cDNA was synthesised using Oligo(dt)$_{20}$ primer and super script IV enzyme, the cDNA synthesis consists of three steps; primer annealing, reverse transcription and RNA digestion.

Reagents	Supplier	Catalogue number
Oligo(dT)$_{20}$	Eurofins genomics	
dNTPs	Biolabs	N0447S
FS -RT-buffer(5X)	Invitrogen	18057018
DTT (0.1 M)	Invitrogen	18057018
RNase out^{TM}	Invitrogen	10777019
SuperScript^{TM} IV	Invitrogen	18057018
SYBR Green	Roche	04913914001
dH$_2$O	Qiagen	129112
RNase H	Biolabs	M0297S
RNase H buffer	Biolabs	B0297S

Table 2-3 This table represent list of reagents used in cDNA symthesis

2.2.2.1 Primer annealing

The first step of cDNA synthesis was preparing the following reagents then the tubes were incubated in thermocycler at 64^{o}C for 5 minute and cooled for 1 minute on ice, reagents were mixed as follow:

RNA	500 ng
Oligo(dt)$_{20}$	0.5 µl
dNTPs (10 mM)	0.5 µl
dH$_2$O	Up to 10 µl

2.2.2.2 Reverse transcription

For the second step a master mix was prepared, then 5 µl of master mix was added into the tube containing components from previous step. The tubes were incubated in thermocycler at 50°C for 50 minutes then at 85°C for 5 minutes, the master mix was prepared as follow:

FS RT buffer (5X)	3 µl
DTT (0.1M)	1 µl
RNase out™	0.5 µl
SuperScript™ IV	0.5 µl

2.2.2.3 RNA digestion

The third step included adding 1 µl of RNase H to the reaction for digesting the RNA. The tubes were incubated in thermocycler at 37°C for 20 minutes, then cDNA was stored at - 20 °C.

2.2.3 qPCR

To determine the type of genes expressed in G7 and E2 cells in stem cells and differentiated state, cDNA was diluted in 1:5 ratio. 5 µl of diluted cDNA and 20 µl of primer's master mix was added into each well of 96 well plate (Thermo fisher) , making the final volume 25 µl per well.

The primer's master mix was prepared as follow:

SYBR Green mix	12.5 µl
Forward primer	3 µl
Reverse primer	3 µl
dH_2O	1.5 µl

qRT-PCR was performed by selecting SYBR Green dissociation curve using Mx Pro 3000 program. PCR products that have been amplified was detected using SYBR green assay. The thermal cycler profile setup was performed as follow:

Segments	Cycles	Time	Temperature
1	1	10 minutes	95°C
2	40	15 seconds	95°C
		1 minutes	60°C
3	1	1 minutes	95°C
		30 seconds	55°C
		30 seconds	95°C

Genes were amplified using primer sets that were designed by NCBI software except for CD133 primer sets were taken from an article (Brescia, et al., 2013) .The primers were designed to span on exon-exon junction, 70-150 base pair with melting temperature of 58-62°C. Once the primers were ordered (Eurofins Genomics) they were resuspended in TE buffer according to the oligonucleotide synthesis report. TE buffer was prepared from 10 mM Tris (pH 7.5) and 1 mM EDTA (pH 8) in DNase free water.

Primer	sequence
SOX2 Forward	TACAGCATGATGCAGGACCA
SOX2 Reverse	CCGTTCATGTAGGTCTGCGA
NESTIN Forward	CTCAGCTTTCAGGACCCCAAG
NESTIN Reverse	GCACAGGTGTCTCAAGGGTA
OLIG2 Forward	ATAGATCGACGCGACACCAG
OLIG2 Reverse	CTCGGACCCGAAAATCTGGA
GFAP Forward	ACCTGCAGATTCGAGAAACCAG
GFAP Reverse	TCCTGCCTCACATCACATCC
β III Tubulin Forward	TCCATTTCTCGACTTTCCAAACTG
β III Tubulin Reverse	CTTCCCAGAACTGTGGACGC
CD133 Forward	ACCAGGTAAGAACCCGGATCAA
CD133 Reverse	CAAGAA TTCCGCCTCCTAGCACT
NANOG Forward	CAATGGTGTGACGCAGGGAT
NANOG Reverse	TGCACCAGGTCTGAGTGTTC
MYC Forward	ACT CTG AGG AGG AAC AAG AA
MYC Reverse	TGG AGA CGT GGC ACC TCT T
EZH2 Forward	AAT CAG AGT ACA TGC GAC TGA GA
EZH2 Reverse	GCT GTA TCC TTC GCT GTT TCC
MGMT Forward	GCT GAA TGC CTA TTT CCA CCA
MGMT Reverse	CAC AAC CTT CAG CAG CTT CCA
PTEN Forward	CAA GAT GAT GTT TGA AAC TAT TCC AAT G

PTEN Reverse	CCT TTA GCT GGC AGA CCA CAA
P16INK4a Forward	GCC CTG GAG GCG GCG AGA
P16INK4a Reverse	CGA CCG TAA CTA TTC GGT GCG TTG G
CDK2 Forward	GGC AGA CCA GCA TGA CAG ATT
CDK2 Reverse	AAG GCA GAA GAT GTA GAG CGG
β -Actin Forward	ATT GGC AAT GAG CGG TTC
β -Actin Reverse	GGA TGC CAC AGG ACT CCA T

Table 2-4 List of primers used in qRT-PCR and their sequence.

2.2.4 qRT-PCR analysis

For stem and differentiated genes the fold change was calculated from average ΔCt using the formula $2^{\wedge(-\Delta Ct)}$. The average ΔCt represent ΔCt from three biological replicates. Error bars represent standard deviation of ΔCt of three replicates. The ΔCt was calculated by subtracting the Ct from housekeeping gene from interested gene.

For PRC2 targeted genes the average Ct from three Ct values was calculated, the average Ct housekeeping gene was subtracted from average Ct of gene of interest the fold change of gene of interest was calculated using the formula $2^{\wedge(-\Delta Ct)}$.

2.3 Clonogenic assay

2.3.1 Clonogenic assays of EZH2 and BMI1 inhibitors

G7 and E2 cell lines were grown in stem conditions and seeded into Matrigel coated 6 well plates (corning), the seeding density of cells was 250 cells per well

in 1 ml media .The plates were inoculated and incubated for 24 hrs to allow cell attachment to the surface of the plate.

Cells were exposed to different concentrations of EPZ6438 (Selleckchem), GSK343 (Selleckchem), UNC1999 (Selleckchem) and PTC209 (MedChemExpress) or 0.2% DMSO, the concentration of the stock was 10 mM.After treating the cells with different concentrations of drugs , plates were incubated with the drugs for 48 hrs. After 48 hrs, media containing the drugs was aspirated and replaced with new 2 ml media. Plates were left in incubator for 14 days to allow cell to form colonies.

Cells were also seeded at 250/well in 6 well plates in 1 ml media and exposed to increasing doses of radiation (1,2.3.4 and 5 Gy) or TMZ (10 mM stock concentration) for 24 hrs following incubation with increasing concentration of drugs or 0.2% DMSO for 24 hrs. After overnight incubation, the media and drugs was changed with new 2 ml media , the plates were returned to the incubator and left for 14 days to form colonies.

G7 and E2 stem cells were maintained in AdDMEM/F12 medium with supplements and growth factors throughout the entire experiment. After 14 days, media was aspirated and cells were fixed with 1 ml of 50% methanol and PBS for 15 minutes then aspirated and cells were fixed with 1 ml methanol for 15 minutes. After methanol was removed from the plates, cells were stained with crystal violet diluted in PBS (1:25) for 45 minutes.

Colony assay was calculated by taking the mean from independent experiments. The error bars represent standard error of mean of colonies counted from each experiment. For clonogenic assay of cells treated with drugs only, the p value was calculated using Student's T test from means of 3 independent experiment of drug treated vs control. IC50 from three independent experiments was calculated.

Dose modifying ratio (DMR) of cells treated with combination of drugs and radiation was determined. The DMR was calculated by taking the ratio of the radiation dose required to reduce survival to 37% for control and treated samples. p value calculated by comparison of means, sd and sample size (n) of

drug treated vs control was calculated using tools on website https://www.medcalc.org/calc/comparison_of_means.php .

2.3.2 Clonogenic assay of TMZ and BET inhibitors

GBM cell lines were grown in stem and differentiated conditions in 6 well plates, the seeding density of cells was 250 cells per well The plates were inoculated and incubated for 24 hrs to allow cell attachment to the surface. Next day, cells were treated with different concentrations of the drug.

Cells were also exposed to increasing concentrations of TMZ (Selleckchem) with 10 mM stock concentration or BET inhibitor OTX015 (Selleckchem) with 100 mM stock concentration, separately. Cells were incubated with TMZ for 1 hr. After treating the cells with different concentrations of OTX015, plates were incubated for 24 hrs. For assessing the combination of TMZ and OTX015, plates were incubated for 1 hr with TMZ then with 24 hrs of OTX015, or DMSO (0.1%) Media was changed after treating the cells with drugs every 3 days for 10 days.

For counting the colonies, cells were fixed with methanol and stained with 0.1% crystal violet (sigma). Colonies were counted manually. Colony assay was calculated by taking the mean from independent experiments. The error bars represent standard error of mean of colonies counted from each experiment. IC50 of three independent experiments was calculated. p value was calculated using Student's T test from means of 3 independent experiment of drug treated vs control.

2.4 Cell Titer –Glo assay

2.4.1 Glo assays for EZH2 and BMI1 inhibitors

Cells were seeded into 96 well plates coated with Matrigel and grown in stem condition. Each well of 96 well plate was inoculated at density 2500 cells in 100 µl media , then the plates were incubated for 24 hrs overnight. The seeding

density of cells was calculated with haemocytometer. Cells were treated with increasing concentration of EPZ6438, UNC1999, GSK343 and PTC209 or 0.2% DMSO then retuned to the incubator and left for 5 days..

After 5 days of incubation with drugs, number of viable cells were detected using Cell Titer- Glo (Promega). This assay depends on luciferase reaction in which the amount of ATP from viable cells were quantified following cell lysis. 100 µl of Cell Titer- Glo reagent was added into each well containing cells and left for 10 minutes at room temperature to induce cell lysis. Luminescence signal of each sample was detected using Luminoskan Ascent using Cell Titer-Glo assay following manufacturer's instruction. p value of means of 3 independent experiments was calculated using Student's T test in drug treated vs control. IC50 was calculated from three independent experiments.

2.4.2 Glo assays for TMZ and BET inhibitors

Cells were grown in stem and differentiated conditions in 96 well plates. Each well of 96 well plate was inoculated with 5000 cells and 100 µl of media, plates were incubated for 24 hrs to allow cells to attach to the surface of the plate. The next day, cells were treated with 0.2% DMSO or increasing concentration of OTX015 and TMZ separately and in combination for 3 days. Luminescence signal of each sample was detected with Luminoskan Ascent using Cell Titer- Glo assay following manufacturer's instruction. IC50 was calculated from three independent experiments. p value of means of 3 independent experiments was calculated using Student's T test in drug treated vs control.

2.5 RNA sequencing

2.5.1 Initial analysis of data with Galaxy server

G7 and E2 were grown in stem condition on Matrigel coated 10 cm dishes and seeded at 600000/dish. Cells were incubated with 2 µM of EZH2 inhibitors for

5 days. RNA extraction was performed on the samples as explained in qRT-PCR section.

RNA samples were sent to BGI genomics in Hong Kong for RNA sequencing, this resulted in generating FastQ files for each samples. The low level analysis of Fastq files was performed using Galaxy server (Afgan *et al.*, 2018) that is hosted by University of Glasgow polyomics. The FastQC was selected to determine the quality of sequenced data for each sample. HISAT2 (Kim, Langmead and Salzberg, 2015), a sequence alignment mapping program, used to map RNA sequence and produce BAM files. This spliced alignment tool used to map reads to reference human genome. From the software the unstranded option was selected in specified standard information and GTF file was chosen from advanced option to determine exon-intron junction.

The aligned reads were then assembled using StringTie program into transcript. The unstranded option and GTF file were selected again. The read length was set at 100 bp with reference transcription only being selected along with BAM files that were selected as input files. The count files that produced by StringTie were selected in Deseq2 (Love, Huber and Anders, 2014). In the first factor level, gene counted data for treated sample was chosen and compared to gene counted data for control from second factor level. Three different types of files were generated from Deseq2 analysis these include normalised count, plots and result files.

2.5.2 Visualisation of the data using Searchlight2

To visualise RNA- seq data searchlight2 with single comparison was selected from Galaxy server . Searchlight2 (Cole *et al.*, 2020) is visualisation tool that is used for unlimited differential datasets. Three input files were needed to run searchlight2; expression matrix, sample sheet and differential expression. All the input files that were used in Searchlight2 were created in excel and saved as Tab delimited format file. Deseq2 result file was modified into differential expression file while Deseq2 count file was formatted into expression matrix. Sample sheet was also modified from Deseq2 count file that only includes the name and the group of samples . After the output files created from

searchlight2, the files were download and the R program was used to modify the plots and export as images.

2.5.3 RNA-seq analysis using Gene Ontology

To identify biological processes and pathways that are involved with differentially expressed genes (DEGs) Gene Ontology (GO) analysis was performed. Before GO analysis, the Deseq2 differentially expressed files were filtered with adjusted p value < 0.05. the DEGs were filtered into upregulated genes with Log2 fold change > 0 and downregulated genes with Log2 fold change < 0. The analysis of GO was performed using Toppgene, which is a program that is used for the gene enrichment analysis. The list of all of upregulated and downregulated DEGs from DESeq2 files were copied into Toppgene website separately. The ensemble gene IDs were copies into Toppfun column and the analysis was run through the software. The output file generated from Toppgene website was modified using excel sheet. The file was filtered to include only Biological process with q value (Bonferroni) < 0.05 that was plotted on graph against - Log10 of q value calculated for upregulated genes and Log10 q value for downregulated genes separately.

2.5.4 InteractiVenn

The Venn diagram was created using InteractiVenn tool (Heberle *et al.*, 2015), this software was used to identify similarities between G7 and E2 stem cell lines. The Deseq2 result file was modified with adj. p value < 0.05 and Log2 fold change > 0 for upregulated genes while for down regulated genes, Log2 fold change < 0 with adj. p value < 0.05. The upregulated and downregulated genes for G7 stem and E2 stem were ran separately using InteractiVenn creating diagrams that were exported as images.

p value was determined by calculating representation factor using the website http://nemates.org/MA/progs/overlap_stats.html. The representation factor was calculated as fellow: Expected number of genes = number of genes in group 1 *

number of genes in group 2 / total number of genes, Representation factor= number of genes common in both groups / expected number of genes.

2.5.5 RNA-seq analysis using Gene Set Enrichment Analysis

Gene Set Enrichment Analysis (GSEA) (Subramanian *et al.*, 2005) can be more accurate in identifying pathways that are changed in cell lines compared to GO analysis. GSEA not only looks at the gene expressions that are significantly changed but also looks at the genes with the smallest change in expression. The count files from Deseq2 were formatted into two type of files (expression data set and phenotype label files) and uploaded into GSEA program. In phenotype label option treated vs control sample file was chosen and gene set as per mutation type was selected. The output file generated from GSEA website was modified using excel sheet. The file was filtered with nominal (NOM) p value < 0.05 and false discovery rate (FDR) q value < 0.25. A graph was plotted with normalised enrichment score (NES) against pathways, NES < 0 for upregulated pathways and NES > 0 for downregulated pathways.

2.5.6 Open cravat

The interpretation of genomic variants of the sample was made through Open cravat https://opencravat.org/.This web toolkit analysis the variants and creates a file with variants annotation, scores and impact. The VCF files of the each sample was created by uploading BAM files of G7 and E2 controls into Free Bayes BAM dataset after selecting Merge output VCFs using Galaxy platform, the VCF files that were uploaded into Open Cravat web tool. Hg 38 was selected as reference genome and from annotation tab; Sequence Ontology Summery, Gene Ontology, Cancer Genome Interpreter, CHASM plus and CHASM plus GBM . From filter tab CHASM plus p value < 0.01 and CHASM plus GBM p value < 0.05 were selected. From variant tab a file with variant annotation was created.

2.6 ChIP sequencing

2.6.1 Chromatin sample preparation (cross linking)

G7 and E2 were grown in stem condition on Matrigel coated 10 cm dishes and seeded at 600000/dish. Cells were incubated with 2 µM EPZ6438 for 5 days then ChIP-seq was performed. One plate was used for cell counting and the others were used for chromatin collection. When the cells reaches 80-90% confluence, the media was changed with pre-warmed media (with no supplements). The 16% formaldehyde stock was diluted in solution consisted of(1 mM EDTA, 0.1 M NaCl, 50 mM HEPES pH 8.0, and 0.5 mM EGTA) to make 10% formaldehyde. Cells were cross linked on shaker for 10 minutes at room temperature by adding 10% formaldehyde to make 1% final concentration.

The cross linking reaction was quenched on shaker for 5 minutes by adding 0.75 ml of 1 M glycine. After that cells were washed with 10ml prechilled PBS and scraped with 5 ml pre chilled PBS. Cells were centrifuged for 5 minutes at 1200 rpm at 4^{o}C, the pellet was resuspended in PBS and centrifuged again. Finally, the pellet was resuspended in RIPA buffer(0.1% sodium deoxycholate, 10 mM Tris-HCl pH 8, 1 mM EDTA pH 8, 0.5 mM EGTA pH 8, 0.1% SDS, 1 X protease inhibitor cocktail, 1% triton X-100, and 10 µM of sodium butyrate). The Amount of RIPA buffer was calculated: 7.5 x 10^{7} cells in 2 ml RIPA buffer. Samples were incubated on ice for 10 minutes then stored at -80.

2.6.2 Chromatin sonication

The samples were thawed on wet ice, then chromatin was sheared using sonication (Sonicator 3000) for 30 minutes, high power voltage and amplitude 30 seconds on/30 seconds off.

2.6.3 Reverse crosslinking reaction

Chromatin sample was reverse cross linked in tube that contained 4 µl of sonicated chromatin, 2 µl distilled water, 1 µl of proteinase K (1:5 diluted in water) 1 µl RNase A (1:10 diluted in water) and 2 µl of 1 M NaCl.The reaction

was incubated at 65ºC for 2 hrs, the tubes were allowed to cool at room temperature then the DNA was purified using Qiagen mini elute column kit and eluted in 12 µl elution buffer. The concentration of DNA was determined with nanodrop then 4 ul of 25% glycerol was added to 2 µl of DNA sample, the samples were ran in 1% agarose gel electrophoresis for 50 minutes.

2.6.4 Chromatin immunoprecipitation

The chromatin sample (10 µl) was thawed on wet ice and spun in 12000 rpm for 5 minutes at 4ºC, the supernatant was transferred into new tube, 900 µl of cold RIPA buffer(1 mM EDTA pH 8, 10 mM Tris-HCl pH 8, 140 mM NaCl, 0.5 mM EGTA pH 8, 0.1% sodium deoxycholate, 0.1% SDS, 1 X protease inhibitor cocktail, 1% triton X-100 and 10 mM sodium butyrate) was added into chromatin samples.

The magnetic beads were washed twice with 200 µl of blocking buffer (0.5% BSA and 0.5% tween-20 in PBS). The antibody was bound to magnetic beads by adding 2-3 µl of antibody to 200 µl of blocking buffer and incubated on a rotator at room temperature for 1 hr. The supernatant was removed by placing the antibody conjugated beads on magnet.

400 µl of chromatin sample was applied to antibody conjugated beads and incubated for 3 hrs at 4ºC on a rotator. The beads were washed using the magnet to remove the supernatant with a pipette each time; twice with 500 µl of cold RIPA buffer, twice with 500 µl of cold RIPA-500 (500 mM NaCl, 1 mM EDTA pH 8, 10 mM Tis-HCl pH 8, 0.5 mM EGTA pH 8, 0.1% SDS, 0.1% sodium deoxycholate, 1 X protease inhibitor cocktail, 1% triton X-100 and 10 mM sodium butyrate). once with 500 µl of cold RIPA-LiCl (1 mM EDTA pH 8, 10 mM Tis-HCl pH 8, 0.5 mM EGTA pH 8, 0.1% SDS, 0.5% NP40, 250 mM LiCl, 1 X protease inhibitor cocktail, and 10 mM sodium butyrate), twice with 500 µl of room temp TE pH 8 (1 mM EDTA and10 mM Tris-HCl pH 8). With the last wash, the sample with beads were spun briefly then the magnet was used to remove all of the supernatant.

The beads and the input were resuspended by pipetting up and down in 70 µl of elution buffer (5 mM EDTA, 10 mM Tris-HCl pH 8, 300 mM NaCl and 0.5% SDS) and 4 µl of proteinase K , 1 µl of RNase A was added to the input only, The beads and the input were incubated at 55ºC for 1hr. After incubation, the samples were allowed to sit at room temperature for 10 minutes then stored at -20.

Antibody	Species raised	Supplier	ul per IP	Catalogue number
H3K4me3	Rabbit	EMD Millipore	2.5	07-473
H3K27me3	Rabbit	EMD Millipore	3	07-449
H3 pan ct	Rabbit	EMD Millipore	2	07-690

Table 2-5 List of antibodies used in ChIP sequencing experiment.

The next day, tubes were warmed at 37ºC to allow samples to resuspend, then the samples were spun briefly and supernatant were collected after applying magnet to the beads. The samples containing the DNA was purified using Qiagen mini elute PCR purification kit,50 µl of Qiagen elution buffer was added to the samples. At this stage samples were frozen at -80 until they were shipped for ChIP- seq.

2.7 ChIP-seq analysis

ChIP DNA was combined from 2 – 3 immunoprecipitations to yield at least 10 ng for sequencing. DNA was quantified by Glasgow Polyomics using Qubit technology. Samples were sequenced by Novogene using paired end sequencing to give 150 bp reads. Fastq files were processed by tools using the Galaxy server hosted by Glasgow Polyomics. Bowtie2 (Langmead *et al.*, 2009) was used to align reads to the Hg38 genome, which was imported from the UCSC genome browser server in May 2021. The sensitive end to end alignment setting was chosen to maximise the number of correctly aligned reads.

2.7.1 UCSC genome browser and ChIPseeker

To view the ChIP-seq data on the UCSC genome browser, the bamCoverage (Ramírez *et al.*, 2016) tool was used to create BigWig files. The bin size was 50 bases, reads were normalised to reads to kilobase per million, and reads were extended to 300 bases for visualisation purposes. BigWig files were uploaded to the Cyverse Discovery Environment, from where a public link was used to load the data into the UCSC genome browser.

MACS2 was used to call peaks from ChIP samples using the data from input chromatin as the control. Several settings were tested in order to generate peaks that best matched those observed on the BigWig traces. The final settings used were: band width of 500 bases and a q value of 0.05 for peak detection (Zhang and Su, 2012), along with the broad peak setting with an FDR of 0.05. The default settings for model building were used. The broad peak setting combines nearby highly enriched regions into one broad region. The tool ChIPseeker was used to annotate the MACS output bed file with genomic regions. The reference was a gtf file containing transcript information that was downloaded from the UCSC genome browser server in May 2021.

2.7.2 Seqmonk

To analyse the peaks, bam files were downloaded and imported into Seqmonk version 1.48.0 (Babraham Bioinformatics). Hg38 version 102 was used as the reference genome. Probes were defined using the MACS2 peaks for the control (non drug treated) sample in each experiment, and read counts across these probes were quantified in both the control and drug treated samples. Read counts were corrected per total million reads to allow for differences in library size. Read counts are expressed in log2. Upregulated DEGs from the DESeq2 output described in the RNA-seq analysis section (adj.p < 0.05) were used to create an annotation list. Genome co-ordinates were ascribed to each DEG using the function vlookup in excel, referring to the gtf file as the source of the co-ordinates. The DEG.gtf file was imported into Seqmonk, and used to filter the MACS2 probes so as to select peaks that overlapped with an upregulated DEG. These probes were then filtered for TSS, so that only peaks overlapping with the TSS of an upregulated DEG were retained. The “filter on values differences”

function was used to filter H3K27me3-DEG up-TSS peaks that had a decrease of 0.5 log2 in the drug treated samples compared to the control. For H3K4me3, DEG up-TSS peaks were selected that had an increase of 0.4 log2 in the drug treated compared to control. Plots were created using the scatter plot function.

The exported lists of peaks from Seqmonk were annotated in excel. Growth factors, receptor tyrosine kinase genes and genes involved in neurogenesis or central nervous system development were identified based on GO terms within Toppgene. Transcription factors were annotated using the database created by Lambert et al (2018), using the vlookup function in excel.

To see if there is any correlation between ChIP quantification and expression level, Seqmok was used to quantify the peaks from control samples, then it was filtered for those that overlaps TSS eponine. The Seqmonk file was exported that contained prob list with gene names and quantification. Vlookup was used to import gene count from each replicate of Deseq2 count file into Seqmonk output file. The average count from the 3 replicates were calculated and converted to Log2 using excel sheet. The Log2 quantification > -5 of each ChIP peak against Log2 average count > 0 was plotted in scatter plot.

The Seqmonk output file was also used to create box and whiskers plots. The formula vlookup was used to look for all gene names in the list of genes with ChIP peaks. A list of all genes was created with based on whether they have a ChIP peak or don't have ChIP peak. The Log2 (> 0) of average count from Deseq2 count file was calculated to create box and whiskers plot.

2.8 Senescence β- galactosidase staining

G7 and E2 stem cells were seeded in 6 well plates coated with Matrigel at density of 2000 cells/well and left overnight to allow cells to attach to the wells. Next day, E2 and G7 cells were treated with 2 μM of drugs (EPZ6438, GSK343, PTC209 and UNC1999) then left in the incubator. After 5 days incubation with the drugs the media was removed, the plates were rinsed once

with 2 ml 1x PBS, the Senescence- ß -Galactosidase staining kit (Cell Signalling Technology #9860).1 ml of 1X fixative solution was added into each well, cells were allowed to fix for 15 minutes at room temperature. Plates were rinsed twice with 1X PBS then 1 ml of ß- galactosidase staining solution was added into each well, plates were sealed with parafilm to prevent evaporation and incubated overnight at 37ºC in incubator with no CO2. The Next day, cells (with ß- galactosidase still on the plate) were checked under microscope to see the blue colour have been developed.

The images of the cells were captured using Confocal microscope with ZEN microscope software. The images from treated and control cells of each well were captured in 3 different fields. The cells within the image was counted using Image J program.This assay was performed as 3 independent experiment. p value was calculated using Student's T test from means of 3 independent experiment of drug treated vs control

2.9 Apoptosis assay

Cells were seeded at 600000 in 10 cm dish, both G7 and E2 cells were grown in stem culture media on Matrigel coated plates. Cells were incubated for 24 hrs to allow cells to attach to the surface of the plates. The next day, cells were incubated with 2 µM of drugs (EPZ6438, GSK343, PTC209 and UNC1999) for 5 days.

Cells were detached with cell scraper and centrifuged at 1200 rpm for 5 minutes. The supernatant was discarded,1 ml of Hank's Balanced salt solution (HBSS) was added then centrifuged and the supernatant was discarded again. The total of working solution was prepared per sample was (40 µl HBSS, 5 µl AnnexinV and 5 µl 7AAD). 50 µl of stock was added to the sample. For single dye control, 45 µl of HBSS and 5 µl of dye were added. For cells only control nothing was added to the sample. The racks containing the tubes were shaken then incubated for 15 minutes at room temperature in the dark. 300 µl of HBSS was added into each tube. Each tube was vortexed before reading, The flow cytometric analysis was carried out using FlowJo program

Reagent	Supplier	Catalogue number
HBSS	Merck	55037C
7AAD	BD Bioscience	559925
AnnexinV	Biolegend	640906

Table 2-6 List of reagents used in Apoptosis assay.

Chapter 3 Characteristics of GBM cell lines

3.1 Aims

This chapter presents initial characterisation of the two GBM cell lines used in this study, G7 and E2.

Aims:

1) GBM cells typically express several genes associated with cancer stem cells (CSC) and neural stem cells (NSC). The first objective is to investigate the effect of culturing the cell lines under "stem" and "differentiated" culture conditions on the expression of various stem cell marker genes.

2) To investigate the sensitivity of the GBM cell lines to the standard chemotherapy drug, TMZ.

3) To investigate the sensitivity of the GBM cell lines to epigenetic drugs that inhibit BMI1 and BET proteins, and to investigate whether these drugs can increase the sensitivity of the cells to the standard treatments of radiation or TMZ.

4) To identify genetic mutations in cancer driver genes in the GBM cell lines.

3.2 Introduction

G7 and E2 cell lines were derived from resected GBM tumours. Cells were maintained in stem media and differentiated media. To assess the sensitivity of CSCs to conventional chemotherapy and epigenetic drugs, GBM cell lines were cultured *in vitro* in under conditions that either promote the maintenance of GSC characteristics, or promote a more differentiated state that is typical of the bulk of cells within a GBM tumour (Ledur *et al.*, 2017). Previous studies have focused on distinguishing CSCs from the rest of the cancer cell population using different approaches. The expression level of stem cell markers that are highly expressed in CSCs population has been utilised as one of the methods to identify GSC population. Brescia *et al.*, classified GBM cell lines by quantifying their high and low mRNA expression of the same stem cell marker (Brescia *et*

al., 2013). This study suggested not to rely on single stem marker to isolate GSC population, since there is not universal marker for CSCs. Facs sorting analysis of GBM tumour cells showed mixed population of CSCs that are expressing different levels of stem cell surface markers (Brown *et al.*, 2017).

Previous investigations using clonogenic survival assays showed that the GSC population in GBM tumour is radioresistant (Ali *et al.*, 2020). SOX2 and NESTIN are considered NSC markers that are expressed in stem cells of the central nervous system (Zhang and Jiao, 2015). OLIG2 is also considered a NSC marker that prevents astrocyte differentiation (Setoguchi and Kondo, 2004).In cancer, stem cell's markers such as SOX2 and OLIG2 are expressed in GSCs found to be correlated with radioresistance (Kowalski-Chauvel *et al.*, 2018). Lee *et al.*, demonstrated that SOX2 overexpression correlates with promoting clonogenic growth in GBM cells (Lee *et al.*, 2015). They have shown that a significant increase in levels of SOX2 was observed as a results of irradiation of GBM tumour cells. Recent finding also indicates the involvement of some CSCs markers in signalling pathways that enhances the chemoresistance of GSCs population. Overexpression of NANOG in GBM tumour cells, was found to play a vital role in HEDGEHOG-GLI signalling pathways that are involved in DNA repair mechanism (Soni *et al.*, 2017).

The first objective of this chapter is to characterise the "stemness" of the GBM cell lines being studied, by investigating the expression level of various CSC markers.

3.3 Characteristics of G7 and E2 cell lines in stem and differentiated cultures

In order to maintain the CSC characteristics, GBM cell lines were cultured in media without serum in the presence of growth factors (EGF and FGF), and allowed to adhere to a Matrigel coated surface (stem cell conditions). Conversely, cells grown under differentiated conditions were cultured in the presence of serum without additional growth factors or Matrigel.

Studies have focused on identifying GSCs and distinguishing them from the rest of non stem cell population. Since there is not a universal marker for GSCs, it is important not to rely on a single marker for identification of CSCs. CD133 is usually expressed in GSCs, although some GBM cells are found to have CSCs characteristics despite exhibiting low CD133 expression (Brown *et al.*, 2017). Common CSCs markers that are expressed in GSCs are SOX2, OLIG2, NESTIN and NANOG, while GFAP is an astrocytic marker that is usually expressed in differentiated GBM cells (Hattermann *et al.*, 2016).

Here, GBM cells cultured under stem (S) and differentiated (D) conditions and were characterised by a panel of CSCs makers (Figure 3-1). E2S cells had significantly higher expression of several CSC markers than G7S cells, including *OLIG2*, *CD133* and *NESTIN*. In contrast, G7S cells had higher expression of the astrocyte marker, *GFAP*. Growing the E2 cells under stem conditions led to significant increases in *OLIG2*, *SOX2* and *GFAP* compared to the differentiated conditions, and a trend towards increased expression of *CD133* and *NESTIN*. For the G7 cells, the only gene showing a significant reduction in expression under differentiated conditions was *NESTIN*.

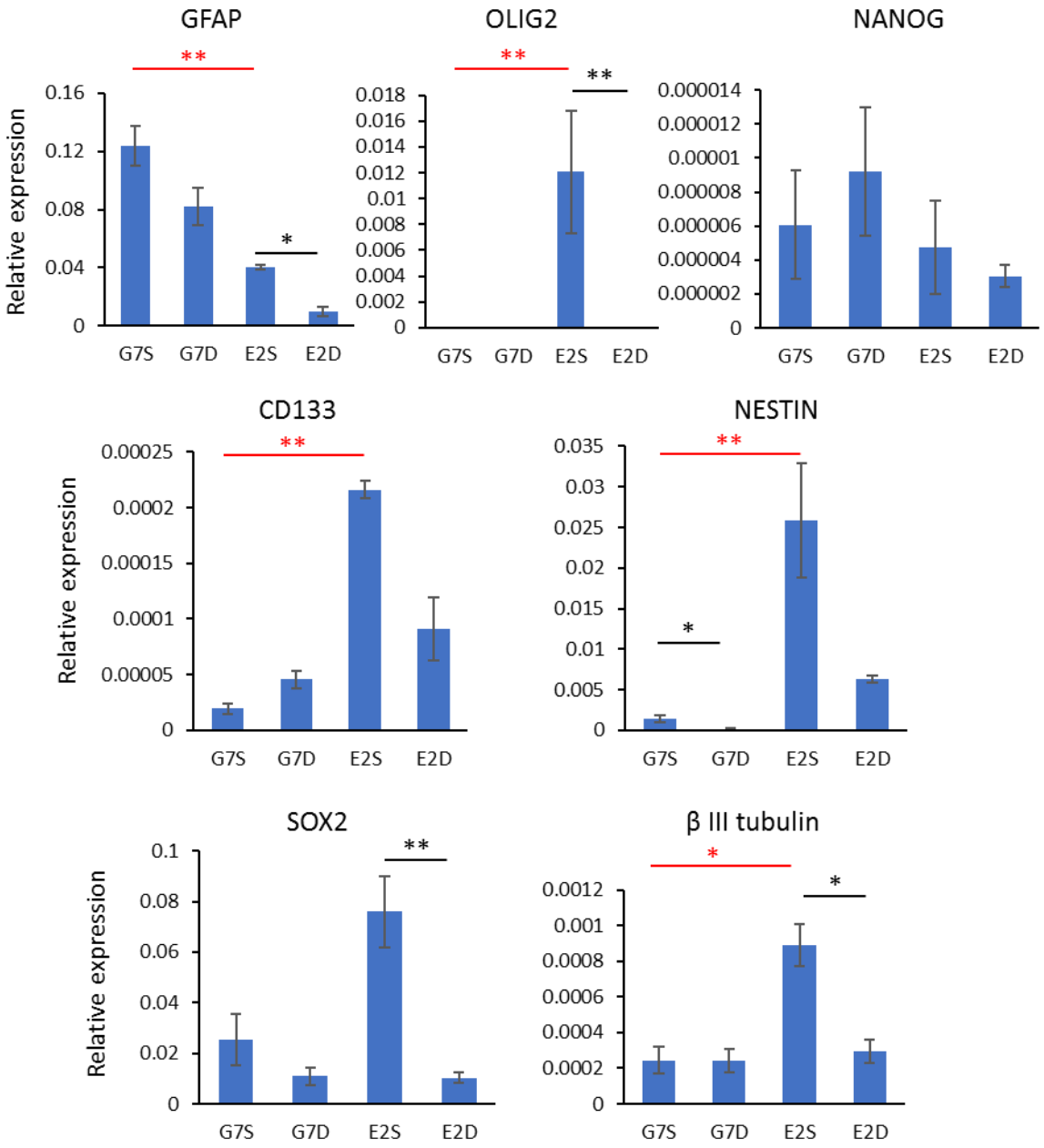

Figure 3-1 Marker gene expression in G7 and E2 cells grown under stem and differentiated conditions.

mRNA expression of the indicated genes was quantified by qRT-PCR and normalised to actin. The mean expression relative to actin from three independent experiments is plotted for G7 cells grown under stem (G7S) and differentiated (G7D) conditions, and for E2 cells grown under stem (E2S) and differentiated (E2D) conditions. Error bars represent the SEM. The media for stem conditions lacks serum but contains EGF and FGF, and cells are grown on Matrigel. The media for differentiated conditions contains FBS. Student's T test was used to compare expression between stem vs differentiated media (black bars), and to compare expression between G7 and E2 cells under stem conditions (red bars). * $p \leq 0.05$, ** $p \leq 0.01$.

3.4 Effect of TMZ on GSCs

TMZ is a cytotoxic drug that is widely used to treat GBM. However, many GBM tumours are resistant to TMZ due to overexpression of the DNA repair enzyme MGMT. In order to investigate the sensitivity of the G7 and E2 cells to TMZ *in vitro*, colony assays were performed. Colony assays are considered to be the "gold standard" method of assaying sensitivity to DNA damaging drugs, as cells have to be able to proliferate in order to form a colony. Cells with damaged DNA that are still alive but cannot proliferate are therefore excluded from this assay.

Figure 3-2 illustrates the effect of TMZ on the growth of G7 and E2 cells cultured under stem and differentiated conditions. In this assay, cells were only exposed to TMZ for one hour. The drug was then washed out and the cells allowed to grow for 10 days. In most experiments, the number of colonies increased at 10 μM TMZ, then decreased as the TMZ concentration was increased. The IC50 for TMZ in G7 stem cells (29 μM) was similar to that for G7 differentiated cells (37 μM) and E2 differentiated cells (35 μM). The IC50 for E2 stem cells could not be determined as the reduction in colony numbers was more than 50% at the highest concentration tested.

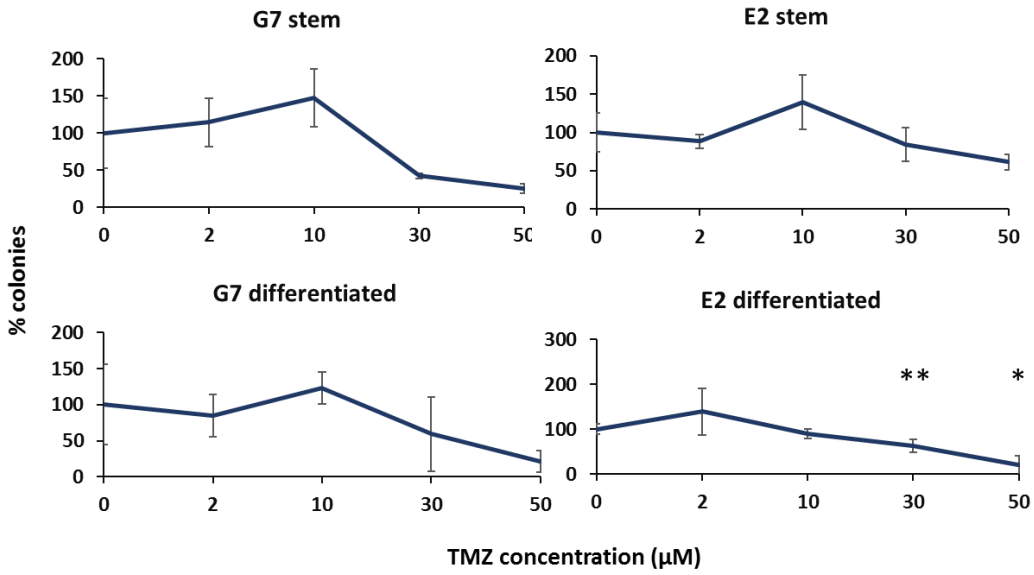

Figure 3-2 The effect of TMZ on cell survival in G7 and E2 cell lines grown in stem and differentiated conditions.

Each experiment determining the effects of different concentrations of TMZ was performed in three independent experiments. The seeding density was 250 cells per well of a six well plate. Cells were plated either in stem cell media on Matrigel, or in differentiated media in the absence of Matrigel. Cells were exposed to TMZ or DMSO for 1hr then allowed to grow for 10 days. Cells were fixed and stained, and the number of colonies was counted manually. The graph represents the mean and SEM of three independent experiments. Student's T test was performed to determine the significance of data in control and treated cells. * $p \leq 0.05$ and ** $p \leq 0.01$.

Cell proliferation assays can also be used to assess the effect of cytotoxic drugs, as they measure the number of cells present in the sample. In this assay, the TMZ remained in the cell culture media for the duration of the experiment. Cells were allowed to proliferate for 3 days. Cell proliferation was assayed using Cell Titer Glo reagents (Promega) that measure the amount of ATP, which is proportional to the number of viable cells in the sample. Figure 3-3 proliferation assay shows the inhibitory effect of TMZ on G7 and E2 cell lines (under stem and differentiated conditions) as a single agent. The data shows that increasing concentration of TMZ did not have significant effect on cell proliferation in GBM cell lines. The IC50 of G7 and E2 cell lines grown in stem and differentiated condition could not be determined as the assay didn't show reduction in number of viable cells.

Taken together, the colony assays and proliferation assays indicate that TMZ is not very effective on G7 and E2 cells under these conditions . These data form a baseline for subsequent experiments in this thesis, which investigate whether

the combination of TMZ with epigenetic drugs could be more effective at killing the GBM cells than using single agent.

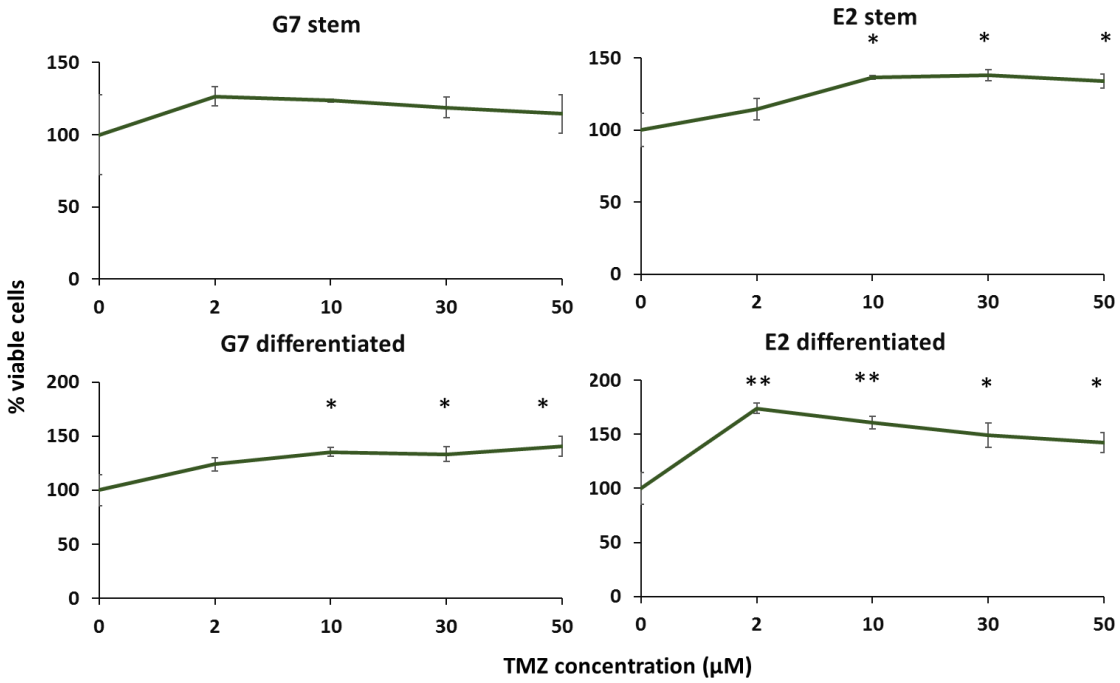

Figure 3-3 The effect of TMZ on proliferation of G7 and E2 cells grown under stem and differentiated conditions.

Cells were seeded at 5000 per well in stem or differentiated conditions, then incubated with DMSO or increasing concentrations of TMZ for three days. Cell density was determined using the Cell Titer Glo kit (Promega) that quantifies the amount of ATP present in the samples. The experiment was repeated on three separate occasions, and with technical triplicates for each sample within each experiment. The mean number of viable cells from three independent experiments is plotted, with the vehicle control set to 100%. Error bars represent the SEM. Student's T test was used to compare data of control and treated in G7 and E2 cell lines. * $p \leq 0.05$ and ** $p \leq 0.01$.

3.5 Effect of PTC209 on GBM cell lines alone and combined with radiation

PTC209 is a drug that is reported to inhibit expression of BMI1 (Li, Vangundy and Poi, 2020). Clonogenic and proliferation assays were performed to investigate whether G7 and E2 cells are sensitive to this drug when grown under stem conditions. In the clonogenic assays, cells were incubated with the drug for 48 hrs, then allowed to form colonies over the next 14 days. Clonogenic assays indicated that both cell lines are sensitive to incubation with PTC209, with

fewer than 40% of colonies remaining at 2 μM treatment (Figure 3-4). The IC50 for G7 was 2.8 μM and for E2 was 2.7 μM.

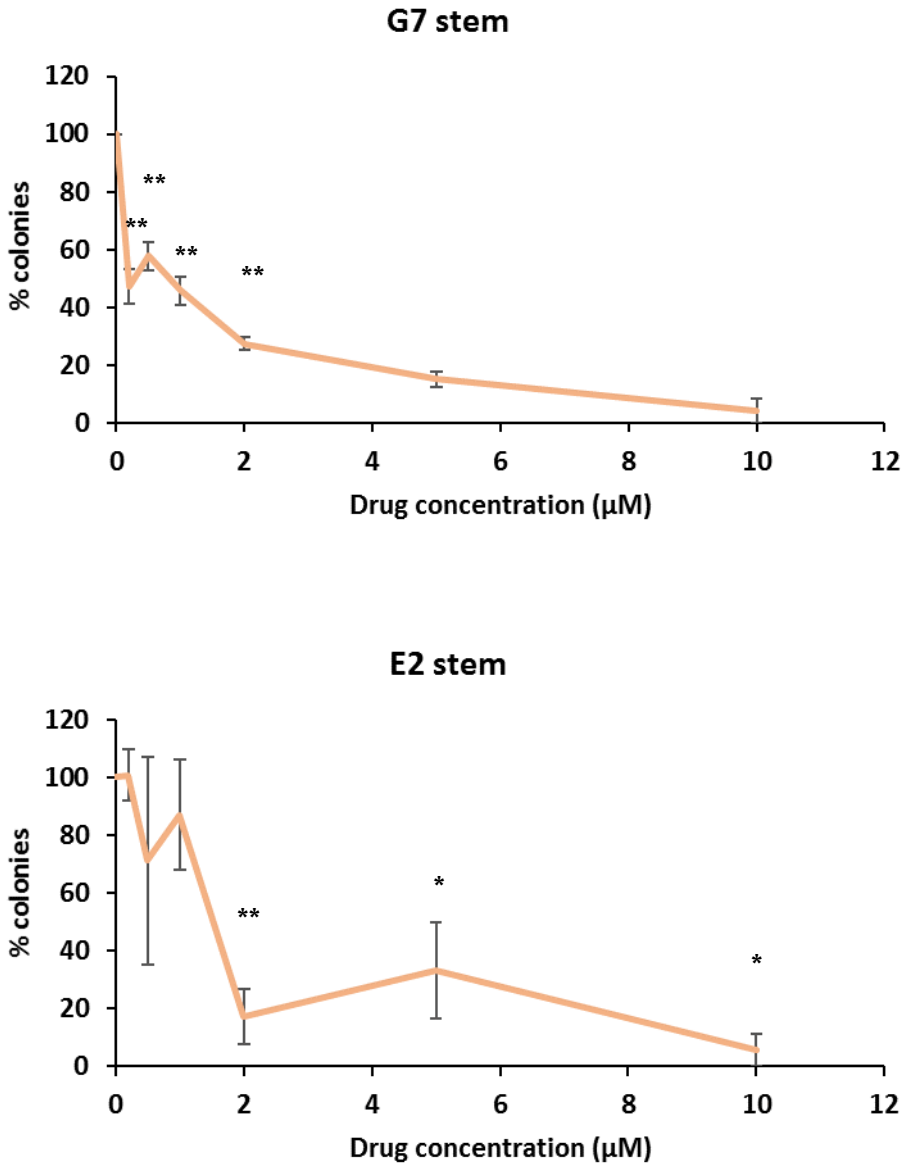

Figure 3-4 Assessing the effect of increasing concentrations of PTC209 on colony formation in G7 and E2 cell lines grown in stem condition .

Clonogenic assay was used to measure the capacity of cells to form colonies after treatment with PTC209. After 48 hrs incubation with increasing concentrations of PTC209, media was changed and plates were incubated to allow cells to form colonies for 14 days. . GBM stem cell lines were seeded in 6 well plates at 250 cells/well. The colony numbers were counted manually.Results are mean values of three independent experiments with error bars representing the SEM. Student's T test was used to compare data of control and treated cells. * $p \leq 0.05$ and ** $p \leq 0.01$.

Cell proliferation assays were also performed, allowing the cells to proliferate in the presence of drug for 5 days. Treating GSCs with PTC209 showed a decrease in percentage of viable cells with increasing dose. As shown in Figure 3-5, PTC209 inhibited cells proliferation for both G7 and E2 stem cells at higher concentrations (10 μM and 20 μM). G7 cell lines showed significant reduction of colonies at higher concentration of PTC209. However, E2 cells were more sensitive to PTC209 than the G7 cells, with a 60% reduction in cell numbers at 2 μM. The value of IC50 in G7 was 14.97 μM and in E2 was 1.13 μM, indicating that PTC209 has more potent effect on E2 cell lines than G7 cells..

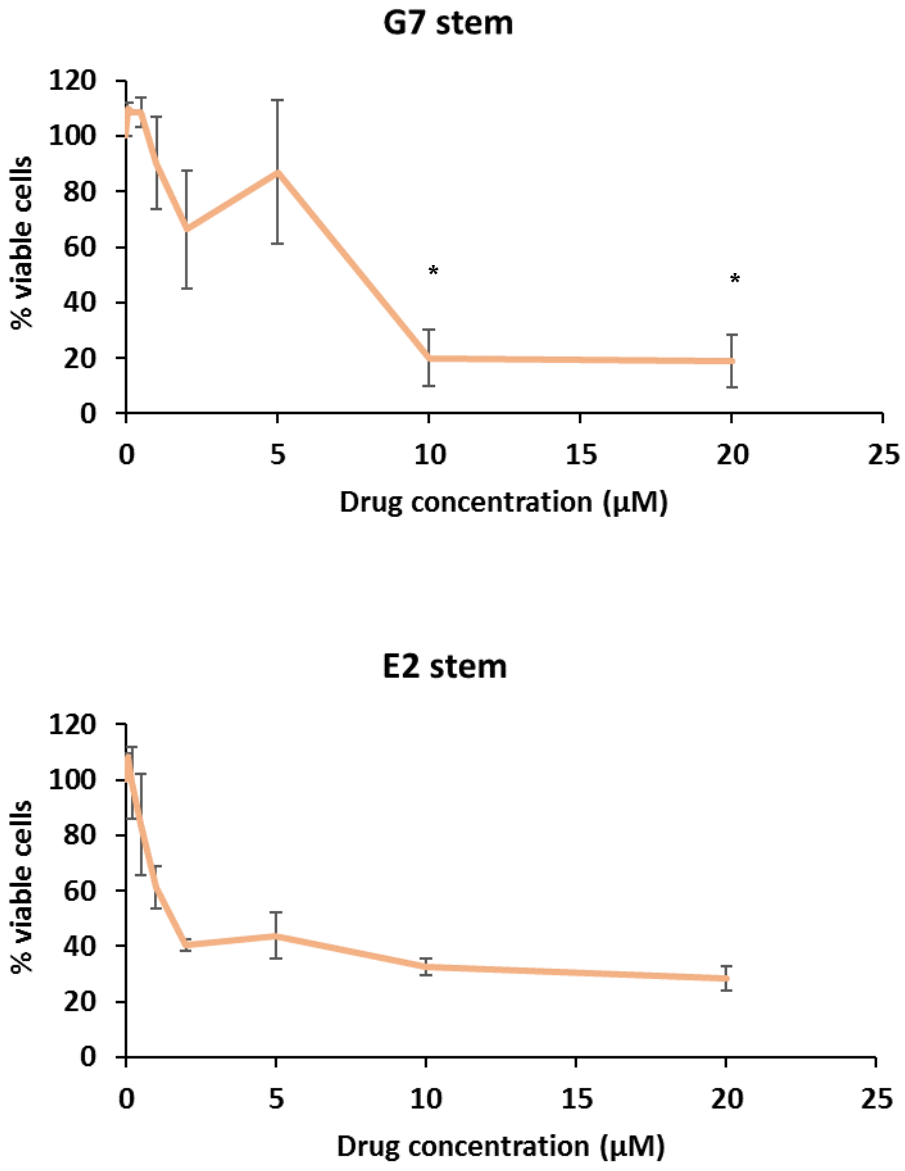

Figure 3-5 Dose dependent effect of PTC209 on cell proliferation in G7 stem and E2 stem cell lines.

GBM stem cell lines were seeded at 2500 cells per well in triplicates in 96 well plates at different concentrations of PTC209. Percentage of viable cells was determined with Cell Titer Glo assay after 5 days of treatment. This assay detects luminescence signal generated from the amount of ATP released from lysed cells that is proportional to the number of viable cells. Results are mean values of three independent experiment. Error bars represent SEM. Student's T test was performed to determine the significance of data in control and treated cells. * $p \leq 0.05$.

Epigenetic therapies often have broad effects that are not specific to cancer cells, so there is much interest in using epigenetic drugs to sensitise tumours to standard therapies such as radiation or cytotoxic agents. The mechanism of these epigenetic drugs involved epigenetic changes of genes associated with DNA repair, apoptosis or cell cycle (Smits *et al.*, 2014). To investigate this possibility, colony assays were performed to determine whether combining PTC209 with radiation has an effect on GSC survival . Cells were treated with low concentrations of PTC209 (0.5 – 2 μM) or DMSO for 24 hrs prior to irradiation. Figure 3-6 shows that the clonogenic survival of stem cells was decreased following radiation of up to 5 Gy. Addition of PTC209 to radiation treatment does not have a significant effect on the survival of G7 cells. However, the addition of PTC209 decreases the survival of E2 cells irradiated with 5 Gy in a dose responsive manner. The dose modifying ratio (DMR) was used to quantify the radiosensitisation of control and treated cells with PTC209 by calculating the ratio of doses needed to reduces the survival fraction to 0.37 (Table 3-1). E2 cell have significantly higher DMR values at 1 μM and 2 μM compared to G7. These data are consistent with the earlier observation that E2 cells are more sensitive to PTC209 than the G7 cells at concentrations of 5 μM or lower . This shows that PTC209 sensitise E2 cells to radiation more effectively than G7.

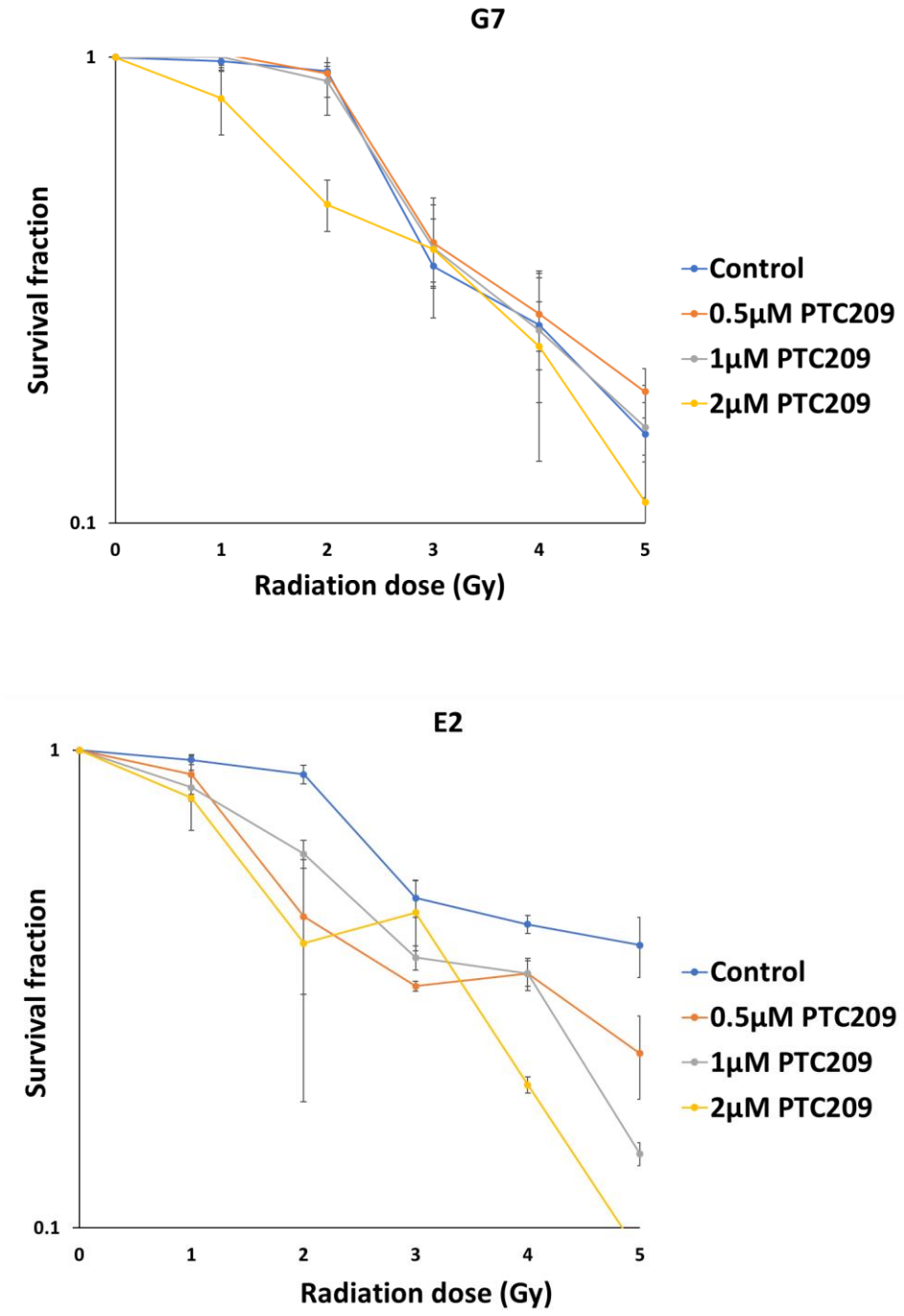

Figure 3-6 Clonogenic survival analysis of GSC cell lines treated with combination of PTC209 and radiation.

Cells were seeded for colony formation, and exposed to various doses of radiation from 0-5 Gy following treatment with (0.5, 1 and 2 µM) PTC209. Cells were seeded in triplicates, incubated with the drug for 24 hrs then exposed to radiation for 24 hrs. Result shows mean survival fraction from three independent experiments. Error bars represent SEM.

G7	$DMR_{(0.37)}$
0.5 μM PTC209	0.69
1 μM PTC209	0.99
2 μM PTC209	1.18*

E2	$DMR_{(0.37)}$
0.5 μM PTC209	0.3
1 μM PTC209	1.46***
2 μM PTC209	1.71***

Table 3-1 These tables show DMR values of G7 and E2 cell lines.

The DMR represents the dose required to reduce survival fraction to 0.37 in control vs treated with increasing concentration of PTC209. p value is calculated by comparing the means, sd and n of drug treated vs control. * $p \leq 0.05$ and *** $p \leq 0.001$

3.6 Effect of OTX015 alone and combined with TMZ on GBM cell lines

Colony assays were used to investigate the sensitivity of OTX015, a potent bromodomain inhibitor, in G7 and E2 cell lines . Cells were incubated with OTX015 for 24 hrs, then the drug was washed out and the cells allowed to form colonies over the next 10 days. Results from figure 3-7 shows that various concentrations of OTX015 did not have an effect on colony formation, either in G7 or E2 cells, or under stem or differentiated conditions. There was no clear downward trend of colony formation with increasing OTX015 concentrations, even at the highest dose of 500 nM. The IC50 for both cell lines could not be calculated because the percentage survival did not drop below 50% in all graphs.

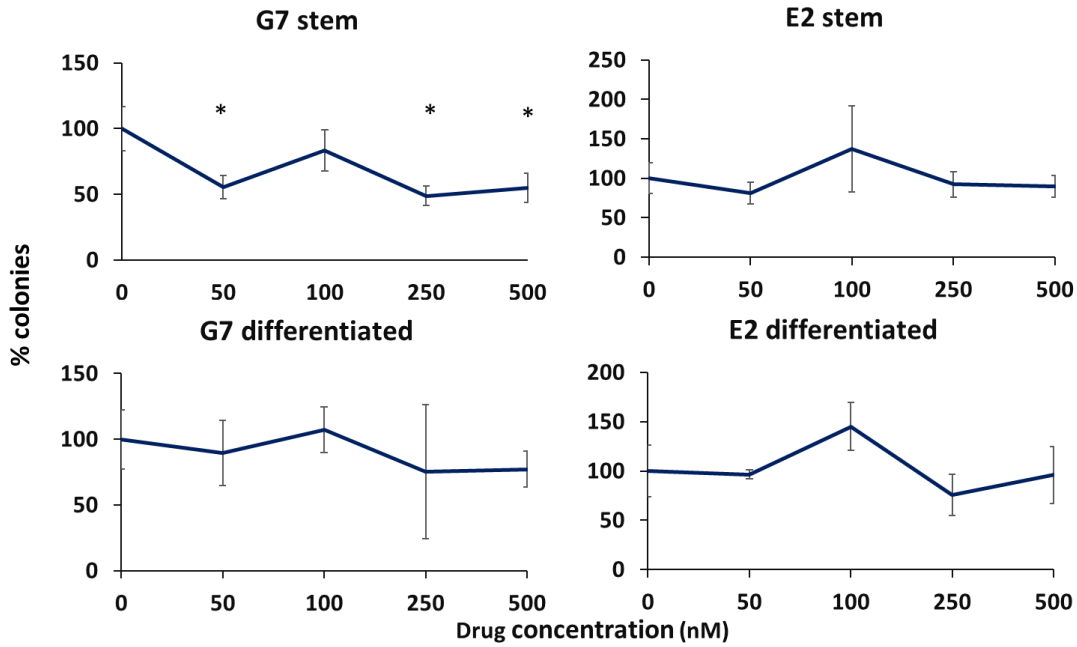

Figure 3-7 The effect of OTX015 on stem and differentiated GBM cell lines.

OTX015 effect on GBM cells was determined with colony formation assay over a range of concentrations. Cells were seeded at 250 per each well, after incubation with OTX015 for 24 hrs, cells were allowed to form colonies for 10 days. At each concentration of OTX015 cells were seeded in triplicates, Data points represents mean of three independent experiments with error bars indicating SEM. Student's T test was used to compare control with treated samples in G7 and E2 cells. * p ≤ 0.05.

Although the GBM cells were not sensitive to OTX015 as a single agent, it is possible that the combination of OTX015 with TMZ would be more effective at

preventing colony formation. G7 and E2 cell lines were cultured in stem and differentiated conditions. To investigate this, cells were incubated with TMZ for one hour then with OTX015 for 24 hrs. Figure 3-8 shows colony formation for TMZ and OTX015 individually and in combination. In E2 cells, the combination of TMZ and OTX015 did not reduce colony formation any further than using either drug alone. Similar results were observed for G7 cells grown under stem conditions. Intriguingly, the combination of TMZ and OTX015 appeared to stimulate colony formation in G7 cells grown under differentiated conditions .

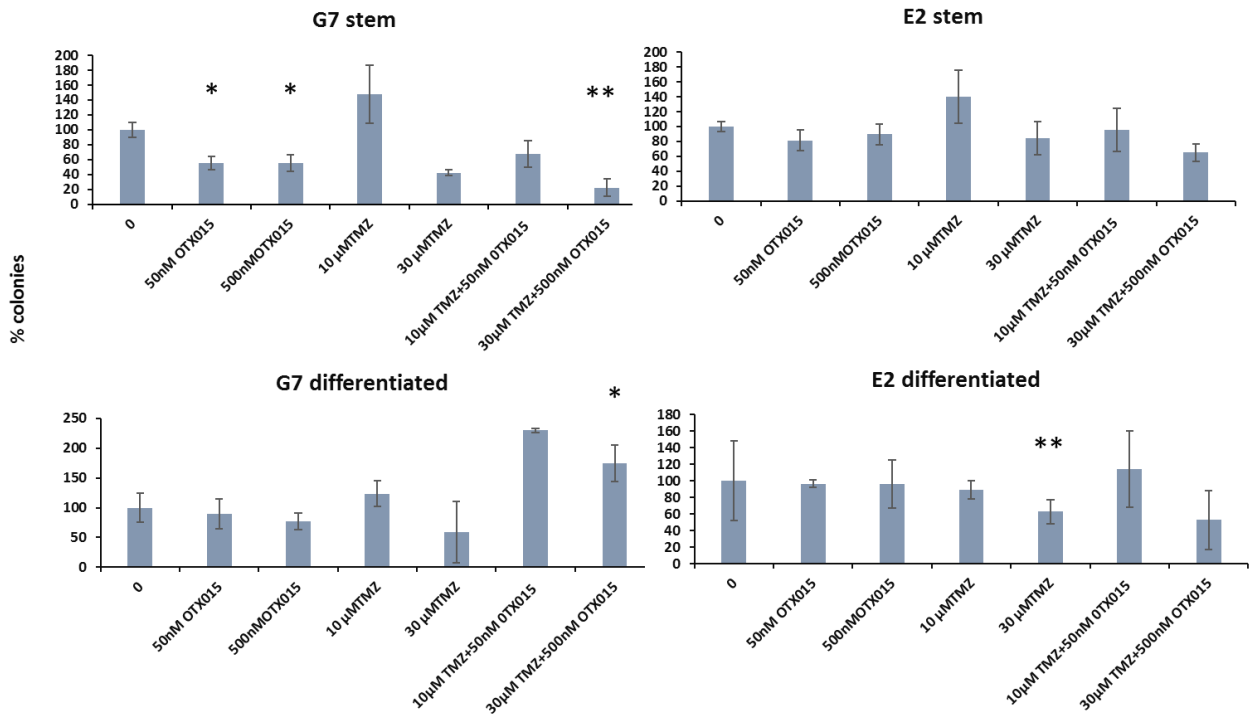

Figure 3-8 The effect of combined treatment of TMZ and OTX015 on colony formation in GBM cell lines grown in stem and differentiated conditions.

The seeding density of cells was 250 cells/well .Cells were treated with TMZ for 1 hr followed by 24 hrs treatment with OTX015 then allowed to form colonies for 10 days. Cell were seeded in triplicates at each combination of TMZ and OTX015 with the respect to 0.1% DMSO as a control. The linear graph shows mean value and SEM of three independent experiments. Student's T test was used to compare control with treated samples in G7 and E2 cells.* $p \leq 0.05$ and ** $p \leq 0.01$.

The above data show that treatment with OTX015 for 24 hrs does not have an impact on colony formation over the subsequent 10 days, either in the presence or absence of TMZ. To investigate whether the drug affects cell proliferation when it is present continuously in the culture, proliferation assays were performed. Figure 3-9 shows that the BET inhibitor OTX015 does not strongly affect GBM cell proliferation, even at higher concentrations. When cells were treated with increasing concentrations of OTX015, the growth of cells remained almost the same except for G7 stem in which number of cells was higher at 250 nM. The values of IC50 for stem and differentiated cell lines were undetermined, the assay didn't show reduction in number of cells at higher concentration.

The combination of OTX015 with TMZ did appear to be more effective in inhibiting cell proliferation. Figure 3-10 shows the effect of increasing concentrations of both drugs on G7 and E2 cells under stem and differentiated conditions. There is a downwards trend in proliferation as the concentrations of the drugs are increased in the combination, which was not observed when the drugs were used individually (Figures 3-3 and 3-9). Indeed, cell numbers at the higher concentrations, especially at 100 μM TMZ and 500 nM OTX015, are significantly lower than 500 nM OTX015 when is used alone, for G7 differentiated , E2 stem and E2 differentiated experiments ($p < 0.05$). Therefore, the use of TMZ and OTX015 together is more effective at reducing cell proliferation. However, it should be noted that these concentrations are still much higher than those used in previous studies.

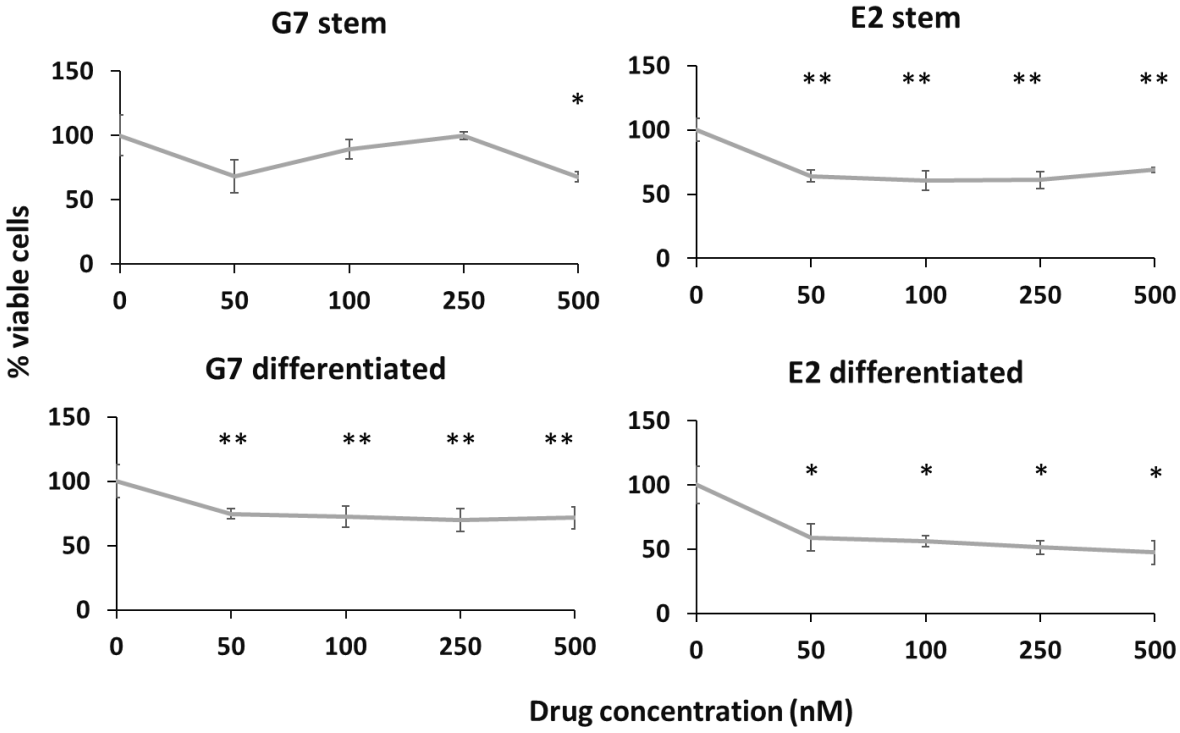

Figure 3-9 The effect of increasing concentrations of OTX015 on GBM cell proliferation.

Cells were seeded at 5000 cells/well in 96 well plates under stem or differentiated conditions, then incubated with OTX015 for 3 days. Cell viability was determined by measuring the amount of ATP present in the samples Cell Titer- Glo assay (Promega). Each condition was carried out in triplicate wells, and three independent experiments were performed. The mean value represents number of viable cells from three independent experiments as a percentage of the DMSO control; error bars represent the SEM. Student's T test was used to determine significance of data in control and treated samples.* $p \leq 0.05$ and ** $p \leq 0.01$.

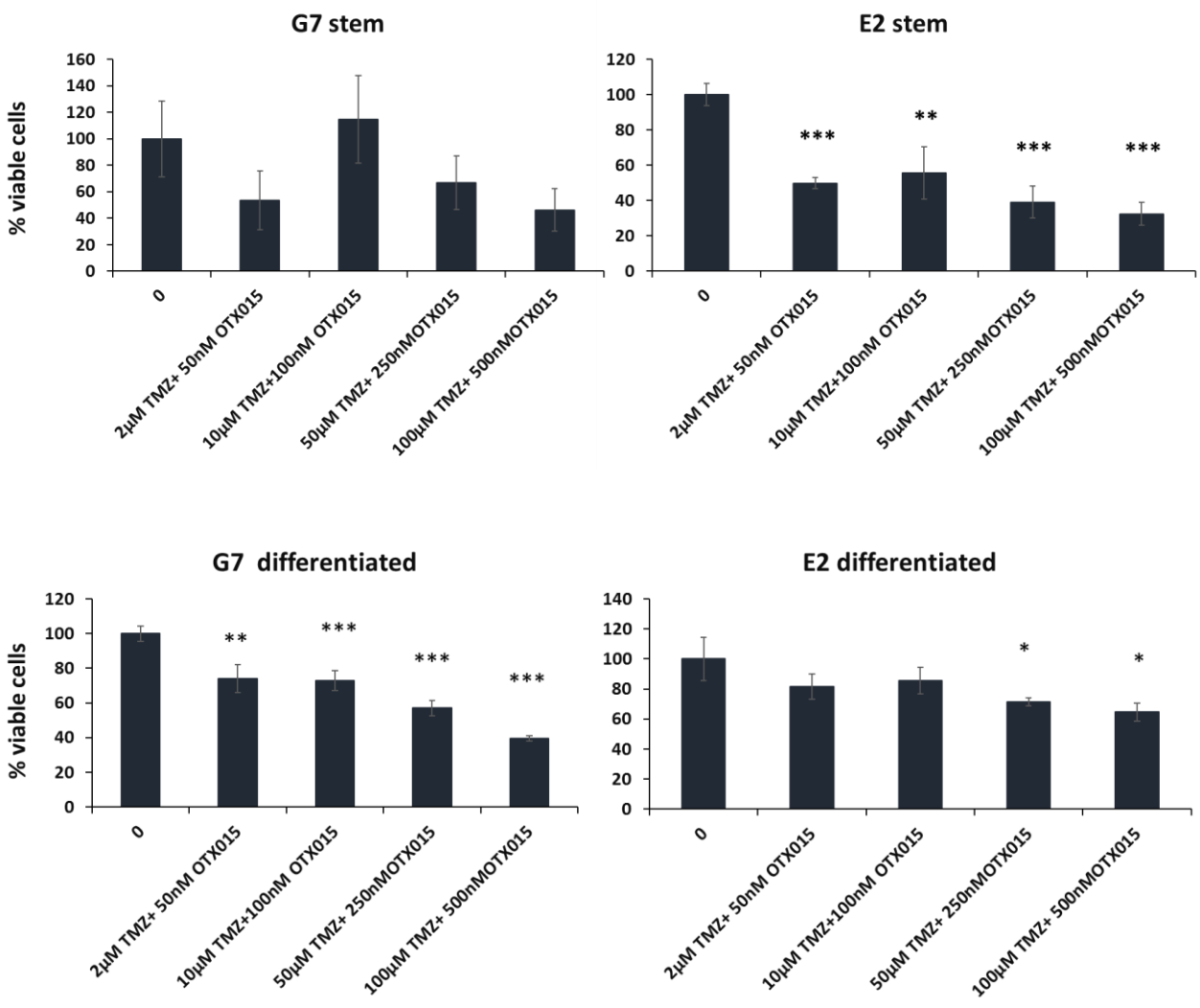

Figure 3-10 Effect of OTX015 combined with TMZ on cell proliferation in GBM stem and differentiated cell lines.

Proliferation assay after 3 days exposure to a different combination of TMZ and OTX015, cells were seeded at 5000 cells/well. Cell proliferation was measured using Cell Titer Glo assay (Promega), by measuring the amount of ATP present in GBM cells. Each combination of TMZ and OTX015 was performed in triplicates. The final concentration of DMSO was kept constant in all experiments. Student's T test was used to compare data between control and treated samples * $p < 0.05$, ** $p < 0.01$ and *** $p < 0.001$.

3.7 Identifying missense mutation in G7 and E2 cells

In order to try and identify key genes that are mutated in G7 and E2 cells and that might be driving the cancer phenotype of these cells, variant calling was performed using transcript data from RNA-seq analysis (see chapter 4 for details of RNA-seq). The Galaxy tool Free Bayes was used to compared RNA-seq reads from the two cell lines with the reference Hg38 genome sequence in order to identify sequence changes (Garrison and Marth, 2012). The resulting VCF files containing information about sequence variants were analysed using the Open

Cravat platform (Pagel *et al.*, 2020). The use of RNA-seq data means that only variants in the exons of expressed genes can be identified. Variants were filtered using the CHASM plus ($p < 0.01$) and CHASM plus GBM widgets ($p < 0.05$) (Tokheim and Karchin, 2019). "CHASM plus" aims to identify variants that are likely to be cancer driver mutations (as opposed to passenger mutations), and "CHASM plus GBM" categorises variants based on how likely they are to be drivers of GBM.

After filtering, 10 variants were identified in G7 cells and 9 in E2 cells that are likely to be cancer driver genes (Table 3-2). The CHASM plus GBM scores for these genes are plotted in Figure 3-11. G7 cells have two heterozygous mutations in TP53, two heterozygous mutations in MAP3K1, and one homozygous and one heterozygous mutation in PIK3R2. It cannot be determined from the RNA-seq data whether the heterozygous mutations are on the same allele or different alleles, as the mutations are too far apart to be on the same read or mate-pair. E2 cells have heterozygous mutations in EGFR and TP53, and two heterozygous mutations in MAP3K1. It is notable that both cell lines have the same loss of function mutations in MAP3K1 and APC (Xue *et al.*, 2018; Wang *et al.*, 2018), and the same gain of function mutation in PIK3R2 (Cheung *et al.*, 2011).

A:G7

Gene	Protein	VCF Phred	Zyg.	Alt. reads	Total reads	VAF	Chr	Position	Ref	Alt	UniProt	CHASM plus Score	CHASM plus GBM Score
TP53	Arg248Gln	7489	het	292	603	0.48	chr17	7674220	C	T	P04637	0.85	0.80
TP53	Arg282Trp	10846	het	431	902	0.48	chr17	7673776	G	A	P04637	0.79	0.70
MAP3K1	Asp806Asn	264	het	11	17	0.65	chr5	56881616	G	A	Q13233	0.62	0.32
SETD2	Pro1962Leu	9043	hom	303	303	1.00	chr3	47083895	G	A	Q9BYW2	0.32	0.21
MAP3K1	Val906Ile	528	het	21	35	0.60	chr5	56881916	G	A	Q13233	0.35	0.18
APC	Val1822Asp	556	het	25	49	0.51	chr5	112841059	T	A	P25054	0.49	0.16
PIK3R2	Ala415Thr	12598	het	489	1026	0.48	chr19	18163100	G	A	O00459	0.40	0.14
CDKN1A	Asp149His	39	het	5	18	0.28	chr6	36684546	G	C	P38936	0.59	0.13
PIK3R2	Ser234Arg	14405	hom	464	464	1.00	chr19	18161380	A	C	O00459	0.35	0.13
ARID1A	Pro683Ser	1407	het	65	196	0.33	chr1	26760982	C	T	O14497	0.67	0.12

B: E2

Gene	Protein	VCF Phred	Zyg.	Alt reads	Total reads	VAF	Chr	Position	Ref	Alt	UniProt Accession	CHASM plus Score	CHASM plus GBM Score
EGFR	Ala289Val	617	het	25	36	0.69	chr7	55154129	C	T	P00533	0.80	0.85
TP53	Arg273His	13568	het	504	587	0.86	chr17	7673802	C	T	P04637	0.82	0.75
MAP3K1	Asp806Asn	2134	het	91	234	0.39	chr5	56881616	G	A	Q13233	0.62	0.32
MAP3K1	Val906Ile	2833	het	113	251	0.45	chr5	56881916	G	A	Q13233	0.35	0.18
USP9X	Gln640His	731	hom	23	23	1	chrX	41162812	A	C	Q93008	0.52	0.18
PTCH1	Pro1315Leu	563	het	26	57	0.46	chr9	95447312	G	A	Q13635	0.33	0.17
LZTR1	Gly301Ser	4774	hom	161	161	1	chr22	20991737	G	A	Q8N653	0.34	0.16
APC	Val1822Asp	1889	hom	61	61	1	chr5	112841059	T	A	P25054	0.49	0.16
PIK3R2	Ser234Arg	13717	hom	437	437	1	chr19	18161380	A	C	O00459	0.35	0.13

Table 3-2 Potential GBM cancer driver mutations in G7 and E2 cell lines grown in stem condition.

VCF files were generated from combined RNA-seq data from control (untreated) cells compared to Hg38 references sequence using FreeBayes. Files were uploaded to Open-Cravat tool, and filtered to only analyse variants that lead to change in protein sequence, have a Chasm plus p value < 0.01 and Chasm plus GBM p value < 0.05. The variants were

then filtered to remove those with a VCF PHRED score of less than 20 (ie >1% chance of error), fewer than 15 total reads, or a variant allele frequency of less than 0.25, in order to remove variants that are less reliable. Zyg: zygosity. Alt reads: number of reads matching the alternate allele. VAF: variant allele frequency. Chr: chromsome. Ref: reference base. Alt: alternate base. Variants in grey are found in both G7 and E2 cells.

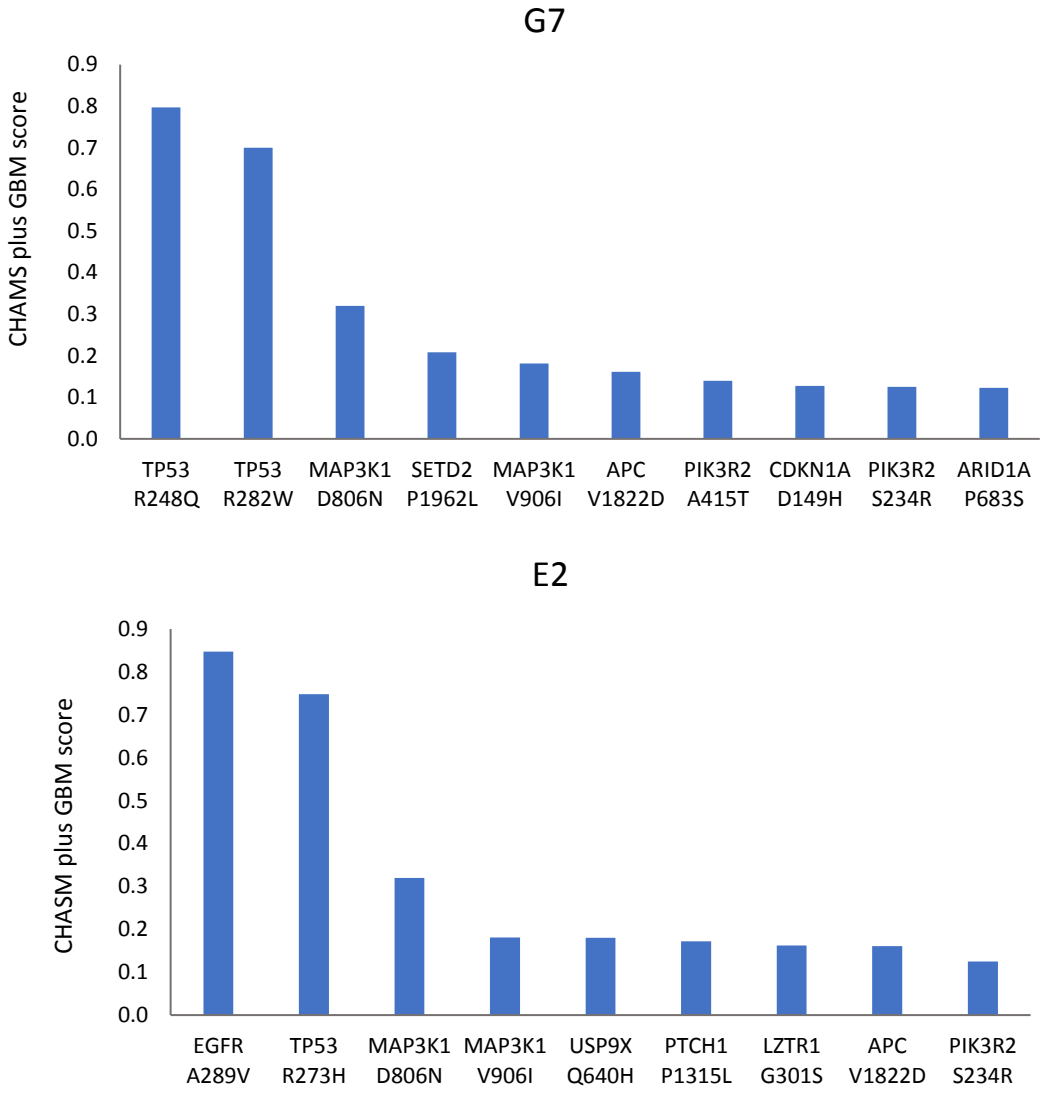

Figure 3-11 Chasm plus GBM scores for variants in G7 and E2 cells gown in stem condition.

VCF files were generated from combined RNA-seq data from control (untreated) cells compared to Hg38 references sequence using FreeBayes. Files were uploaded to Open-Cravat tool, and filtered to only analyse variants that lead to change in protein sequence, have a Chasm plus p value < 0.01 and Chasm plus GBM p value < 0.05. The variants were then filtered to remove those with a VCF PHRED score of less than 20 (ie >1% chance of error), fewer than 15 total reads, or a variant allele frequency of less than 0.25. The CHASM plus GBM score is plotted for all variants that pass the filters. The higher the score the greater the likelihood that the mutation in the gene is a driver mutation in GBM cell line.

3.8 Discussion

G7 and E2 cell lines were characterised for expression of stem cell markers after being cultured in stem and differentiated cancer cell media. E2 stem exhibited higher levels of CSC marker expression compared to G7 stem, including *CD133*, *NESTIN,* and *OLIG2*. E2 stem cells also had higher expression of the neuronal marker *β III tubulin*, whereas G7 stem had higher expression of the glial marker *GFAP*. Culturing E2 cells under stem conditions increased expression of *SOX2*, *OLIG2* and *β III tubulin* compared to differentiated conditions, while G7 showed significant higher expression of *NESTIN* under stem compared to differentiated conditions. These data reveal the importance of stem culture conditions in maintaining the CSCs characteristics of the two cell lines, in particular E2 cells. The data also emphasise that G7 and E2 cells have different gene expression patterns, with E2 appearing to be more stem cell-like, which may impact on how these cells respond to different epigenetic drug treatments

TMZ is an oral alkylating agent that is often given as a first line of treatment for GBM. Despite the antiproliferative effect of TMZ, patients tend to develop resistance to the drug after prolonged treatment. Current studies focus on developing new epigenetic therapies that are aiming to target specific pathways involved in mechanism of resistance and enhance the cytotoxic effect of TMZ on GBM cells. The data showed that at higher concentrations, TMZ has an inhibitory effect on the growth of colonies. For G7 cells and E2 cells cultured in differentiated conditions, treatment with 30 μM and 50 μM TMZ resulted in reduction of number of colonies compare to control. E2 cells cultured under stem conditions appeared to be less sensitive. The results for the proliferation assay showed that TMZ did not have any effect on proliferation rate when compared with DMSO treated control. This indicates that treatment with TMZ does not have an effect on the number of viable cells in these GBM cell lines in short term culture, while it reduces colony formation at higher concentrations when cells are allowed to grow over a longer period.

OTX015 is an epigenetic inhibitor that binds to BET proteins and prevents their binding to chromatin, thus by inhibiting transcription. The efficacy of OTX015 on GBM cells was tested both *in vitro* and *in vivo* and also the ability to cross

blood-brain barrier (Berenguer-Daizé *et al.*, 2016). However, the data presented here shows that OTX015 alone did not have an effect on the survival of colonies or on proliferation in G7 and E2 GBM cells. Combined treatment of TMZ and OTX015 was not more effective than TMZ alone in the colony assays, and actually increased colony survival above the no drug control in G7 differentiated cells. These results show that treating GBM cells with OTX015 as a single agent does not reduce proliferation or colony formation, and suggest that OTX015 may interfere with the inhibitory effect of TMZ when the two drugs were combined. This has potential implications for the use of these two drugs in treating GBM.

The anticancer activity of PTC209, a specific BMI1 inhibitor, has been evaluated in different types of cancer. It was reported that PTC209 targets the expression of BMI1 at post transcriptional level (Mayr *et al.*, 2016). In GBM cells, treatment with PTC209 lead to derepression of tumour suppressor genes involved with cell cycle regulation and proliferation (Kong *et al.*, 2018). Here, our data showed that PTC209 exhibited an antiproliferative effect and also showed cytotoxic effect on colony formation in GBM cell lines. Colony assays were also performed to determine the drug efficacy of PTC209 when combined with radiation on GBM cells. A recent literature determined that ubiquitination of H2AK119 with BMI1 along with PRC1 subunits contributed to DNA repair mechanism (Ginjala *et al.*, 2011). In this study results showed increase sensitivity of E2 cells to PTC209 at higher doses of radiation. The graphs and DMR values indicate that treatment of PTC209 in combination with radiation reduces the survival fraction in E2 at higher concentrations.

The gene expression data in this chapter highlights some of the differences between the G7 and E2 cell lines. In order to investigate these cell lines further, data from our RNA-seq analysis, which is described in detail in later chapters, was used to identify missense mutations in the coding regions of expressed genes. In cancer, missense mutations are found to be the most common types of mutations(Vogelstein *et al.*, 2013). New methods have been developed to separate driver missense mutations from passenger missense mutations in cancer genomes. Chasm plus is a new approach to predict the oncogenic effect of a missense mutation based on its score. This method was developed to classify somatic missense mutations as driver or passenger (Tokheim and Karchin, 2019) . Chasm plus analysis finds that genes with high scores are usually associated with

metastases and deregulation of cell proliferation and survival. The analysis showed high score associated with TP53 in G7 and EGFR in E2. Both genes are associated with cell division and growth and their Mutations is linked with lung cancer progression (Qin *et al.*, 2020).

In conclusion, G7 stem and E2 stem cell lines showed increased expression of common CSC markers. Both stem cell lines also carried mutations that are likely to be driver mutations in GBM. Targeting the CSC population is thought to be an important strategy in eliminating GBM tumour growth and metastasis. While the effects of TMZ and OTX015 on these cells were weak, the BMI1 inhibitor PTC209 inhibited cell proliferation and suppressed colony formation at higher doses. This indicates that targeting PRC subunits might be a promising strategy to treat GBM.

Chapter 4 Efficacy of EPZ6438 on GBM cell lines

4.1 Introduction

EPZ6438 is a selective and potent inhibitor of EZH2 . Recent reports have demonstrated the antiproliferative effects of EPZ6438 and its effect on derepression of genes targeted by PRC2 complex (Zhang *et al.*, 2020) . This compound shares similar *in vitro* characteristics as the previous inhibitor EPZ005687, only it has superior pharmacokinetic properties. EPZ6438 disrupts PRC2 function by inhibiting the enzymatic activity EZH2 through a SAM competitive mechanism. *In vitro* data also revealed that EPZ6438 inhibits cancer progression in multiple myeloma (Tremblay-LeMay *et al.*, 2018). Consistent with this, EPZ6438 was found to inhibit both wild type and mutant EZH2 . This *in vivo* study demonstrated that treatment with EPZ6438 showed potent antitumour activity in a xenograft model of rhabdoid tumour. EPZ6438 is 35 fold more selective to EZH2 compared to EZH1 (Knutson *et al.*, 2013) . Exposing cancer cells to EPZ6438 resulted in re-expression of PRC2 targeted genes as well as an increase in the percentage of cells at the G1 phase of cell cycle and induction of apoptosis (Knutson *et al.*, 2013). Treatment with EPZ6438 leads to inhibition of cellular growth and reduction in H3K27me3 in cancer cell lines (Knutson *et al.*, 2014a). Inhibition of proliferation was observed after treating cancer cells with EPZ6438 for 6-11 days (Knutson *et al.*, 2014b).

This chapter investigates the effect of EPZ6438 on G7 and E2 cell lines grown under stem cell conditions. The anti-tumour effect of EPZ6438 was evaluated with cell survival and viability assays, and RNA-seq analysis was performed to investigate the mechanistic basis of the drug action.

4.2 Effect of EPZ6438 on survival assay and proliferation assay

The effect of EPZ6438 was determined by performing clonogenic survival assay to evaluate the potency EPZ6438 has on colony formation in GSCs. Figure 4-1 demonstrate the effect of EPZ6438 on number of colonies formed in G7 and E2 cell lines after plating the cells on Matrigel coated 6 well plates and incubating with the drug for 48 hrs then allowed to form colonies for 14 days. Treating G7 cell lines with 2 μM EPZ6438 caused a slight decrease in percentage of colonies formed 82% then followed by an abrupt increase 133% at 1 μM. At higher concentration data showed reduction in percentage of colonies formed. Similar results were obtained with E2 cell lines treated with increasing concentration of EPZ6438. The data showed an increase in percentage of colonies at 1 μM followed by significant decrease at higher concentrations. The IC50 was similar for G7 (1.90 μM) and E2 (1.64 μM) treated with EPZ6438.

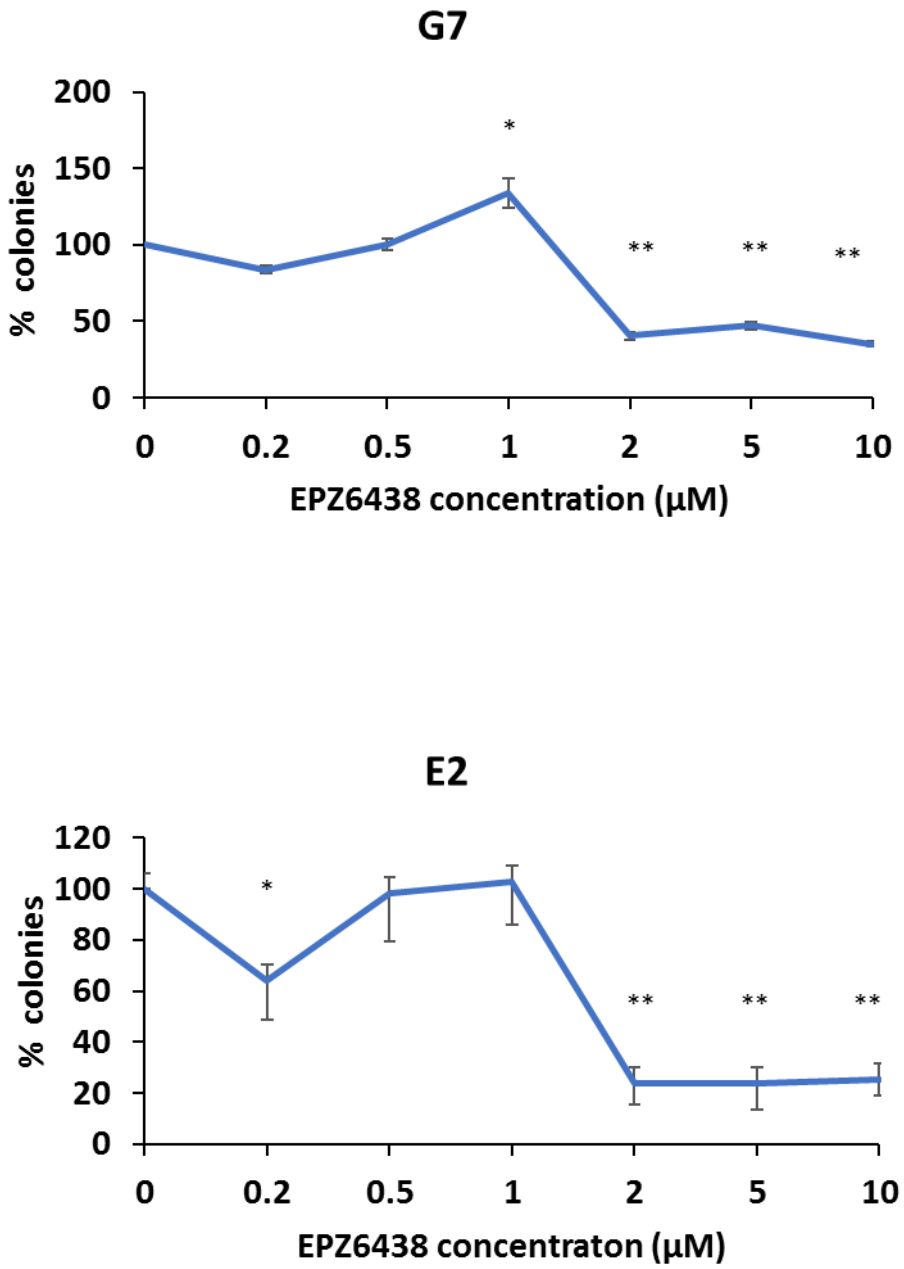

Figure 4-1 Clonogenic survival curves of G7 and E2 treated with EPZ6438.

Clonogenic assay was used to measure the capacity of cells to form colonies after 48 hrs incubation with increasing concentrations of the drug.. Cells were fixed and colonies were counted manually after 14 days of incubation. A graph is plotted that shows the effect of increasing concentration of EPZ6438 on number of colonies formed in both cell lines . Cells were seeded at each concentration in triplicates. Data points represents mean values and SEM of three independent experiments. Student's T test was performed to determine the significance of data in control and treated cells. * $p \leq 0.05$ and ** $p \leq 0.01$.

The assessment EPZ6438 potency was also determined by conducting viability assay in GBM cell lines. G7 and E2 cell lines were seeded into 96 plates coated with Matrigel at density of 2500 per well. Cells were incubated with the increasing concentration of EPZ6438 or corresponding DMSO as a control for 5 days. Results were normalised with control and plotted as shown in Figure 4-2. The treatment of G7 cell lines with 1 μM of the drug showed an increase to 118% when compared with the DMSO control. Then followed by a slight decrease at higher concentrations. The same was observed with E2 cell lines treated with EPZ6438 when compared to control. The data shows EPZ6438 exposure did not have significant effect on viable cells in GSCs. The value of IC50 in the E2 cell line was higher (11.48 μM) than in the G7 cell line (2.01 μM) in the proliferation assay.

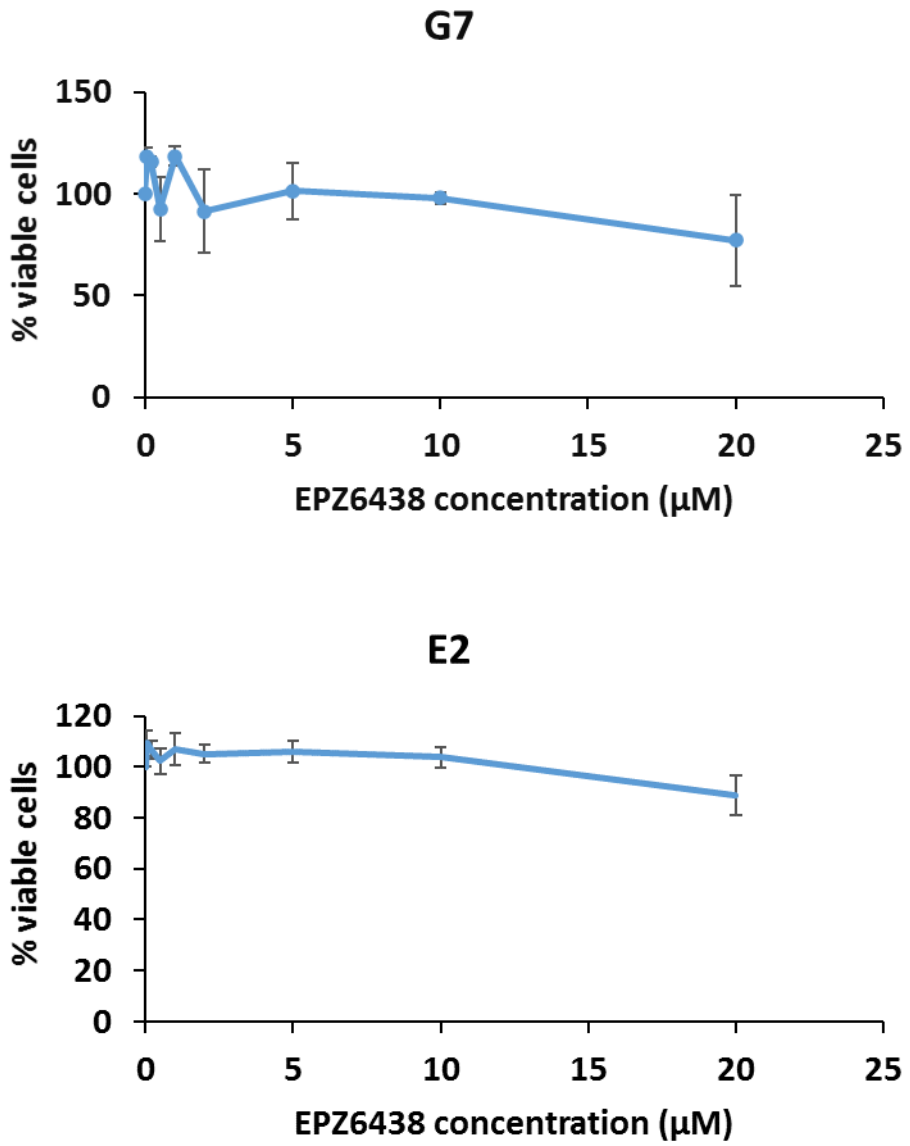

Figure 4-2 Dose dependent effect of EPZ6438 on cell proliferation in G7 and E2 cell lines.

GBM cells were seeded in triplicate in 96 well plates in the presence of varying concentrations of EPZ6438, and allowed to grow for five days. DMSO at 0.2% was used as the control. The Cell Titer Glo kit (Promega) was used to quantify viable cells. Cell viability was calculated as a percentage of the DMSO control, and results are plotted as the mean value of three independent experiments. Error bars show the SEM.

The combined effect of TMZ and EPZ6438 on GBM cell lines was confirmed with clonogenic survival assay. G7 and E2 cell lines were seeded into Matrigel covered 6 well plates at seeding 250 per well. Cell culture where then incubated with increasing concentration of EPZ6438 for 24 hrs followed by treatment with 10 μM of TMZ for 24 hrs. Cells were left to form colonies for 14 days. As can be seen in Figure 4-3, treatment of TMZ and EPZ6438 reduced colony formation in both cell lines compared to DMSO control. There was a significant reduction in colony formation at 0.5 μM EPZ6438 with 10 μM TMZ. At higher concentration of EPZ6438 with 10 μM TMZ the number of colonies were abolished.

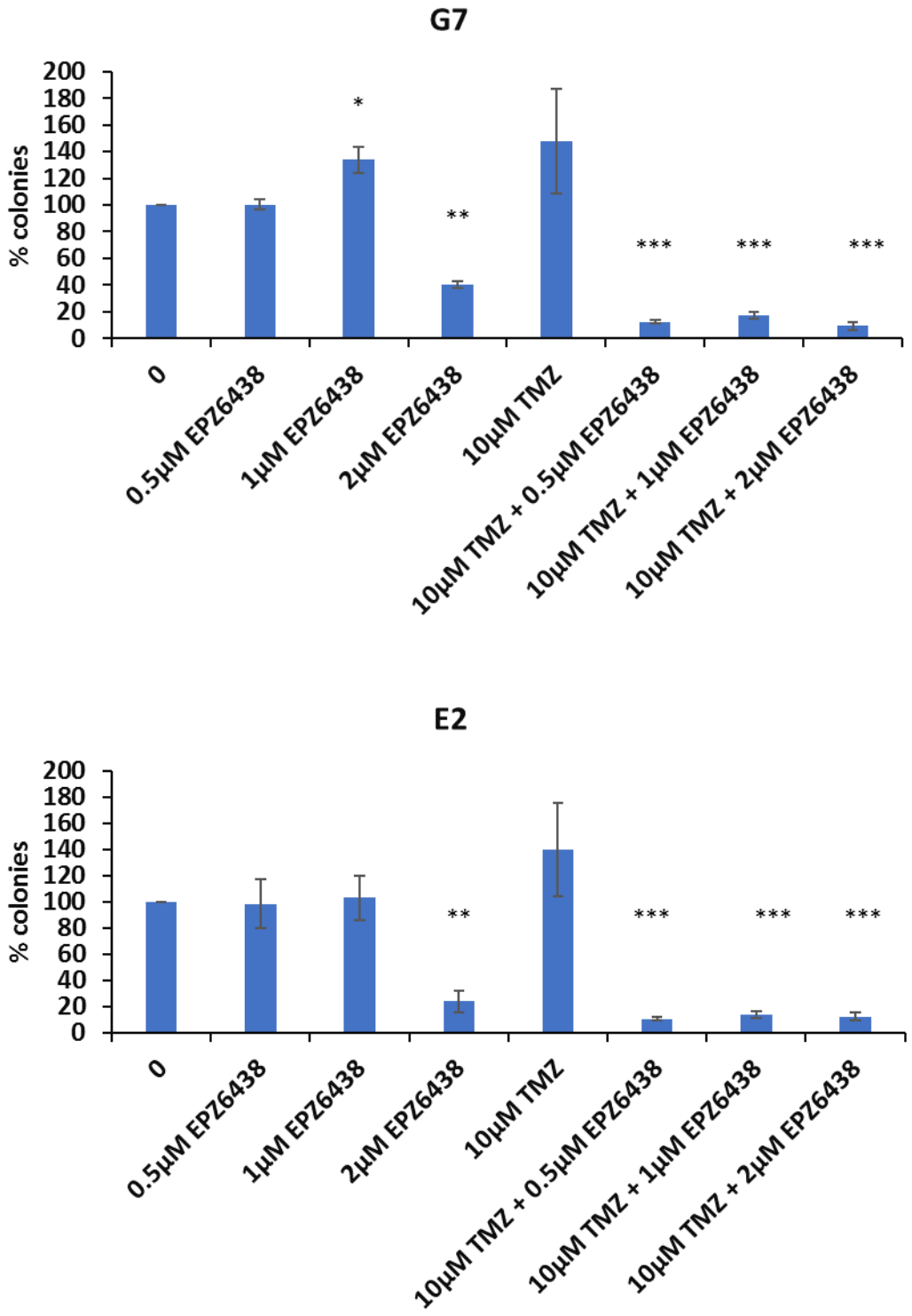

Figure 4-3 Clonogenic assay plot showing combined treatment of TMZ with EPZ6438 in G7 and E2 cell lines.

The survival assay was performed to determine the ability of treated cells to form colonies. Data shows the combined effect of 10 µM TMZ with increasing dose of EPZ6438. Cells were incubated with increasing concentration of EPZ6438 for 24 hrs then with 10 µM TMZ for 24 hrs. Data point represent mean of number of colonies from three independent experiment with error bars representing SEM. Student's T test was used to determine the significance of data in control vs treated cells. **p ≤ 0.01 and *** p ≤ 0.001.

The effect of EPZ6438 with radiation was investigated with clonogenic survival assays. G7 and E2 cell lines were incubated with EPZ6438 or the corresponding concentration of DMSO for 24 hrs, then plates were irradiated with 0-5 Gy, and incubation in the presence of drug was then continued for an additional 24 hrs. The 6 well plates were then incubated for 14 days and allowed to form colonies. The resulting clonogenic survival curve of both cell lines is shown in Figure 4-4.In G7 cells, the mean survival fraction was below 0.8 at 3 Gy at all concentrations of EPZ6438. At higher doses of radiation, the survival fraction was further decreased especially at 2 μM EPZ6438 when compared with control. There is a trend towards reduced survival when EPZ6438 is added, but the differences are not significant. In E2 cell line, there is a clear decrease in the surviving fraction when increasing concentrations of EPZ6438 are added at both 3 Gy and 5 Gy. For example, the surviving fraction after 5 Gy in the absence of drug is 0.33, and this is reduced to 0.11 in the presence of 2 μM EPZ6428. Table 4-1 shows the DMR values generated from survival fraction data in both cell lines. The highest DMR of 1.3 was obtained for E2 cells treated with 2 μM EPZ6438. This means that 1.3 fold more radiation is needed to reduce the survival fraction to 0.37 in control cells compared to cells treated with 2 μM EPZ6438. These data confirm that treatment with EPZ6438 makes E2 cells more sensitive to radiation, but does not affect G7 radiosensitivity.

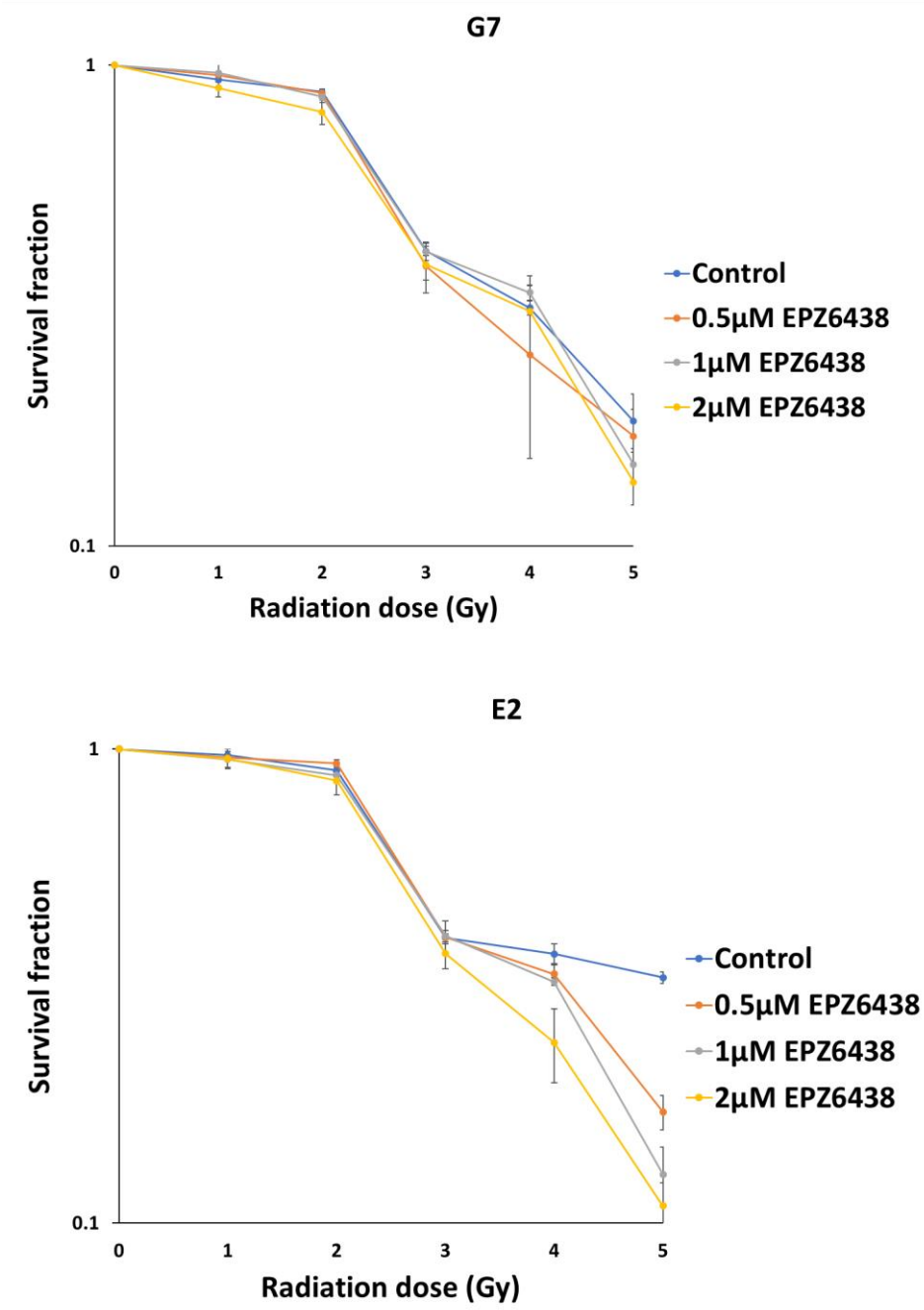

Figure 4-4 Clonogenic survival assay plot showing the combined effect of radiation with EPZ6438 in G7 and E2 cells.

Result shows mean survival fraction from three independent colony formation assay experiment, error bars represent SEM. Cells were seeded under stem conditions in 6 well plates in triplicate, incubated with different concentration of EPZ6438 for 24 hrs, exposed to radiation at 0 to 5 Gy, then incubation in the presence of the drug was continued for 24 hrs. The drug was then washed out and colonies allowed to form over 14 days. Cells were fixed then colonies were counted manually.

G7	$DMR_{(0.37)}$
0.5 μM EPZ6438	1.05
1 μM EPZ6438	1.01
2 μM EPZ6438	1.06

E2	$DMR_{(0.37)}$
0.5 μM EPZ6438	1.2*
1 μM EPZ6438	1.2**
2 μM EPZ6438	1.3**

Table 4-1 The DMR of G7 and E2 cell lines.

The DMR represents the dose required to reduce survival fraction to 0.37 in control vs treated with increasing concentration of EPZ6438. p value is calculated by comparing the means, sd and n of drug vs control. * $p \leq 0.05$ and ** $p \leq 0.01$.

4.3 Assessment of EPZ6438 in apoptosis and senescence assays

The previous experiments established that EPZ6438 inhibits colony formation in G7 and E2 cells. In order to investigate the biological processes occurring in these cells, assays for senescence and apoptosis were performed. Although cancer cell lines are immortal, usually due to the re-expression of telomerase, it is well established that chemotherapeutics and radiation can still induce cellular senescence in cancer cells. Therapy induced senescence is characterised by enhanced expression of senescence-associated ß-galactosidase and prolonged growth arrest, and usually involves induction of p21 and p16 (Saleh *et al.*, 2020).

An assay for senescence-associated ß-galactosidase was performed to determine whether EPZ6438 induces senescence in G7 or E2 cells. A concentration of 2 μM EPZ6438 was chosen for this experiment as this is the lowest concentration that has a significant effect on colony formation (Figure 4-1). Cells were incubated with EPZ6438 or corresponding DMSO as control for 5 days. Cells were fixed and stained with ß-galactosidase staining kit.

Figure 4-5 (A) shows an increase in number of senescence-ß-galactosidase stained cells in G7 cell line incubated with EPZ6438 when compared with control. The GBM cell lines that were not stained were graded as live cells while those with blue stain were classified as senescent cells. The result summarised in Figure 4-5 (B) suggested that EPZ6438 at 2 μM promotes senescence in G7 cells. The same observation can be found with E2 cell lines treated with 2 μM EPZ6438. The graph Figure 4-5 (B) indicates a significant increase in number of ß-galactosidase stained cells compared to control.

A)

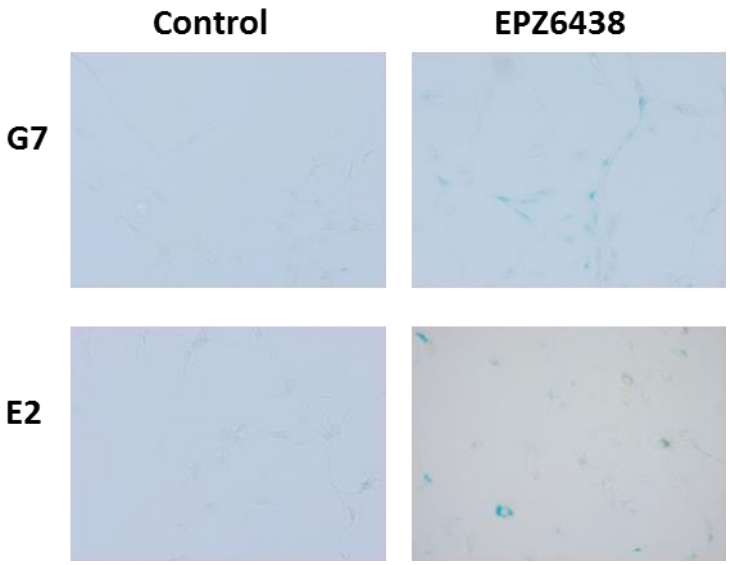

B)

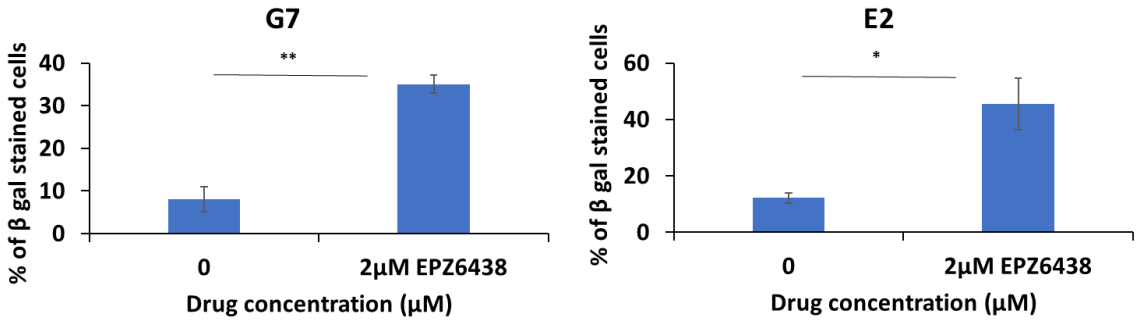

Figure 4-5 Senescence assay plots in G7 and E2 cell lines after treatment with 2 μM EPZ6438 or corresponding DMSO.

The images β-galactosidase stained cells was captured using confocal microscope (A). After 5 days of incubation with the drug ,cells were fixed and stained with β-galactosidase staining solution, β- galactosidase positive cells were quantified and plotted in a graph (B) with mean and SEM of three independent experiments. p value was calculated using student's T test. *p ≤ 0.5 and **p ≤ 0.01.

Flow cytometry analysis was performed to examine the apoptotic effect EPZ6438 on GBM stem cells lines. G7 and E2 cell lines were seeded into Matrigel coated 10 cm dishes. Cells were treated with 2 μM EPZ6438 or corresponding concentration of DMSO as control. Quantification of apoptotic cells was determined with AnnexinV and 7AAD staining kit. Figure 4-6 show apoptosis analysis with flow cytometry determines that EPZ6438 did not induce apoptosis in G7 and E2 cell lines when compared to control. Percentage of early and late apoptotic cells was very low compared to viable cells in plotted graph of treated cells.

A)

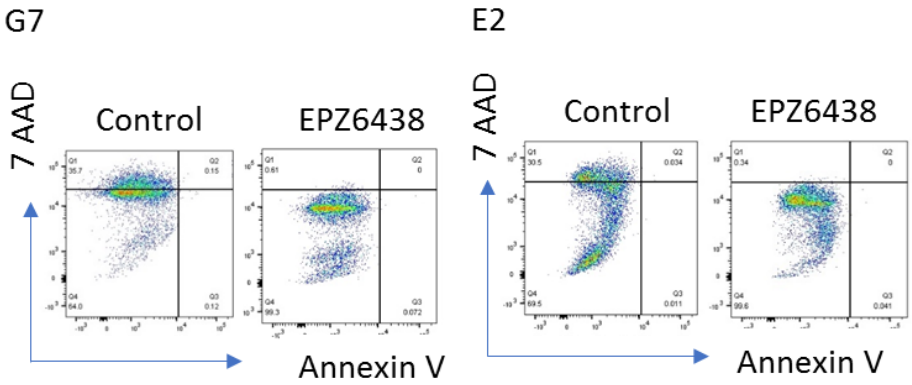

B)

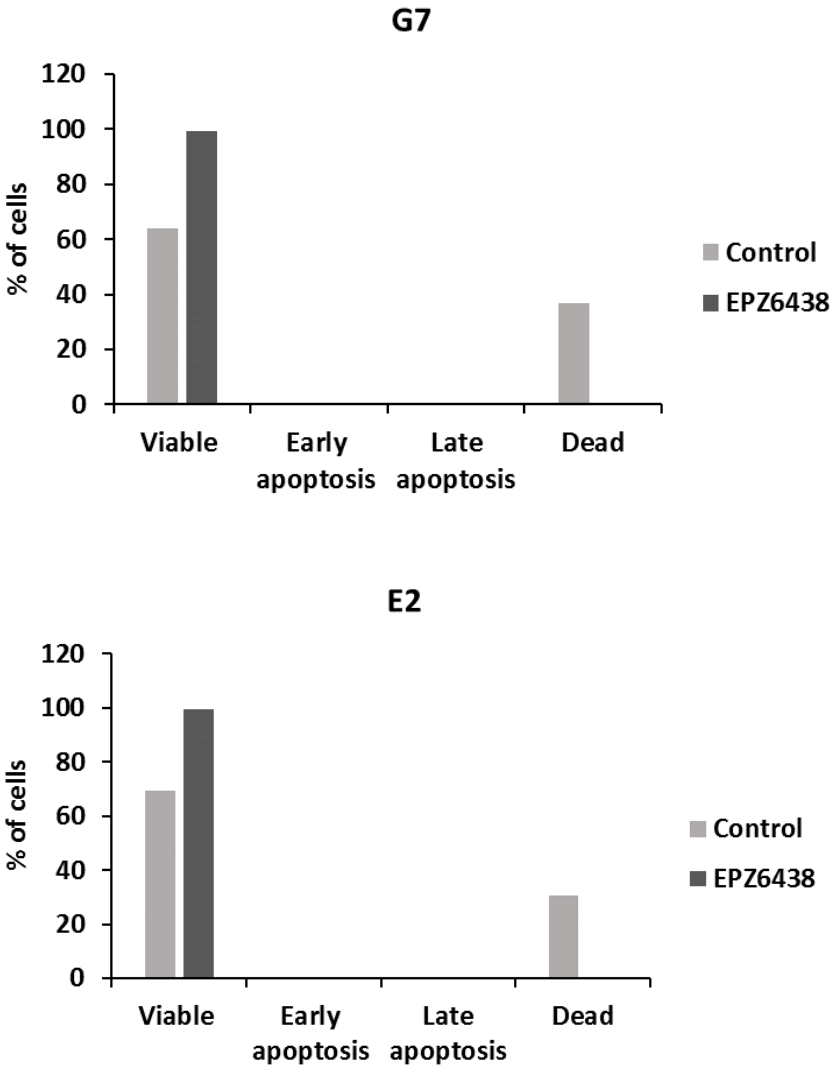

Figure 4-6 Apoptosis assay of G7 and E2 cell line treated with EPZ6438 or corresponding DMSO.

Flow cytometric data shows apoptotic effect of 2 µM EPZ6438 treatment in G7 and E2 cell line. Cells were incubated with the drug or DMSO for 5 days, then fixed and stained with AnnexinV and 7AAD . The percentage of cell (A) was plotted as scatter plots showing live

(Q4), early apoptosis (Q3), late apoptosis (Q2) and dead cells (Q1) . The viable, early , late apoptosis cells are represent in a graph (B).

4.4 Effect of EPZ6438 on genes associated with stemness and tumourgenesis

qRT- PCR was performed to assess the effect of EPZ6438 on genes involved with stemness of stem cells. *SOX2*, *NESTIN*, *CD133* and *OLIG2* are commonly used stem markers to identify GBM stem cells population, while *GFAP*, an astrocyte marker, and βIII tubulin are identified as differentiated markers. G7 and E2 were cultured under stem conditions and incubated for 5 days with the drug . Figure 4-7 shows stem and differentiated gene expression in G7 and E2 cells after exposure to increasing concentration of EPZ6438 or corresponding concentration of DMSO. In G7 cells, most of the genes did not show a consistent trend in changes in expression following drug treatment. Expression of *OLIG2* and *NANOG* increased, but the overall relative expression compared to *B-Actin* is very low compared to genes such as *SOX2* and *NESTIN* .

In the same Figure, the qRT-PCR graph of E2 showed an elevated expression level of *SOX2* and *NESTIN* in treated cells compared to control especially at 0.5 μM EPZ6438. However, the expression level of other genes remained low in both treated and control cells.

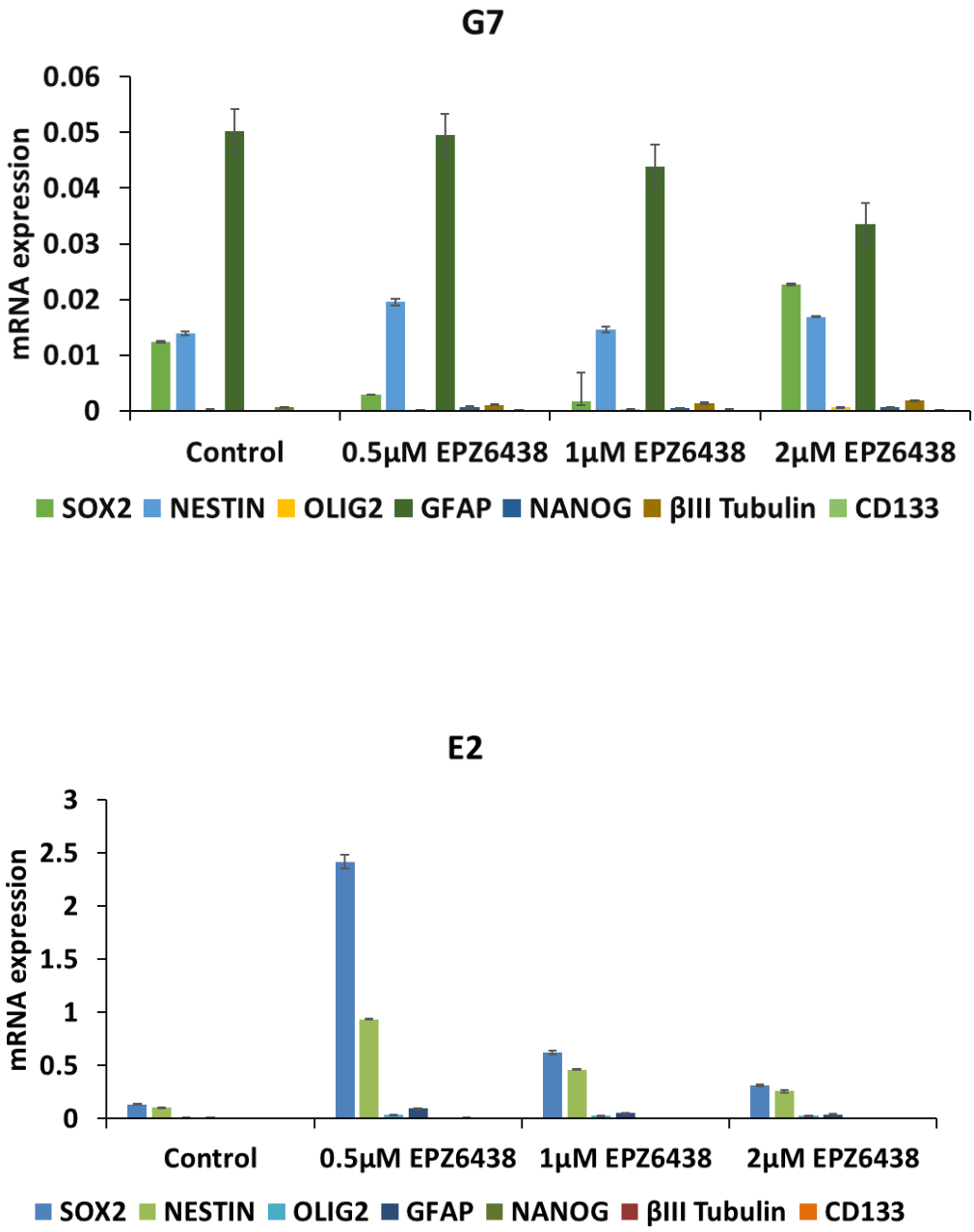

Figure 4-7 The level of mRNA expression of stem cell markers and differentiated markers in G7 and E2 cell lines following treatment with increasing concentration of EPZ6438 or corresponding DMSO as control.

The graph shows qRT-PCR data of G7 and E2 cells treated with (0.5, 1 and 2 µM) of EPZ6438 for 5 days. Data are normalised with β-Actin, the mRNA expression represents the fold change that is calculated from delta Ct with error bars representing SEM .Each RNA sample was loaded into wells in triplicates.

qRT- PCR was also performed to determine the level of genes associated with cell cycle regulation and tumour suppression. GSCs were incubated with increasing concentrations of EPZ6438 on Matrigel coated plates for 5 days The expression level of *p21* and *CDK2*, cell cycle regulators, found to be elevated in G7 at 2 μM EPZ6438 (Figure 4-8). However, the level of tumour suppresser *PTEN* and senescent marker *p16* remained the same for treated and control. Surprisingly, the level of oncogene *MYC* and PRC2 subunit EZH2 was also elevated at 2 μM EPZ6438. Similarly, in E2 the level of *p21* and *CDK2* was increased at 2 μM EPZ6438. The level of *EZH2* was also increased while *MYC* expression level remained low. The *p16* and *MGMT* expression levels were remained the same and the level of *PTEN* increased at 2 μM EPZ6438 .

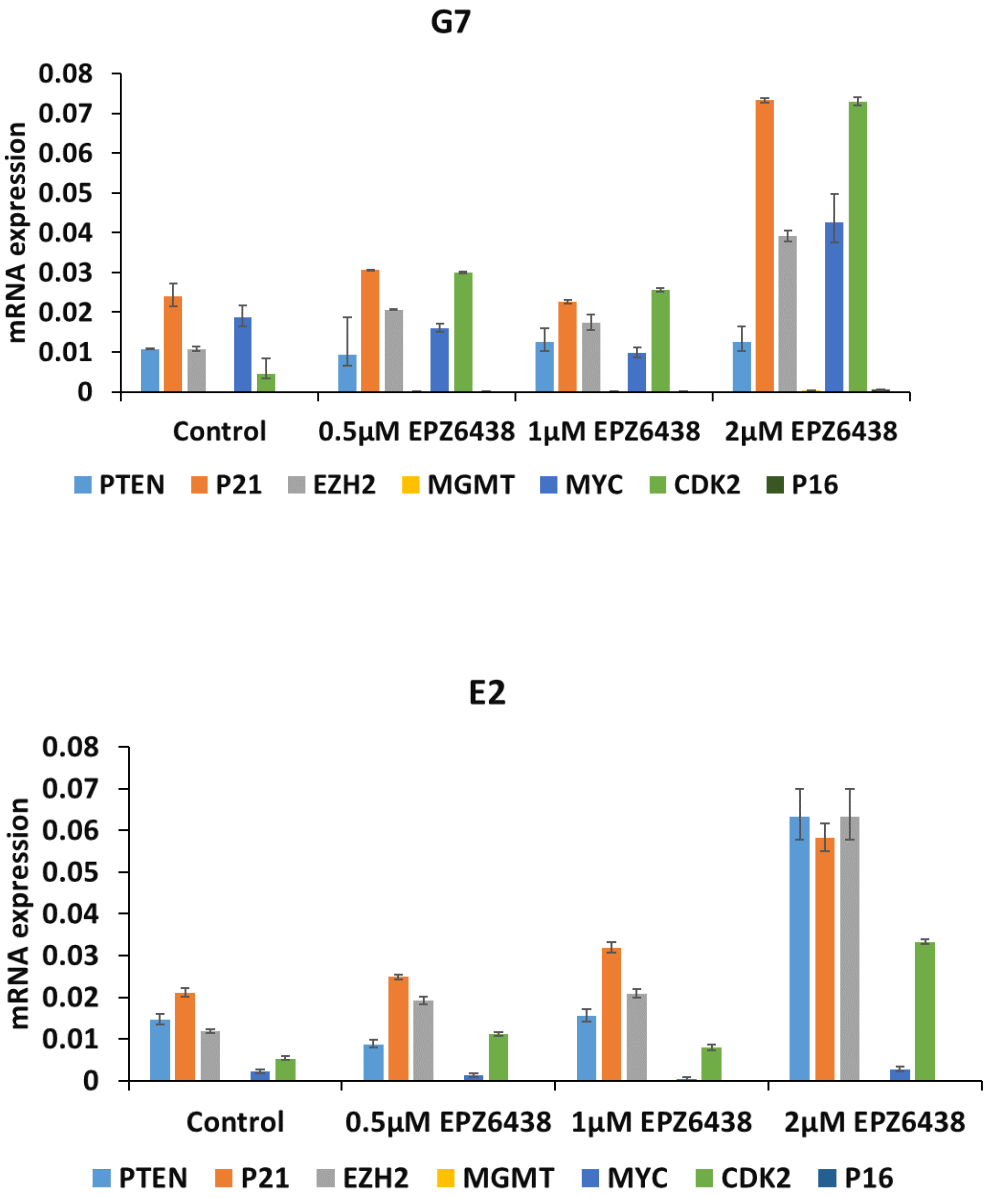

Figure 4-8 The level of mRNA expression of genes involved with cell cycle, apoptosis and senescence in GBM stem cell lines treated with increasing concentration of EPZ6438 or corresponding DMSO as control.

The mRNA relative expression in G7 and E2 treated with (0.5, 1 and 2 µM) EPZ6438 for 5 days were examined with qRT-PCR. Each RNA sample was loaded into wells in triplicates. Data are normalised with β-Actin, error bars represent SEM. The mRNA expression represents the fold change that is calculated from delta Ct.

4.5 RNA sequencing analysis of GBM cell lines treated with EPZ6438

4.5.1 Quality control and data visualisation with searchlight2 using Galaxy

G7 and E2 cell lines were treated with 2 μM EPZ6438 for 5 days. RNA samples were prepared and shipped for paired-end RNA-seq analysis. The Fastq files containing the raw sequencing data were obtained from BGI genomics and were processed through Galaxy server. FastQC was used to assess the quality of data. The samples displayed an overall GC content of 50% and typical PHRED scores of 36 (range of 29- 38). Hisat2 was used to align the samples to the human Hg38 genome, and the percentage of mapped reads was typically 95%. Data were visualised using Searchlight2 to determine the changes that can be observed in DEGs in both cell lines treated with EPZ6438 versus control. In principal component analysis (PCA) plots, the second and third replicates of treated and control experiments in both cell lines formed clusters that indicates similarity in gene expression. However, the first replicates of control and treated in G7 and E2 cell lines did not form cluster with the other replicates. Thus, indicating variability between samples and less significantly changed genes will be identified (Figure 4-9).

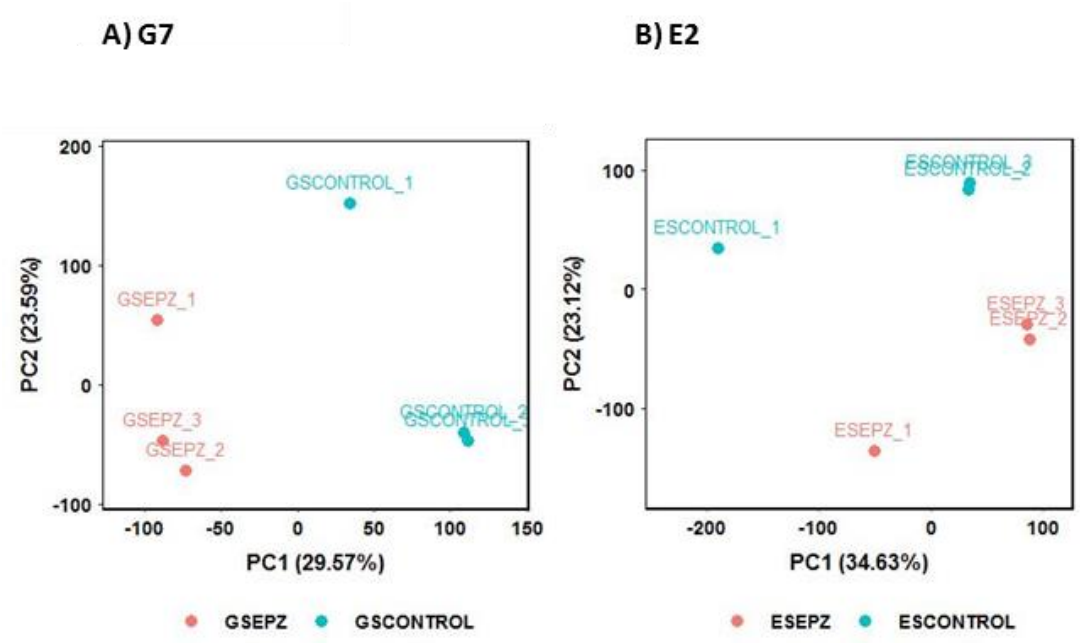

Figure 4-9 PCA plots for G7 and E2 lines treated with 2 µM EPZ6438 and controls.

The scatterplot shows two sample groups control and treated that is distributed and presented as dots. The blue dots represent control and the red dots represent the treated samples. The total variation percentage explained by each component is given in the x and y axis. The PCA plots were generated from searchlight2 .

Searchlight also generated MA plots that is shows log fold change vs normalised gene expression between treated and control (Figure 4-10). The MA plot is presented as scatter plots with normalised mean expression on y axis and Log2 fold change on x axis. The data points > 0 Log2 fold change indicates upregulated genes while data points < 0 Log2 fold change represents downregulated genes.

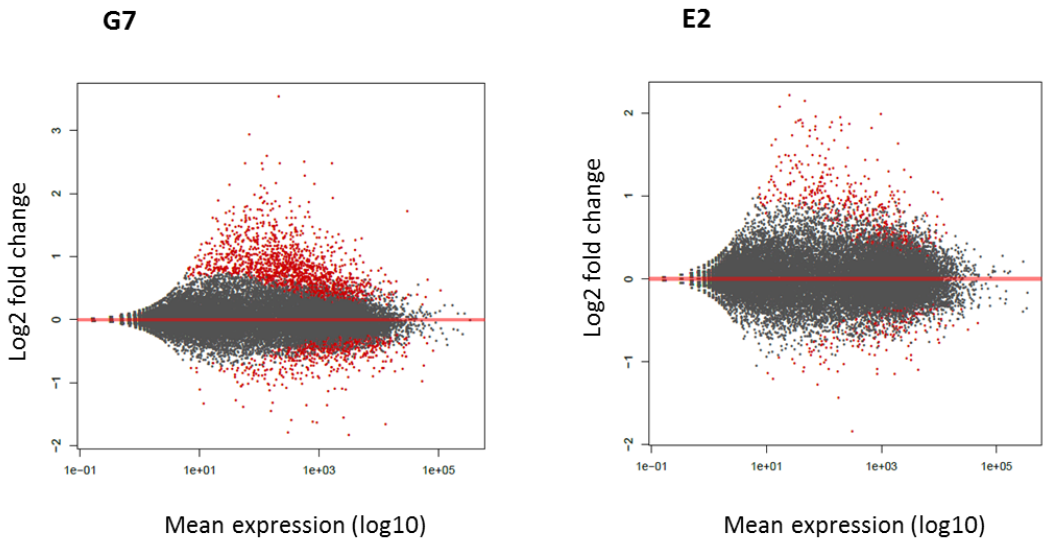

Figure 4-10 MA plots in G7 and E2 treated with 2 μM EPZ6438 .

The MA plot shows the relationship between the mean expression of each gene and its fold change. The plots were created by Deseq2 using RNA-seq data. The x axis indicates the normalised mean expression from all samples, while the y axis indicates the Log2 fold change between treated and control. Significantly changed genes are shown in red and non−significant genes in black .

Similar results were obtained with significant genes heatmaps with p value < 0.05 in G7 and E2 cell treated and control. The heatmap showed the level of significantly genes expressed were similar in all three replicates with red indicating upregulated and blue presenting downregulated (Figure 4-11).

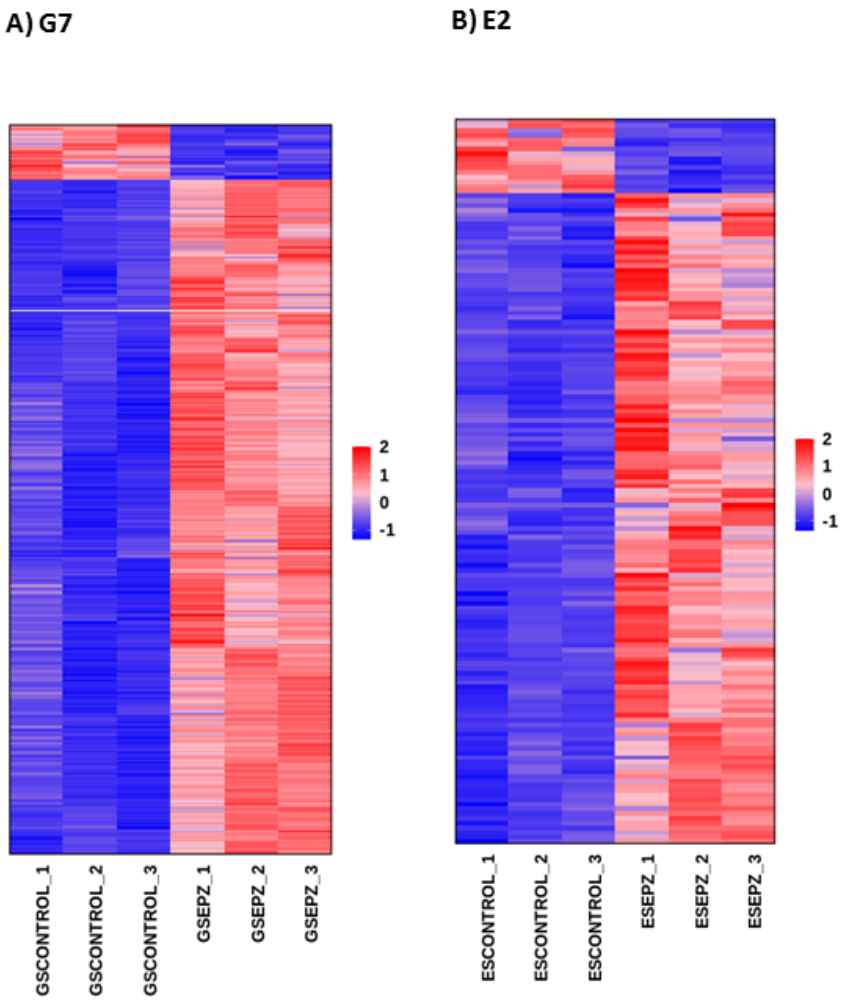

Figure 4-11 Significant genes heatmaps of G7 and E2 treated with 2 μM EPZ6438 and controls.

The plot is generated by modifying and running Deseq2 count and result files on Galaxy server Antioch . The output files from searchlight2 were visualised using R program. Gene expression is represented in a hierarchical cluster heatmap (Spearman) with p value < 0.05. Red represent upregulated genes and blue represent downregulated genes.

4.5.2 Pathway analysis with Gene ontology (GO)

In order to identify pathways that are involved with gene expression, GO analysis was performed using software analysis Toppgene. The Deseq2 file was modified using filter function on excel with p value < 0.05 forming two list of genes upregulated (Log2 fold change > 0) and downregulated (Log2 fold change < 0). The two list of genes were ran through Toppgenes creating an output files of significant DEGs and their pathways.

In G7, the biological process with q value (Bonferroni) < 0.05 from output file of GO analysis showed most of the upregulated genes associated with neurogenesis. However, the biological process for downregulated genes found only 2 pathways one involved with postsynaptic density organisation while the other one associated with noncoding RNA metabolism. No GO biological process categories were significantly altered in E2 cells.

a)

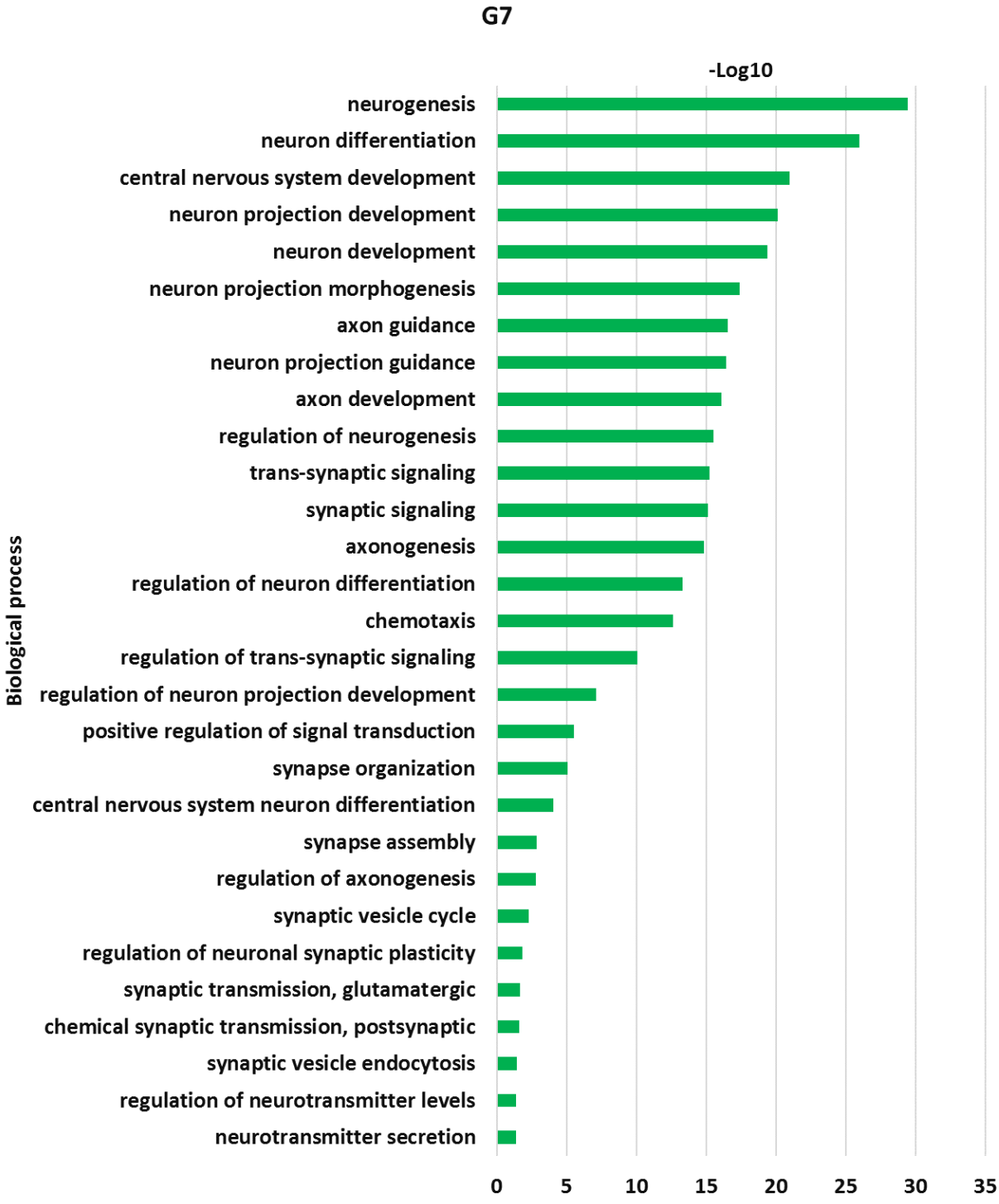
G7
-Log10
Biological process
neurogenesis
neuron differentiation
central nervous system development
neuron projection development
neuron development
neuron projection morphogenesis
axon guidance
neuron projection guidance
axon development
regulation of neurogenesis
trans-synaptic signaling
synaptic signaling
axonogenesis
regulation of neuron differentiation
chemotaxis
regulation of trans-synaptic signaling
regulation of neuron projection development
positive regulation of signal transduction
synapse organization
central nervous system neuron differentiation
synapse assembly
regulation of axonogenesis
synaptic vesicle cycle
regulation of neuronal synaptic plasticity
synaptic transmission, glutamatergic
chemical synaptic transmission, postsynaptic
synaptic vesicle endocytosis
regulation of neurotransmitter levels
neurotransmitter secretion
0
5
10
15
20
25
30
35

b)

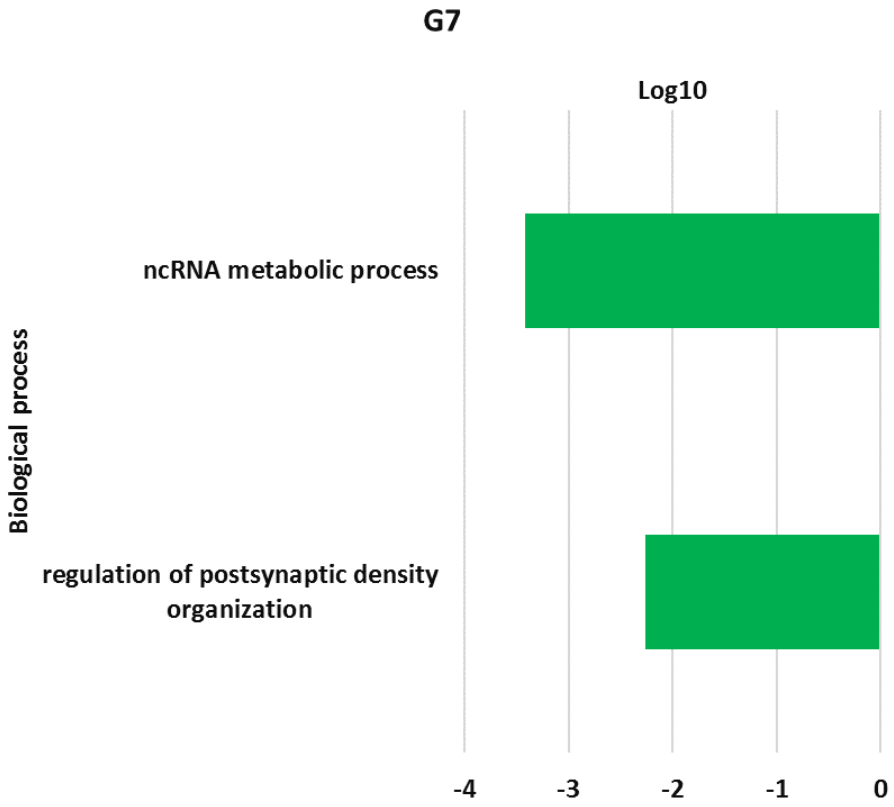

Figure 4-12 Significantly enriched GO biological processes in G7 cells treated with 2 μM EPZ6438.

GO analysis (biological processes) was performed using Toppgene. Significantly upregulated (- Log10 q value) and downregulated (Log10 q value) biological process categories with q value (Bonferroni) < 0.05 are shown. The Log10 q value is plotted as a horizontal bar; upregulated categories (a) have a positive value and downregulated categories (b) have a negative value. The GO analysis was performed on DEGs (adj p value < 0.05), treating upregulated genes (Log2 fold change > 0) and downregulated genes (Log2 fold change < 0) separately.

4.5.3 Comparative analysis with InteractiVenn and GO analysis

A Venn diagram was plotted using InteractiVenn to identify similarity in DEGs that are associated in G7 and E2 treated with 2 μM EPZ6438. The Deseq2 files was modified with filter function to form a list of significant upregulated genes (Log2 fold change > 0 and p value < 0.05) then the list for both cell lines were run through InteractiVenn (Figure 4-16). The output file generated Venn diagram with 1149 for G7 and 248 for E2, with 98 common genes. However, the

downregulated (Log2 fold change < 0 and p value < 0.05) list of both cell lines showed 440 for G7 and 98 for E2 with 8 genes in common. The overlap significance was determined by calculating the representation factor of upregulated common genes (13.4) and downregulated common genes (9.9). Indicating more significant overlaps between G7 and E2 cells treated with EPZ6438.

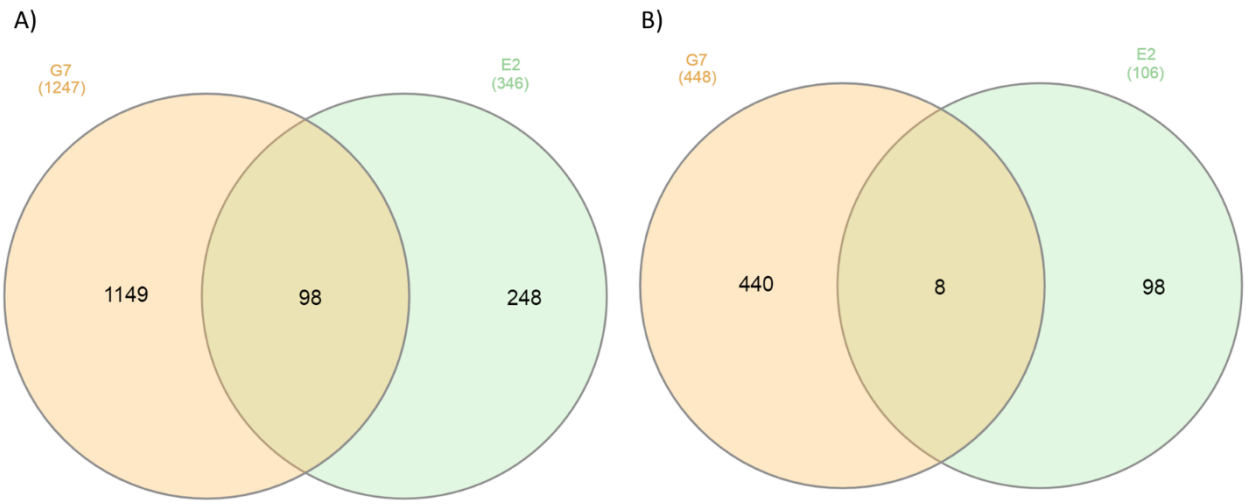

Figure 4-13 Venn diagram for upregulated (A) and downregulated (B) genes in G7 and E2 cell lines treated with EPZ6438.

The Deseq2 result file was modified with the adj. p value < 0.05 creating a list for upregulated genes (log2 fold change > 0) and downregulated genes (log2 fold change < 0). The lists of upregulated and downregulated genes were run through InteractiVenn to show common genes associated in both cell lines. p value was determined by calculating the representation factor of overlapped genes for both upregulated and downregulated genes. p ≤ 0.001.

The list of upregulated and downregulated genes common in both G7 and E2 produced from InteractiVenn was ran through Toppgene for GO analysis. This created output files modified with p value < 0.05 for upregulated genes (Log 2 fold change > 0) and downregulated genes (Log2 fold change < 0). The biological process showed 11 pathways for only upregulated genes involved in neurogenesis and synaptic signalling, while GO analysis did not show any downregulated pathways.

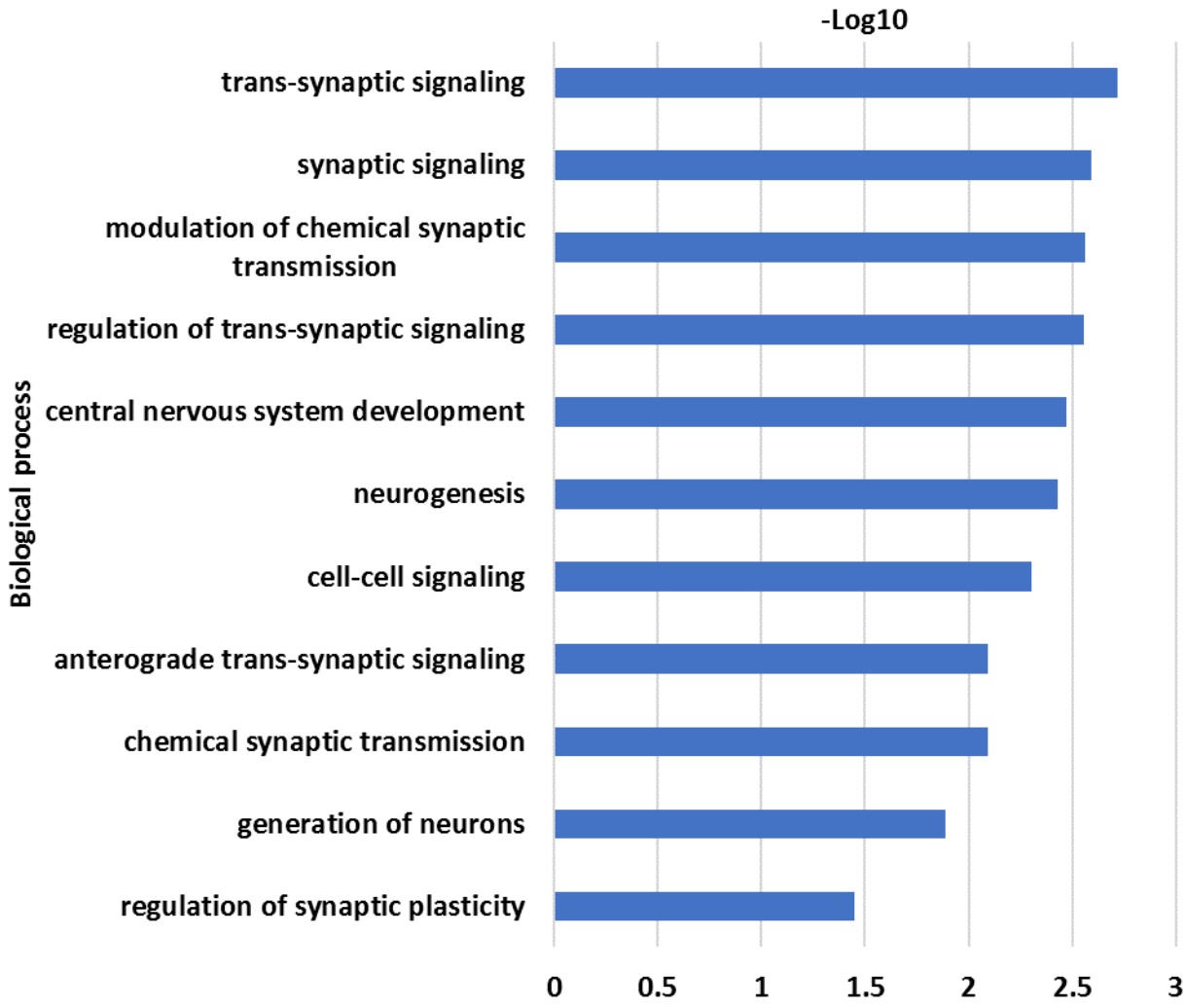

Figure 4-14 Biological process significantly upregulated in both G7 and E2 cell lines treated with EPZ6438.

GO analysis was carried out on list of upregulated common genes obtained from InteractiVenn analysis of G7 and E2 treated with EPZ6438. The horizontal graph is plotted with - log10 on x axis that is calculated from q value Bonferroni and biological process on y axis. The list biological process was filtered on excel with q value (Bonferroni) < 0.05.

4.5.4 Pathway analysis with GSEA

GSEA was used to identify pathways involved in G7 stem and E2 stem treated with 2 μM EPZ6438. This is a powerful tool that can analyse small gene expression changes across the whole data set rather than just using the list of DEGs that pass a certain cut off. The Deseq2 file was modified and uploaded into GSEA software, and analysed using the Hallmarks group of gene sets (Liberzon *et al.*, 2015) . The Hallmarks group contains 50 gene sets that been curated to provide lists of genes with coherent expression that represent well defined biological states or processes.

In G7 cells, positive enrichment of 18 gene sets and negative enrichment of 5 gene sets were observed with a nominal (NOM) p value < 0.05 and false discovery rate (FDR) q value < 0.25 (Figure 4-15). Figure 4-16 shows two enrichment plots from G7 that were generated by GSEA. The plots shows the set of genes that are downregulated in response to KRAS signalling (HALLMARK _KRAS_SIGNALLING_DN, FDR q value 0.026), and a subset of genes that are targets of MYC (HALLMARK_MYC_TARGETS_ V2,FDR q value 0).

a)

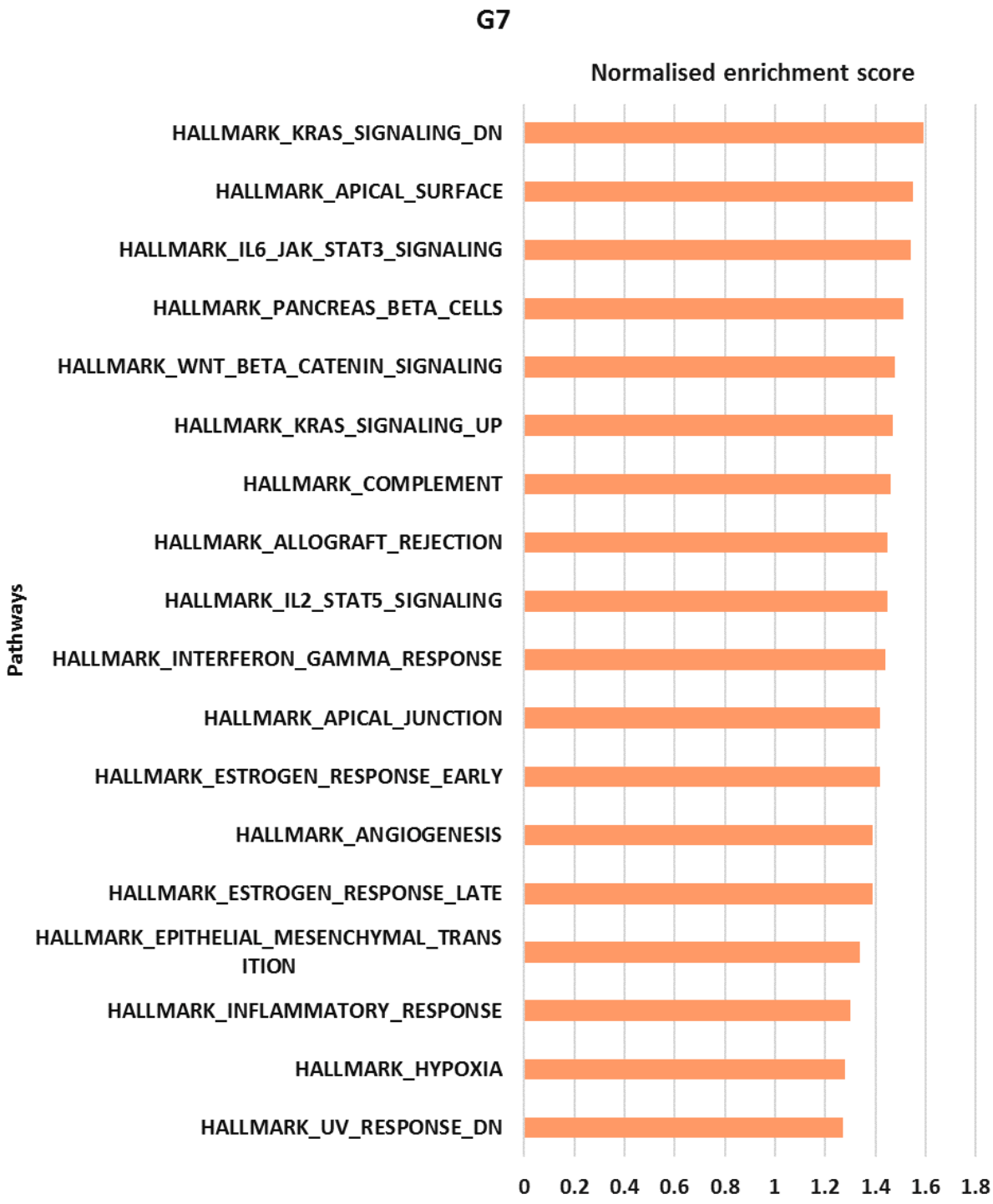
G7
Normalised enrichment score
Pathways
HALLMARK_KRAS_SIGNALING_DN
HALLMARK_APICAL_SURFACE
HALLMARK_IL6_JAK_STAT3_SIGNALING
HALLMARK_PANCREAS_BETA_CELLS
HALLMARK_WNT_BETA_CATENIN_SIGNALING
HALLMARK_KRAS_SIGNALING_UP
HALLMARK_COMPLEMENT
HALLMARK_ALLOGRAFT_REJECTION
HALLMARK_IL2_STAT5_SIGNALING
HALLMARK_INTERFERON_GAMMA_RESPONSE
HALLMARK_APICAL_JUNCTION
HALLMARK_ESTROGEN_RESPONSE_EARLY
HALLMARK_ANGIOGENESIS
HALLMARK_ESTROGEN_RESPONSE_LATE
HALLMARK_EPITHELIAL_MESENCHYMAL_TRANSITION
HALLMARK_INFLAMMATORY_RESPONSE
HALLMARK_HYPOXIA
HALLMARK_UV_RESPONSE_DN
0
0.2
0.4
0.6
0.8
1
1.2
1.4
1.6
1.8

b)

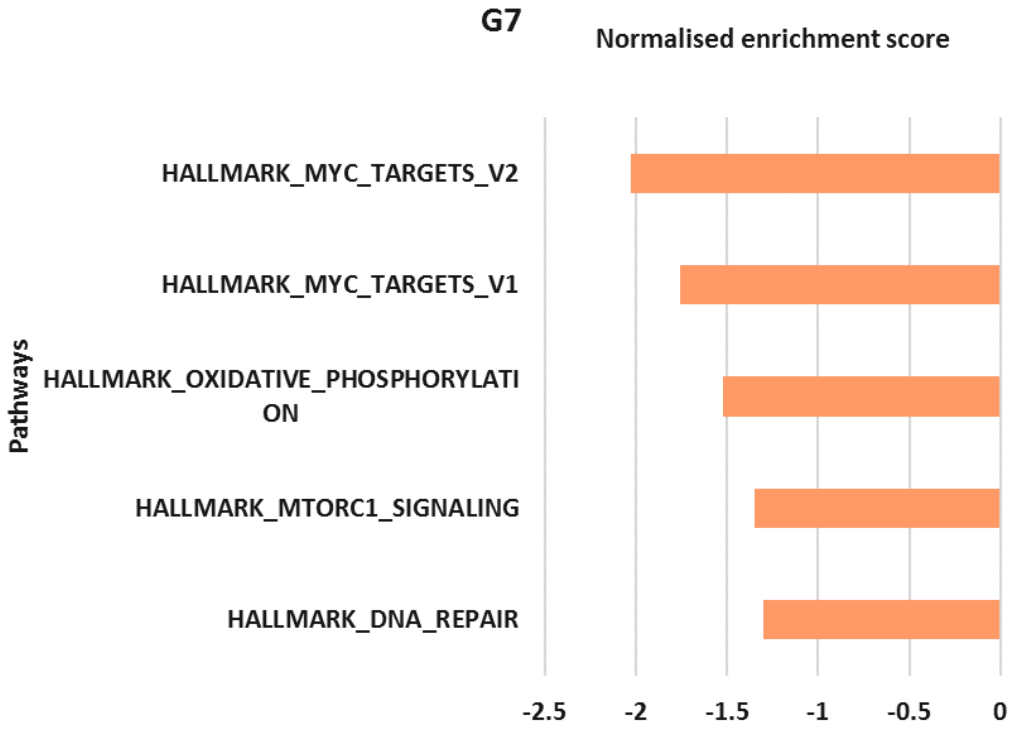

Figure 4-15 Horizontal bar chart of enriched GSEA Hallmarks gene sets in G7 treated with 2 μM EPZ6438.

Normalised enrichment score (NES) is indicated on x axis that is plotted against gene sets represented on y axis. The plot represents significant gene sets that was filtered using GSEA report output file with NOM p value < 0.05 and the FDR < 0.25. (a) plot with NES > 0 indicates gene sets that are positively enriched and (b) plot with NES < 0 indicates gene set negatively enriched in GBM treated cells.

A)

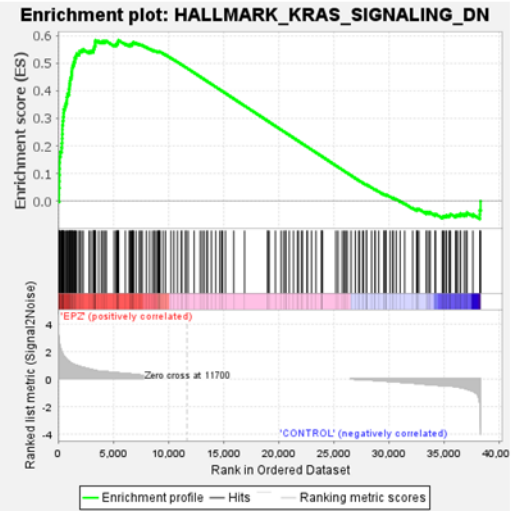

B)

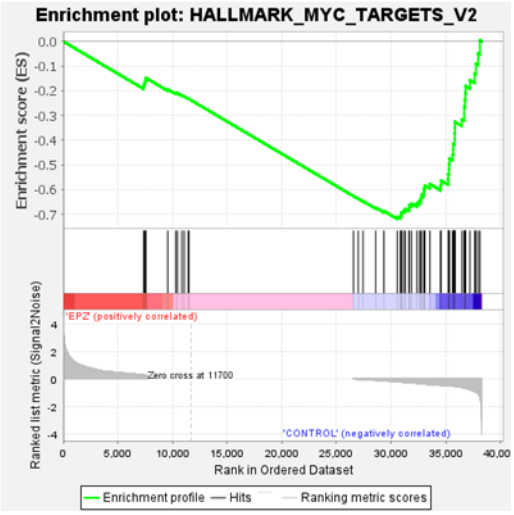

Figure 4-16 The enriched plot of GSEA in G7 treated with 2 μM EPZ6438 and G7 Control.

Plot (A) represents the top positive enrichment gene set: genes that are downregulated in response to KRAS signalling. Plot (B) represents the top negative enrichment gene set: targets of MYC. The enriched score (ES) is indicated as the green curve; the final ES score is indicated at the peak of the curve of that gene set. The plot is obtained from GSEA output file after running the Deseq2 counts file through GSEA software.

In E2 cells, GSEA indicates significant enrichment of 11 gene sets (NOM p value < 0.05 and FDR q value < 0.25) (Figure 4-17). The plots for the top positive and negative enriched gene sets are shown in Figure 4-18: G2M checkpoints (FDR q value 0) and Oxidative phosphorylation (FDR q value 0).

a)

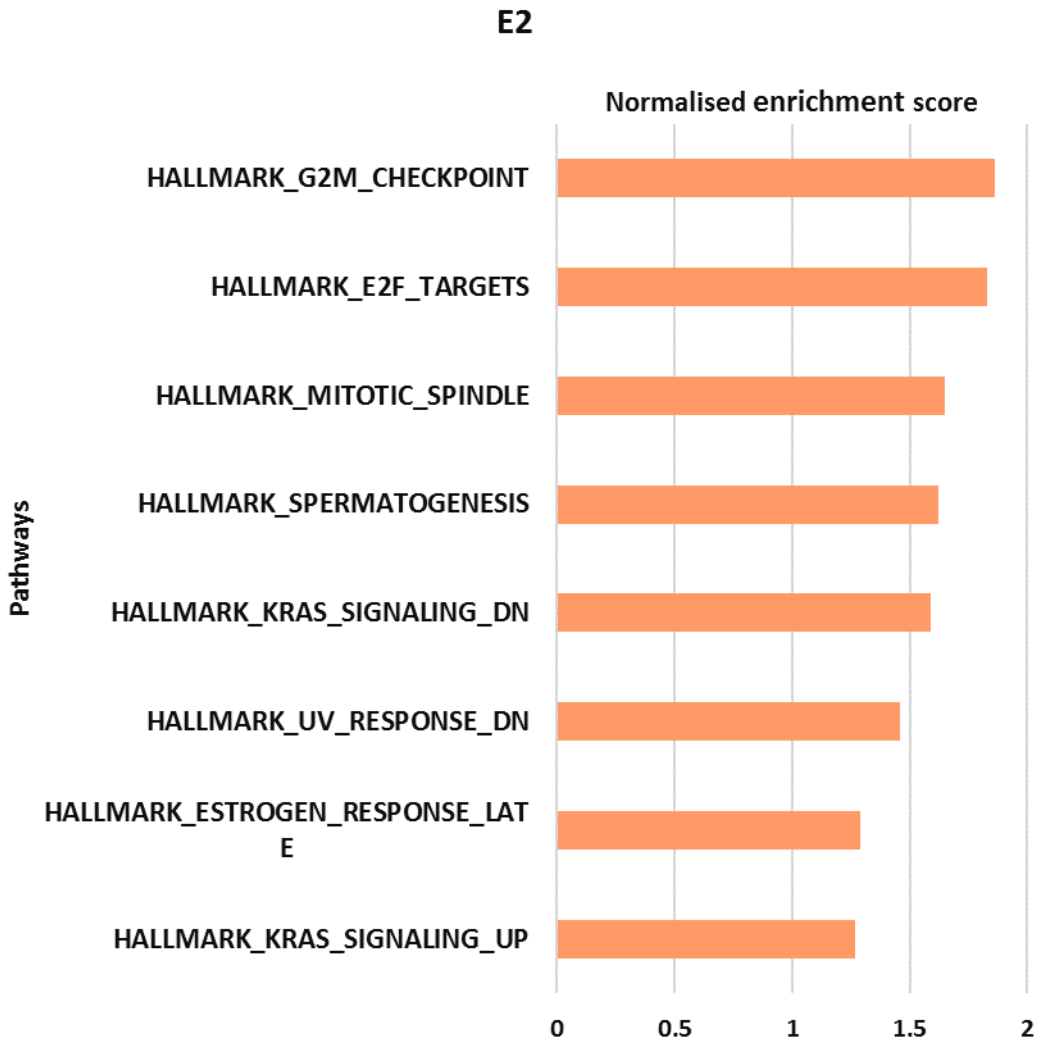

b)

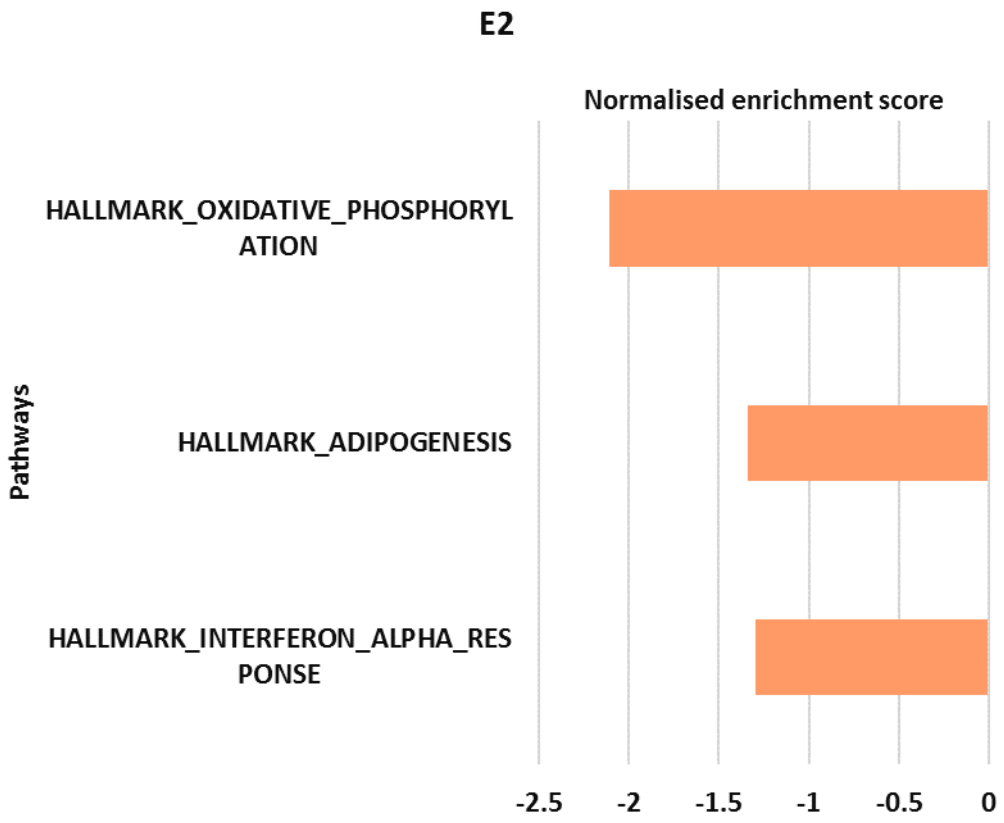

Figure 4-17 Horizontal bar chart of enriched GSEA Hallmarks gene sets in E2 treated with 2 µM EPZ6438.

NES is indicated on x axis while gene sets represented on y axis. The plot represent significant gene sets that was made with NOM p value < 0.05 and the FDR < 0.25 obtained from GSEA report output file of E2 stem treated cells . (a) graph with NES > 0 indicates gene sets that are positively enriched and (b) graph with NES < 0 indicates gene set negatively enriched in E2 stem treated cells.

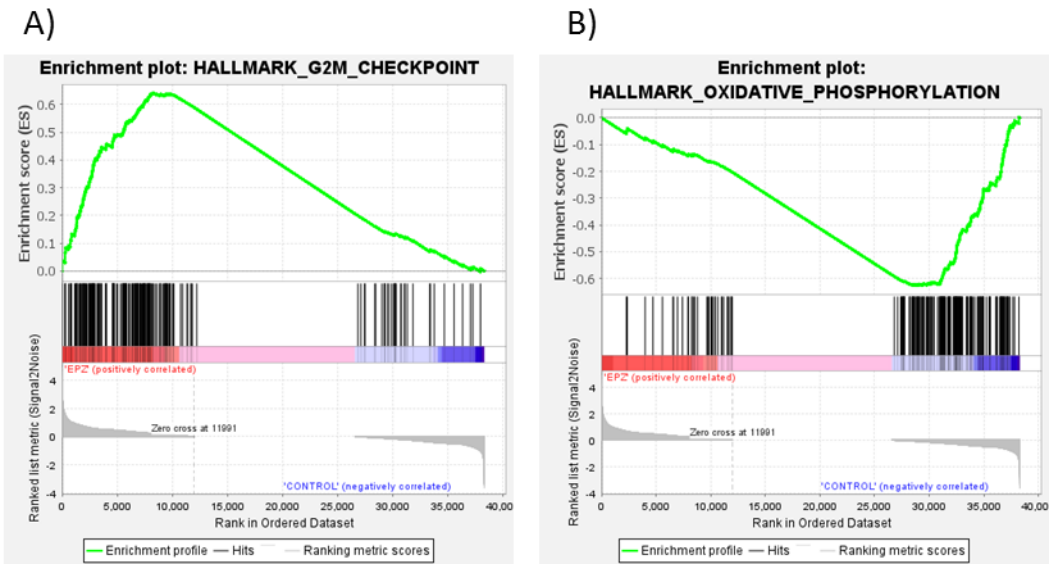

Figure 4-18 The enriched plot of GSEA in E2 treated with 2 μM EPZ6438 and E2 Control.

Plot (A) represents the top enrichment at the top of the list while plot (B) represents top negative enrichment of the horizontal bar. The ES is indicated as the green curve, the final ES score is indicated at the peak of the curve of that gene set. The Deseq2 count file was modified and ran through GSEA software to generate enriched plot.

Comparative analysis was performed based on GSEA analysis of NES values of G7 and E2 cell lines. Table 4-2 shows pathways common in both cell lines treated with EPZ6438. The analysis showed 3 pathways were positively enriched; Hallmarks of KRAS signalling DN, KRAS signalling UP and UV response DN. Only one pathway that include Hallmark of Oxidative phosphorylation was found negatively enriched.

Hallmark	G7 NES	E2 NES
HALLMARK_KRAS_SIGNALING_DN	1.59	1.59
HALLMARK_KRAS_SIGNALING_UP	1.47	1.27
HALLMARK_UV_RESPONSE_DN	1.27	1.46
HALLMARK_OXIDATIVE_PHOSPHORYLATION	-1.52	-2.11

Table 4-2 Hallmark of gene set positively and negatively enriched in G7 and E2 cell line.

This table shows NES values of significant pathways present in both G7 and E2 cells treated with 2 μM EPZ6438. NES > 0 indicates positive enrichment while NES< 0 represents negative enrichment.

4.6 Discussion

This chapter demonstrates the investigation of EPZ6438 and its importance as inhibitor of EZH2 enzymatic activity in GSCs. . Previous reports demonstrated that EPZ6438 inhibits trimethylation of histone H3K27 by inhibiting EZH2 activity. The data presented in this chapter show that treatment with EPZ6438 reduces colony formation in GBM stem cell lines. This shows that exposure to EPZ6438 has a detrimental effect on the ability of cells to survive and proliferate over the long term. However, the drug did not affect cell numbers over a shorter five days period.

In order to further investigate the effect of EPZ6438 on the GBM cells, assays for apoptosis and senescence per performed. The apoptosis assay demonstrated that the percentage of early and late apoptotic cells remained low in treated compared with control cells, providing no evidence that the drug induces apoptosis at these concentrations. However, there was an increase in the percentage of cells expressing senescence-associated- ß-galactosidase following treatment with EPZ6438. Previous reports indicated that p21 and p16 are associated with promoting therapy induced senescence in tumour cells (Saleh *et al.*, 2020) . qRT-PCR analysis clearly indicated higher expression of *p21* in both treated GBM cell lines. Increases in *p16* expression were not detected in either cell line, and, as explained in chapter 3, subsequent analysis revealed that both alleles of *CDKN2a*, the gene that expresses p16, are absent in E2 cells. RNA-seq data indicated that senescence-associated genes such as those associated with the senescence-associated secretory phenotype (SASP) were not enriched in either the GO or the GSEA analyses.The induction of the SASP varies, depending on cell type and the nature of the stimulus, and can depend on the p53 status (Bojko *et al.*, 2019). Variant analysis in chapter 3 indicated that both G7 and E2 cells have heterozygous *p53* mutations, which is likely to influence the senescent phenotype. This data suggests that EPZ6438 can induce senescence in G7 and E2 cells, but further analysis is required to investigate the nature of the senescence-related changes in these cells.

In order to investigate the effect of the drug on the whole transcriptome rather than a few candidate genes, RNA-seq analysis was performed. GO analysis showed that the significantly upregulated genes were strongly linked to

neurogenesis-related pathways in G7 treated cells. The GO analysis of E2 treated cells did not show any significant upregulated genes associated with neurogenesis pathways, probably because there were fewer DEGs. However, Venn diagrams revealed that there were 98 genes upregulated in both G7 and E2 cells, and most of these are associated with synapse regulation in neurons. Thus, increases in neuronal gene expression were present in both G7 and E2 treated cells. Based on this data, we hypothesise that EPZ6438 causes the cells to lose their ability to maintain their stem cell phenotype, and results in differentiation down neuronal-related pathways. Further investigation is required to test this hypothesis; for example, cell imaging and immunofluorescence studies could be used to examine the expression of neuronal marker genes.

GSEA analysis can be a more sensitive approach than GO when identifying pathways or cell types that are altered. This is because it takes into account small changes in many genes along a pathway, rather than relying on significant changes in a few genes. GSEA revealed that sets of genes regulated by KRAS signalling are enriched in both G7 and E2 cells. It is possible that increased signalling through the KRAS pathway drives the increase in the expression of genes related to neurogenesis as observed in the GO analysis. GSEA also indicated that several other signalling pathways were activated in EPZ6438 treated G7 cells, including IL6 and Wnt-ß catenin, both of which have been implicated in neurogenesis.

The MYC target gene set was found to be a negatively enriched dataset in GSEA analysis. However, interrogation of the RNA-seq data set found that the expression of MYC and MYCN were not significantly altered in G7 or E2 cells ($p > 0.25$). MYC is well known as an oncogene that regulates pathways involved in survival of cancer cells such as cell growth and cell cycle progression (Holmen and Williams, 2005). Interestingly, MYC oncogenes have been found to regulate EZH2 at both the transcriptional and post transcriptional level (Koh *et al.*, 2011). It is possible that inhibition EZH2 leads to changes in expression of one or more co-factors that modulate the activity of MYC.

Pathway analysis with GSEA also showed that genes involved in oxidative phosphorylation (OxPhos) appear to be downregulated in both G7 and E2 cells following drug treatment. OxPhos is the mechanism by which ATP is produced in

the mitochondria, and is required for cell proliferation (Vasileiou *et al.*, 2019; Xiong *et al.*, 2012). However, it is not possible to say from our data whether the reduction in OxPhos gene expression is a consequence of reduced proliferation and cell cycle arrest, or vice versa.

Pharmacological inhibition of EZH2 with EPZ6438 with either radiation or TMZ was also assessed. *In vitro* clonogenic assays determined the inhibitory effect of EPZ6438 combined with radiation. DMR showed significantly increased radiosensitivity of E2 treated cells. Indicating the increasing sensitivity of E2 following combined treatment of EPZ6438 with radiation.

Furthermore, the combined treatment of the alkylating agent TMZ with EPZ6438 shows that the two drugs seemingly have a synergistic effect. Interestingly, GSEA revealed that the gene set of DNA repair genes was negatively enriched in G7 cells. This gene set was also negatively enriched in E2 cells, although it didn't reach significance. Based on this data, it is hypothesise that EPZ6438 treatment leads to downregulation of genes involved in DNA repair, thus sensitising the cells to DNA damaging agents such as radiation and TMZ.

In conclusion, treatment with EPZ6438 lead to a reduction in the number of colonies in both GBM cell lines. This did not appear to be due to a significant level of apoptosis, but gene expression analysis indicated it could be due to differentiation of the cells or even induction of senescence. Consistent with above assays, downregulation of genes involved in OxPhos was observed. EPZ6438 also sensitised the cells to the DNA damaging agents' radiation and TMZ. The result detailed above supports further investigation into the mechanism of action of EPZ6438, with a view to its potential use as an anti - tumour agent.

Chapter 5 Efficacy of UNC1999 on GBM cell lines

5.1 Introduction

UNC1999 is orally bioavailable SAM competitive inhibitor that supresses enzymatic activity of EZH2 or EZH1 (Konze *et al.*, 2013). *In vitro* analysis showed potency of UNC1999 in inhibiting proliferation and migration in bladder cancer (Chen *et al.*, 2019). *In vivo* xenograft model treated with UNC1999 exhibited reduction in tumour growth and self renewal in colorectal cancer (Lima-Fernandes *et al.*, 2019). UNC1999 also found to prolong survival of murine Leukemia model *in vivo*. It was observed treatment with UNC1999 re-expressed genes that are usually targeted by the PRC2 complex (Xu *et al.*, 2015).

In this chapter the efficacy of UNC1999 as an EZH2 inhibitor in GBM cells was investigated. Gene expression changes in drug treated cells compared to controls were further examined. All experiments were performed on G7 and E2 cell lines that were grown in stem conditions on Matrigel coated plates.

5.2 Effect of UNC1999 on survival assay and proliferation assay

The effect of increasing concentrations of UNC1999 was evaluated using clonogenic assays in GBM cell lines. Figure 5-1 shows the effect of UNC1999 on colony formation in G7 and E2 cell lines. There was no consistent effect in G7 cell lines at concentrations of 1 μM and below, then colony numbers were reduced at higher concentrations. The E2 cell line was a little more sensitive, with the percentage of colonies decreasing to 73% at 0.5 μM, then higher doses led to complete loss in colony formation. The IC50 was higher in G7 (1.66 μM) compared to E2 (0.73 μM).

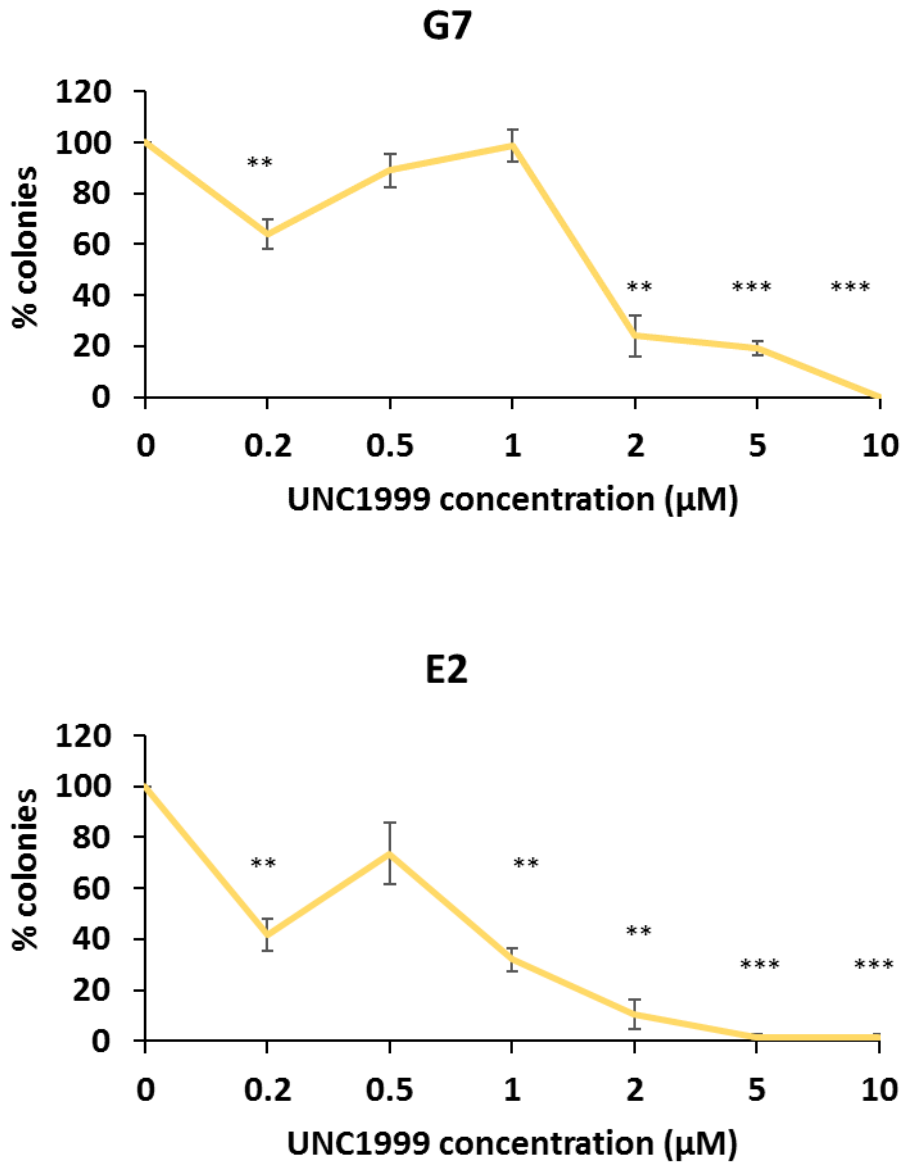

Figure 5-1 Clonogenic survival curves of G7 and E2 exposed to increasing doses of UNC1999.

Cells were seeded on 6 well plates at 250 per well. Cells were incubated with the drug or DMSO for 48 hrs. The drug was then washed out and cells allowed to grow for 14 days. Cells were then fixed, and colonies were counted manually. At each drug concentration cells were seeded in triplicates. A graph is plotted that shows the effect of increasing concentration of UNC1999 on number of colonies formed in G7 and E2. Data points represents mean values and SEM of three independent experiments. p value was determined using student's T test in control vs treated cells. **p ≤ 0.01 and *** p ≤ 0.001.

Viability assays were performed with the Cell Titer Glo kit to determine the effect of increasing dose of UNC1999 on GBM cell lines over the short term (Figure 5-2). The percentage of viable cells in the G7 cell line showed a slight increase at low drug concentrations up to 113% at 0.5 μM, then higher concentrations resulted in a reduction in viable cells. In the E2 cell line, treatment with UNC1999 showed steeper reduction in cell viability, especially at higher concentration that resulted in complete eradication of live cells. In G7 cell, the IC50 was 6.72 μM while in E2 it was 2.86 μM.

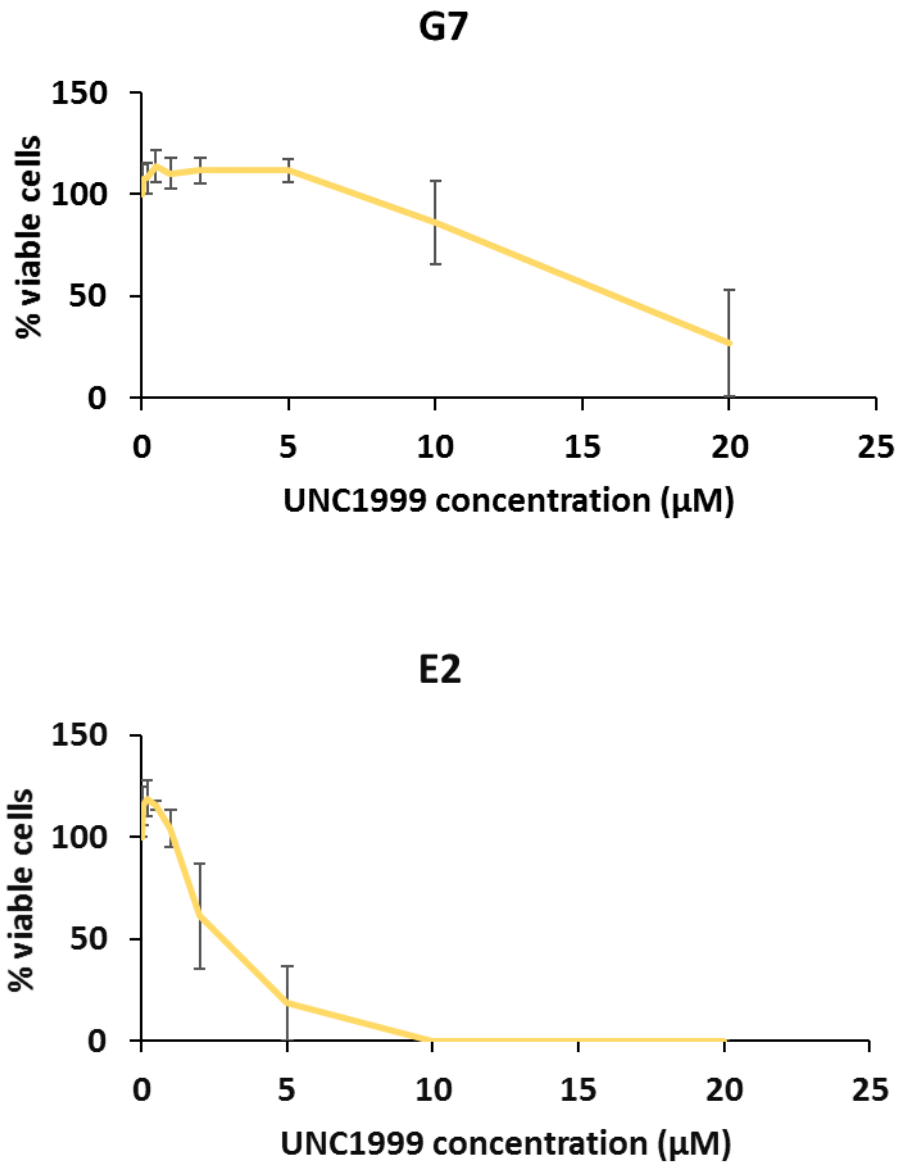

Figure 5-2 Cell viability assay shows the effect of UNC1999 on cell proliferation in G7 and E2 cell lines.

Cells were seeded in triplicate in 96 well plates at 2500 per well in the presence of varying concentrations of UNC1999 and allowed to grow for five days. DMSO at 0.2% was used as the control. The Cell Titer Glo kit (Promega) was used to quantify viable cells. Cell viability was calculated as a percentage of the DMSO control, and results are plotted as the mean value of three independent experiments. Error bars show the SEM.

The combined effect of TMZ and UNC1999 was assessed with clonogenic assays. Cells were incubated with UNC1999 for 24 hrs then with TMZ for 24 hrs. The data shows that the 10 μM TMZ more potently reduced the number of colonies when combined with increasing concentration of UNC1999. Figure 5-3 represents the synergistic effect of TMZ with UNC1999 in G7 and E2 cell lines.

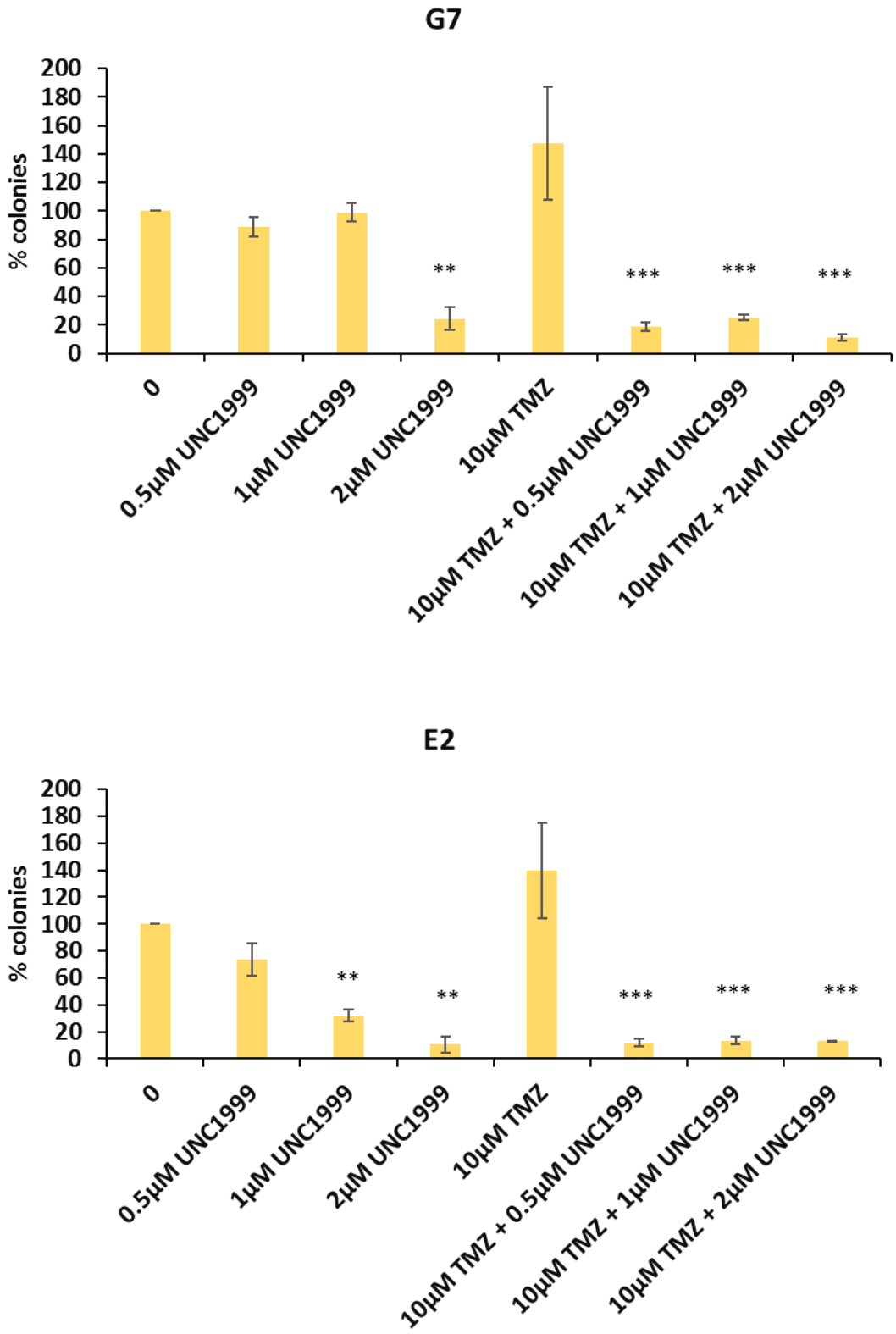

Figure 5-3 Clonogenic assay plots of G7 and E2 shows combined treatment of TMZ with UNC1999 .

The survival assay was performed to determine the ability of treated cells to form colonies. Cells were seeded at 250 / well on Matrigel coated 6 well plates, then incubated with UNC1999 for 24 hrs then with 10 μM TMZ for 24 hrs. Data shows the combined effect of 10 μM TMZ and with increasing dose of UNC1999. Data points represent mean of number of colonies from three independent experiment with error bars representing SEM. Student's T

test was performed to determine the significance of data in control vs treated cells. **p ≤ 0.01 and *** p ≤ 0.001

The effect of UNC1999 on the response of the cells to gamma radiation was investigated using colony assays. G7 and E2 cell lines were exposed to varying concentrations of UNC1999 for 24 hrs then irradiated and allowed to form colonies. Figure 5-4 shows that the survival fraction of GBM cell lines decreased at 3 Gy and higher. Pre-treatment with UNC1999 did not have a significant effect on the survival fraction in G7 cells. However, UNC1999 did significantly decrease colony formation in irradiated E2 cells, especially at 4 Gy and 5 Gy. This effect was apparent even at the lowest dose of UNC1999 tested, where the survival fraction reduced from 0.346% with 5 Gy alone to 0.198% with 5 Gy and 0.5 μM UNC1999. At this concentration, UNC1999 only causes a 27% reduction in colony numbers when used as a single agent (Figure 5-1). This data indicates that UNC1999 sensitises E2 cells to gamma radiation. Table 5-1 shows the values of DMR in G7 (0.88 - 0.94) and E2 (1.17 -1.25). The DMR for G7 was less than 1 indicating cells were less sensitive to radiation after treatment with UNC1999. However, The values of DMR in E2 increased significantly with increasing concentration of UNC1999, indicating that higher concentrations of the drug increases radiosensitivity of E2 cell line.

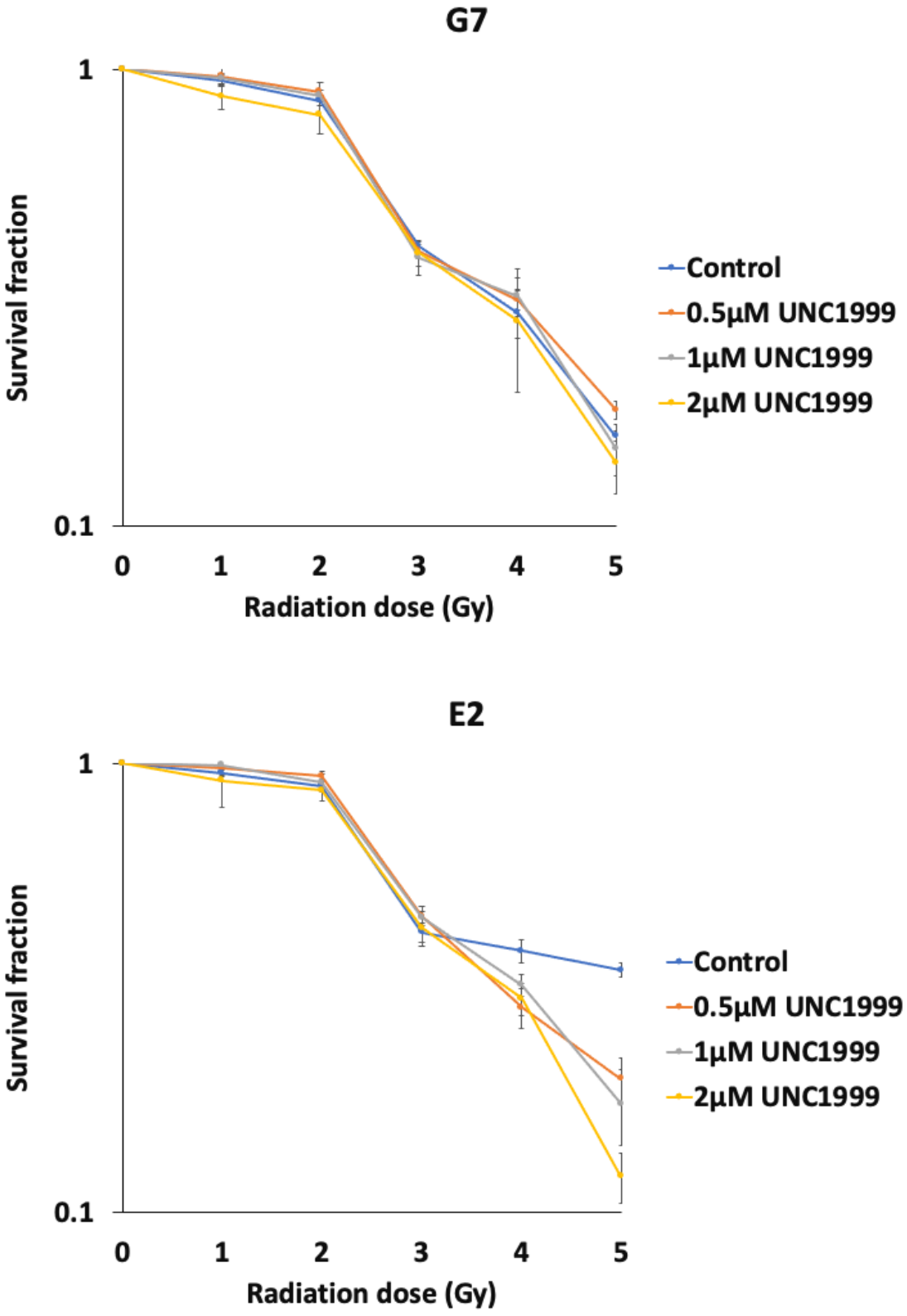

Figure 5-4 Clonogenic survival assay plot showing the combined effect of radiation with UNC1999 on G7 and E2 cells.

The mean survival fraction from three independent colony assay experiment is plotted in a graph, error bars represent SEM. After 24 hrs incubation with different concentration of UNC1999, cells were exposed to different doses of radiation at 0 to 5 Gy for 24 hrs.Cells were fixed then colonies were counted manually. The mean of number of colonies were counted and calculated as survival fraction and plotted in a graph with radiation dose.

G7	$DMR_{(0.37)}$
0.5 μM	0.88
1 μM	0.90
2 μM	0.94

E2	$DMR_{(0.37)}$
0.5 μM	1.17*
1 μM	1.17**
2 μM	1.25**

Table 5-1 These tables represent DMR values of G7 and E2 cell lines.

The DMR represents the dose required to reduce survival fraction to 0.37 in control vs treated with increasing concentration of UNC1999. p value is calculated by comparing the means, sd and n of drug treated with control. * $p \leq 0.05$ and ** $p \leq 0.01$

5.3 Assessment of UNC1999 in senescence and apoptosis assay

To investigate whether UNC1999 induces senescence in the GBM cells, cells were incubated with 2 μM UNC1999 for 5 days and then fixed and stained with ß-galactosidase staining solution. Figure 5-5 (B) shows that the percentage of ß-galactosidase stained cells was significantly increased at 2 μM UNC1999 compared to the DMSO control in G7 and E2 cell lines. The graph indicates induction of senescence in GBM cell lines following treatment with UNC1999.

Flow cytometry was used to assay for early and late apoptosis after 5 days incubation with UNC1999. Figure 5-6 shows that there is no increase in apoptotic cells in the G7 population following EPZ6438 treatment. Indeed, the percentage of dead cells was decreased compared to the DMSO control (< 1.62% and 35.7%, respectively). This is consistent with the cell viability assays shown in Figure 5-2, where 2 μM UNC1999 does not decrease the percentage of viable G7 cells after 5 days, and in fact increases cell numbers to 111% of the control. In contrast, E2 cells had 10.8% of cells in early apoptosis and 38% of cells in late apoptosis after 5 days incubation with 2 μM UNC1999 (Figure 5-6). This is consistent with the 61% reduction in viable E2 cells that was previously observed in Figure 5-2.

A)

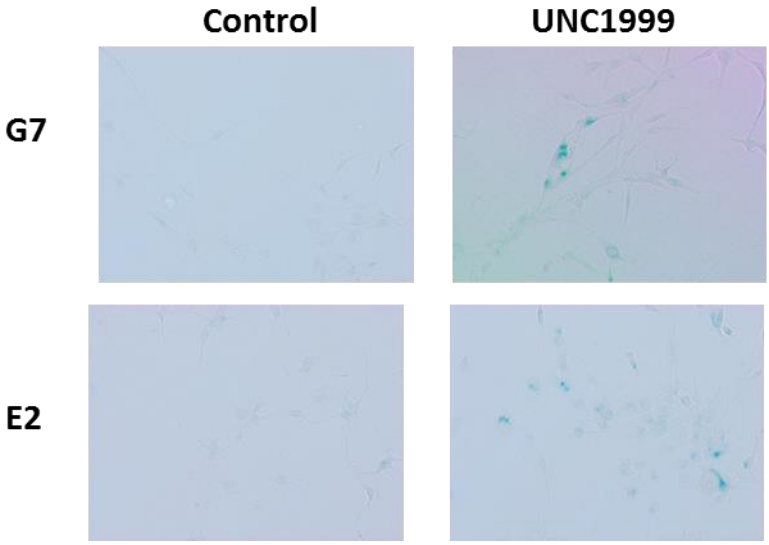

B)

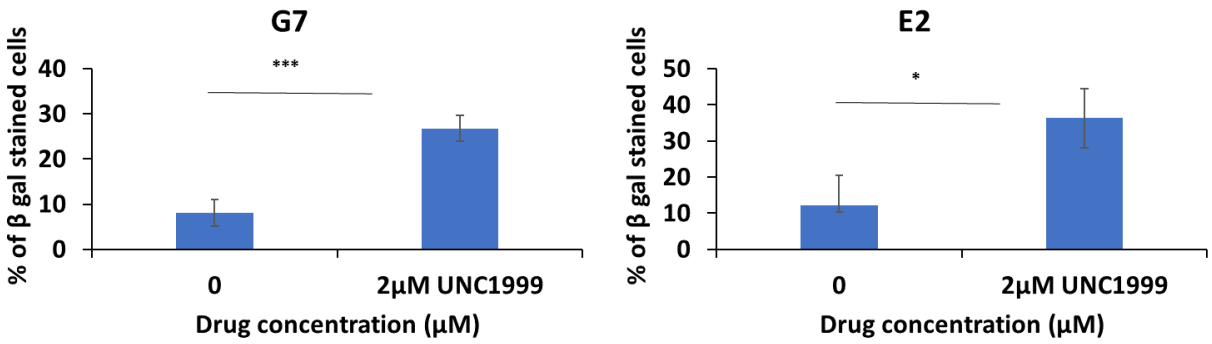

Figure 5-5 Senescence assay plots in G7 and E2 cell line after treatment with 2 μM UNC1999 or corresponding DMSO.

The treated cells were incubated for 5 days the were fixed and stained with β- galactosidase staining solution. Picture of β- galactosidase stained cells (A) was captured using confocal microscope. β- galactosidase positive cells were quantified and plotted in a graph (B) with mean and SEM of three independent experiments, p value was calculated using student's T test. *p ≤ 0.05 and ***p ≤ 0.001.

A)

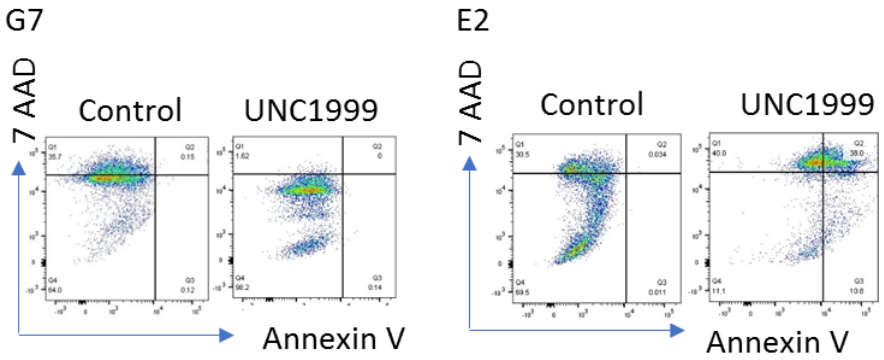

B)

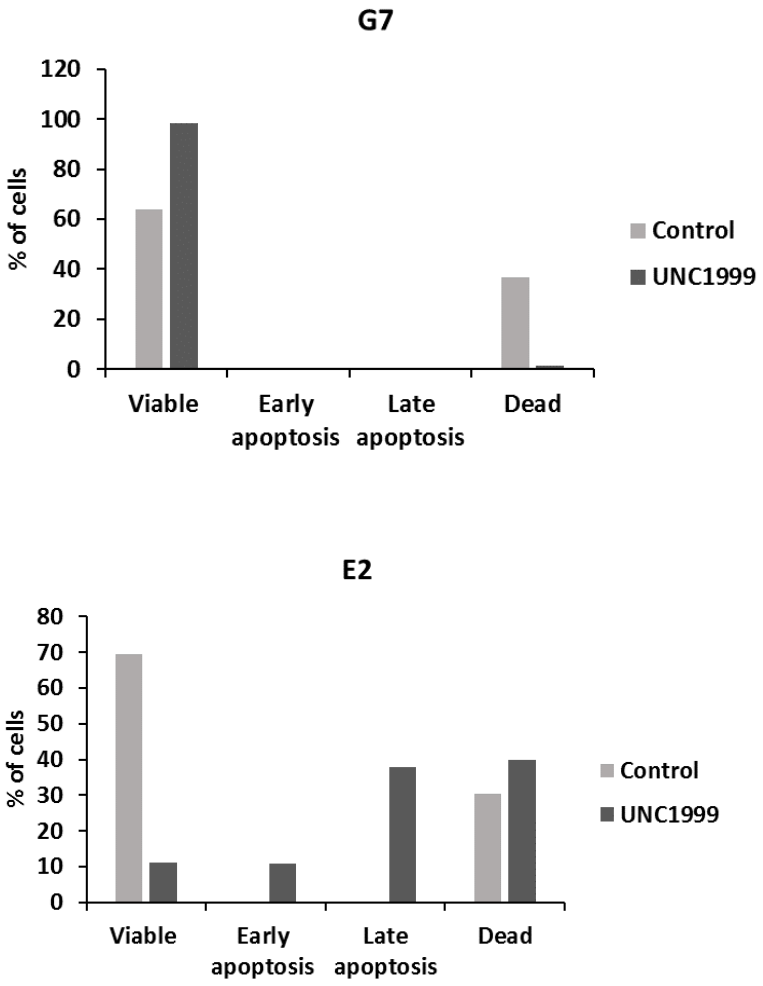

Figure 5-6 Apoptosis assay determining the effect of UNC1999 in G7 and E2 cell lines.

Flow cytometric analysis showing the apoptotic effect of 2 μM UNC1999 in G7 and E2 cell lines. Cells were incubated with the drug for 5 days, then fixed and stained with AnnexinV and 7AAD . The percentage of viable, early apoptosis, late apoptotic and dead cells are

represented in a graph (B). The percentage of cells (A) was plotted as scatter plots showing live (Q4), early apoptosis (Q3), late apoptosis (Q2) and dead cells (Q1) .

5.4 Effect of UNC1999 on genes associated with stemness and tumourgenesis

qRT-PCR was performed to determine whether UNC1999 affects the expression of stem cell marker genes. Figure 5-7 shows the expression of stem and differentiated marker genes in G7 and E2 cells after treatment with increasing concentrations of UNC1999 over 5 days. The relative expression of the *SOX2* and *NESTIN* are elevated in treated G7 and E2 cell lines when compared to the control, particularly at 0.5 μM. In E2 cells the level of the astrocyte maker *GFAP* increases as the drug concentration increases, whereas in G7 cells, *GFAP* expression decreases at the higher drug concentrations. However, these data are from single biological samples so caution should be taken when drawing any conclusions.

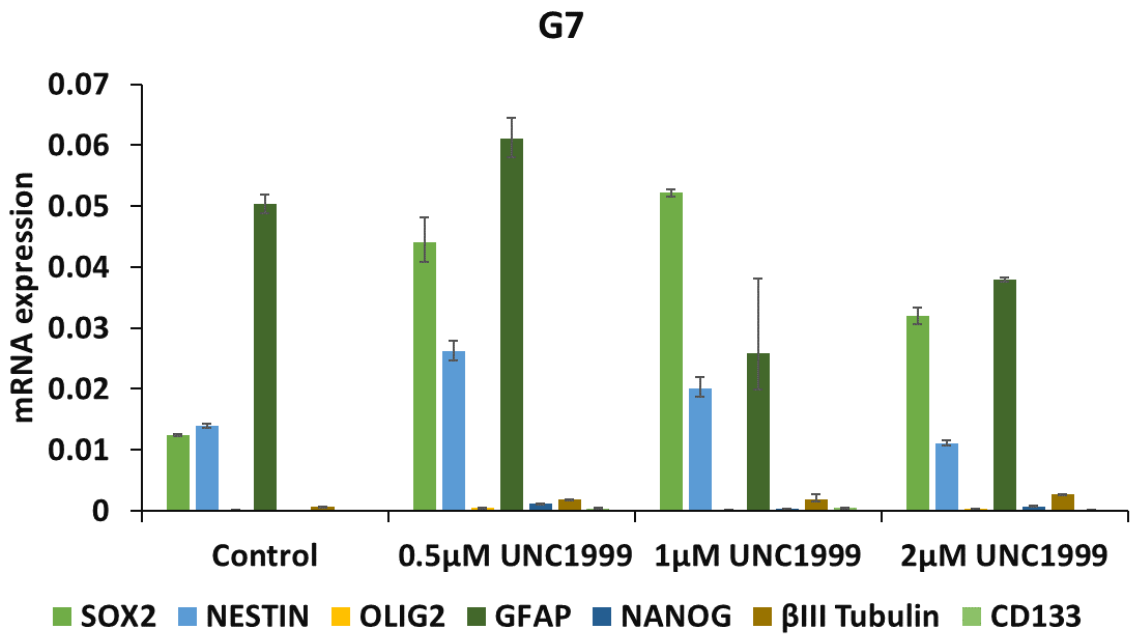

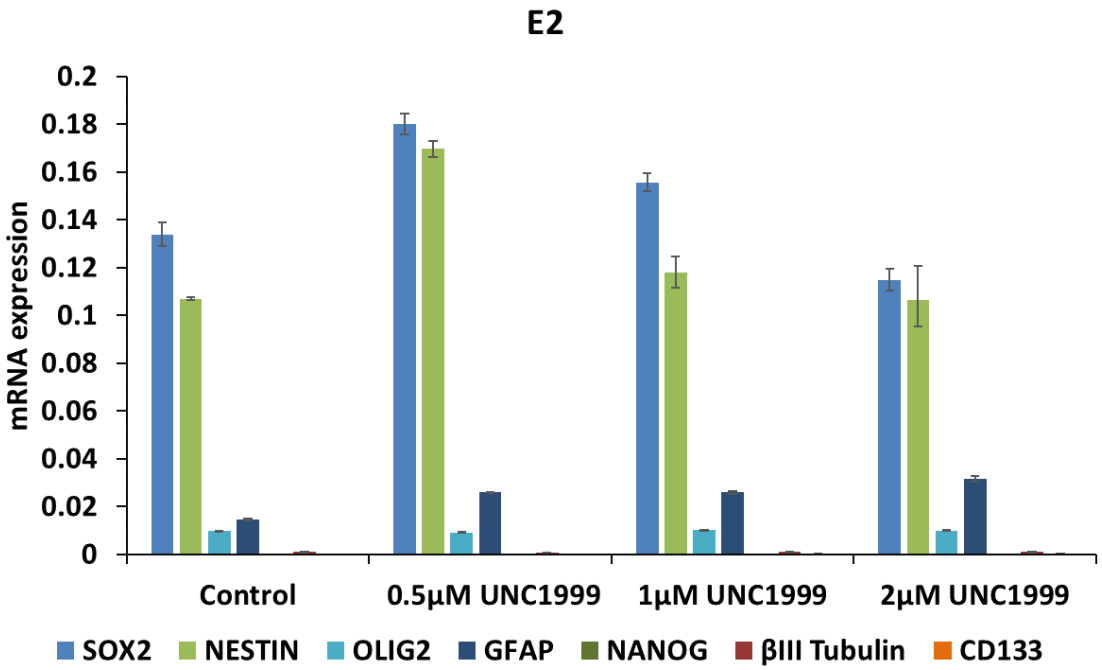

Figure 5-7 The effect of UNC1999 on the level of mRNA expression of stem cell markers and differentiated markers in G7 and E2 cell lines.

qRT-PCR was performed following treatment of G7 and E2 cells with (0.5, 1 and 2 µM) of UNC1999 or corresponding DMSO for 5 days. Data were normalised with β-Actin, the mRNA expression represents the fold change that is calculated from delta Ct with error bars representing SEM. Each RNA sample was loaded into wells in triplicates.

The expression of genes involved in cell cycle regulation and tumorigenesis was also evaluated with qRT-PCR (Figure 5-8). The expression of *P21*, *PTEN* and *CDK2* was found to be elevated in G7 treated cells compared to control, particularly at 2 μM. *CDK2* expression was also elevated in E2 cells, whereas *PTEN* was increased at 0.5 μM but decreased at higher concentrations.

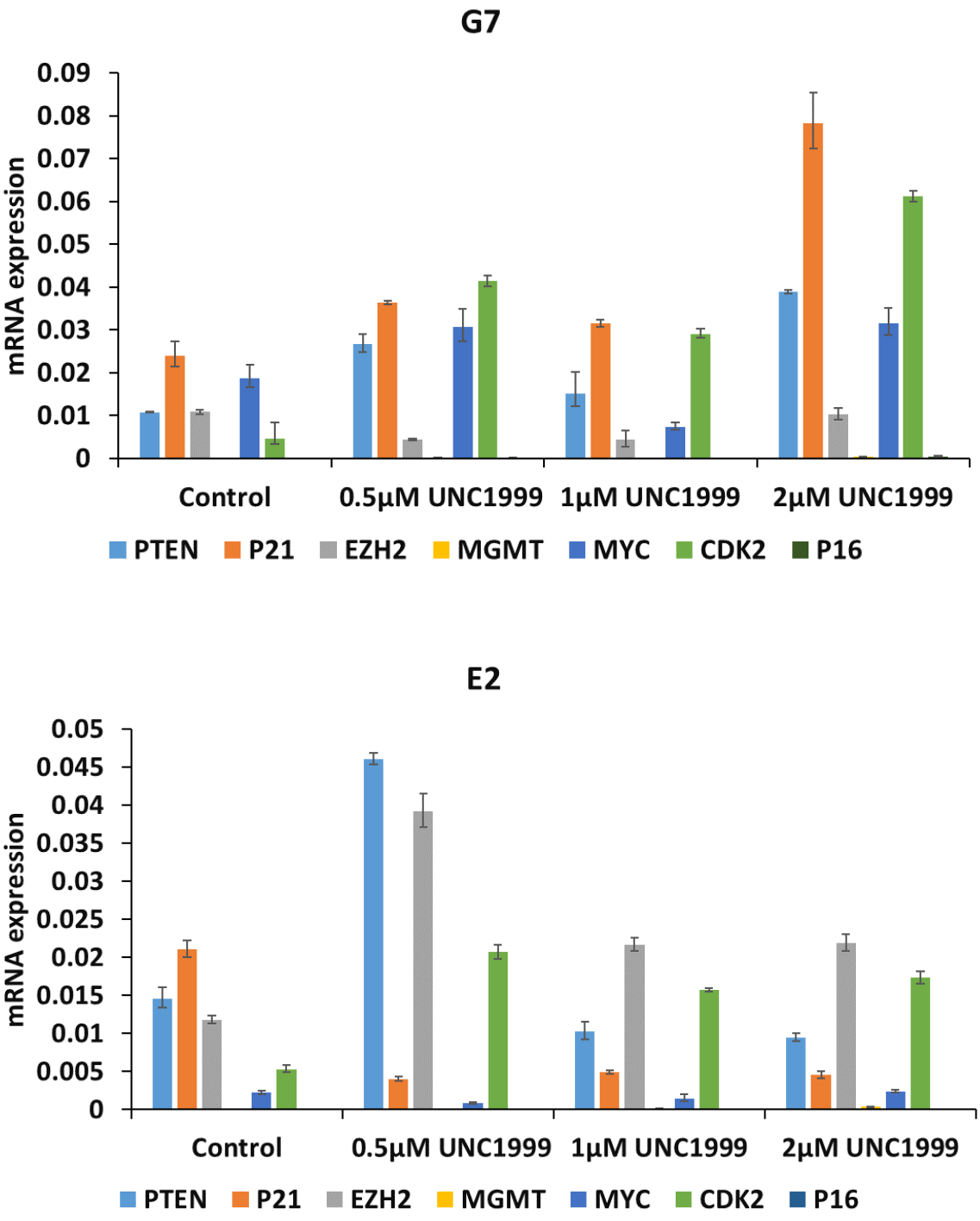

Figure 5-8 The level of mRNA expression of genes involved with cell cycle, apoptosis and senescence in G7 and E2 cell lines exposed to increasing dose of UNC1999.

The mRNA relative expression in G7 and E2 treated with (0.5, 1 and 2 µM) UNC1999 or corresponding DMSO for 5 days were examined with qRT-PCR. Each RNA sample was loaded into wells in triplicates. The mRNA expression represents the fold change that is calculated from delta Ct. Data are normalised with β- Actin, error bars represent SEM.

5.5 RNA sequencing analysis of GBM cells treated with UNC1999

5.5.1 Quality control and data visualisation with Searchlight2

In order to investigate the changes in gene expression on a genome-wide basis, RNA-seq was performed. The concentration of 2 μM UNC1999 was chosen for these experiments as changes in cell survival and gene expression were apparent at this concentration, but there were sufficient surviving and proliferating cells to obtain a high quality RNA sample that should give meaningful gene expression data. Cells were treated with drug or DMSO for 5 days, and RNA samples were collected from three biological replicates. FastQC was used to assess the quality of data. The samples displayed %GC of 50, average PHRED score of 36 and the percentage of mapped reads was typically 95%.

RNA-seq data was aligned to the Hg38 genome using Hisat2, Stringtie was used to assemble and quantity transcripts, and Deseq2 was used to generate a statistical model of the transcript distribution and calculate the differences in expression between drug treated and control samples. The RNA-seq analysis of E2 treated and control showed variability between the three replicates. The analysis was repeated with one of the E2 replicate was excluded in both treated and control samples. PCA plots of RNA-seq samples treated with 2 μM UNC1999 and control were illustrated in Figure 5-9 . In G7, the PCA plot showed that second and third replicates are closer together than first replicate in both treated and control groups. Whereas PCA plot for E2 showed that treated samples formed good cluster unlike control samples.

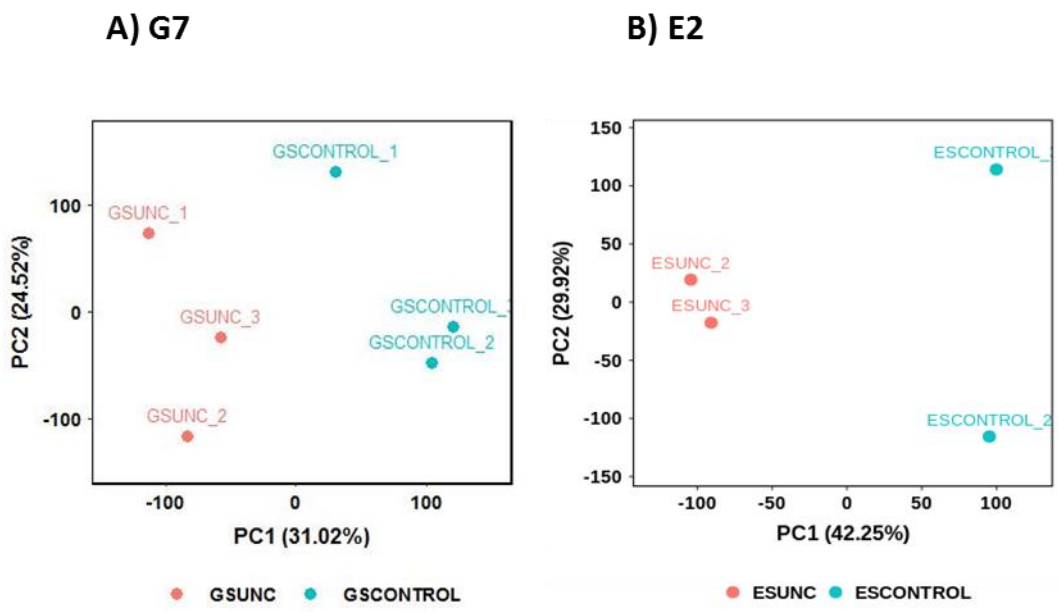

Figure 5-9 PCA plots for G7 and E2 lines treated with 2 μM UNC1999 and control.

The total variation percentage explained by each component is given in the x and y axis. The scatterplot represents two sample groups; control and treated that is distributed and presented as dots. The blue dots indicate control group while red dots present the treated group. The values of expressed genes were transformed using the z-score , prior to the PCA plot.

Figure 5 -10 shows the MA plot of the Log2 fold change and normalised mean expression in for all genes in G7 and E2 cells. Significantly upregulated genes are shown in red above the x axis, and significantly downregulated genes are shown in red below the x axis. It can be seen that there are more DEGs in the G7 cells than in the E2 cells.

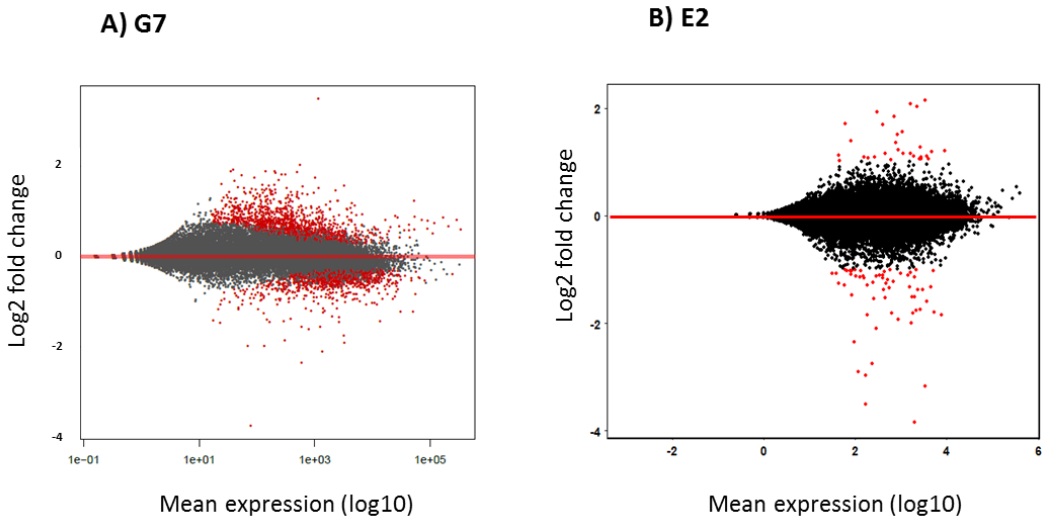

Figure 5-10 MA plots of G7 and E2 treated with UNC1999 .

The MA plot shows the relationship between the mean expression of each gene and its fold change. The plots were created by Deseq2 using RNA-seq data. The x axis indicates the normalised mean expression from all samples, while the y axis indicates the Log2 fold change between treated and control. Significantly changed genes are shown in red and non−significant genes in black.

The hierarchical clustered heatmaps show the significant DEGs in control and UNC1999-treated G7 and E2 cells. The replicates are presented in the G7 and E2 heatmaps (Figure 5-11) as being clustered together into control and treated groups. The figure demonstrates that the differences in expression for the significant DEGs are consistent across all replicates.

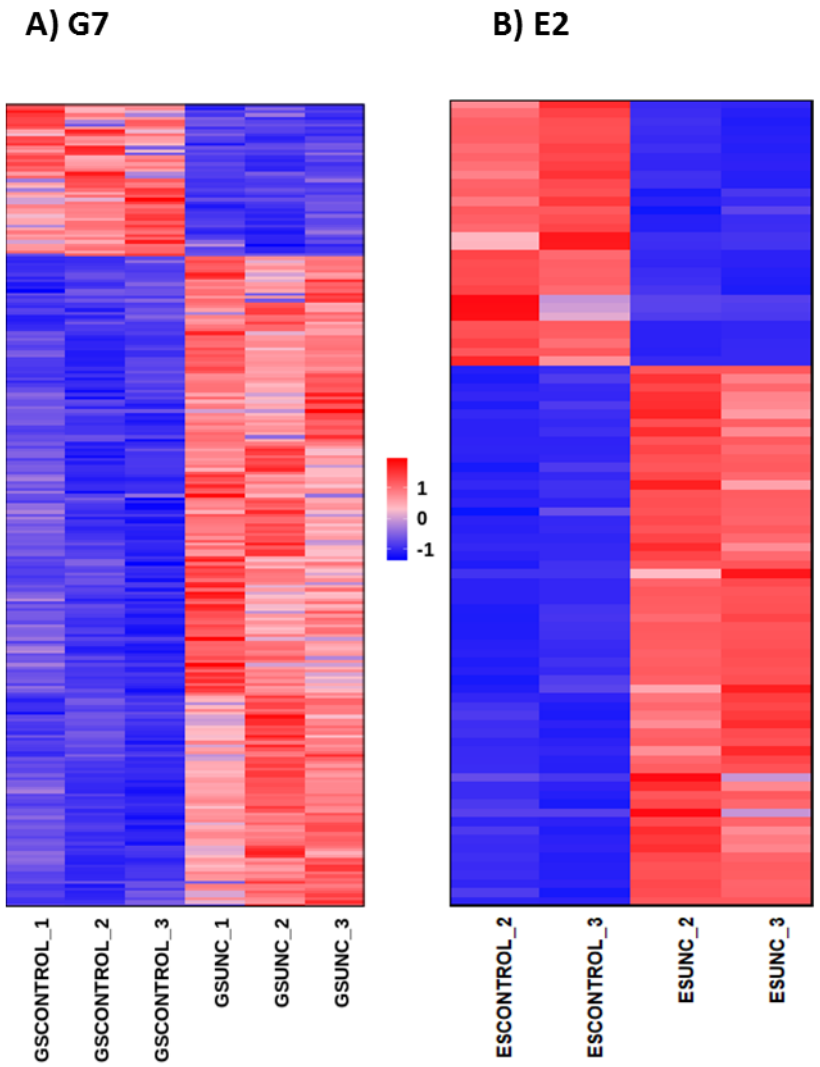

Figure 5-11 Significant genes heatmaps of G7 and E2 treated with 2 μM UNC1999 and controls.

The plot is generated using Deseq2 files that were modifies and uploaded into Galaxy server Antioch using searclight2. The output file was visualised using R program. Gene expression is represented in a hierarchical cluster heatmap (Spearman) with p value < 0.05. The intensity of the colour represents gene expression with Red indicating upregulated genes and blue represent downregulated genes.

5.5.2 Pathway analysis with GO

DEGs with an adjusted p value of less than 0.05 were taken forward into GO analysis in order to get an overview of the pathways and processes that were altered following UNC1999 treatment. Upregulated DEGs (893 for G7 and 370 for E2) were considered separately from downregulated DEGs (661 for G7 and 478 for E2), as this gives more meaningful GO data. Figure 5-12 shows the biological process GO categories that were significantly enriched in the lists of upregulated and downregulated DEGs from G7 cells. It can be seen that most of the GO categories for the upregulated genes are related to neurogenesis, neuron morphology and neuronal function. GO categories enriched in the downregulated genes in G7 cells are mainly related to RNA processing, ribosome function, cell number homeostasis and organelle organisation.

The GO analysis for E2 DEGs showed 31 significantly upregulated and 34 significantly downregulated genes in biological process categories. Most of upregulated genes were associated with metabolic and catabolic processes. Whereas downregulated biological processes were mostly involved in cell cycle processes, cell division, DNA replication and DNA repairs (Figure 5-13).

a)

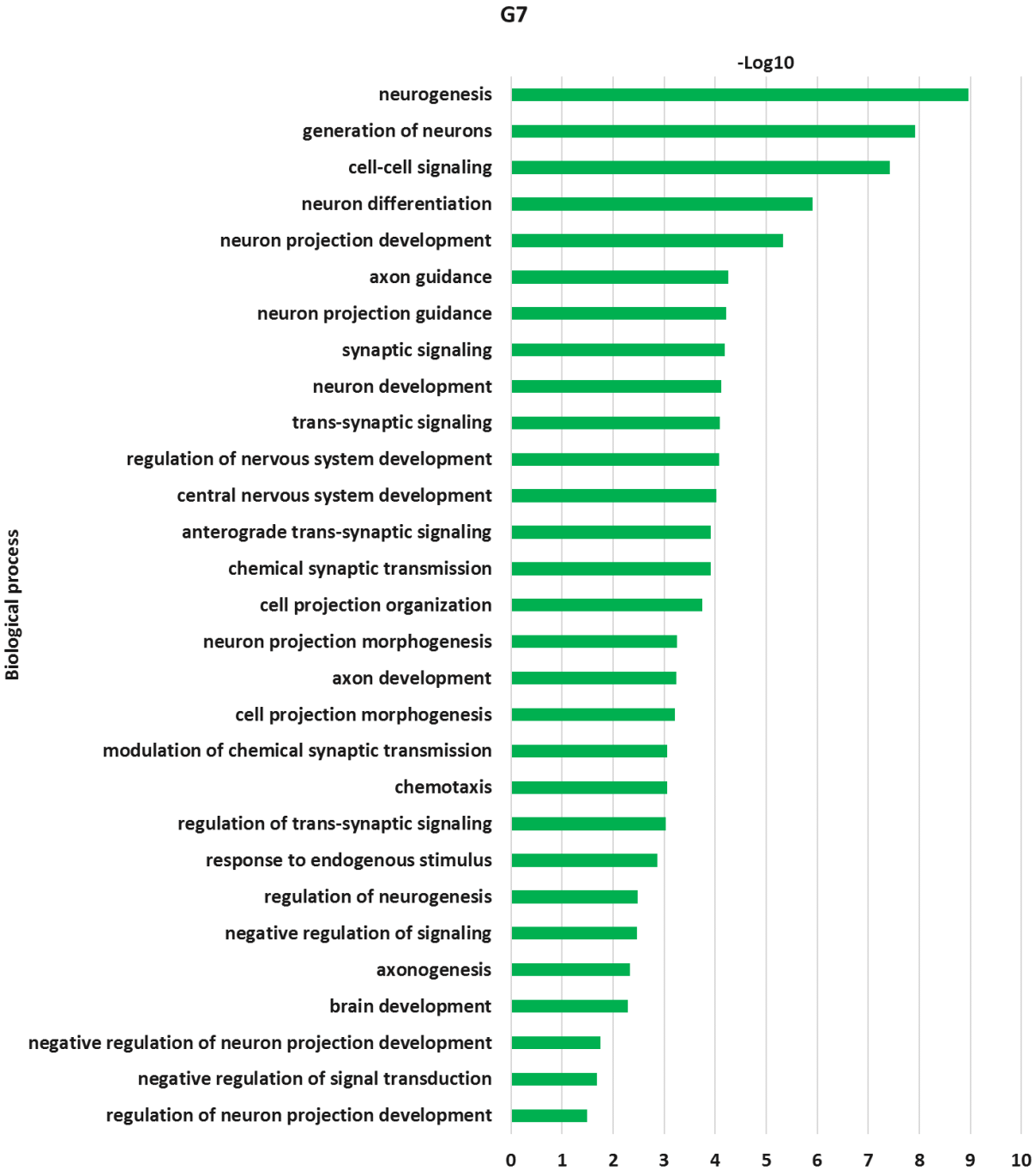
G7
-Log10
Biological process
neurogenesis
generation of neurons
cell-cell signaling
neuron differentiation
neuron projection development
axon guidance
neuron projection guidance
synaptic signaling
neuron development
trans-synaptic signaling
regulation of nervous system development
central nervous system development
anterograde trans-synaptic signaling
chemical synaptic transmission
cell projection organization
neuron projection morphogenesis
axon development
cell projection morphogenesis
modulation of chemical synaptic transmission
chemotaxis
regulation of trans-synaptic signaling
response to endogenous stimulus
regulation of neurogenesis
negative regulation of signaling
axonogenesis
brain development
negative regulation of neuron projection development
negative regulation of signal transduction
regulation of neuron projection development
0
1
2
3
4
5
6
7
8
9
10

b)

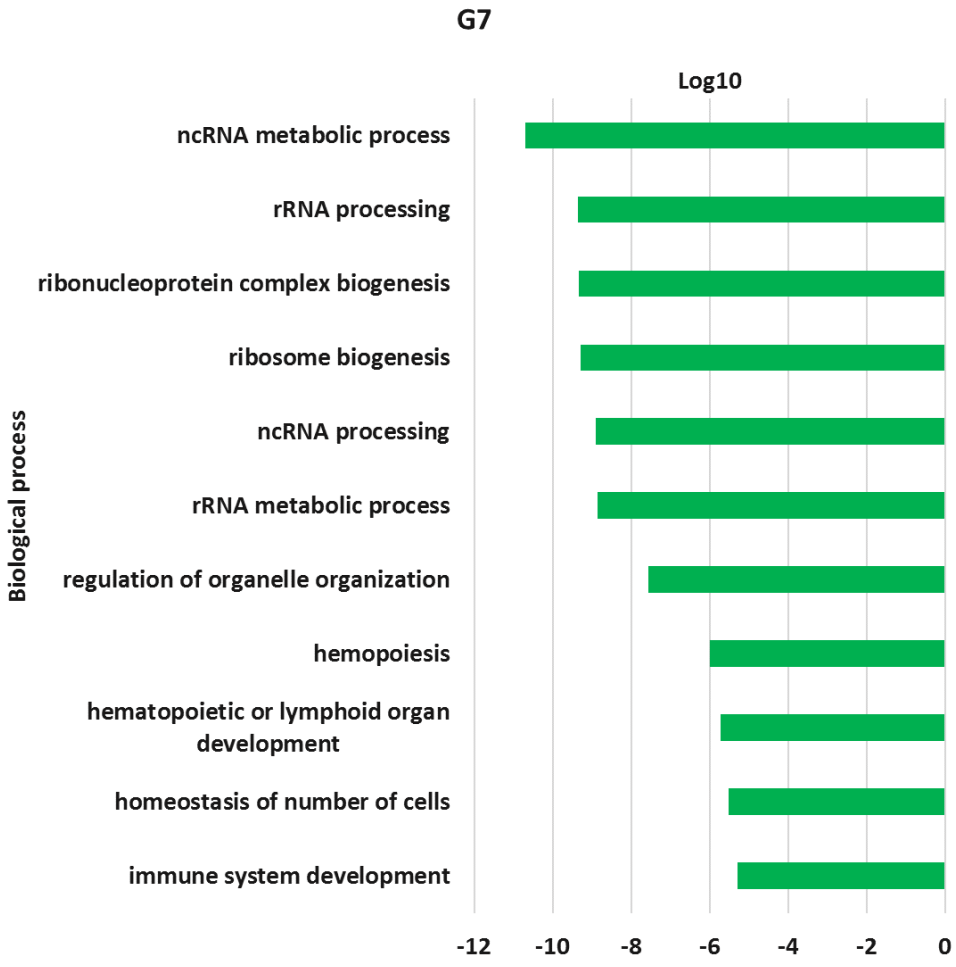

Figure 5-12 Significantly enriched GO biological processes in G7 cells treated with 2 μM UNC1999.

GO analysis (biological processes) was performed using Toppgene. Significantly upregulated (a) and downregulated (b) biological process categories with q value (Bonferroni) < 0.05 are shown. The upregulated categories have a positive value (- Log10 q value) and downregulated categories have a negative value (Log10 q value). The GO analysis was performed on DEGs (adj p value < 0.05), treating upregulated genes (Log2 fold change > 0) and downregulated genes (Log2 fold change < 0) separately.

a)

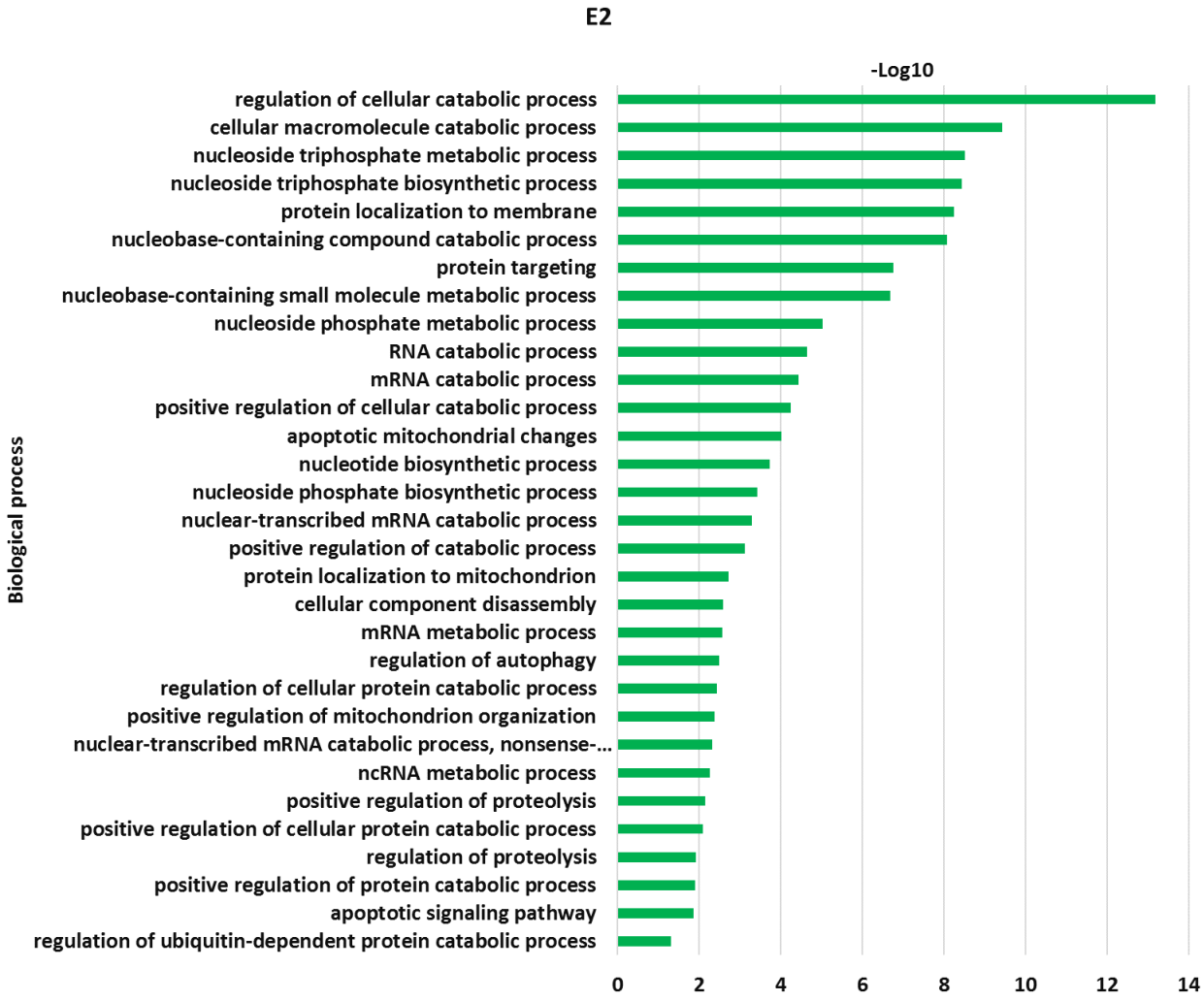
E2
-Log10
Biological process
regulation of cellular catabolic process
cellular macromolecule catabolic process
nucleoside triphosphate metabolic process
nucleoside triphosphate biosynthetic process
protein localization to membrane
nucleobase-containing compound catabolic process
protein targeting
nucleobase-containing small molecule metabolic process
nucleoside phosphate metabolic process
RNA catabolic process
mRNA catabolic process
positive regulation of cellular catabolic process
apoptotic mitochondrial changes
nucleotide biosynthetic process
nucleoside phosphate biosynthetic process
nuclear-transcribed mRNA catabolic process
positive regulation of catabolic process
protein localization to mitochondrion
cellular component disassembly
mRNA metabolic process
regulation of autophagy
regulation of cellular protein catabolic process
positive regulation of mitochondrion organization
nuclear-transcribed mRNA catabolic process, nonsense-...
ncRNA metabolic process
positive regulation of proteolysis
positive regulation of cellular protein catabolic process
regulation of proteolysis
positive regulation of protein catabolic process
apoptotic signaling pathway
regulation of ubiquitin-dependent protein catabolic process
0
2
4
6
8
10
12
14

b)

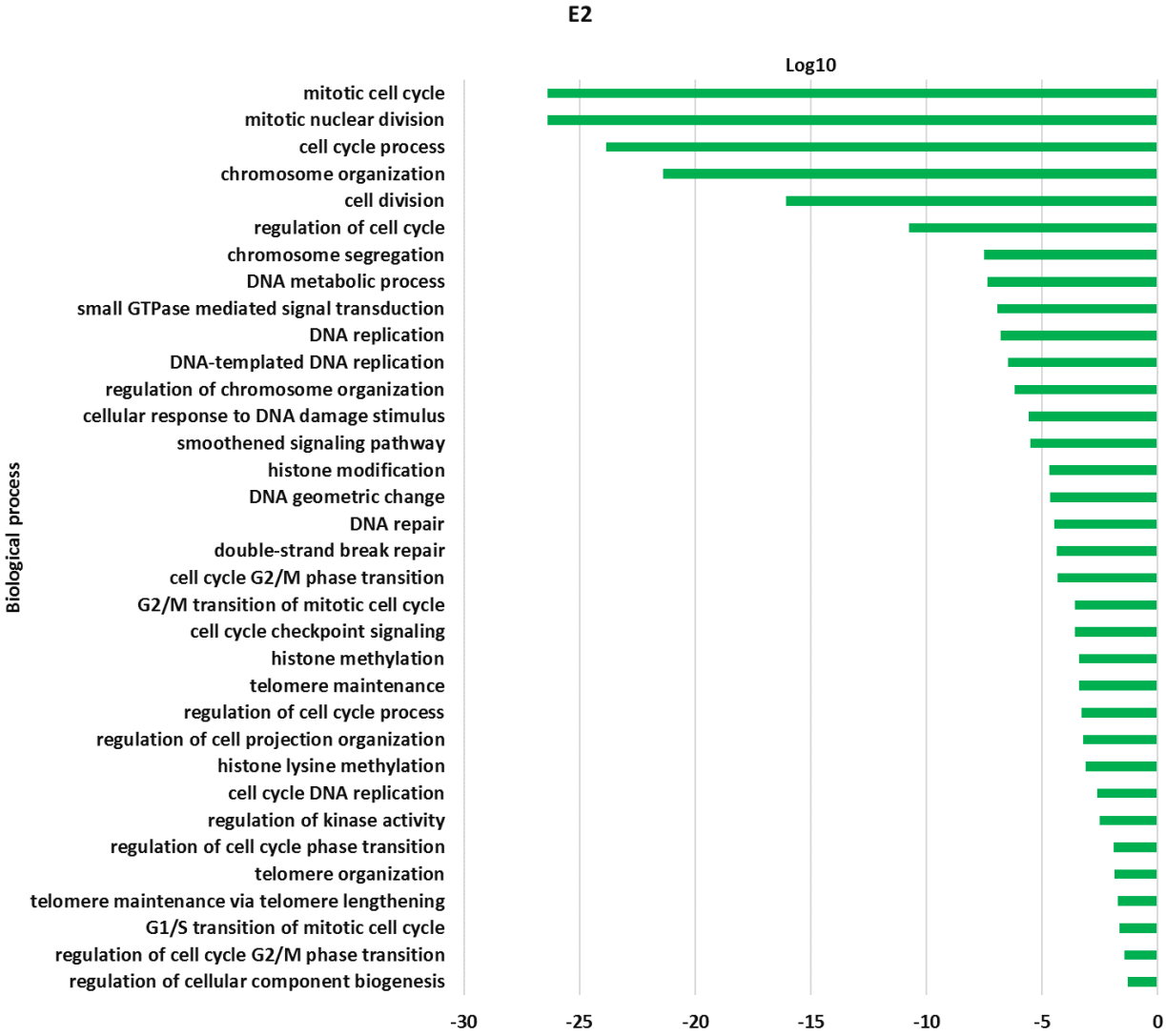

Figure 5-13 Significantly enriched GO biological processes in E2 cells treated with 2 μM UNC1999.

GO analysis was performed using Toppgene. Significantly upregulated (a) and downregulated (b) biological process categories with q value (Bonferroni) < 0.05 are shown. The upregulated categories have a positive value (- Log10 q value) and downregulated categories have a negative value (Log10 q value). The GO analysis was performed on DEGs (adj p value < 0.05), treating upregulated genes (Log2 fold change > 0) and downregulated genes (Log2 fold change <0) separately.

5.5.3 Comparative analysis with InteractiVenn and GO

The common significantly upregulated and downregulated genes in G7 and E2 cell lines were illustrated in Venn diagrams. The comparative analysis with InteractiVenn identified 22 significantly upregulated genes common between G7 and E2 cell lines (Figure 5-14 (A)). Both cell lines had 10 common significantly downregulated genes as shown in Figure 5-14 (B). The GO analysis showed only 4 significant upregulated biological process common in both cell lines. The Figure 5-15 shows two common biological processes were related to neurogenesis, one related to central nervous system development and one associated with regulation of multicellular organismal development . The overlap significance was determined by calculating the representation factor of upregulated common genes (4.3) and downregulated common genes (1.9). Indicating more significant overlaps between G7 and E2 cells.

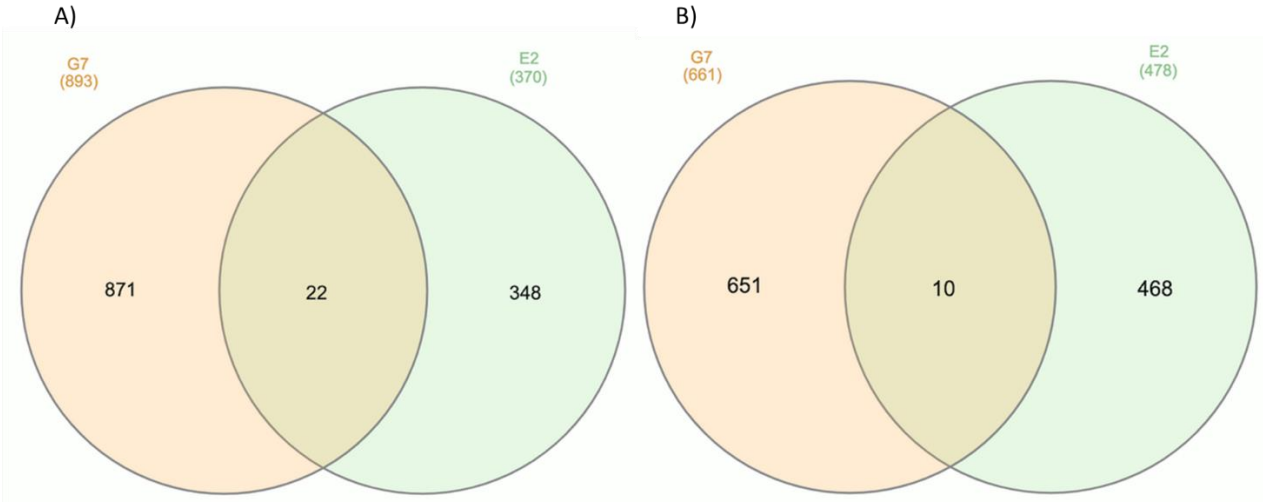

Figure 5-14 Venn diagram of upregulated (A) and downregulated (B) genes in G7 and E2 cell lines treated with UNC1999.

The Deseq2 result file was filtered, the adj. p value < 0.05: Log2 fold change > 0, resulting upregulated genes; and Log2 fold change < 0 resulting in downregulated genes. The list of upregulated and downregulated genes was run through InteractiVenn to show common genes associated in both cell lines. . p value was determined by calculating the representation factor of overlapped genes for both upregulated and downregulated genes. p ≤ 0.001.

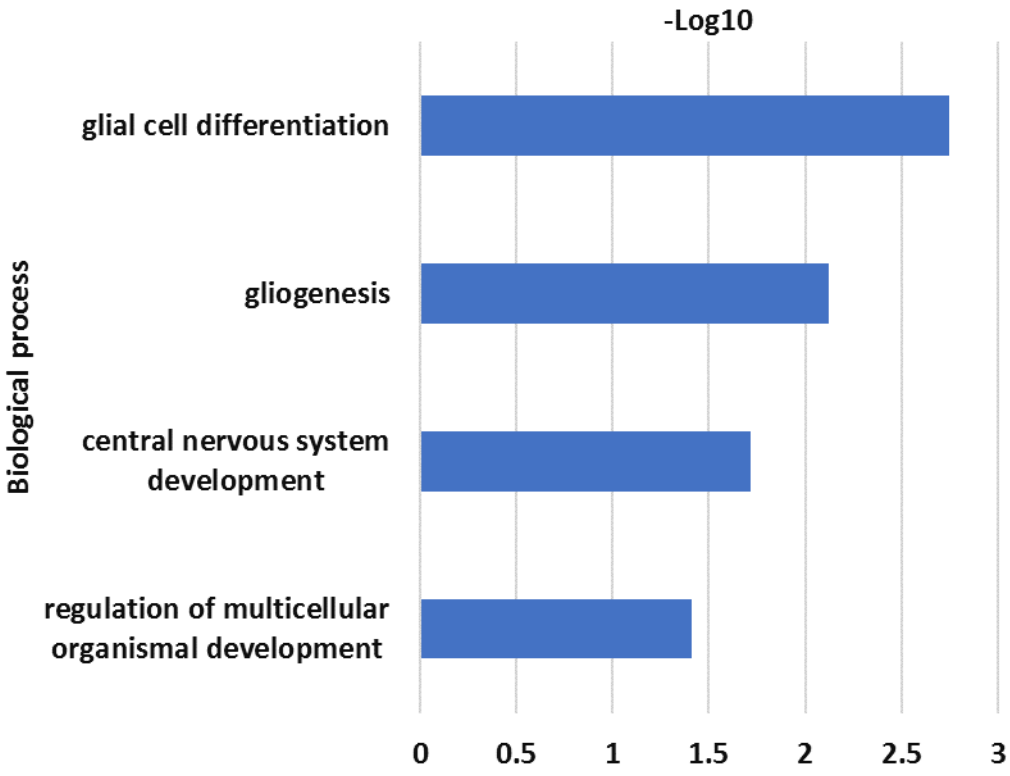

Figure 5-15 Biological process significantly upregulated in both G7 and E2 cell lines treated with UNC1999.

GO analysis was performed on list of upregulated common genes in G7 and E2 treated that is obtained from InteractiVenn analysis. The horizontal graph is plotted with - Log10 on x axis that is calculated from q value Bonferroni and biological process on y axis. The list biological process was filtered on excel with q value (Bonferroni) < 0.05.

5.5.4 Pathway analysis with GSEA

GSEA analysis was carried out on data from G7 and E2 cell using the Hallmarks list of gene sets, as previously described in chapter 4. G7 cells treated with 2 μM UNC1999 identified 9 positive enrichment gene sets and 8 negatively enriched gene sets. Figure 5-16 is a horizontal bar chart plotting the normalised enrichment score for gene sets from G7 cells that have a NOM p value < 0.05 and FDR q value < 0.25. The Hallmark gene set of genes expressed in pancreatic beta cells is the most positively enriched (FDR q value 0.034), and Hallmark gene set of MYC target genes is the most negatively enriched (FDR q value 0) in G7 as shown in Figure 5-17.

a)

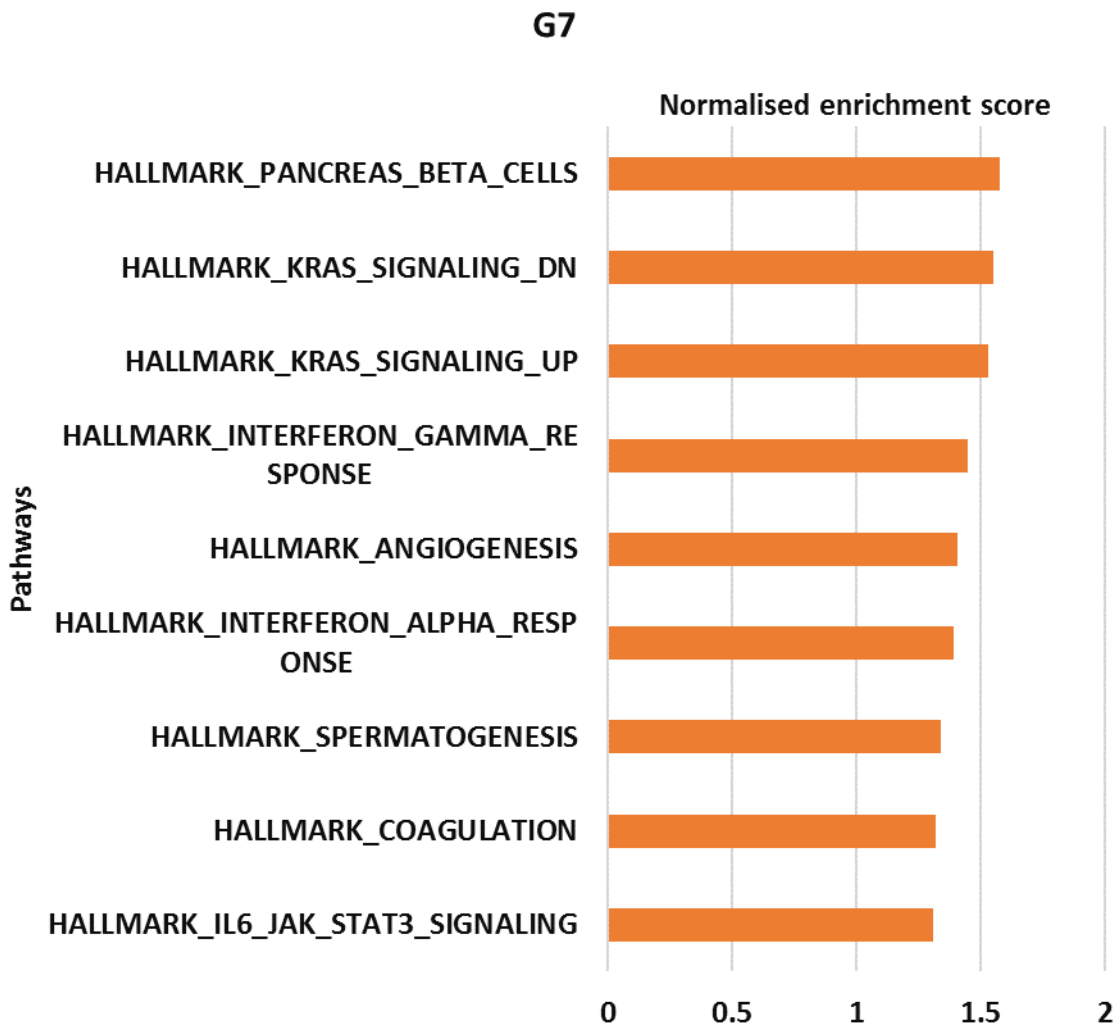

b)

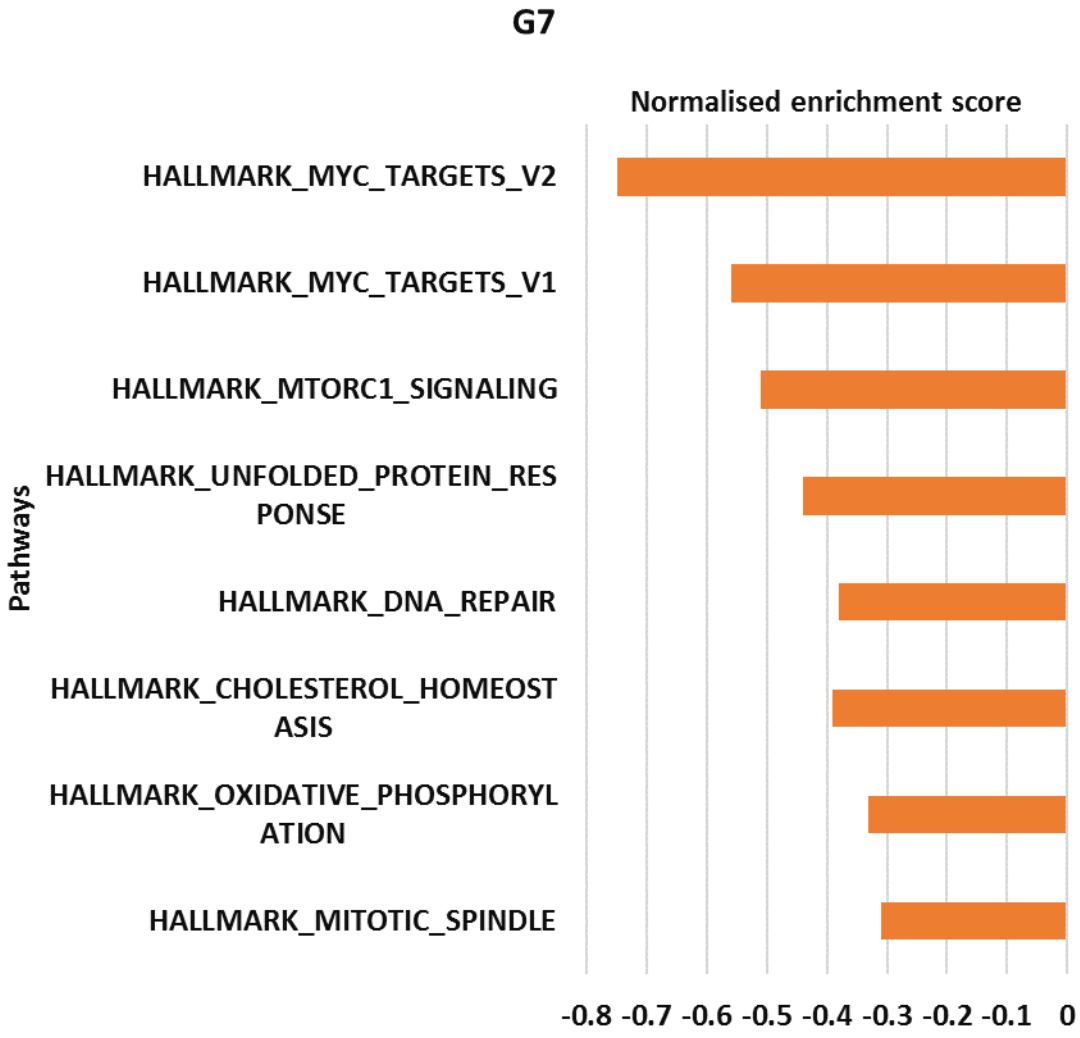

Figure 5-16 Bar plot of significantly enriched GSEA in G7 treated with 2 μM UNC1999. showing hallmarks gene sets.

The plot represents significant gene sets that was filtered using GSEA report output file with NOM p value < 0.05 and the FDR < 0.25. Normalised enrichment score (NES) is indicated on x axis that is plotted against gene sets represented on y axis.. NES > 0 indicates gene sets that are positively enriched (a) while NES < 0 indicates gene set represents negatively enriched (b) in G7 cell line.

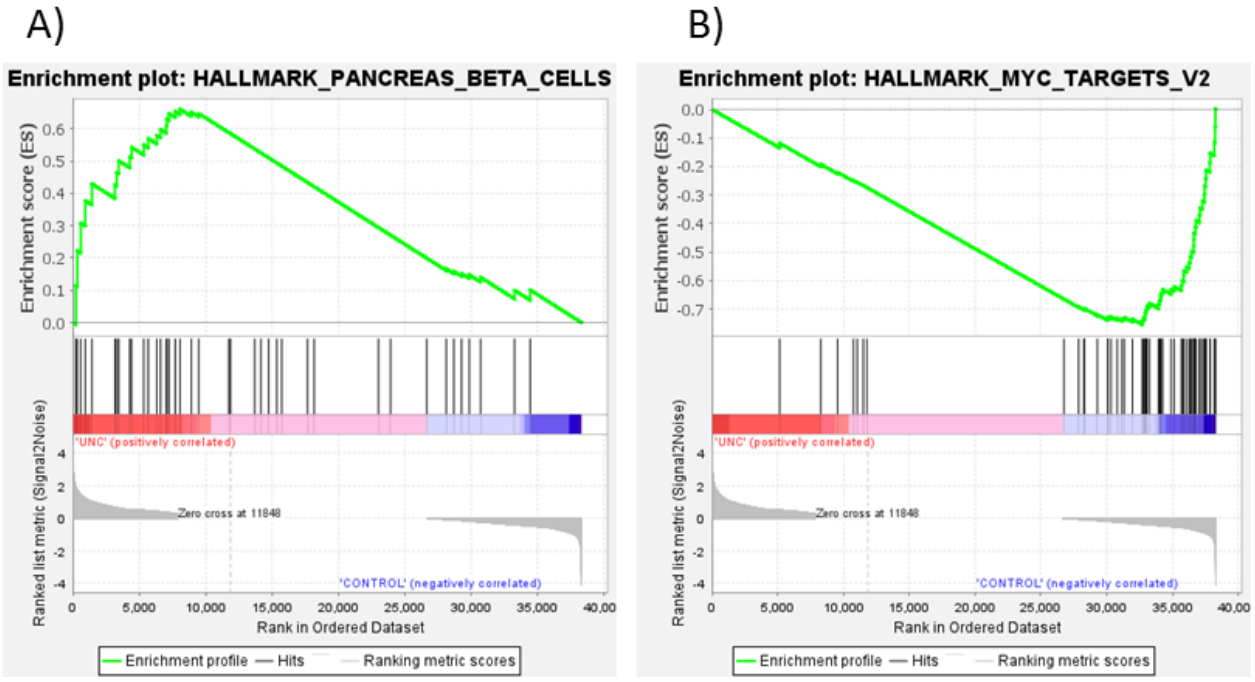

Figure 5-17 The two plots of GSEA showing enrichment in G7 treated with 2 μM UNC1999 and G7 Control.

The ES is indicated as the green curve, the final ES score is indicated at the peak of the curve of that gene set. The top positive enriched plot (A), and the top negative enriched plot (B) of the GSEA horizontal bar. The plot is obtained from GSEA output file after running Deseq2 count file through GSEA software.

The GSEA analysis of E2 cells treated with 2 μM UNC1999 only presented 6 positively enriched gene sets with NOM p value < 0.05 and FDR q value < 0.25 (Figure 5-18). The GSEA plot in Figure 5-19 shows top positively enriched Hallmark gene set of Estrogen response early. No comparative analysis was found to identify significantly positive and negative enriched gene sets in both cell lines treated with 2 μM UNC1999.

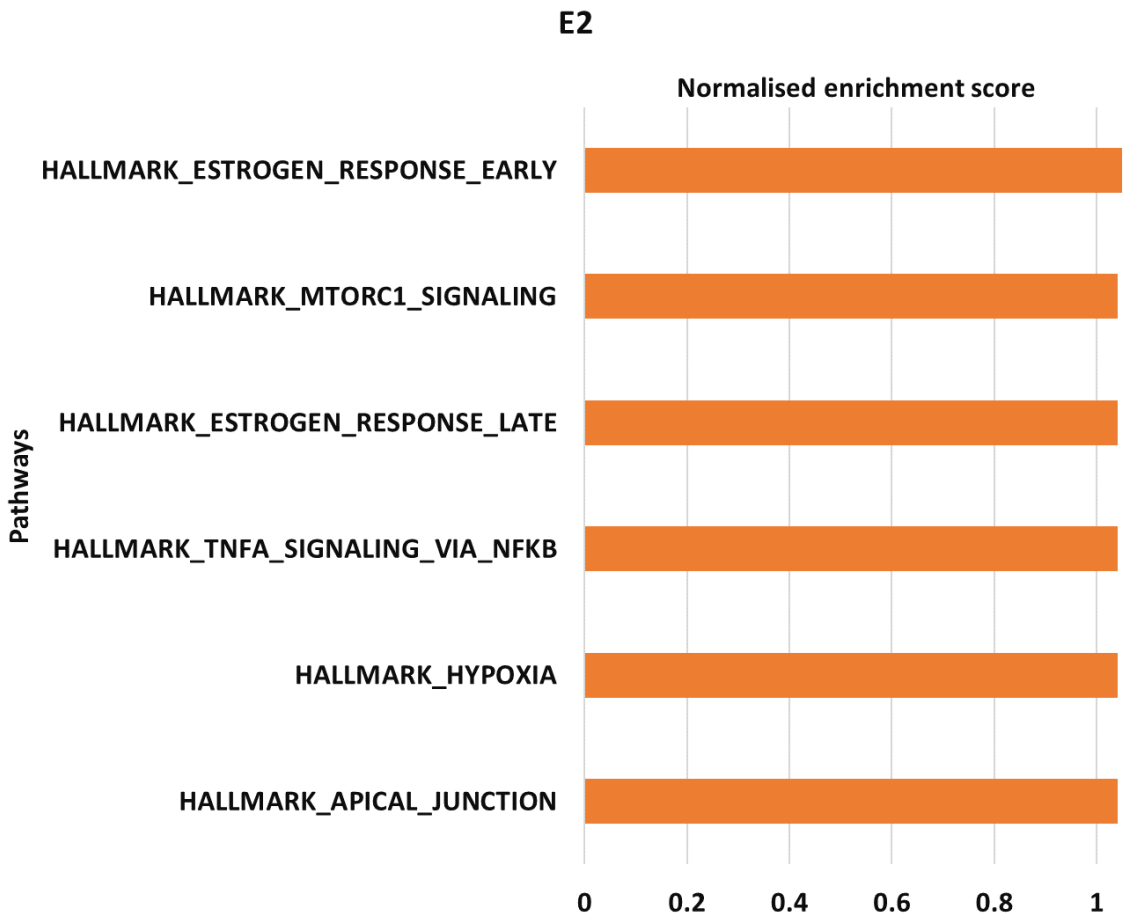

Figure 5-18 Enriched GSEA is plotted in a graph that showing hallmarks gene sets in E2 treated with 2 μM UNC1999.

The plot represent significant gene sets that was made with NOM p value < 0.05 and the FDR < 0.25 obtained from GSEA report output file of E2 treated cells . Normalised enrichment score (NES) is indicated on x axis while gene sets represented on y axis. NES > 0 indicates gene sets that are positively enriched in E2 treated cells.

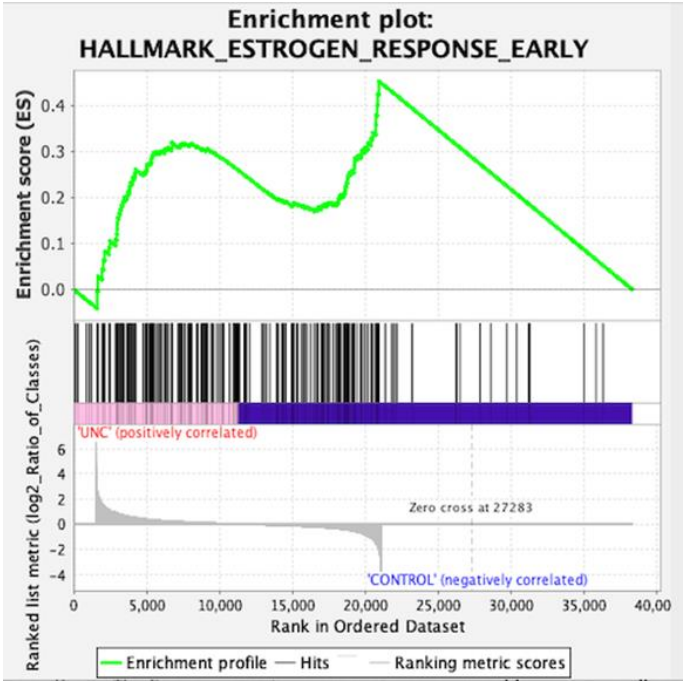

Figure 5-19 The enriched plot of GSEA in E2 treated with 2 μM UNC1999 and E2 Control.

The Deseq2 count file was modified and ran through GSEA software to generate GSEA top positive enriched plot of the horizontal bar. The ES is indicated as the green curve, the final ES score is indicated at the peak of the curve of that gene set.

5.6 Discussion

In this chapter the efficacy of UNC1999 was investigated in GBM cell lines. The clonogenic and proliferation assays was determined following treatment with increasing concentration of UNC1999. The survival assay showed detrimental effect of UNC1999 especially at higher concentration. However, UNC1999 showed to have more potency on proliferation rate in E2 cell compared to G7 cell line. The survival rate was also measured following combined treatment with GBM conventional therapies. The synergistic effect of UNC1999 combined with 10 μM TMZ was evaluated with clonogenic assays. The two drugs worked together to eliminate colonies formed enhancing the mechanism of action of one another. In addition, combined UNC1999 with radiation demonstrated inhibition of survival rate at higher doses in E2 cells. In E2 cells, the DMR values showed increased radiosensitivity of cells with increasing concentration of UNC1999. Thus, indicating that UNC1999 sensitises E2 to radiation.

The effect of UNC1999 on inducing senescence and apoptosis was assessed. The percentage of cells expressing senescence-associated ß-galactosidase was significantly elevated following exposure to UNC1999 in both G7 and E2 cell lines. However, senescence-related categories were not enriched in GO or GSEA analysis. Flow cytometry did not detect apoptosis in the G7 population, but did detect up to 40% of cells in early or late apoptosis in the E2 population. This difference between the G7 and E2 is consistent with the greater sensitivity of E2 cells to UNC1999 as shown by the colony and cell viability assays.

GO analysis of upregulated genes in G7 cells revealed many significantly enriched categories related to neurogenesis and neuronal characteristics. As previously discussed in Chapter 4, G7 cells treated with EPZ6438 also showed upregulation of genes involved in neurogenesis and neuronal structure and function. Thus, it appears that both UNC1999 and EPZ6438 may cause G7 cells to differentiate down neuronal-related pathways. The GO analysis of E2 showed upregulation of genes involved in catabolic and metabolic processes unlike E2 treated EPZ6438 that did not show any significant biological process.

GSEA analysis of UNC1999 treated G7 cells revealed enrichment in targets of KRAS and IL6 signalling. This implies that KRAS and IL6 signalling is upregulated

in these cells, and could be driving the increase in expression of neurogenesis and neuronal-related genes. These pathways were also enriched in the EPZ6438-treated cells (Chapter 4), as was the negative enrichment of gene sets for MYC target genes and genes involved in DNA repair.

In E2 cells, the gene sets enriched following UNC1999 treatment included upregulation of mTORC1 and TNFA signalling both Hallmarks have roles in neurogenesis. GSEA analysis also showed upregulation of Hallmarks of Hypoxia. These pathways were not upregulated in E2 treated with EPZ6438.

The GO pathways associated with downregulated genes in G7 cells are mainly associated with RNA processing, ribosome function, cell number homeostasis and organelle organisation. Interestingly, one of the two downregulated categories following EPZ6438 treatment was ncRNA metabolic processes, which is also one of the downregulated categories in the UNC1999 data. Whereas, the GO analysis of E2 showed downregulation of genes involved in cell cycle progression and telomere organisation.

GSEA indicated that genes involved in oxidative phosphorylation are downregulated in G7 cells following UNC1999 treatment, as previously observed for EPZ6438 treated cells. Taken together, this data is consistent with reduced growth and metabolic activity in G7 cells treated with 2 μM UNC1999, which is consistent with the reduction in clonogenic survival. However,E2 treated with UNC1999 did not show any negatively enriched gene sets.

In conclusion, treatment with UNC1999 was found to inhibit colonies formation in G7 and E2 cell lines, both as a single agent and combined with either TMZ or radiation. Pathway analysis of G7 cells showed upregulation of neurogenesis related genes and downregulation of genes related to oxidative phosphorylation and RNA metabolism, revealing similarities in the response to UNC1999 and EPZ6438. Whereas E2 cells showed downregulation of genes involved with cell division.

Chapter 6 Efficacy of GSK343 on GBM cell lines

6.1 Introduction

GSK343 is one of the EZH2 inhibitors that selectively inhibits trimethylation of H3K27 by competing with SAM methyl donor. Recent studies demonstrate the inhibitory effect of GSK343 in various types of cancer (Ihira *et al.*, 2017; Gong *et al.*, 2020) . Anti tumour effect GSK343 was measured in xenograft model of neuroblastoma . Treatment with GSK343 lead to significant decrease in *in vivo* tumour growth (Bownes *et al.*, 2021). It has been reported that GSK343 induces apoptosis in osteosarcoma (Xiong *et al.*, 2020). Additional evidence also suggests that GSK343 reduced stemness in spheroid formation assay and attenuated cell motility in glioma cells (Yu *et al.*, 2017).

In this chapter, clonogenic survival assays were used to assess the effect of GSK343 on GBM cell lines grown under stem conditions. The effect of GSK343 on colony formation was determined alone or in combination with conventional DNA damaging approaches. The levels of senescence and apoptosis were also assayed, along with analysis of gene expression changes associated with treatment with GSK343.

6.2 Effect of GSK343 on survival assay and proliferation assay

Clonogenic assays were conducted to evaluate the efficacy of increasing concentration of GSK343 on colony formation in GBM cell lines. The effect of GSK343 on colony formation in G7 and E2 cell lines is shown in Figure 6-1. In G7 cells, colony formation was largely unaffected at concentrations up to 2 μM, but was substantially reduced at 5 μM and above. E2 cells were more sensitive, showing a 53% reduction in colony formation at 2 μM, and 16% reduction at 5 μM. The IC50 of G7 and E2 was 4 μM and 1.7 μM respectively.

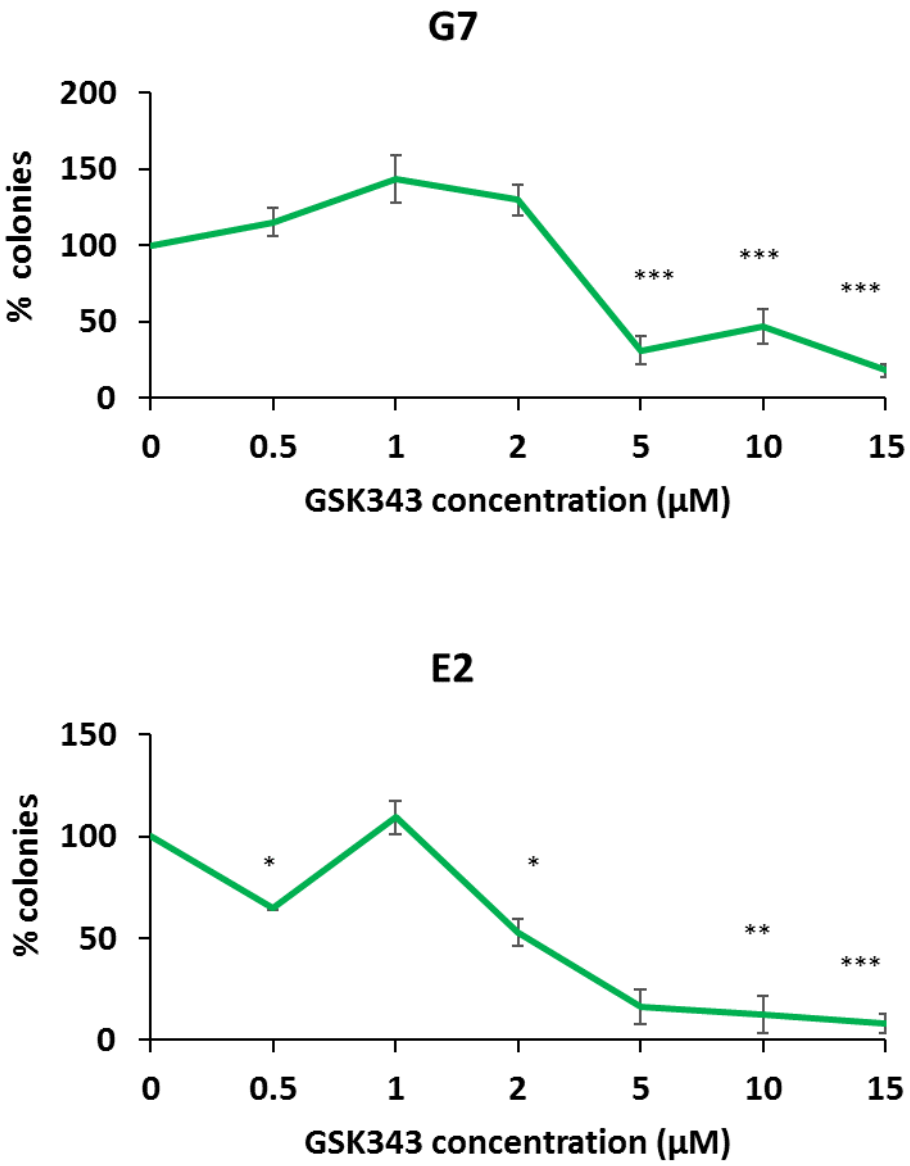

Figure 6-1 Clonogenic survival curves of G7 and E2 cells exposed to different doses of GSK343.

Clonogenic assays were performed to assess the ability of cells to form colonies after exposure to increasing concentrations of the GSK343. Cells were seeded at 250 per well on 6 well Matrigel coated plates. After 48 hrs incubation with the drug or DMSO, media was changed and cells were left to form colonies for 14 days. Then cells were fixed, and colonies were counted. A graph is plotted that shows the effect of increasing concentration of GSK343 on number of colonies formed in both cell lines. Cells were seeded in triplicates at each concentration. Data points represents mean values and SEM of three independent experiments. p value was determined using student's T test in control vs treated cells. *p ≤ 0.05, **p ≤ 0.01 and *** p ≤ 0.001.

The effect of GSK343 on cell viability following continuous incubation for 5 days was determined with the Cell Titer Glo assay (Figure 6-2). In G7 cells, there was a gradual decrease in the number of viable cells between 5 and 20 μM. E2 cells were more sensitive, showing a decrease in viable cells between 1 and 10 μM. The values of IC50 were 6.09 μM for G7 and 0.45 μM for E2 cells.

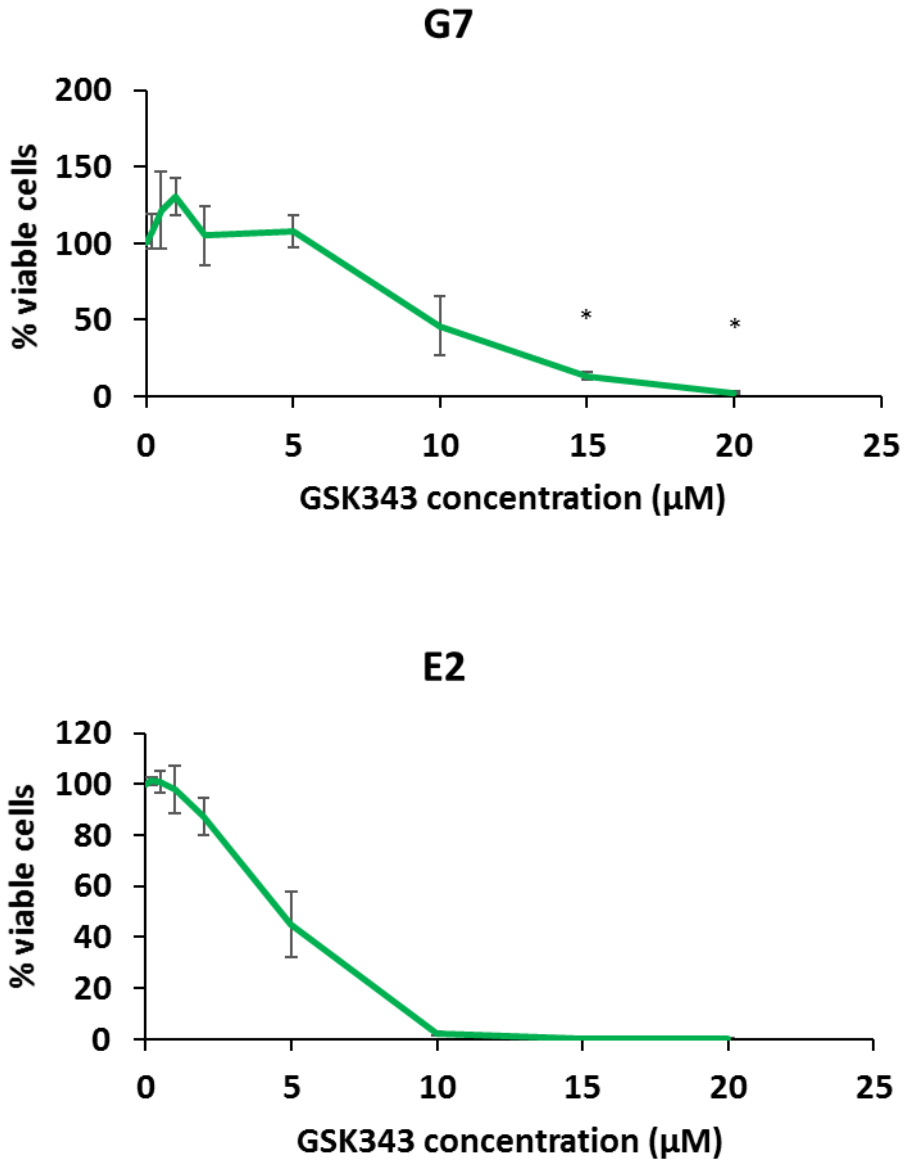

Figure 6-2 Cell survival assay showing the effect of increasing concentration of GSK343 on cell proliferation in G7 and E2 cell lines.

Cells were plated at 2500 per well in triplicate on 96 well Matrigel coated plates. GSK343 or 0.2% DMSO was added and cells allowed to grow for five days. The Cell Titer Glo kit (Promega) was used to quantify viable cells. Cell viability was calculated as a percentage of the DMSO control, and results are plotted as the mean value of three independent experiments. Error bars show the SEM. Student's T test was performed to calculate p value in control vs treated cells *p ≤ 0.05.

The ability of GSK343 to sensitise cells to TMZ was investigated using clonogenic assays. Cells were treated with GSK343 for 24 hrs then with TMZ for 24 hrs. Figure 6-3 demonstrates the effect of increasing concentration of GSK343 with 10 μM TMZ in G7 and E2 cell lines. Both graphs indicate that the combination of the two drugs together more potently inhibited the percentage of colonies than each drug individually. It seems that GSK343 acted synergistically with TMZ to completely diminish the survival rate of both cell lines.

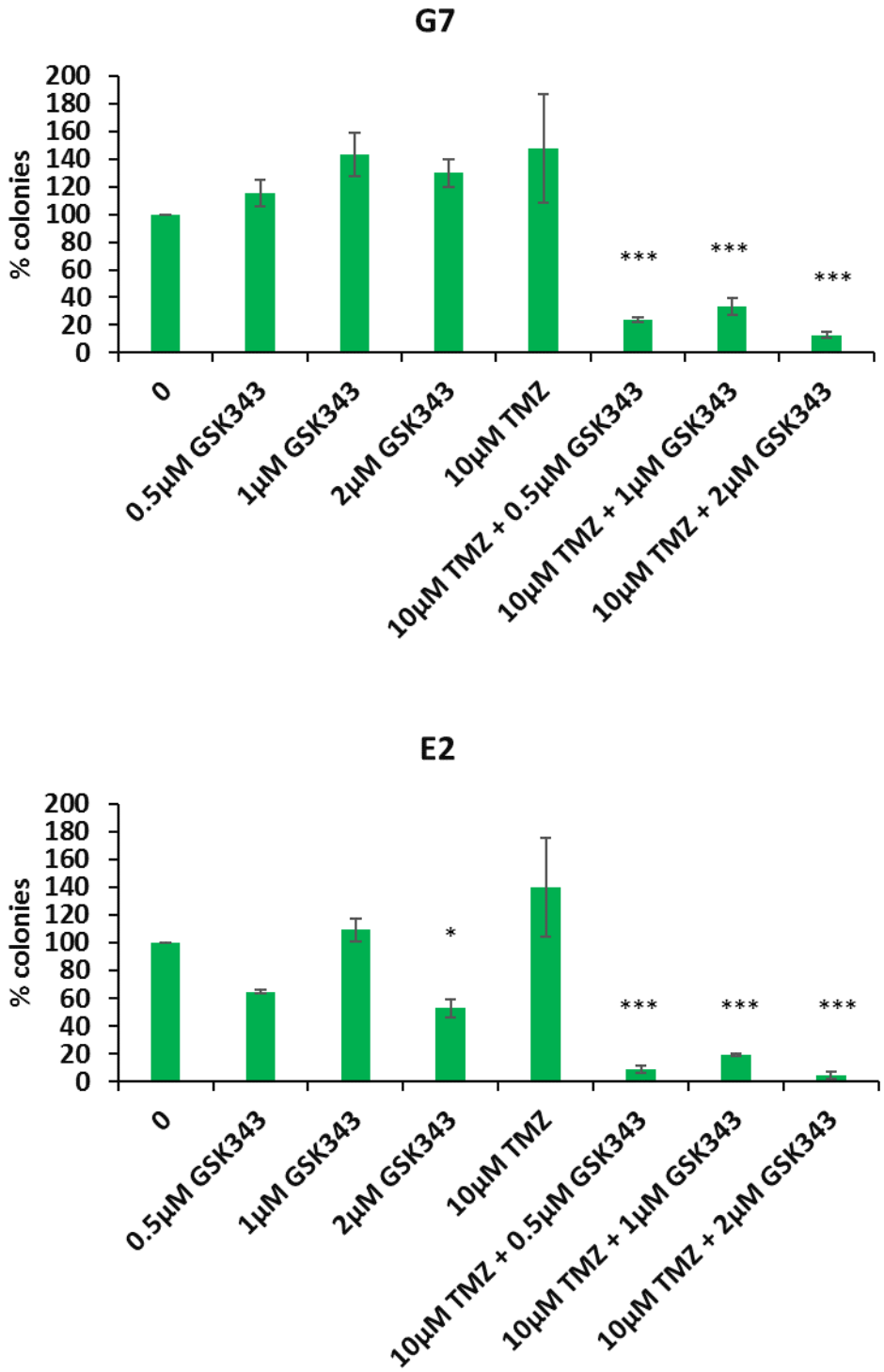

Figure 6-3 Clonogenic assay plot determining the effect of combination of TMZ with GSK343 in G7 and E2 cell lines.

The graph represents the combined effect of 10 μM TMZ and with increasing dose of GSK343. Cells were seeded at 250/well on Matrigel coated 6 well plates, then were incubated with increasing concentration of GSK343 for 24 hrs then with 10 μM TMZ for 24 hrs. Result indicates the percentage of colonies calculated from three independent with error bars representing SEM. Student's T test was used to determine p value in control vs treated cells *p ≤ 0.05 and ***p ≤ 0.001.

Clonogenic assays were also used to investigate whether GSK343 sensitises cells to radiation treatment. GBM cell lines were exposed to increasing doses of radiation following exposure to varying concentrations of GSK343 (Figure 6-4). In G7 cells, pre-treatment with 2 μM GSK343 reduced the surviving fraction at 4 Gy and 5 Gy radiation. In E2 cells, pre-treatment with 0.5 μM, 1 μM or 2 μM GSK343 also reduced the survival fraction at the highest dose of radiation. The DMR values of G7 and E2 cells are shown in Table 6-1. The DMR values showed that G7 is significantly sensitive to radiation at 2 μM. Whereas in E2 cells the DMR values ranged from (1.33, 1.29 and 1.44) indicating that GSK343 significantly induced radiosensitisation.

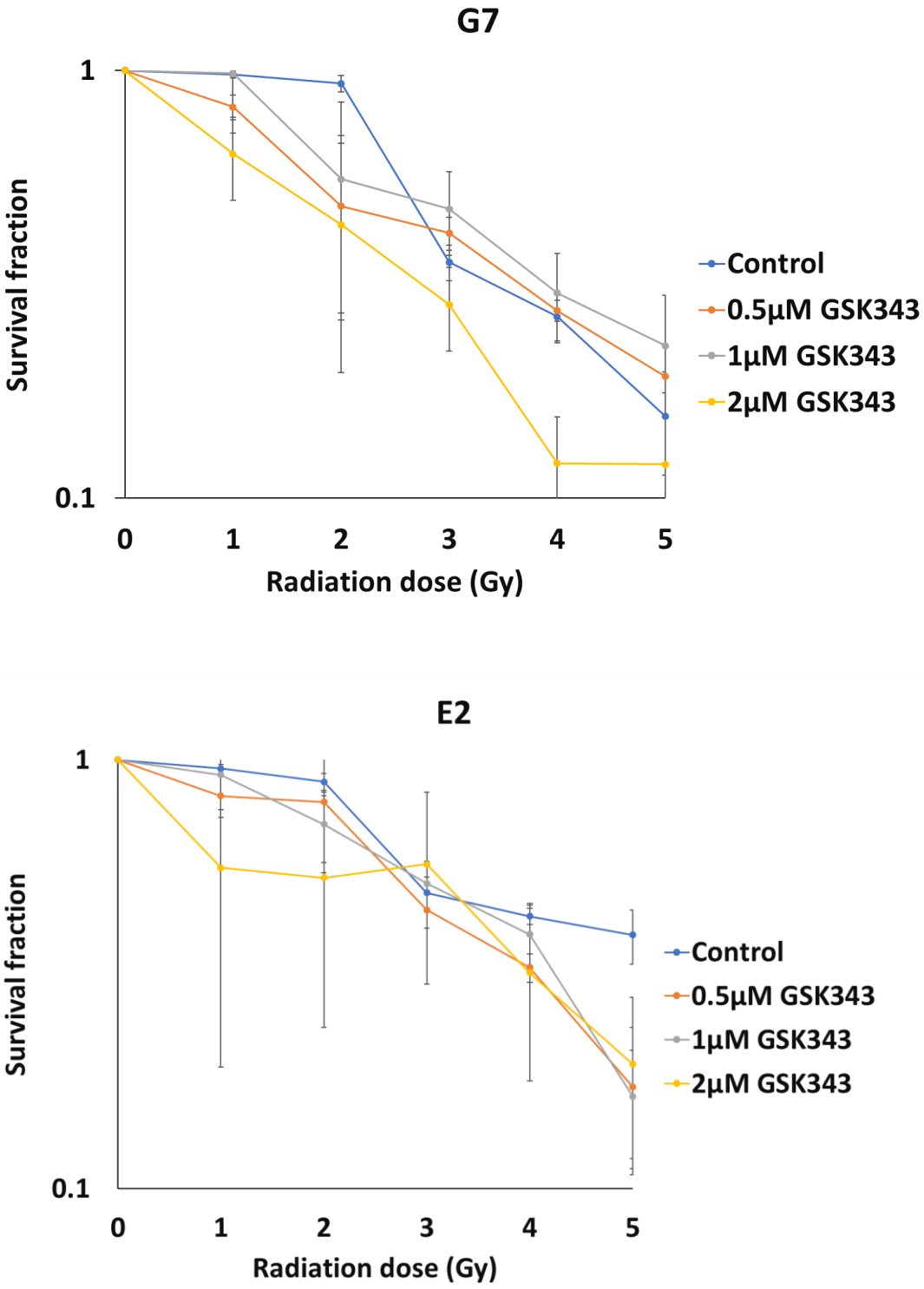

Figure 6-4 Clonogenic survival assay plot showing the combined effect of radiation with GSK343 in G7 and E2 cells.

The graph shows survival fraction on y axis calculated from counting colonies and increasing dose of radiation on x axis. Cells were seeded at 250/well on Matrigel coated 6 well plates in triplicates, then incubated with different concentration of GSK343 for 24 hrs before being exposed to radiation at 0 to 5 Gy. Colonies were allowed to grow for 14 days before being fixed and counted. The curve represents mean survival fraction from three independent experiments with error bars indicating the mean.

G7	$DMR_{(0.37)}$
0.5 μM	1.11
1 μM	0.97
2 μM	1.62***

E2	$DMR_{(0.37)}$
0.5 μM	1.33***
1 μM	1.29***
2 μM	1.41***

Table 6-1 The values of DMR in G7 and E2 cells.

The DMR represents the dose required to reduce survival fraction to 0.37 in control vs treated with increasing concentration of GSK343. p value is calculated by comparing the means, sd and n of drug treated with control. ***p ≤ 0.001.

6.3 Assessment of GSK343 in apoptosis and senescence assays

Senescence and apoptosis assays were conducted to determine the efficacy of GSK343 in cell cycle arrest and cell death. Senescence assay was performed following treatment with 2 μM GSK343 for 5 days. The graphs in Figure 6-5 indicate a significant increase in the percentage of cells expressing ß-galactosidase when compared with the control. These results suggest that GSK343 may be inducing cellular senescence in GBM cell lines.

In contrast, the apoptosis assay performed with flow cytometry demonstrated that 2 μM GSK343 did not appear to induce apoptosis. Figure 6-6 represents flow cytometric analysis of cells that were stained with AnnexinV and 7AAD after treatment for 5 days. In G7 and E2 plots the graphs showed a low percentage of

cells in early and late apoptosis in both treated and control comparing to viable cells. The percentage of dead cells increased in both G7 and E2 cells, but without evidence of early or late apoptosis it is not possible to determine the mechanism of cell death.

A)

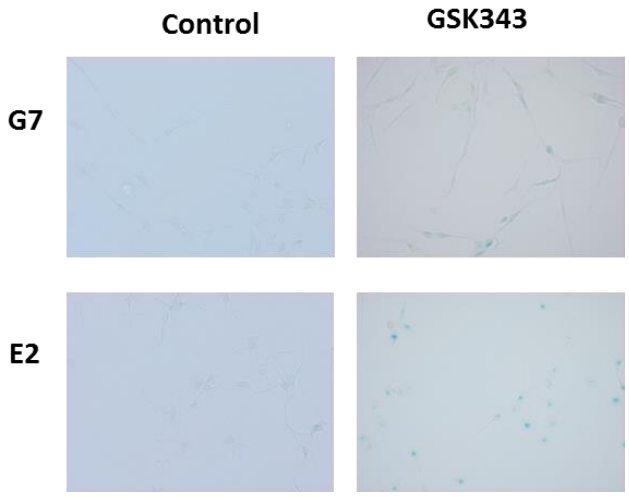

B)

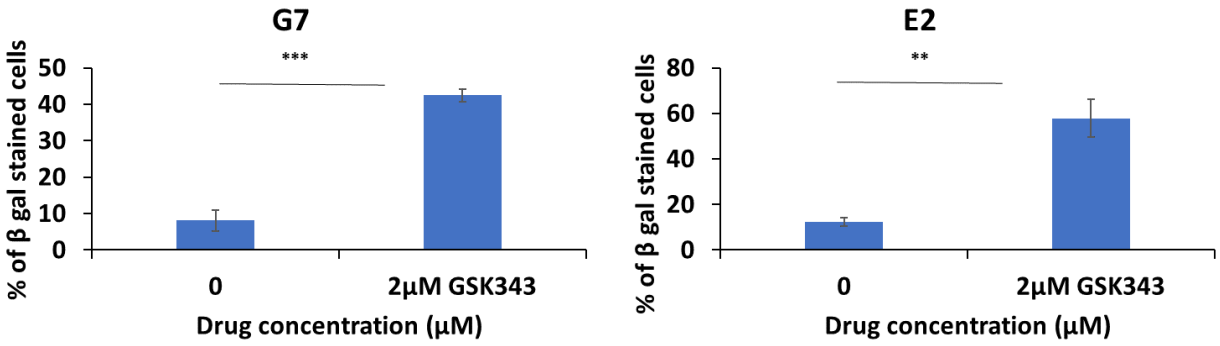

Figure 6-5 Senescence assay plots after exposing G7 and E2 cell lines to 2 μM GSK343 or corresponding DMSO.

Senescence associated β- galactosidase is used to identify senescent cell in culture media treated with GSK343. The picture of β- galactosidase cells was captured with confocal microscopes (A). After cell fixation and staining with β- galactosidase solution, β--galactosidase positive cells were quantified and plotted in a graph (B) with mean and SEM of three independent experiments, p value was calculated using student's T test in drug treated vs control. **p ≤ 0.01 and ***p ≤ 0.001.

A)

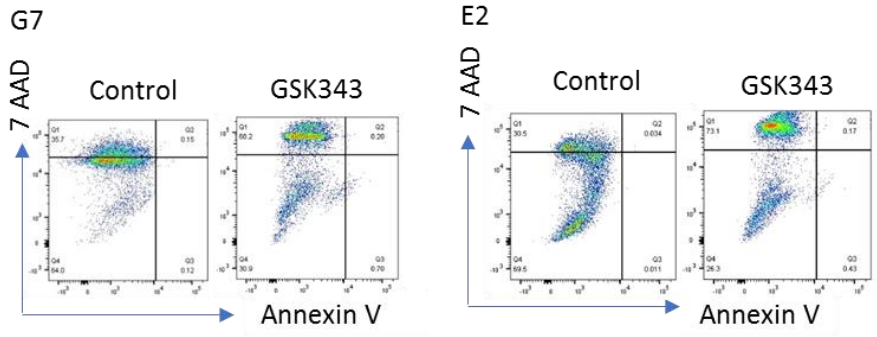

B)

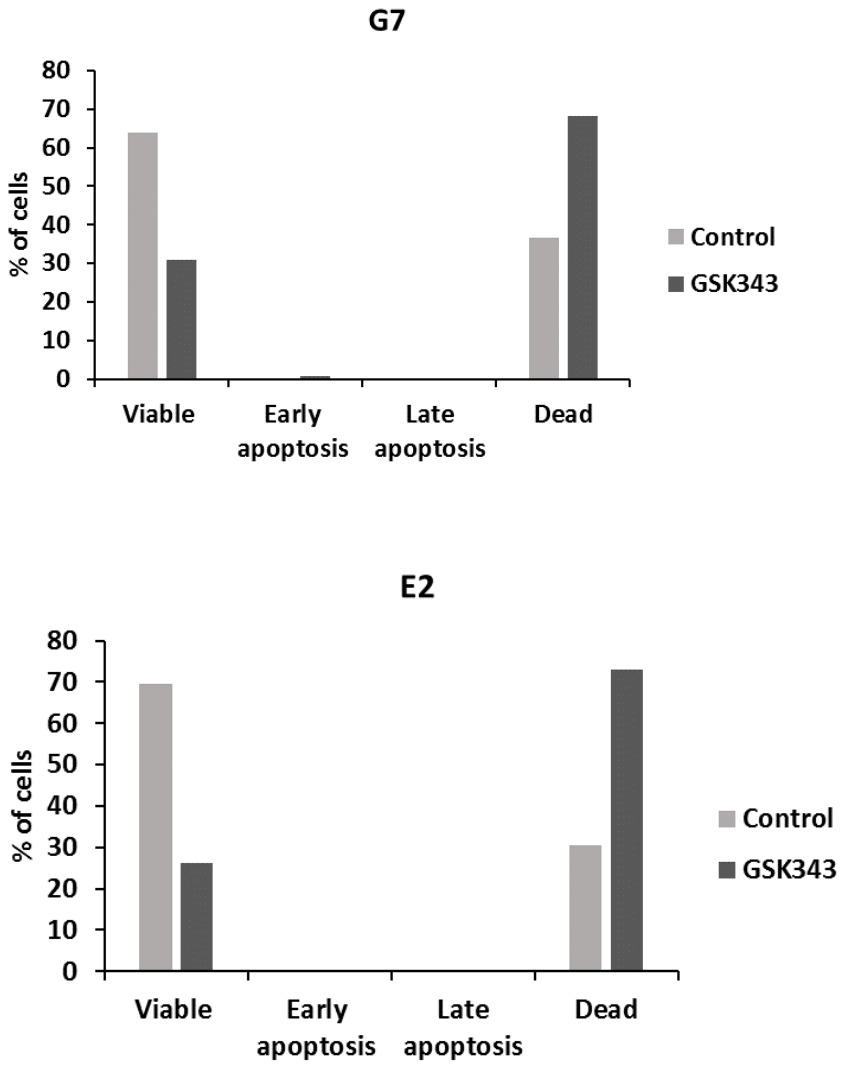

Figure 6-6 Apoptosis analysis by flow cytometry of G7 and E2 cell line treated with GSK343 or corresponding DMSO.

Data shows apoptotic effect of 2 µM GSK343 treatment in G7 cell line. After 5 days of incubating cells with GSK343 or DMSO, cells were fixed and stained with AnnexinV and 7AAD .The percentage of cell (A) was plotted as scatter plots showing live (Q4), early

apoptosis (Q3), late apoptosis (Q2) and dead cells (Q1). The graph (B) indicates the viable, early, late apoptosis and dead cells.

6.4 Effect of GSK343 on genes associated with stemness and tumourgenesis

qRT-PCR was performed to determine the effect of GSK343 on expression of genes involved in stemness and genes associated with cell cycle regulation and tumorigeneses. The experiment was conducted following incubation with the drug for 5 days. A graph was plotted based on the mRNA expression of each gene normalised to *B -Actin* in treated and no drug control. Figure 6-7 shows the expression of stem and differentiated genes after exposure to increasing concentration of GSK343 for 5 days. *SOX2* expression was elevated while the level of GFAP expression reduced in treated G7 cells compared to control. The E2 graph shows that there was no substantial difference in gene expression in cells treated and no drug control. However, caution should be used when interpreting these data as they are from single biological replicates.

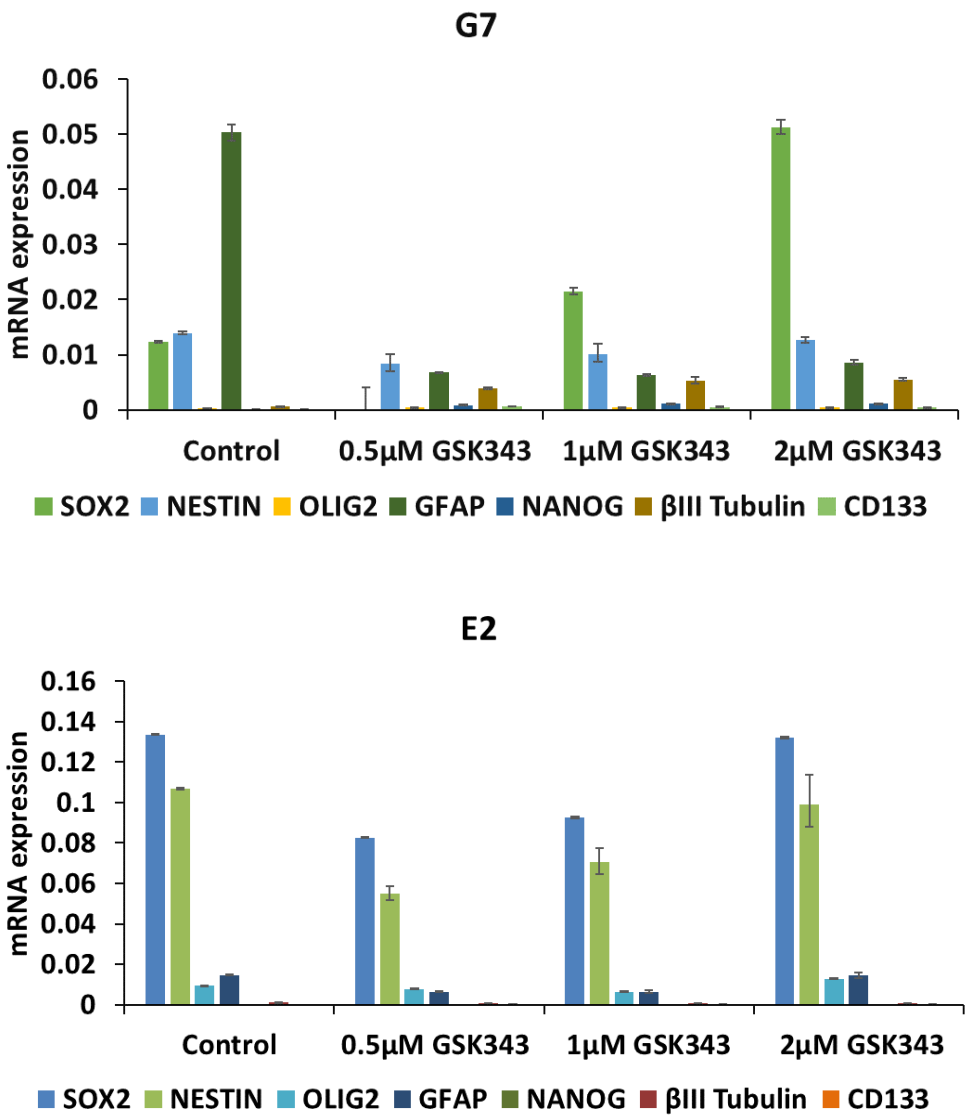

Figure 6-7 mRNA expression level of stem cell markers and differentiated markers in G7 and E2 cell lines after exposure to increasing concentration of GSK343.

G7 and E2 cells were incubated with GSK343 or DMSO for 5 days. Gene expression was determined by qRT-PCR with data normalised to β-Actin. The mRNA expression represents the fold change that is calculated from delta Ct with error bars representing SEM .Each RNA sample was loaded into wells in triplicates.

Interestingly, treatment with GSK343 increased the expression level of *P21* and *CDK2* (Figure 6-8). *P21* is an inhibitor of cell cycle progression, whereas *CDK2* is a cyclin-dependent kinase that drives the cell cycle. The level of *PTEN* increased in both cell lines while the level of *EZH2* was only elevated in E2. The expression of the senescence marker *P16* remained low in treated cell lines compared to the control.

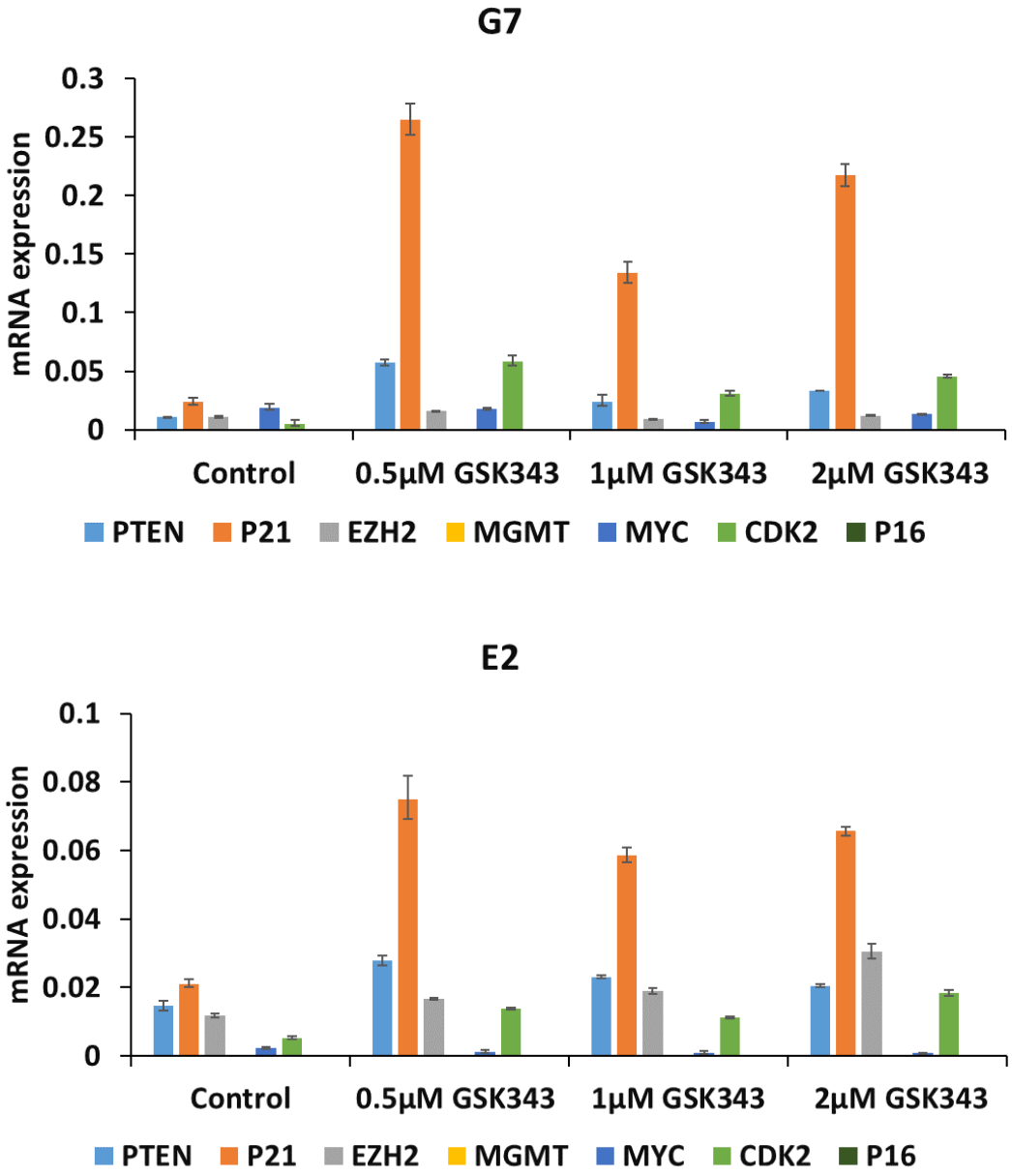

Figure 6-8 mRNA expression level of cell cycle, apoptosis and senescence markers in G7 and E2 cell lines after exposure to increasing concentration of GSK343.

G7 and E2 cells were incubated with GSK343 or DMSO for 5 days. Gene expression was determined by qRT-PCR with data normalised to β-Actin. The mRNA expression represents the fold change that is calculated from delta Ct with error bars representing SEM . Each RNA sample was loaded into wells in triplicates.

6.5 RNA sequencing analysis of GBM cells treated with GSK343

6.5.1 Quality control and data visualisation with searchlight2 using Galaxy

In order to investigate the changes in gene expression on a genome-wide basis, RNA-seq was performed. Cells were treated with 2 μM GSK343 or DMSO for 5 days, and RNA samples were collected from three biological replicates. Paired end sequencing was carried out by BGI genomics. FastQC was used to assess the quality of data. The samples displayed %GC of 50, PHRED score of 36 and the percentage of mapped reads was 95%. RNA-seq data was aligned to the Hg38 genome using Hisat2, Stringtie was used to assemble and quantify transcripts, and Deseq2 was used to generate a statistical model of the transcript distribution and calculate the differences in expression between drug treated and control samples.

PCA plots of G7 and E2 RNA-seq samples treated with 2 μM GSK343 and control were illustrated. The plots presented show that the 3 replicates of control and treated in both G7 and E2 cell lines did not form cluster. This indicates differences in gene expression between the three replicates of the same group of samples (Figure 6-9).

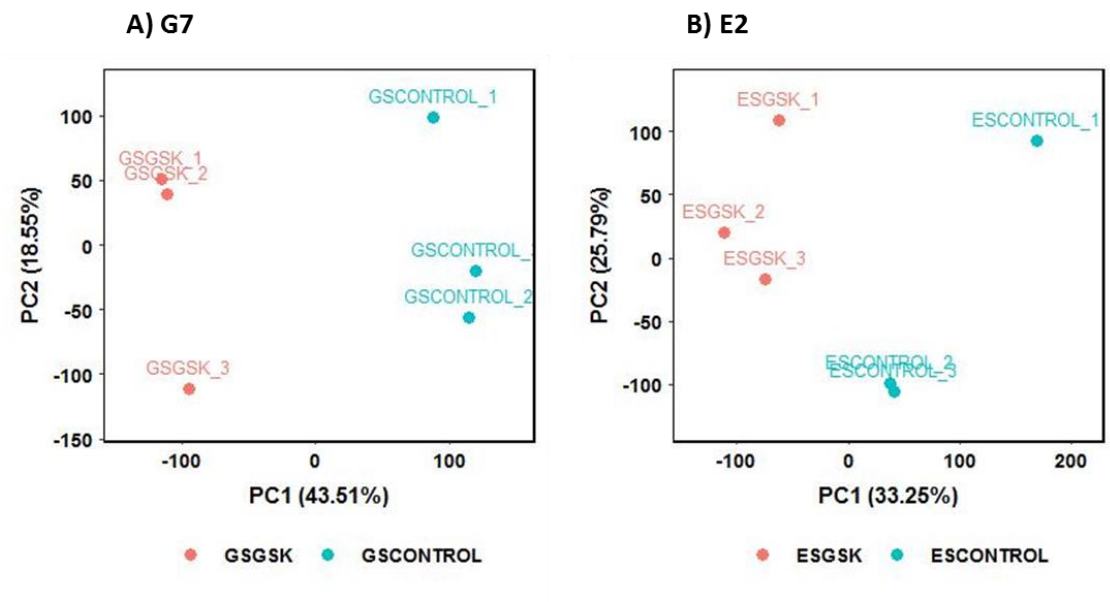

Figure 6-9 Scatterplots of gene expression data PCA showing PC1 vs PC2 in G7 and E2.

Searchlight 2 was used to generate the PCA plots. The dots represent individual samples, the blue dot represent the control and red dots represent treated samples with 2 μM GSK343. The total variation percentage explained by each component is indicated in the x axis and y axis. All gene expression values were scaled on a gene by gene basis using the z-score transformation, before PCA plot was generated.

The MA plot is generated from the Log2 fold change and normalised mean expression of each gene in 2 μM GSK343 treated and control samples for both cell lines (Figure 6-10). The plots show the overall distribution of the data, and it can be seen there are more significantly changed genes than for UNC1999 and EPZ6438 treated cells.

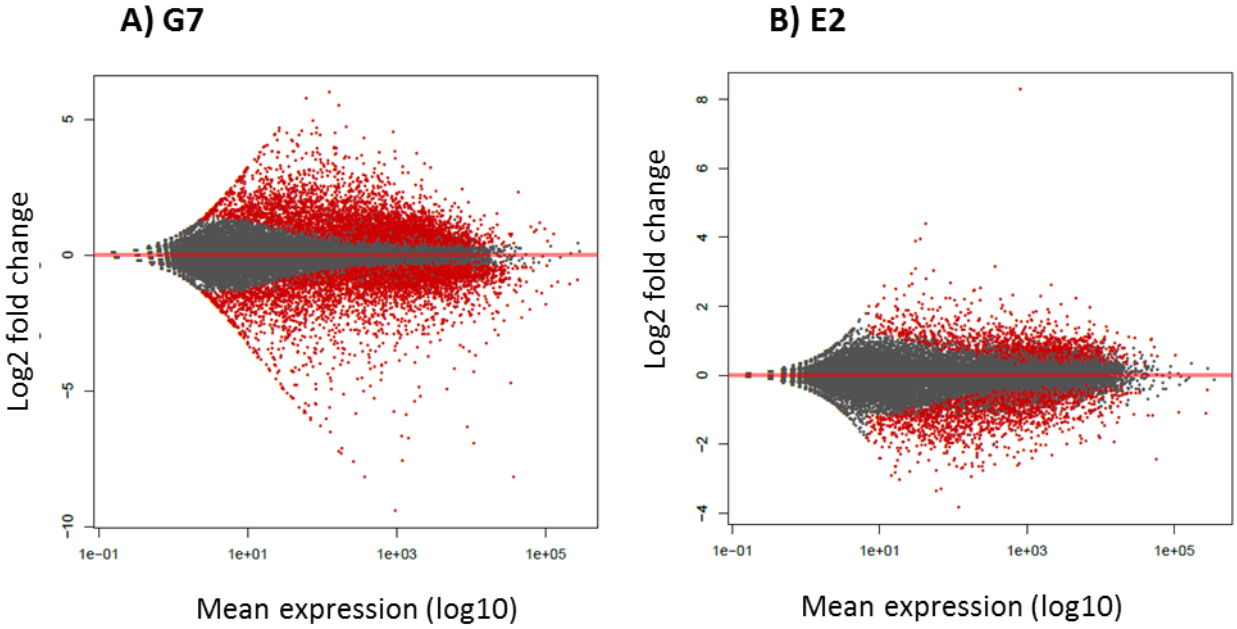

Figure 6-10 MA plots in G7 and E2 treated with GSK343.

The MA plot shows the relationship between the mean expression of each gene and its fold change. The plots were created from Deseq2 using RNA-seq data. The x axis indicates the normalised mean expression from all samples, while the y axis indicates the Log2 fold change between treated and control. Significantly changed genes are shown in red and non−significant genes in black .

The hierarchical clustered heatmaps show the significant DEGs in control and GSK343 treated cells (Figure 6-11). The heatmaps show the 3 replicates of samples are clustered together into control and treated groups, and illustrate how expression is similar between experimental replicates and significantly different to that in the control replicates.

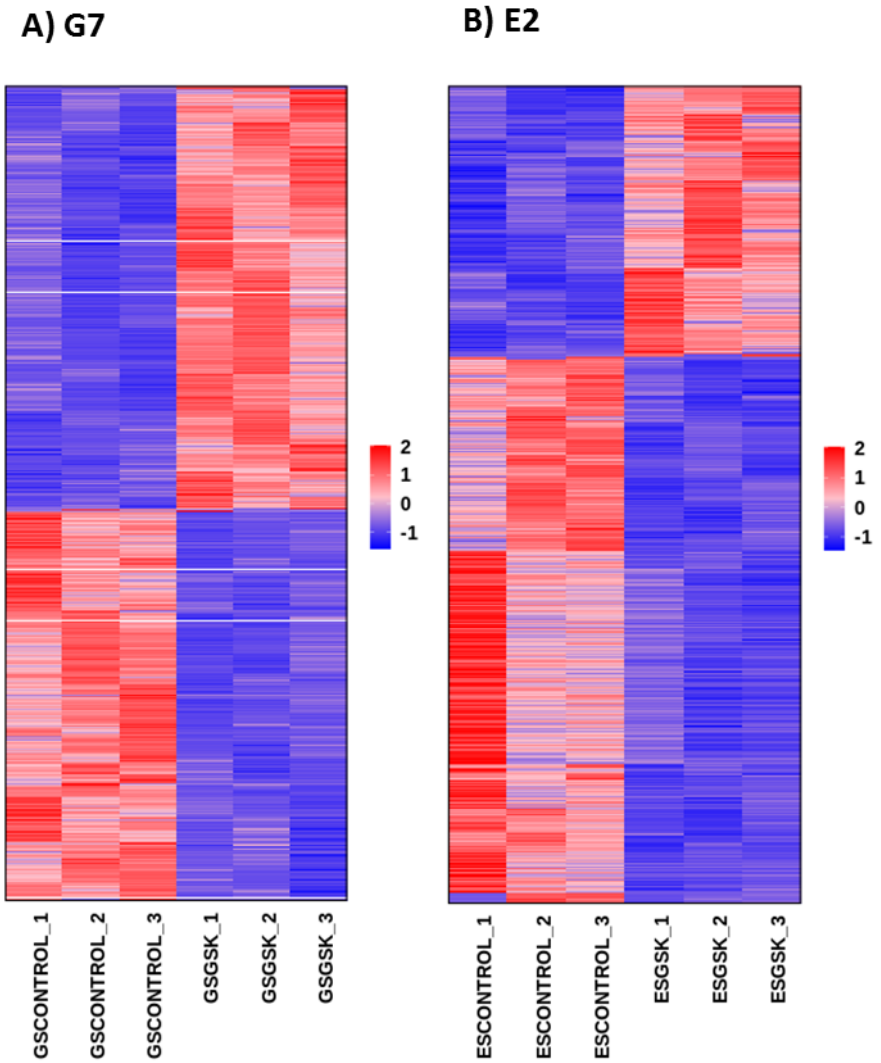

Figure 6-11 Hierarchically clustered heatmap that shows significantly DEGs with log2 fold change >1 and p adj < 0.05 between treated with GSK343 and control samples.

The plot shows samples on x axis with colour intensity representing expression level of genes. Low expression is presented in blue , and high expression is presented in red. Expression levels have been row scaled into z−scores. The x and y axis have been hierarchically clustered using Spearman distances.

6.5.2 Pathway analysis with GO

Filtering of the Deseq2 output files using an adjusted p value < 0.05 revealed 4342 upregulated genes and 4064 downregulated genes p value < 0.05. In E2 cells, there were 1244 upregulated and 1376 downregulated genes. GO analysis with Toppgene was carried out to identify significantly upregulated and downregulated biological processes associated with GBM cell lines in treated and control cells. Figure 6-12 shows the top two significantly upregulated genes were involved with microtubule bundle formation and movement, while the rest of the upregulated biological processes were mostly related to cell cycle and synaptic signalling. Significantly downregulated pathways were associated with a range of other biological process including RNA metabolism and subcellular protein localisation.

a)

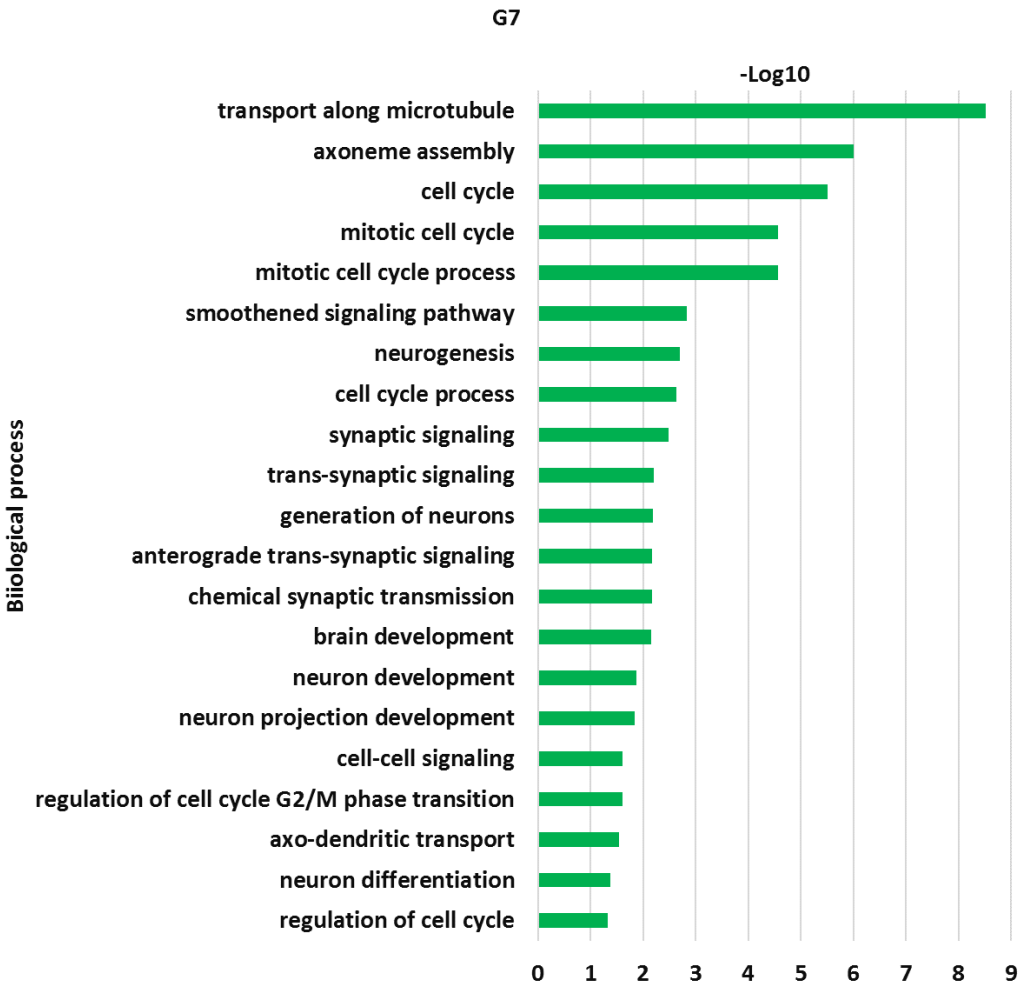

b)

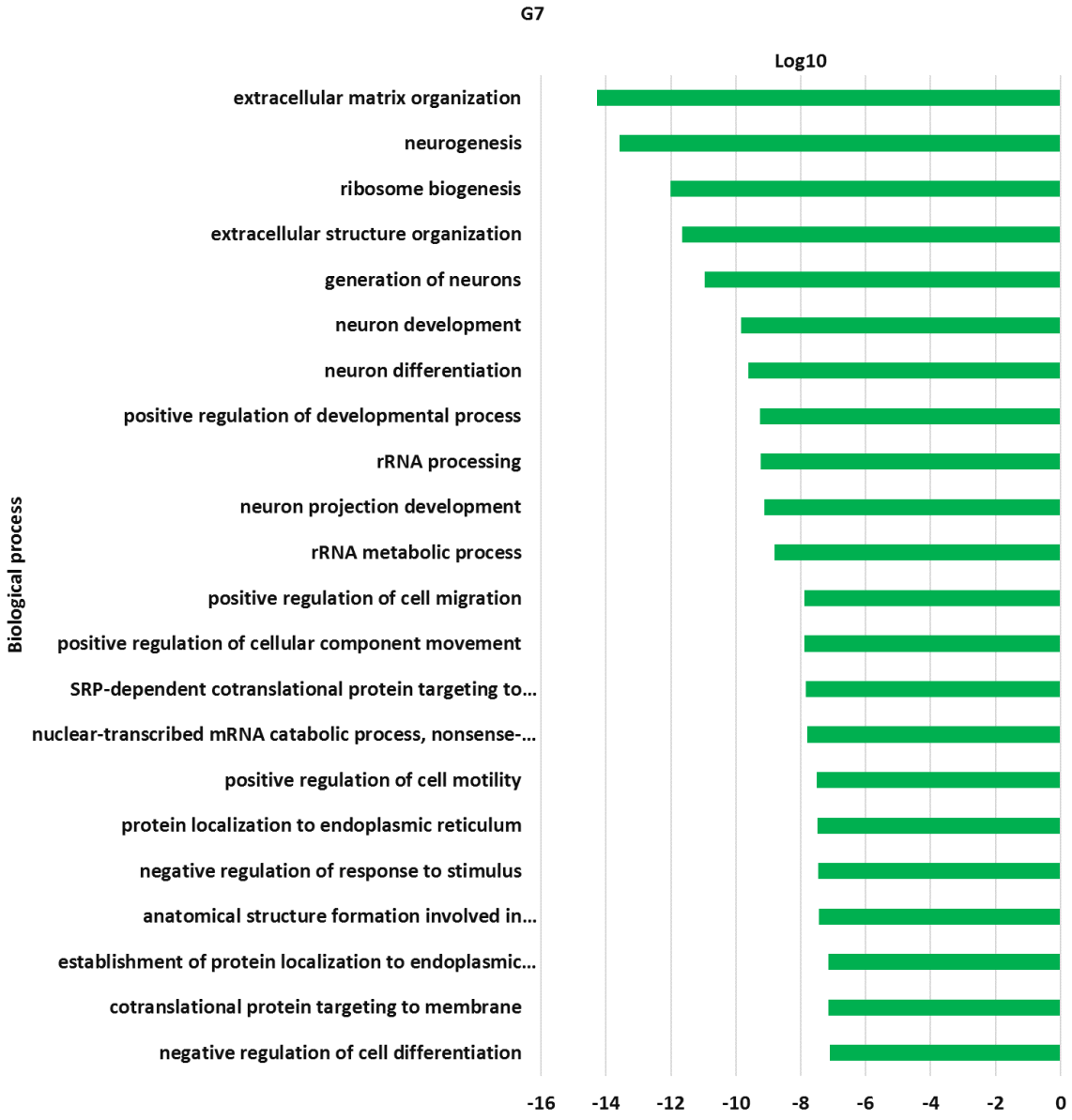

Figure 6-12 Significantly enriched GO biological processes in G7 cells treated with 2 μM GSK343.

GO analysis (biological processes) was performed using Toppgene. Significantly upregulated (- Log10 q value) and downregulated (Log10 q value) biological process categories with q value (Bonferroni) < 0.05 are shown. The Log10 q value is plotted as a horizontal bar; (a) upregulated categories have a positive value and (b) downregulated categories have a negative value. The GO analysis was performed on DEGs (adj p value < 0.05), treating upregulated genes (Log2 fold change > 0) and downregulated genes (Log2 fold change < 0) separately.

The E2 cell line showed significantly upregulated pathways mostly related to neurogenesis (Figure 6-13). The significant downregulated pathways include several signalling pathways associated with the innate immune response, for example response to interferons, virus, cytokines and lipopolysaccharides.

a)

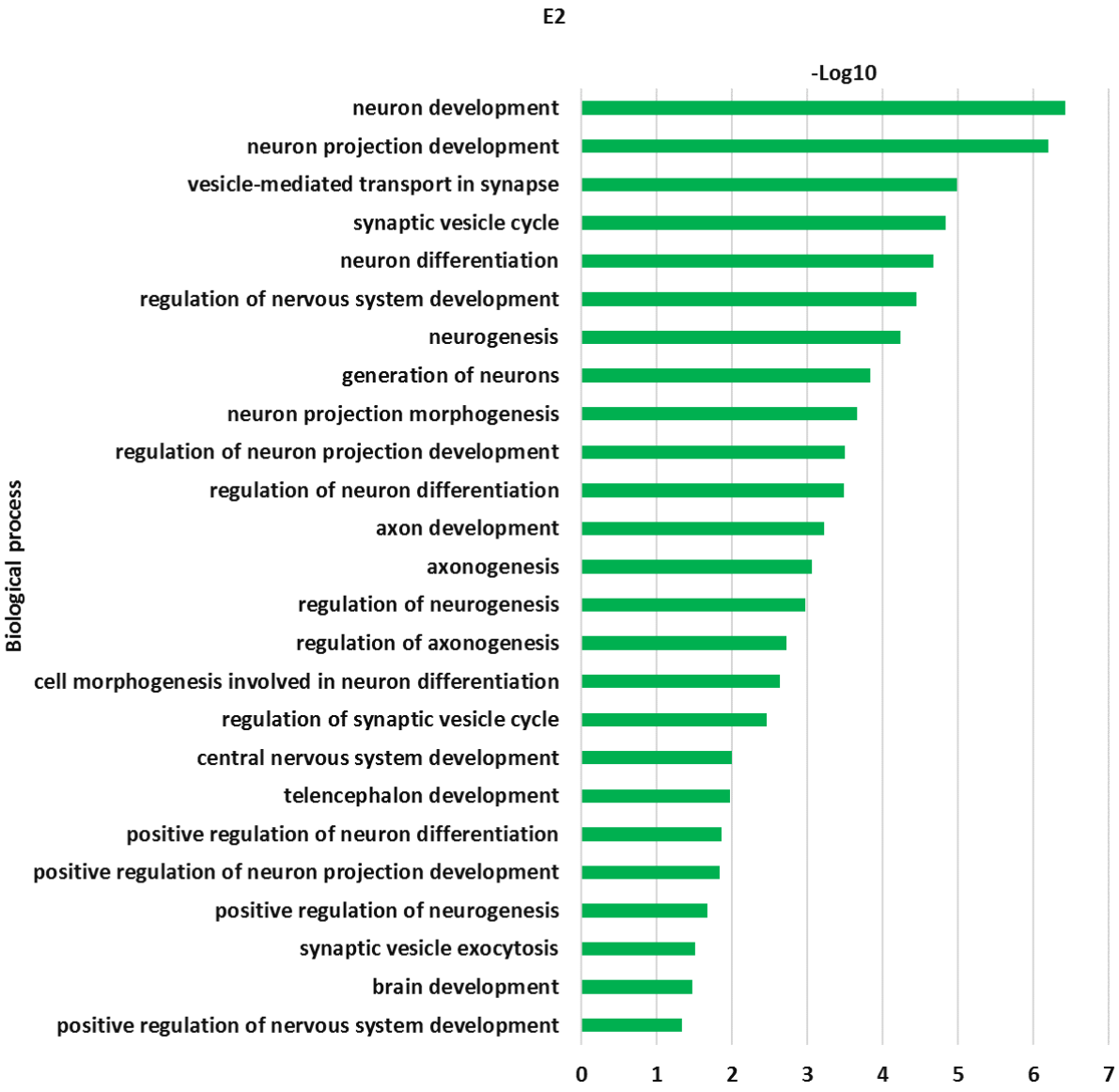

b)

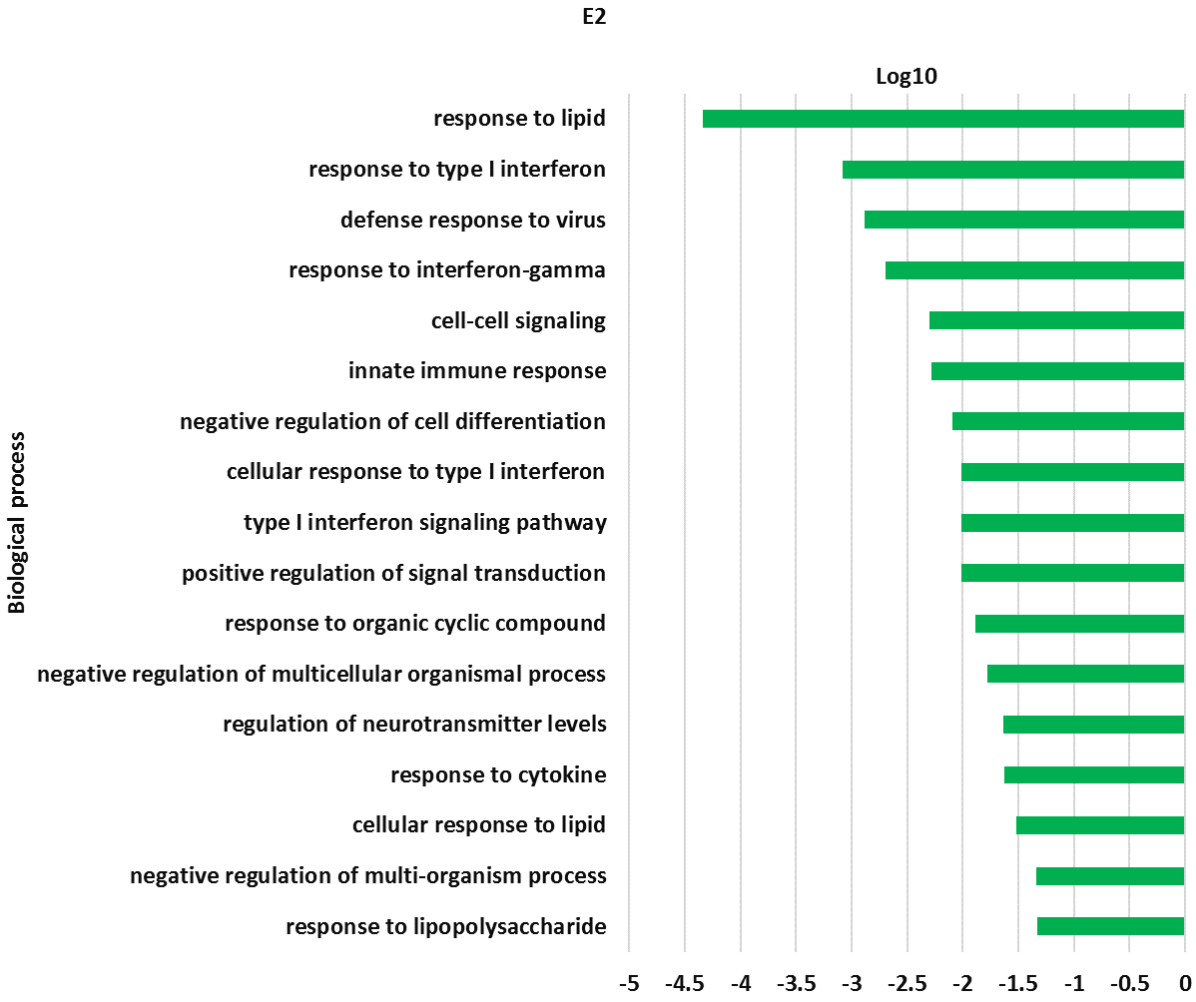

Figure 6-13 Significantly enriched GO biological processes in E2 cells treated with 2 μM GSK343.

GO analysis (biological processes) was performed using Toppgene. Significantly upregulated (- Log10 q value) and downregulated (Log10 q value) biological process categories with q value (Bonferroni) < 0.05 are shown. The Log10 q value is plotted as a horizontal bar; (a) upregulated categories have a positive value and (b) downregulated categories have a negative value. The GO analysis was performed on DEGs (adj p value < 0.05), treating upregulated genes (Log2 fold change > 0) and downregulated genes (Log2 fold change < 0) separately.

6.5.3 Comparative analysis with InteractiVenn and GO analysis

Venn diagrams of G7 and E2 cell lines were generated using InteractiVenn to identify the common DEGs in both cell lines. The list of significant upregulated genes with p value < 0.05 and Log2 fold change > 0 and significantly downregulated genes with p value < 0.05 and Log2 fold change < 0 were ran through InteractiVenn. Figure 6-14 shows 574 upregulated and 604 downregulated DEGs that are common in G7 and E2 cell lines treated with 2 µM GSK343. Representation factor of upregulated common genes is 6.3 and downregulated common genes is 6.4 ,indicating more significant overlaps between G7 and E2 cells treated with GSK343.

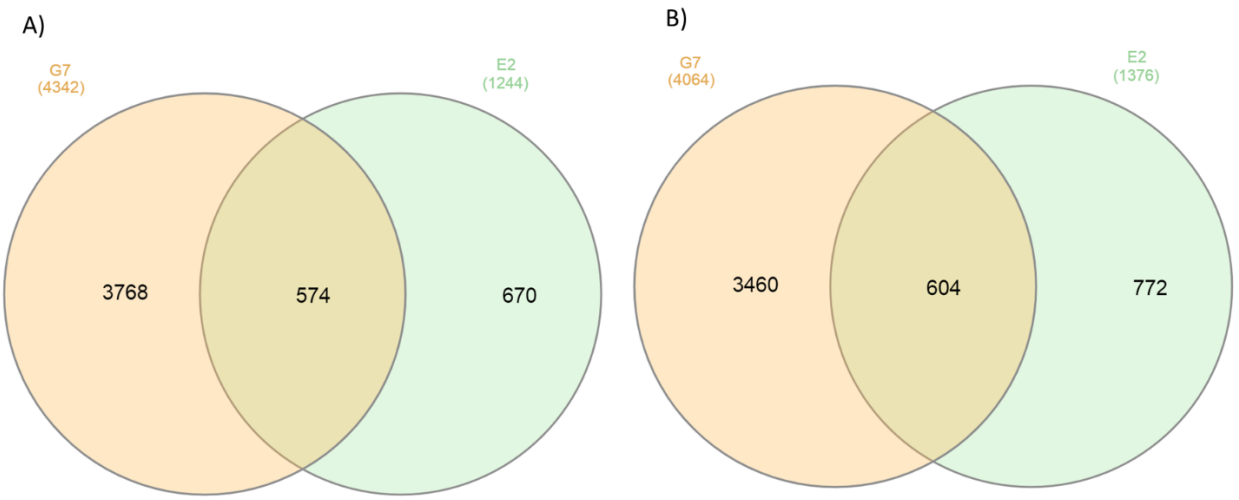

Figure 6-14 Venn diagram of upregulated (A) and downregulated (B) genes in G7 and E2 cell lines treated with GSK343.

Venn diagrams were generated using InteractiVenn which can show the overlap between G7 and E2 lists of genes. The Deseq2 result file was filtered, the adj. p value < 0.05 : Log2 fold change > 0, resulting upregulated genes; and Log2 fold change < 0 resulting in downregulated list of genes that were run on InteractiVenn. p value was determined by calculating the representation factor of overlapped genes for both upregulated and downregulated genes. p ≤ 0.001.

The upregulated and downregulated list of common genes in the two cell lines were run through Toppgene (Figure 6-15). The analysis showed 6 upregulated pathways mostly involved in glycosylation and glycoprotein processes and 8 downregulated pathways related to adhesion, cellular component and signalling.

a)

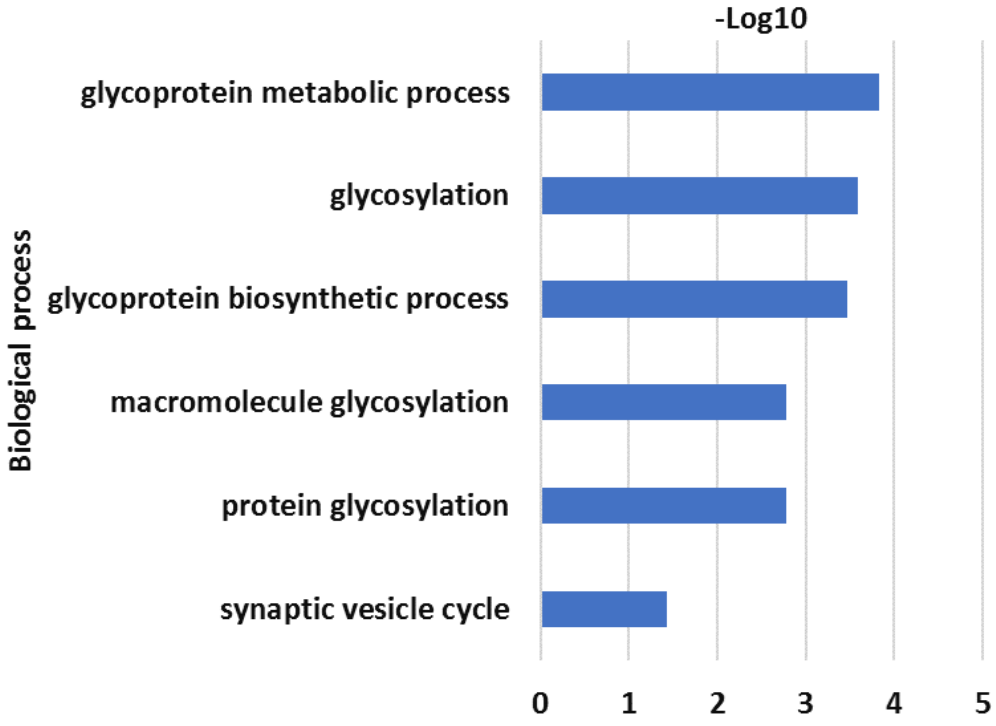

b)

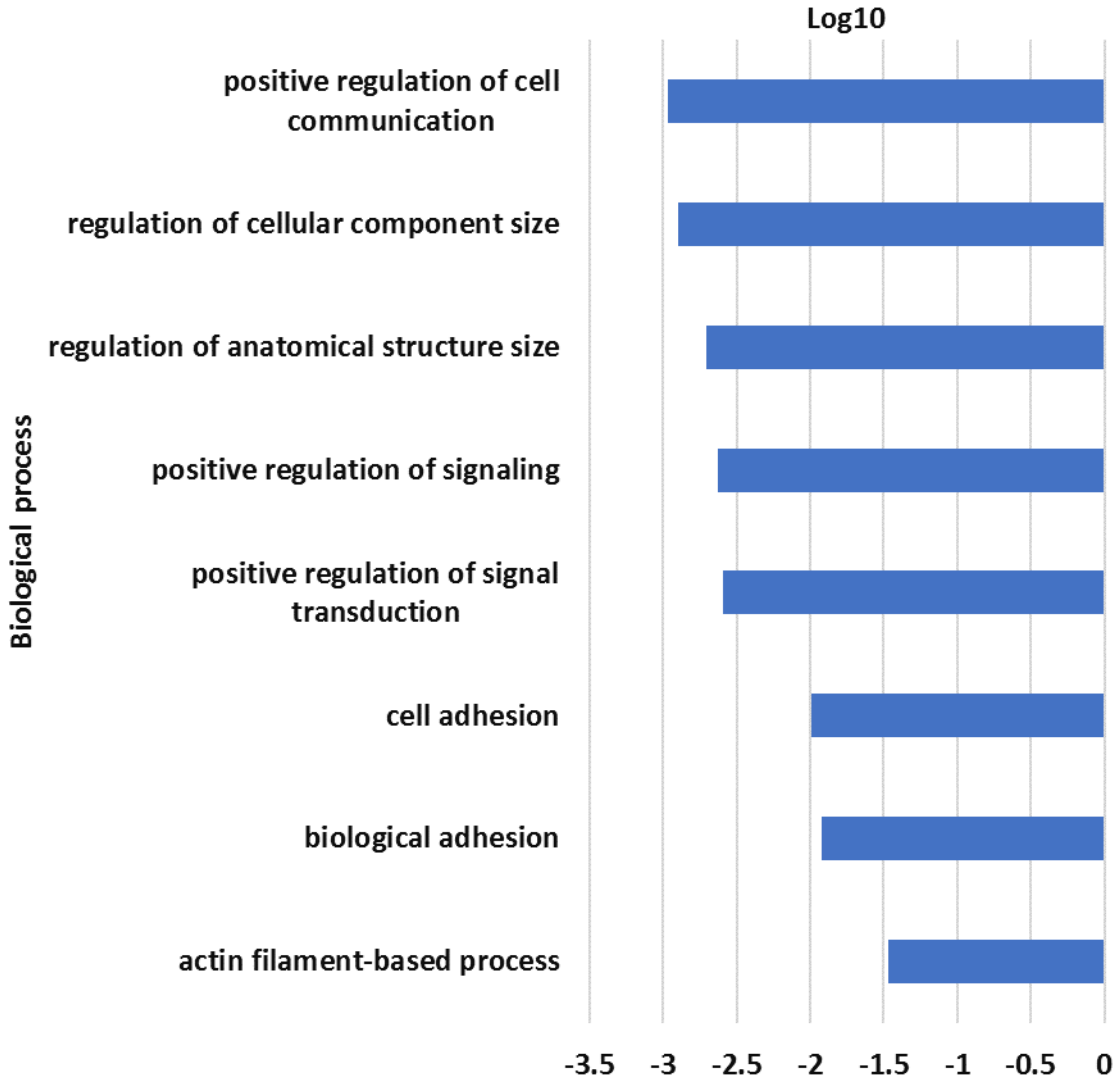

Figure 6-15 Biological processes significantly upregulated (a) and downregulated (b) in both G7 and E2 treated with GSK343.

GO analysis of upregulated (- Log10 q value) and downregulated (Log10 q value) biological process in both treated cell lines obtained from running output files of InteractiVenn on Toppgene. The Log10 q value (Bonferroni) < 0.05 is represented on the x axis, and list of biological process on y axis.

6.5.4 Pathway analysis with GSEA

To analyse the whole data set instead of just DEGs, GSEA analysis was used. This resulted in pathways identified in G7 and E2 cell lines. Figure 6-16 shows the GSEA results from G7 cells plotted into a graph, with 2 positively enriched gene sets and 13 negatively enriched gene sets (NOM p value < 0.05 and FDR q value < 0.25). The plots for the top positively enriched and top negatively enriched gene sets are shown in Figure 6-17: genes upregulated in response to alpha interferon (FDR 0.017) and genes defining the epithelial-mesenchymal transition (FDR 0). It is notable how few positively enriched gene sets there are for G7, particularly when there were over 8400 significant DEGs in this dataset.

a)

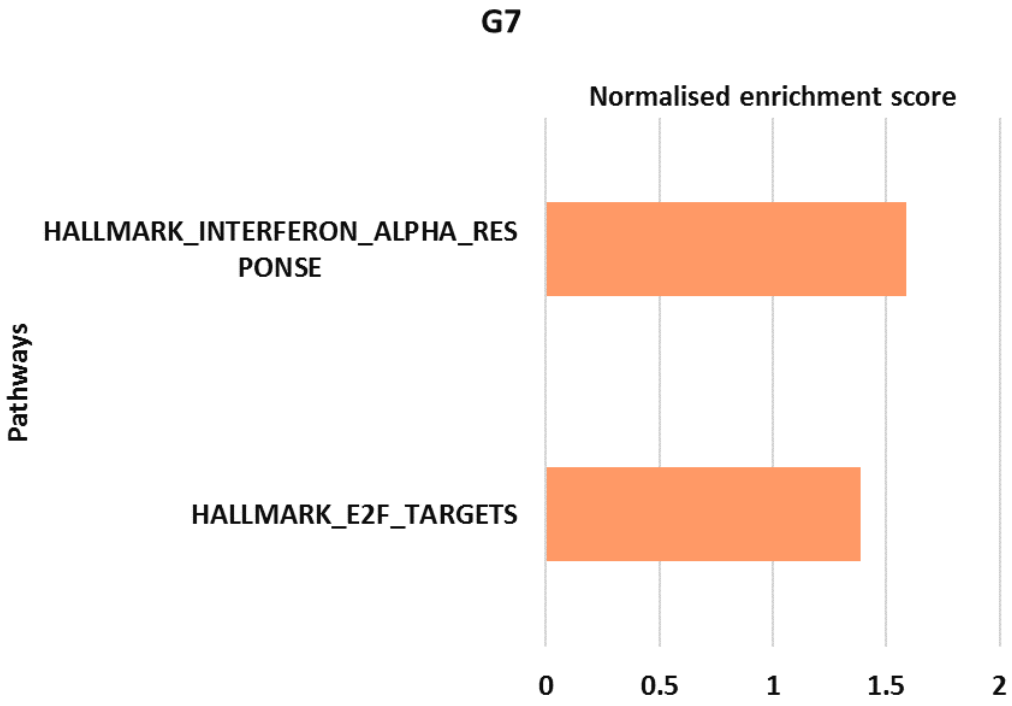

b)

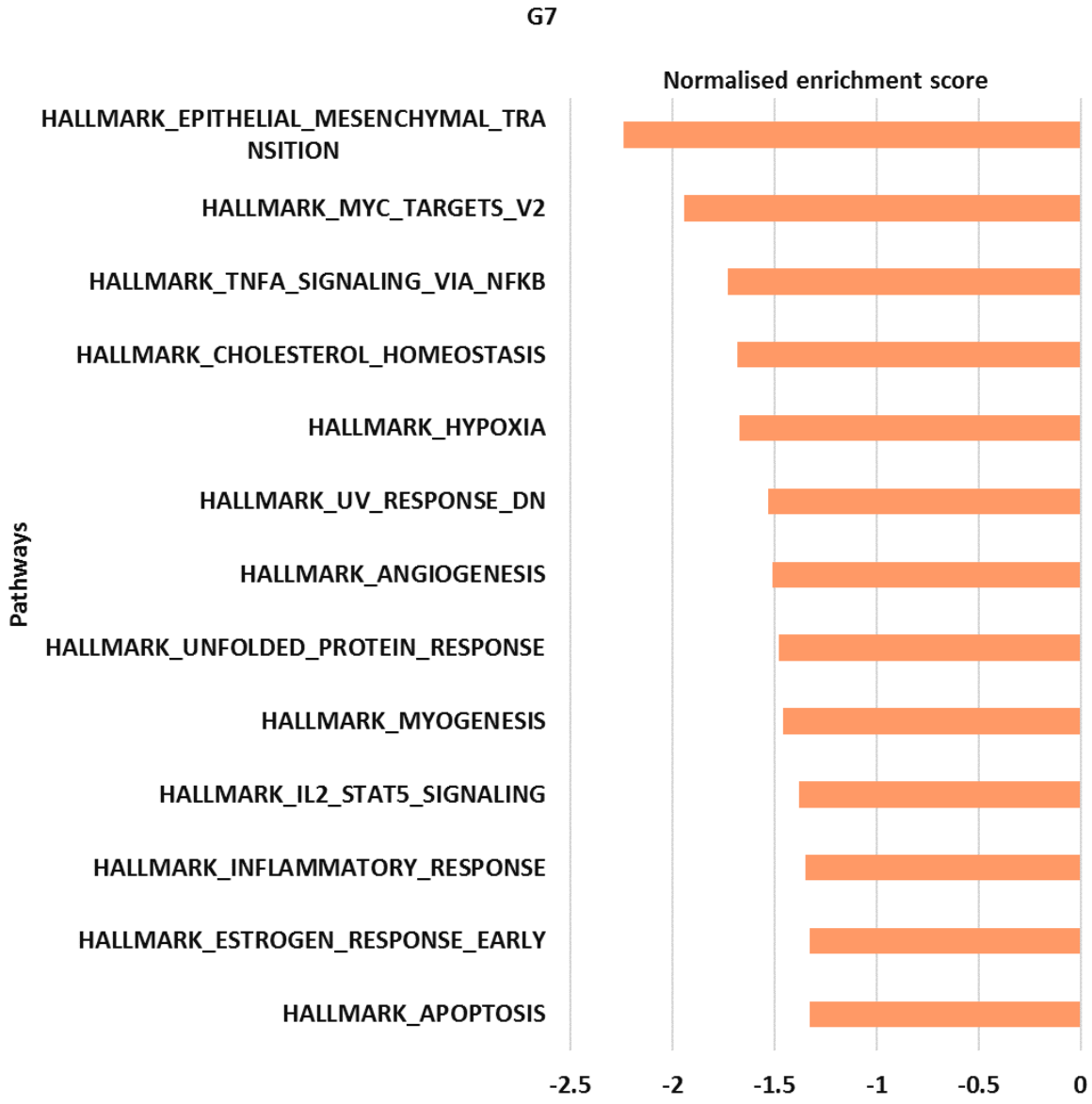

Figure 6-16 The graph of enriched GSEA indicating hallmarks gene sets in G7 treated with 2 µM GSK343.

The plot represents significant gene sets generated from GSEA report output file with NOM p value < 0.05 and the FDR < 0.25. Normalised enrichment score (NES) is indicated on x axis that is plotted against gene sets represented on y axis. Positively enriched gene set (a) have NES > 0 while negatively enriched gene set (b) have NES < 0.

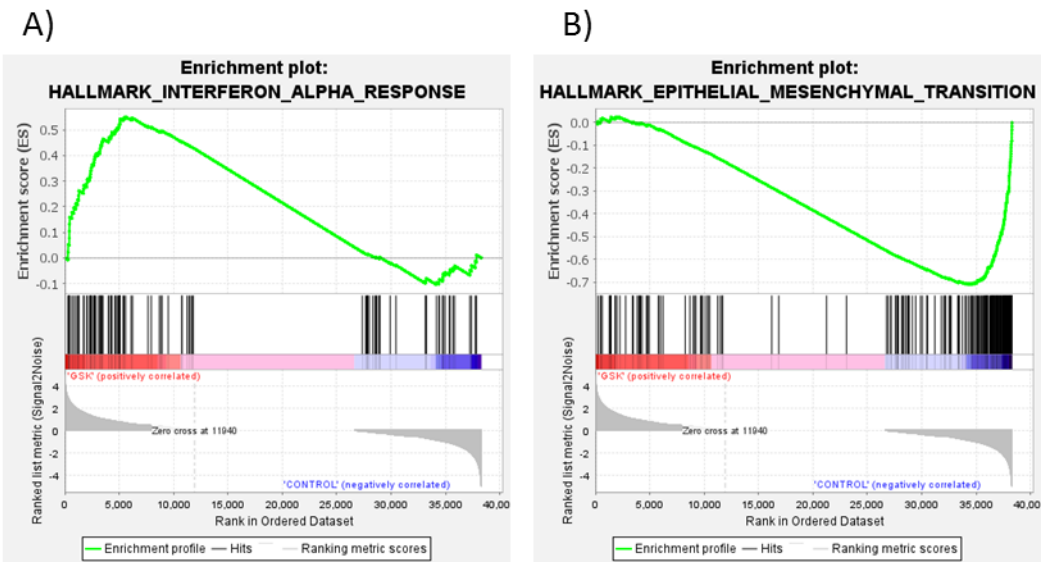

Figure 6-17 GSEA Enriched plots of G7 treated with GSK343.

GSEA enrichment plots represents the top positive enriched plot (A), and the top negative enriched plot (B) in G7 treated GSK343. The green curve indicates the ES for that specific gene with the peak indicating the final ES score. The plot is obtained from GSEA output file after running Deseq2 count file through GSEA software

In E2 cells, the GSEA analysis showed 5 positively enriched gene sets and 2 negatively enriched gene sets (NOM p value < 0.05 and FDR q value < 0.25) (Figure 6-18). Figure 6-19 shows the plots for the top positive enriched gene set, genes involved in the Mitotic spindle, and the top negative enriched gene set, genes upregulated in response to Interferon alpha.

a)

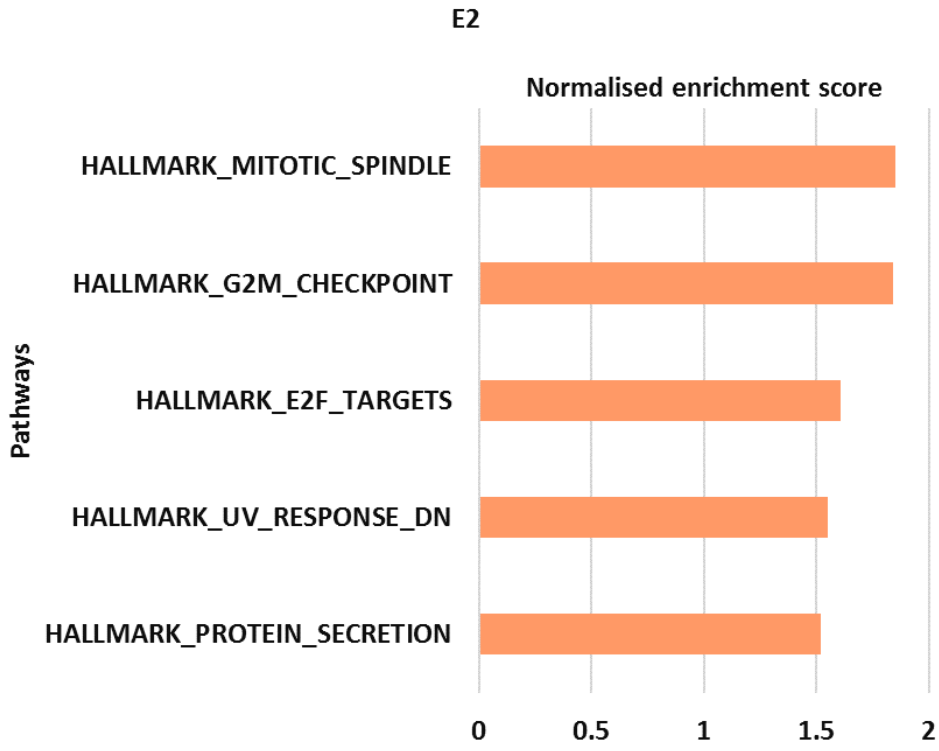

b)

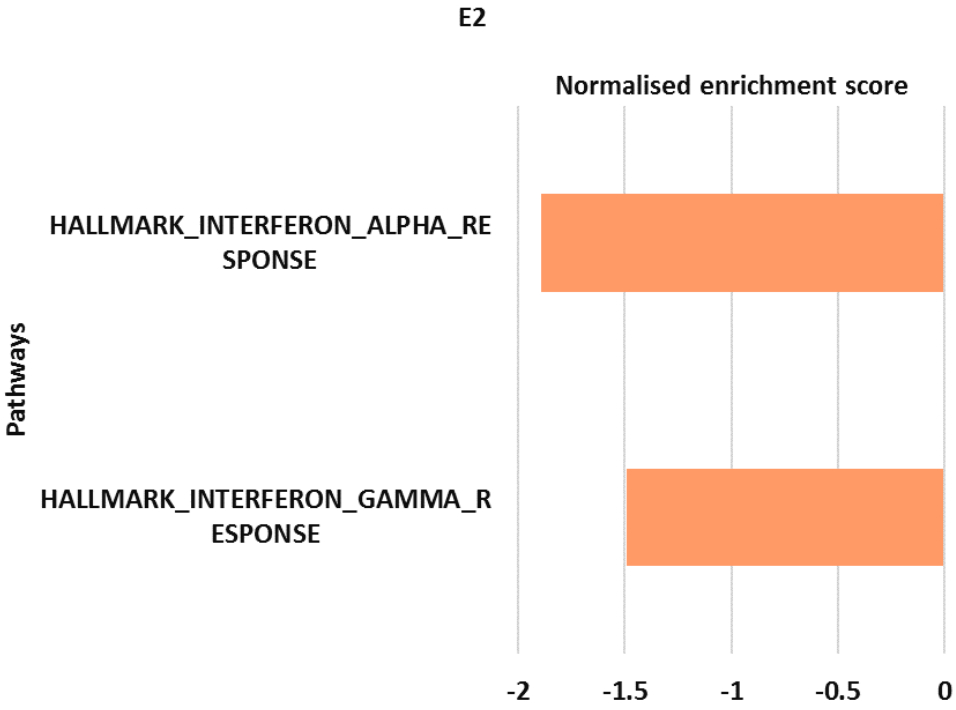

Figure 6-18 The enriched GSEA horizontal graph indicating hallmarks gene sets in E2 treated with 2 μM GSK343.

Normalised enrichment score (NES) is indicated on x axis that is plotted against gene sets presented on y axis.. The plot represents significant gene sets generated from GSEA report output file with NOM p value < 0.05 and the FDR < 0.25. Positively enriched gene set (a) have NES > 0 while negatively enriched gene set (b) have NES < 0.

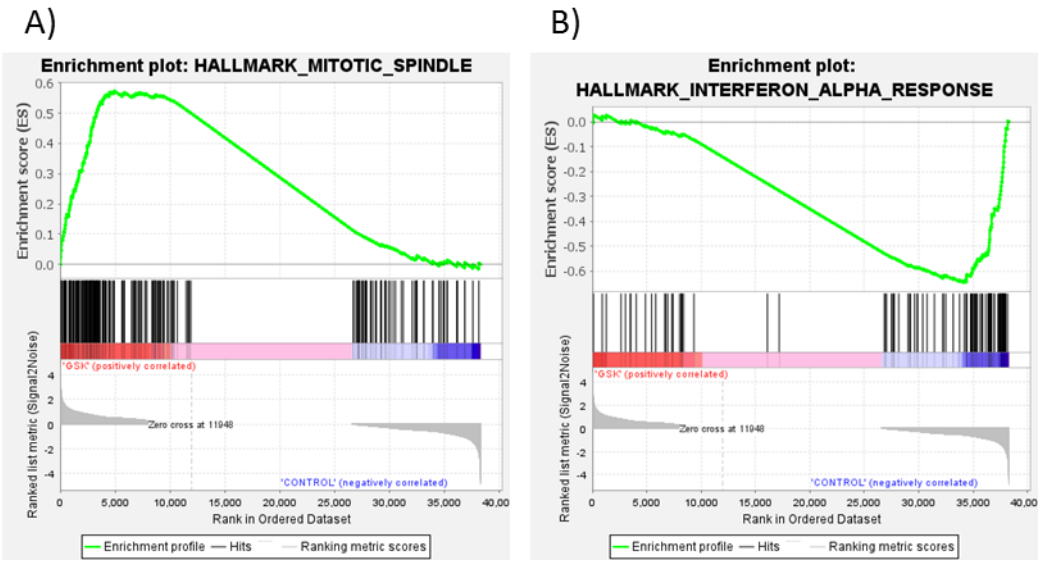

Figure 6-19 The enriched plot of GSEA in E2 treated with 2 μM GSK343 .

GSEA enriched plot represents top positive enriched plot (A), and the top negative enriched plot (B) of the horizontal bar. The ES is indicated as the green curve the final ES score is indicated at the peak of the curve of that gene set.

Table 6-2 shows the NES values of positively and negative enrichment of gene sets of GSEA analysis that is common in G7 and E2 cell lines. The Hallmark gene sets of E2F targets genes are positively enriched in both cell lines. Whereas the Hallmark gene sets of UV response DN genes are negatively enriched in G7 and positively enriched in E2, while Hallmark gene sets of Interferon alpha response genes are positively enriched in G7 and negatively enriched in E2.

Hallmark	G7 NES	E2 NES
HALLMARK_E2F_TARGETS	1.39	1.61
HALLMARK_UV_RESPONSE_DN	-1.53	1.55
HALLMARK_INTERFERON_ALPHA_RESPONSE	1.59	-1.89

Table 6-2 Hallmark of gene set positively and negatively enriched in G7 and E2 cell line.

The NES values of significant pathways is presented in table in G7 and E2 cells treated with 2 μM GSK343. NES > 0 indicates positive enrichment while NES < 0 represents negative enrichment.

6.6 Discussion

GSK343 is a SAM competitive inhibitor that demonstrated potency in several types of cancer. In this chapter, treatment with GSK343 led to a reduction in the number of colonies formed at higher concentrations in G7 and E2 cell lines.The effect of GSK343 on cell viability was also evaluated as an antiproliferative agent. Result obtained showed GSK343 effectively inhibits the number of viable cells thus reducing proliferation, with E2 cells being more sensitive than G7 cells. This confirms recent findings that show that GSK343 suppresses proliferation (Yu *et al.*, 2017).

Assessment was further evaluated to determine the effect of GSK343 combined with either radiation or TMZ. The clonogenic assay showed the cytotoxic effect of GSK343 with increasing doses of radiation on the number of colonies formed. The combination treatment of GSK343 and TMZ caused the two drugs to act synergistically; the experiment yielded a reduction in colony survival, indicating the potency of 10 μM TMZ when combined with GSK343. These data support the effect of GSK343 in sensitising GBM cells to DNA damaging agents.

The mechanism of GSK343 in inducing senescence and apoptosis in GBM cells was also investigated. AnnexinV/7AAD results suggested that GSK343 did not induce early and late apoptosis in GBM cell lines. This contradicts with recent literature that demonstrated GSK343 induces cellular apoptosis (Xiong *et al.*, 2020). Further analysis showed an increase in the expression of senescence-associated ß- galactosidase after exposure to GSK343. Expression of *P21*, which causes cell cycle arrest, was increased, but the senescence marker gene *P16* was not. Furthermore, senescence-related genes were not enriched in the GO or GSEA analyses. Therefore, further investigation would be required to determine whether these cells are actually undergoing senescence or not.

In G7 cell lines, GSK343 induced many more significant changes in gene expression than was observed with EPZ6438 or UNC1999 (Chapter 4 and 5). May be this is due to the fact that there are more off target effects of GSK343 that leads to more changes in gene expression than EPZ6438 and UNC1999. Since the PCA plot did not show the replicates close together. In G7,GO analysis of changes induced by GSK343 showed upregulation of genes related to cell cycle

process and synaptic signalling both associated with cancer progression (Collins, Jacks and Pavletich, 1997; Monje, 2020). Whereas upregulation of neurogenesis and neuronal function genes was found in E2 cells.This may indicate the inhibition of tumour cell progression and increase differentiation. Downregulated pathways in G7 cells included those related to rRNA processing and protein targeting, whereas many of the pathways downregulated in E2 involved the innate immune response, such as the response to interferon and cytokines. This confirms heterogeneity in GBM cell lines, in which E2 cells exhibited more sensitivity to GSK343 treatment and it is consistence with proliferation assay.

However, the comparative analysis with Venn diagrams showed that both cell lines upregulated genes associated with glycosylation, and downregulated genes associated with cell adhesion. Hence, downregulation of genes related to GBM invasiveness (Tysnes and Mahesparan, 2001).

Finally, GSEA analysis was carried out to further investigate the changes in gene expression. Only two upregulated gene sets were enriched in G7 cells, but it is interesting that the most negatively enriched gene set is genes associated with the EMT. This Hallmark is known as an irreversible biological process that is associated with increased resistance and invasiveness of GBM cells (Iwadate, 2016).

Both G7 and E2 cells showed enrichment of the E2F target gene set, and E2 cells also showed enrichment of gene sets associated with the G2M checkpoint and the mitotic spindle, as previously observed in EPZ6438 treated E2 cells (Chapter 4).

Chapter 7 ChIP sequencing analysis of G7 and E2 treated with EPZ6438

7.1 Introduction

Chapter 4 identified DEGs that were upregulated following treatment with EPZ6438. Some of these genes may be direct targets for EZH2, so should show a decrease in H3K27me3 signal over the promoters and transcription start sites (TSS). Other genes may be upregulated due to indirect effects and are not primary targets for EZH2.

In this chapter the ChIP-seq analysis was carried out to identify upregulated genes that are direct targets of EZH2. The analysis was performed following incubation of G7 and E2 cell line under stem conditions with 2 μM EPZ6438 or solvent control for 5 days.

7.2 Characterisation of ChIP peaks in GBM cell lines

ChIP-seq DNA was sequenced by paired-end sequencing, with 150 bp per read. The number of pairs of reads sequenced range from 22.1 million to 41.8 million. PHRED quality scores were greater than 35 for all positions for all samples. Reads were aligned to the human genome build Hg38 using Bowtie 2. This is the same tool that Hisat2 is based on, but it doesn't use a gtf file as there are no introns that need to be accounted. Bowtie2 uses the quality score of each base to guide alignment. 49 – 82% of pairs aligned concordantly exactly 1 time, which is 22.3 – 42.4 million aligned pairs.

MACS2 was used to identify peaks in the H3K27me3 and H3K4me3 data, with comparison to the input control for G7 and E2 samples (Zhang *et al.*, 2008; Feng *et al.*, 2012). ChIPseeker was used to annotate the peaks, to determine whether they overlap with known genetic elements (Figure 7-1). Approximately 50% of H3K4me3 peaks overlap with promoter regions less than 1 kb from a TSS, consistent with the known role of this modification at active promoters. H3K27me3 peaks were found at a range of elements, with the largest category being distal intergenic regions. No significant differences were found when comparing G7 to E2 cells.

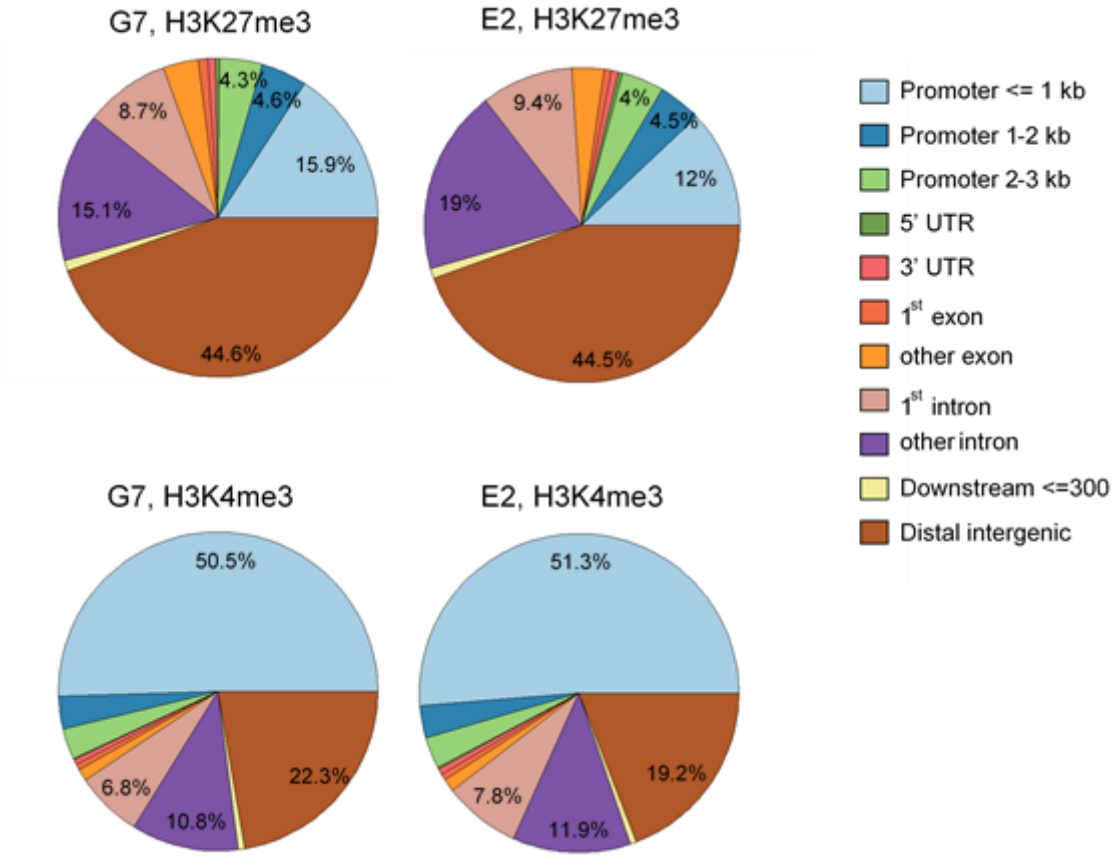

Figure 7-1 Annotation of H3K72me3and H3K4me3 peaks in G7 and E2 cells

MACS2 (broad setting) was used to call peaks from aligned H3K27me3 or H3K4me3 ChIP-seq reads for G7 and E2 cells, using the input reads as the control. The tool ChIPseeker was used to annotate the peaks based on their position with respect to various genomic locations. The pie charts show the percentage of peaks that fall into each annotation category.

Seqmonk was used to quantify peaks and compare ChIP peak intensity against gene expression in control samples. In order to see if there is a correlation between expression level and ChIP quantification, scatter plots were created separately for H3K27me3 and H3K4me3 peaks for each cell line. The quantification of each peak was plotted against the average Log2 RNA-seq count for overlapping genes. The trendline shows a gentle trend of genes with higher expression having less H3K27me3 signal (Figure 7-2). Whereas genes with more H3K4me3 have higher expression than genes with low H3K4me3 (Figure 7-3).

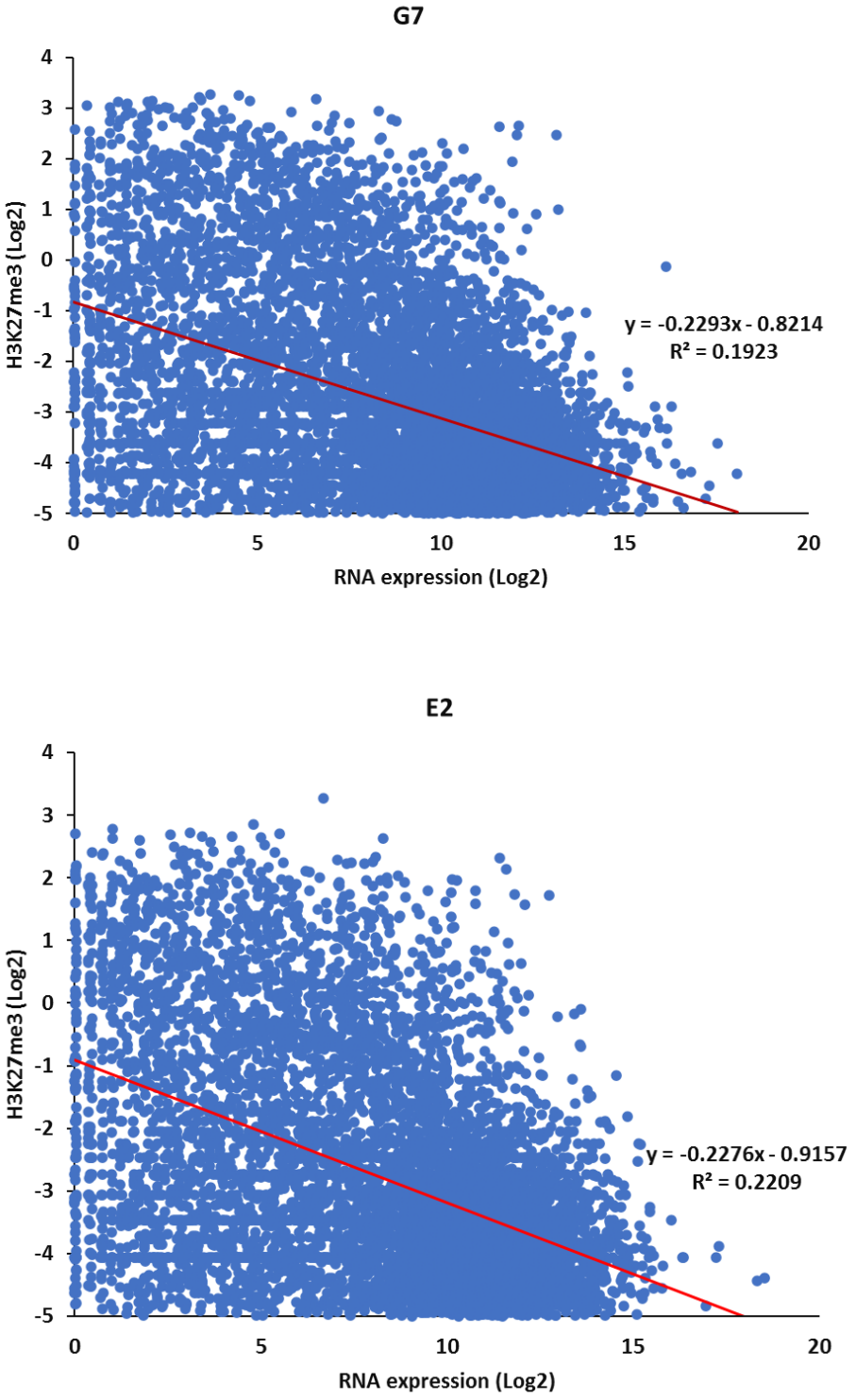

Figure 7-2 The scatter plot of Log2 of quantification of H3K27me3 peaks from the control against Log2 RNA expression.

The quantification of peaks of the control sample was performed using Seqmonk, then filtered for those that overlap TSS eponine. The probe lists were exported that include gene names and quantifications. The Log2 H3K27me3 > - 5 represents quantification of peaks from Seqmonk output file. The Log2 RNA expression > 0 represents average count from the 3 replicates of genes from Deseq2 count file.

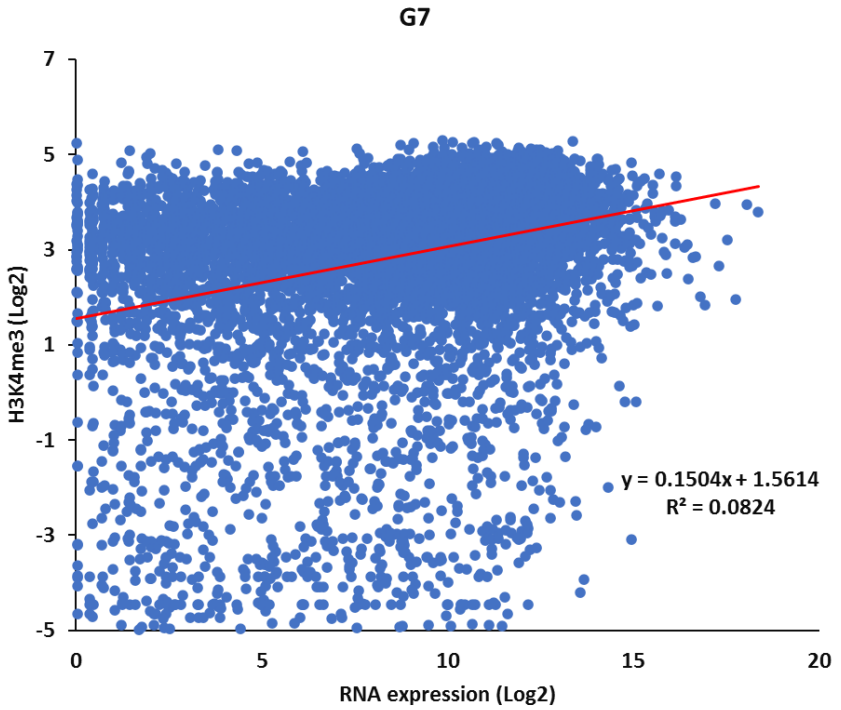

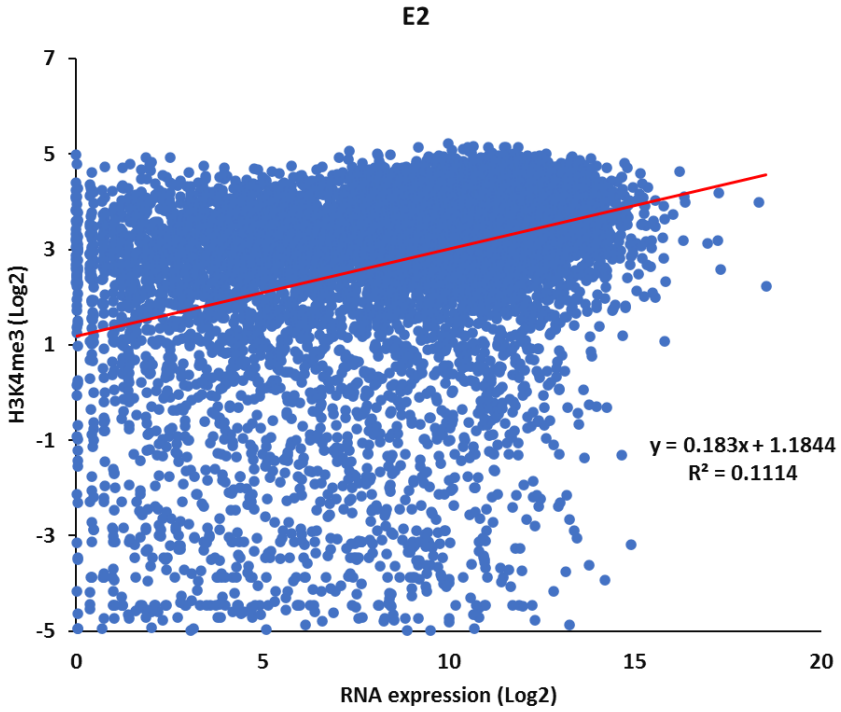

Figure 7-3 The scatter plot of Log2 of quantification of H3K4me3 peaks from the control against Log2 RNA expression.

The quantification of peaks of the control sample was performed using Seqmonk, then filtered for those that overlap TSS eponine. The probe lists were exported containing gene names and quantifications. The Log2 RNA expression > 0 represents average count from the 3 replicates of genes from Deseq2 count file. The Log2 H3K27me3 > - 5 represents quantification of peaks from Seqmonk output file.

In order to compare expression of genes that overlap the ChIP peaks and genes that don't have ChIP peaks, a box plot was created. The same steps for creating scatter plots using Seqmonk output file was performed. Box and whiskers were plotted by separating list of genes that have ChIP peaks and genes that don't have ChIP peaks. Figure 7-4 shows that genes with a H3K27me3 peak have higher expression than genes that don't have H3K27me3 peak in G7 and E2 non treated control cells. The same can be seen in Figure 7-5 that shows genes with H3K4me3 peak have higher expression than genes with no H3K4me3 peaks.

In untreated GBM cells, the box plots showed that average gene expression was higher in genes that have a peak of H3K27me3 in comparison with genes that do not have a H3K27me3 peak. Whilst unexpected, given that H3K27me3 is a repressive mark, this data probably reflects the fact that H3K27me3 is not a universal mechanism for gene silencing, as many genes can be silenced with H3K9me3 (Ninova, Fejes Tóth and Aravin, 2019), DNA methylation (Newell-Price, Clark and King, 2000), or other mechanisms. This will also include bivalent genes that have both H3K4me3 and H3K27me3 and have low levels of expression.

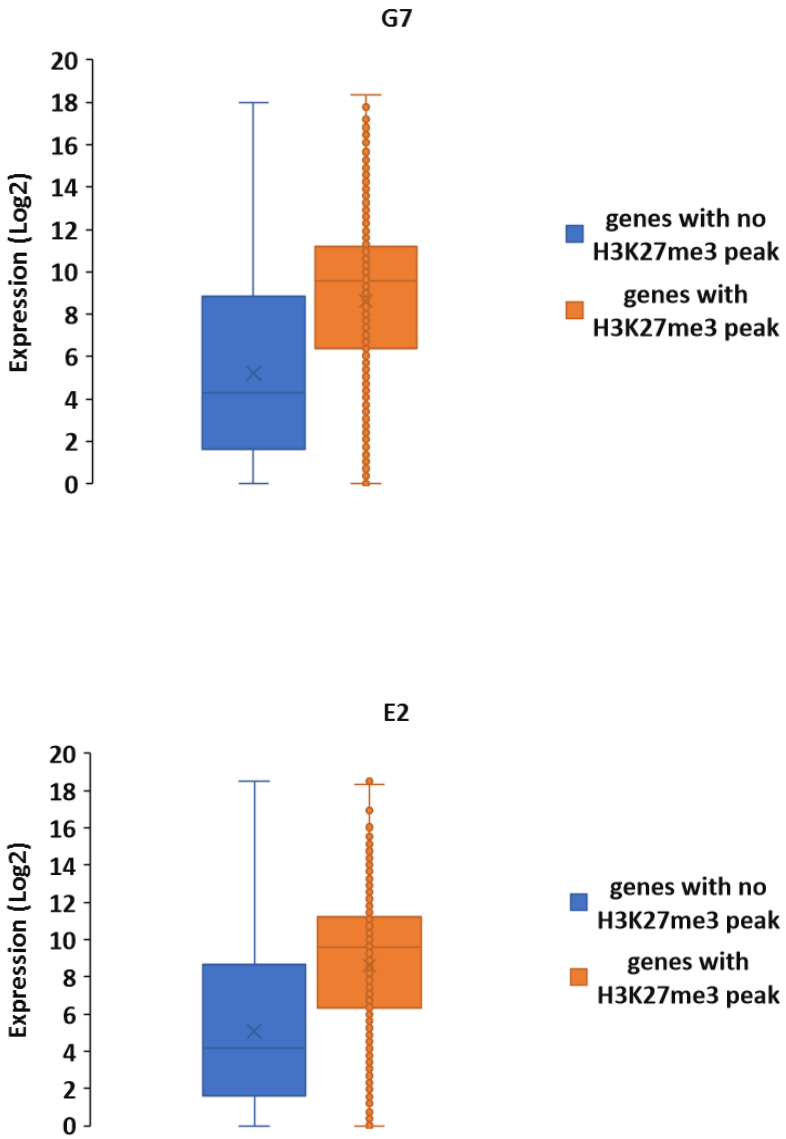

Figure 7-4 Box and whiskers plot compares the RNA expression of genes that have a H3K27me3 peaks with genes those that don't have H3K27me3 peaks.

The probe lists created from Seqmonk were exported that contain gene names and quantifications. The Log2 (> 0) of average expression from triplicates of Deseq2 control file was calculated . Box and whiskers plot were created from list of genes with one box is the combined expression of all genes that overlap ChIP peaks and other box is the data from all genes that don't have ChIP peaks.

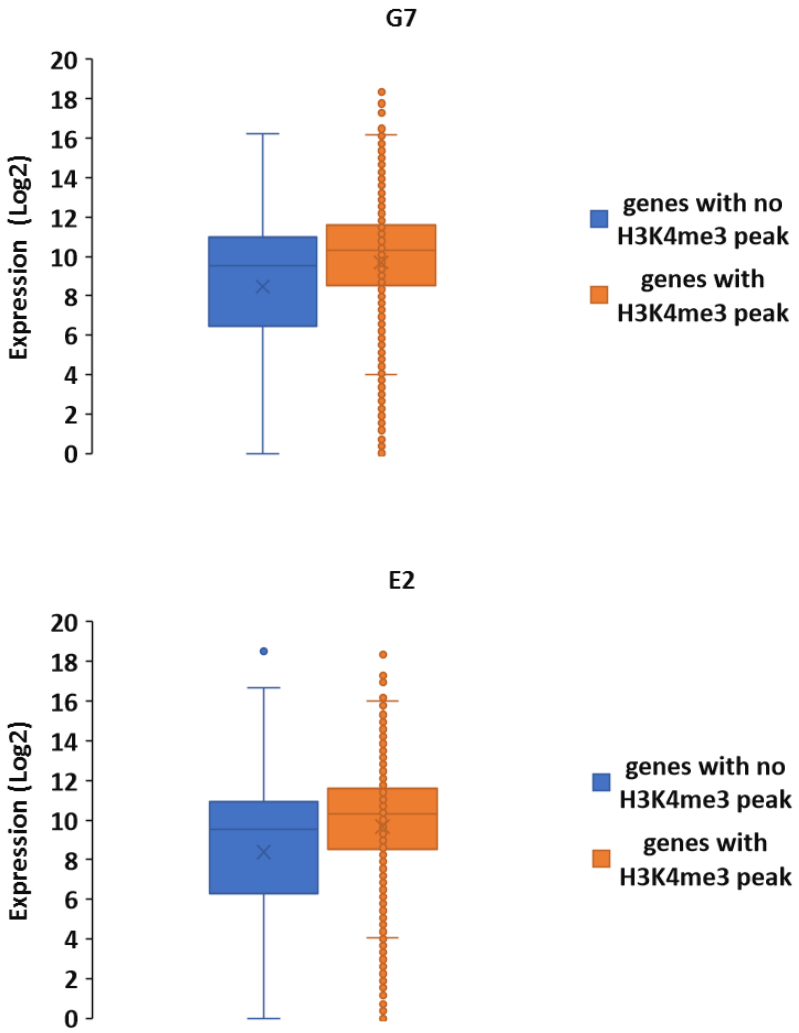

Figure 7-5 Box and whiskers plot compares the expression of genes that have a H3K4me3 peaks with those that don't have H3K4me3 peaks.

The probe lists created from Seqmonk were exported that contain gene names and quantifications. The Log2 (> 0) of average expression from triplicates of Deseq2 control file was calculated . Box and whiskers plot were created from list of genes with one box is the combined expression of all genes that overlap ChIP peaks and other box is the data from all genes that don't have ChIP peaks.

The ChIP-seq data was visualised on the UCSC genome browser in order to confirm enrichment of H3K27me3 at genes that are known to be repressed by this modification. BigWig files were created using bamcoverage tool, and MACS peak was used to call peaks by comparing data to the input control. Figure 7-6 and Figure 7-7 show H3K27me3 ChIP-seq data at haematopoietic genes that are repressed in neural and GBM cells, TAL1 and HBA (the alpha globin gene locus).

The ChIP-seq data of G7 and E2 control cells were compared with other publicly available data for H3K27me3 in normal brain, GBM and oligodendroglioma cell lines. Data from the G7 and E2 cell lines showed a similar profile of H3K27me3 signal compared to the other cell types, with clear enrichment at the TAL1 and HBA genes compared to the surrounding genomic environment. This data is consistent with silencing of these genes in GBM cells, and supports the conclusion that the H3K27me3 ChIP-seq has been performed successfully.

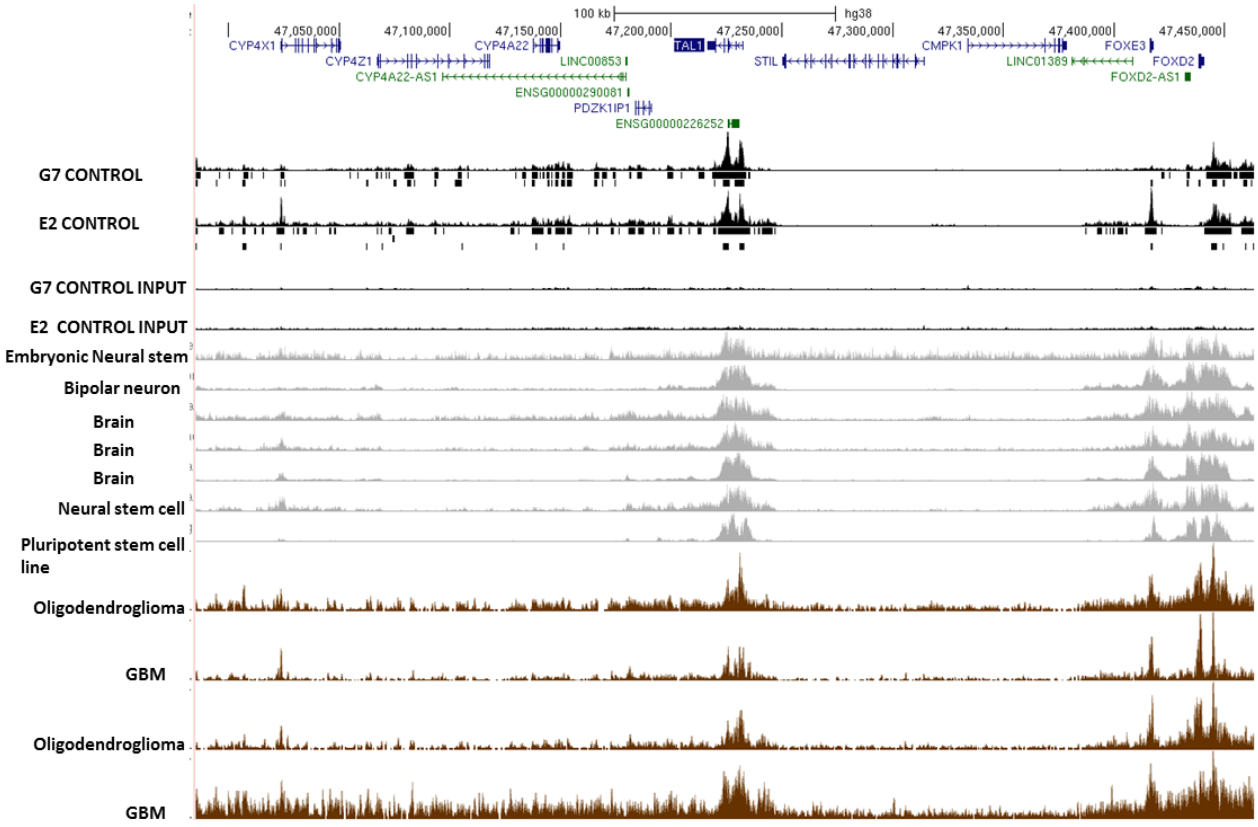

Figure 7-6 ChIP-seq data at the TAL1 gene locus

H3K27me3 ChIP-seq data for G7 and E2 control cells were converted to BigWig files and displayed on the UCSC genome browser. MACS2 peaks are shown as black boxes underneath their respective BigWig track. The TAL1 gene is shown at the top, and it is transcribed from right to left (indicated by arrows). Deep boxes are exons, thin horizontal lines are introns.

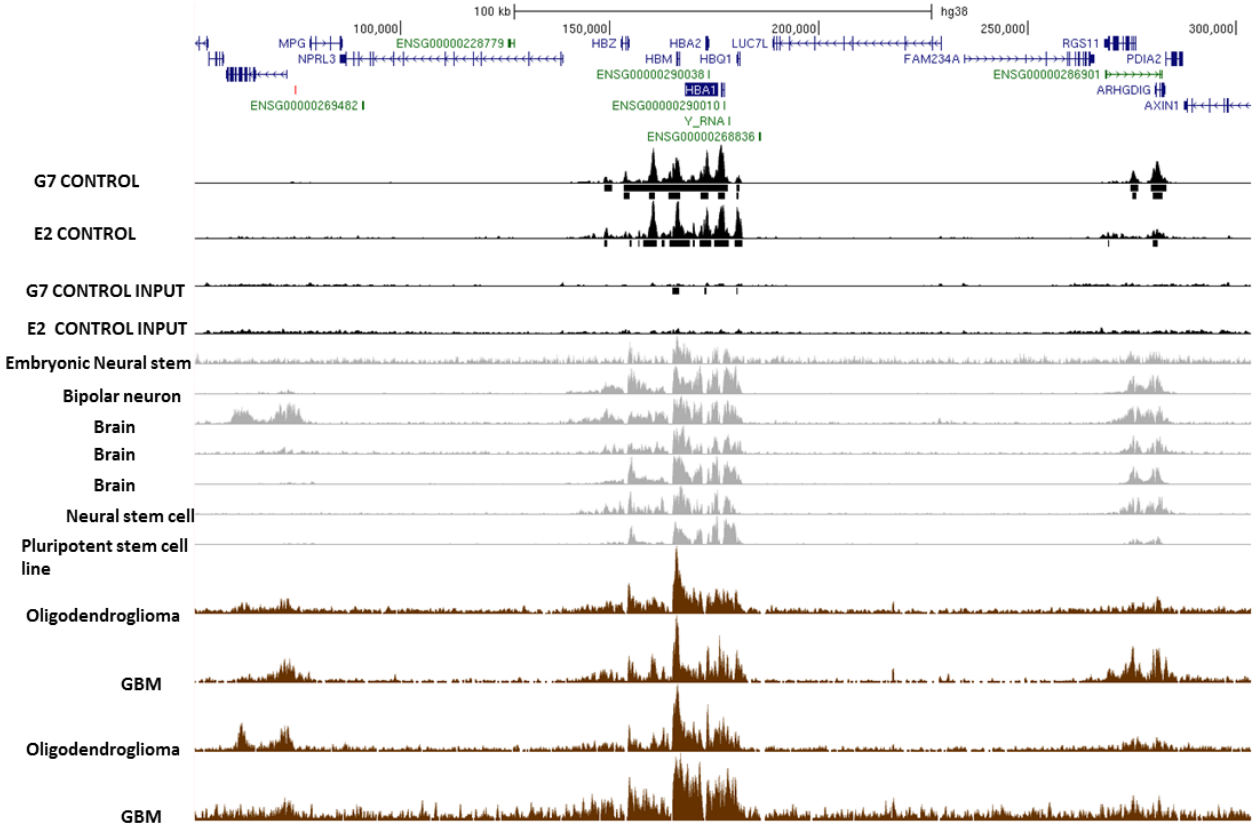

Figure 7-7 ChIP-seq data at the HBA1 gene locus.

H3K27me3 ChIP-seq data for G7 and E2 control cells were converted to BigWig files and displayed on the UCSC genome browser. MACS2 peaks are shown as black boxes underneath their respective BigWig track. The HBA1 gene is shown at the top, and it is transcribed from left to right (indicated by arrows). Deep boxes are exons, thin horizontal lines are introns.

7.3 Investigation of H3K27me3 level in GBM cell lines following treatment with EPZ6438

In order to identify changes that occur in genome wide profile of H3K27me3 and H3K4me3 in cells treated with EPZ6438 versus control, MACS2 was used to define H3K27me3 peaks in untreated cells, and the intensity of signal at these peaks was quantified in the data from both treated and untreated cells. This approach should reveal any changes in H3K27me3 signal resulting from EZH2 inhibition. The grey, red and blue points in the scatter plot in Figure 7-8 show the intensity of signal for all peaks in control and EPZ6438 treated cells. The data show that the intensity of H3K27me3 peaks is stronger in control cells than in treated cells in both cell lines, consistent with inhibition of EZH2 enzymatic activity after drug treatment.

The ChIP-seq data was then intersected with the RNA-seq data in order to identify potential genes that are direct targets of EZH2's histone methylation activity. Potential direct targets were defined as genes that i) have a peak of H3K27me3 overlapping the TSS in untreated cells, and ii) upon EZH2 inhibition, the H3K27me3 peak decreased in intensity and iii) the expression of the gene significantly increased. In Figure 7-8, blue points indicate H3K27me3 peaks that overlap with the TSS of upregulated DEGs, as defined in chapter 4. A decrease in ChIP-seq read counts of at least log2 = 0.5 (i.e. greater than 30% decrease) was then chosen as the cut off to indicate a peak with a decrease in H3K27me3 in EPZ6438 treated cells (red points). This process identified 278 potential EZH2 target genes in G7 cells, and 128 genes in E2 cells.

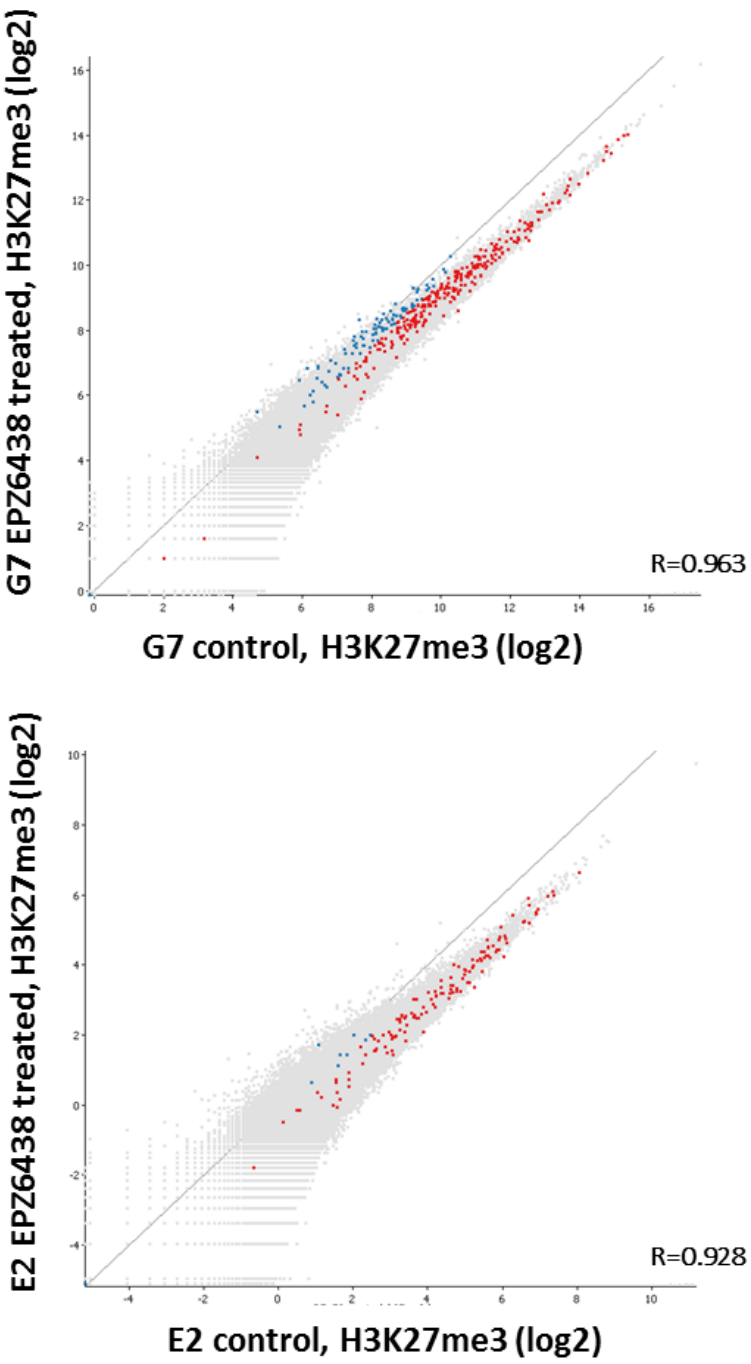

Figure 7-8 Scatter plot showing the H3K27me3 peaks in control and EPZ6438 treated GBM cells.

Scatter plot showing quantification of reads within MACS peaks. The x axis represents the peak in control and the y axis represents the peak in treated cells. The diagonal line corresponds to the same enrichment in control and treated cells.

In addition to a decrease in H3K27me3 signal, it might be anticipated that upregulated DEGs would also show an increase in H3K4me3 signal. To identify these genes, MACS2 peaks were defined for H3K4me3 in untreated G7 and E2 cells using the input chromatin as the control. The peaks were quantified in both treated and untreated cells, and are plotted in a scatter plot in Figure 7-9. In contrast to the H3K27me3 data, there was no general trend indicating a change in H3K4me3 enrichment in treated compared to untreated cells. Peaks were then filtered to highlight those that overlap with the TSS of upregulated DEGs (blue points). A log2 increase of 0.4 was used as a cut off to identify filtered peaks that have an increase in H3K4me3 signal (red points).

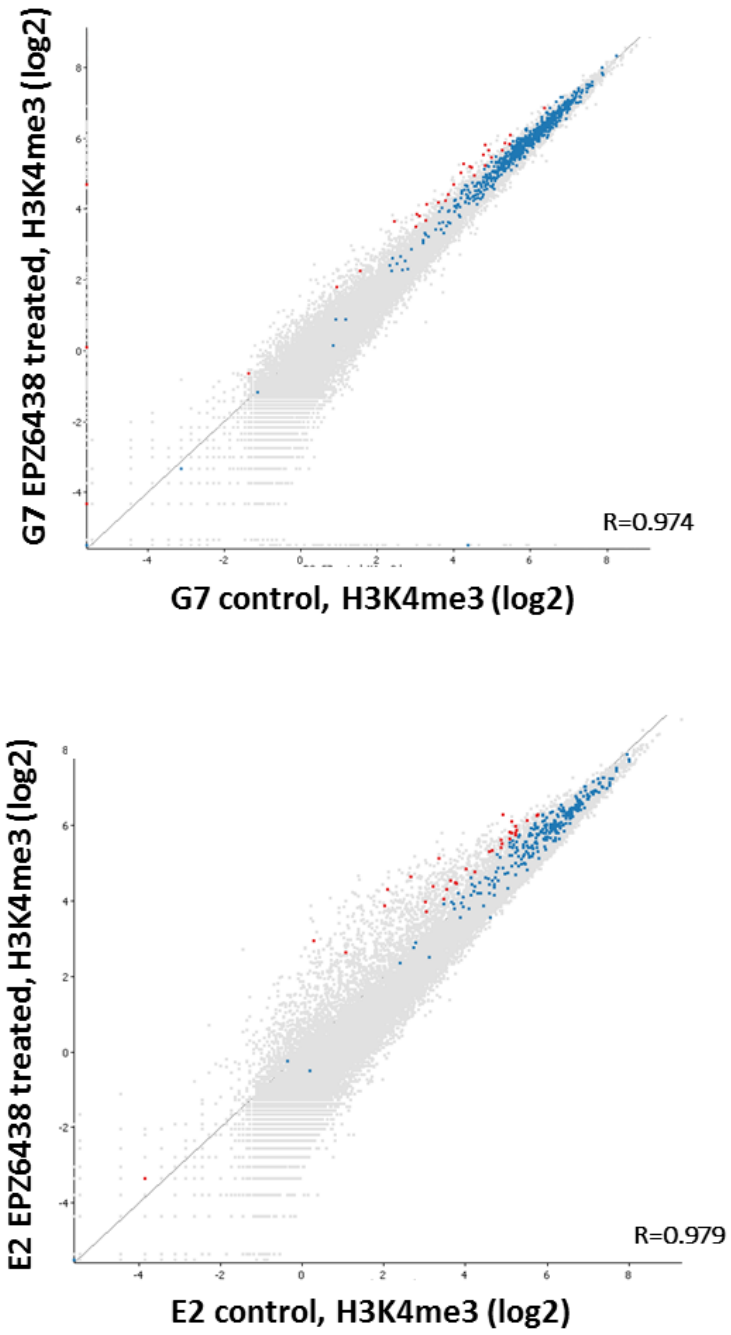

Figure 7-9 Scatter plot showing the H3K4me3 peaks in control and EPZ6438 treated GBM cells.

The x axis represents the peak in control and the y axis represents the peak in treated cells. The diagonal line corresponds to the same enrichment in control and treated cells.

7.4 Investigation of H3K27me3 signal in relation with EZH2 targeted genes

In order to investigate the roles of the 278 genes in G7 cells that were identified as potential EZH2 targets, GO was performed. The top six biological process categories are all related to neurogenesis and neuron development. In order to try and identify which genes might be driving the process of neuronal differentiation, the functional roles of these 278 genes were examined. Transcription factors, growth factors and receptor tyrosine kinases were chosen as categories of regulatory protein that might drive cellular phenotype. The genes that fall into these categories are shown in table 7-1. One of these, BMP7, also showed an increase in H3K4me3 enrichment.

In E2 cells, only 128 genes were found to be upregulated and also show a decrease in H3K27me3 signal. GO analysis revealed enrichment in biological processes including neurogenesis, organ morphogenesis and the response to BMP7 signalling. The gene list was interrogated for regulatory proteins including transcription factors, growth factors and receptor tyrosine kinases, and 6 genes were identified (Table 7-2).

Feature	ID	category	neurogenesis or CNS development	H3K4me3 increased?
BMP7	ENSG00000101144	GF	neurogenesis	H3K4me3 up
CXCL12	ENSG00000107562	GF	neurogenesis	
GDF7	ENSG00000143869	GF	neurogenesis	
NRG4	ENSG00000169752	GF		
PDGFA	ENSG00000197461	GF		
THBS4	ENSG00000113296	GF	neurogenesis	
THPO	ENSG00000090534	GF		
VGF	ENSG00000128564	GF		
WNT11	ENSG00000085741	GF	neurogenesis	
EPHB3	ENSG00000182580	RTK	neurogenesis	
FGFR2	ENSG00000066468	RTK	neurogenesis	
FLT1	ENSG00000102755	RTK		
FLT4	ENSG00000037280	RTK		
KIT	ENSG00000157404	RTK	neurogenesis	
RET	ENSG00000165731	RTK	neurogenesis	
BCL11A	ENSG00000119866	TF	neurogenesis	
BHLHE41	ENSG00000123095	TF	neurogenesis	
EMX2	ENSG00000170370	TF	neurogenesis	
FOXF2	ENSG00000137273	TF		
GLI2	ENSG00000074047	TF	neurogenesis	
HMX3	ENSG00000188620	TF	neurogenesis	
INSM1	ENSG00000173404	TF	neurogenesis	
LEF1	ENSG00000138795	TF	neurogenesis	
MAF	ENSG00000178573	TF		
MAFA	ENSG00000182759	TF		
MAFB	ENSG00000204103	TF	neurogenesis	
NFATC1	ENSG00000131196	TF		
NFIA	ENSG00000162599	TF		
PAX2	ENSG00000075891	TF	neurogenesis	
POU4F2	ENSG00000151615	TF	neurogenesis	
PRDM16	ENSG00000142611	TF	neurogenesis	
PRRX2	ENSG00000167157	TF		
RORA	ENSG00000069667	TF	neurogenesis	
ZBTB46	ENSG00000130584	TF		
ZIC2	ENSG00000043355	TF	neurogenesis	
ZIC5	ENSG00000139800	TF		
ZNF385C	ENSG00000187595	TF		
ZNF467	ENSG00000181444	TF		

Table 7-1 Putative EZH2 target genes that drive neuronal differentiation in EPZ-6438 treated G7 cells.

G7 genes significantly upregulated in the presence of EPZ6438 were filtered for a decrease in H3K27me3 signal. From those 278 genes, transcription factors (TF) were identified from the TF database published by Lambert et al (2016), and growth factors (GF) and receptor tyrosine kinases (RTK) were annotated using GO (Toppgene). The 38 genes with the annotation TF, GF and RTK are shown in this table. Roles in neurogenesis or central nervous system development were identified from GO (Toppgene). Genes with an increase in H3K4me3 are noted.

Feature	ID	TF/GF/RTK	Neurogenesis	H3K4me3
ROR2	ENSG00000169071	RTK		
MAFB	ENSG00000204103	TF	neurogenesis	
PAX2	ENSG00000075891	TF	neurogenesis	
PITX2	ENSG00000164093	TF	neurogenesis	
ZBTB16	ENSG00000109906	TF	neurogenesis	
ZNF467	ENSG00000181444	TF		H3K4me3 up

Table 7-2 Putative EZH2 target genes that drive neuronal differentiation in EPZ-6438 treated E2 cells.

E2 genes significantly upregulated in the presence of EPZ6438 were filtered for a decrease in H3K27me3 signal. From those 128 genes, transcription factors (TF) were identified from the TF database published by Lambert et al (2016), and growth factors (GF) and receptor tyrosine kinases (RTK) were annotated using GO (Toppgene). The 6 genes with the annotation TF or RTK are shown in this table. Roles in neurogenesis were identified from GO (Toppgene). Genes with an increase in H3K4me3 are noted.

It is interesting to note that the transcription factors MAFB, PAX2, and ZNF467 were identified as potential EZH2 target genes in both G7 and E2 cells. In order to examine these genes more closely, the ChIP-seq data was visualised using the UCSC genome browser (Figure 7-10 to 7-14).

Figure 7-10 shows ChIP-seq data at BMP7 gene locus. BMP7 was identified as a EZH2 target in G7 cells but not in E2 cells. In untreated G7 cells, the H3K27me3 track shows high enrichment of H3K27me3 at the BMP7 promoter, and the peaks defined by MACS2 (black bars beneath the trace) extend across most of the visible window. In cells treated with the EZH2 inhibitor, the maximum peak height is decreased, and the bars indicating MACS peaks are more fragmented. This decrease in H3K27me3 signal around the BMP7 TSS is expected, as this is how the EZH2 target genes were defined previously. An increase in H3K4me3 signal at the BMP7 promoter in treated G7 cells can also be observed. Interestingly, there is no H3K27me3 signal across this region in either treated or untreated E2 cells, and the H3K4me3 peak is higher than in G7 cells. This

explains why BMP7 was not identified as an EZH2 target in E2 cells, as there is no H3K27me3 signal to start with.

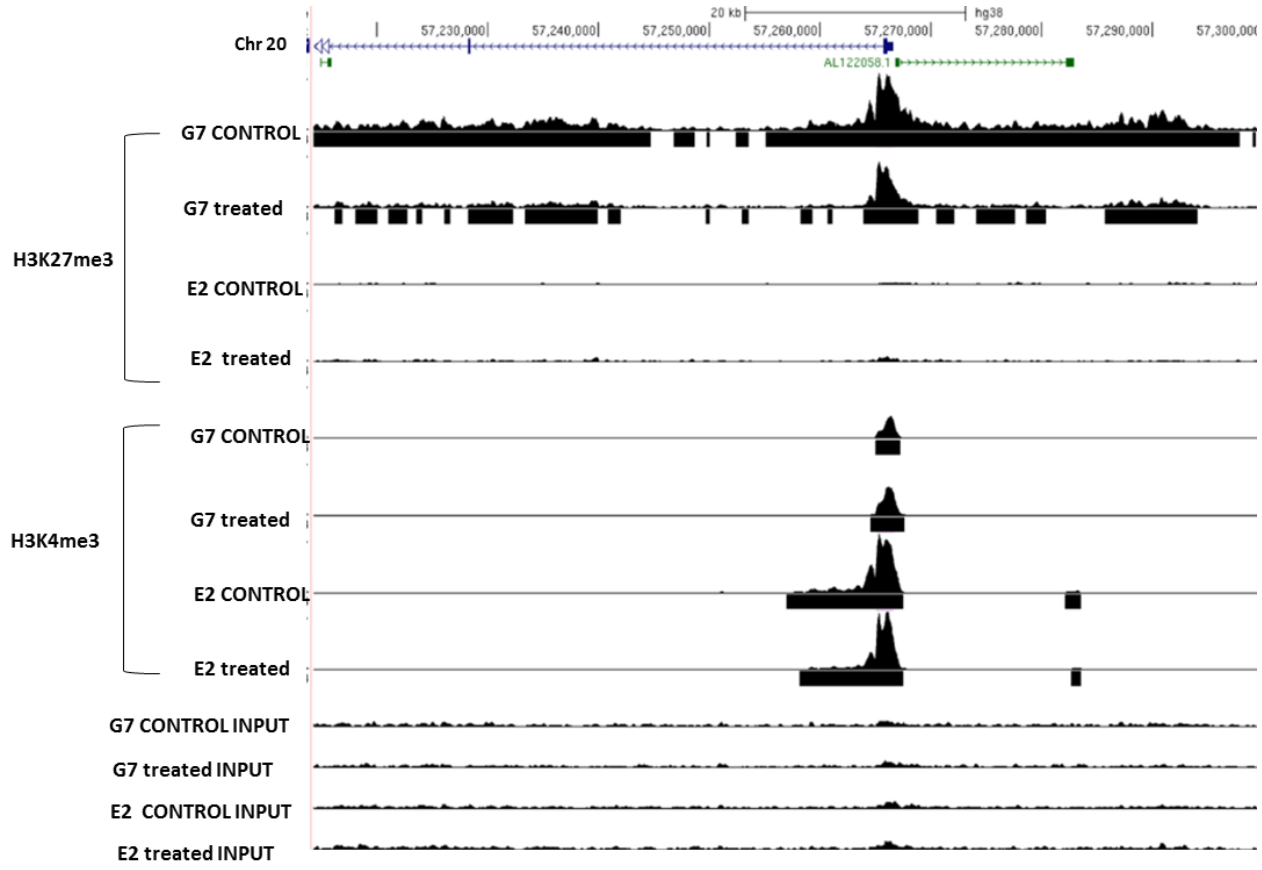

Figure 7-10 ChIP-seq data at the BMP7 gene locus

H3K27me3 and H3K4me3 ChIP-seq data for G7 and E2 cells were converted to BigWig files and displayed on the UCSC genome browser. MACS2 peaks are shown as black boxes underneath their respective BigWig track. The BMP7 gene is shown at the top, and it is transcribed from right to left (indicated by arrows). Deep boxes are exons, thin horizontal lines are introns.

PAX2 was identified as an EZH2 target in both cell lines. Consistent with this, the genome browser view in Figure 7-11 shows extensive H3K27me3 signal in untreated G7 and E2 cells, with MACS2 peaks covering most of the region. The H3K27me3 signal is reduced following EPZ6438 treatment, with smaller peaks defined by MACS2. Enrichment of H3K4me3 at the PAX2 promoter was unchanged in both cell lines following EZH2 inhibition.

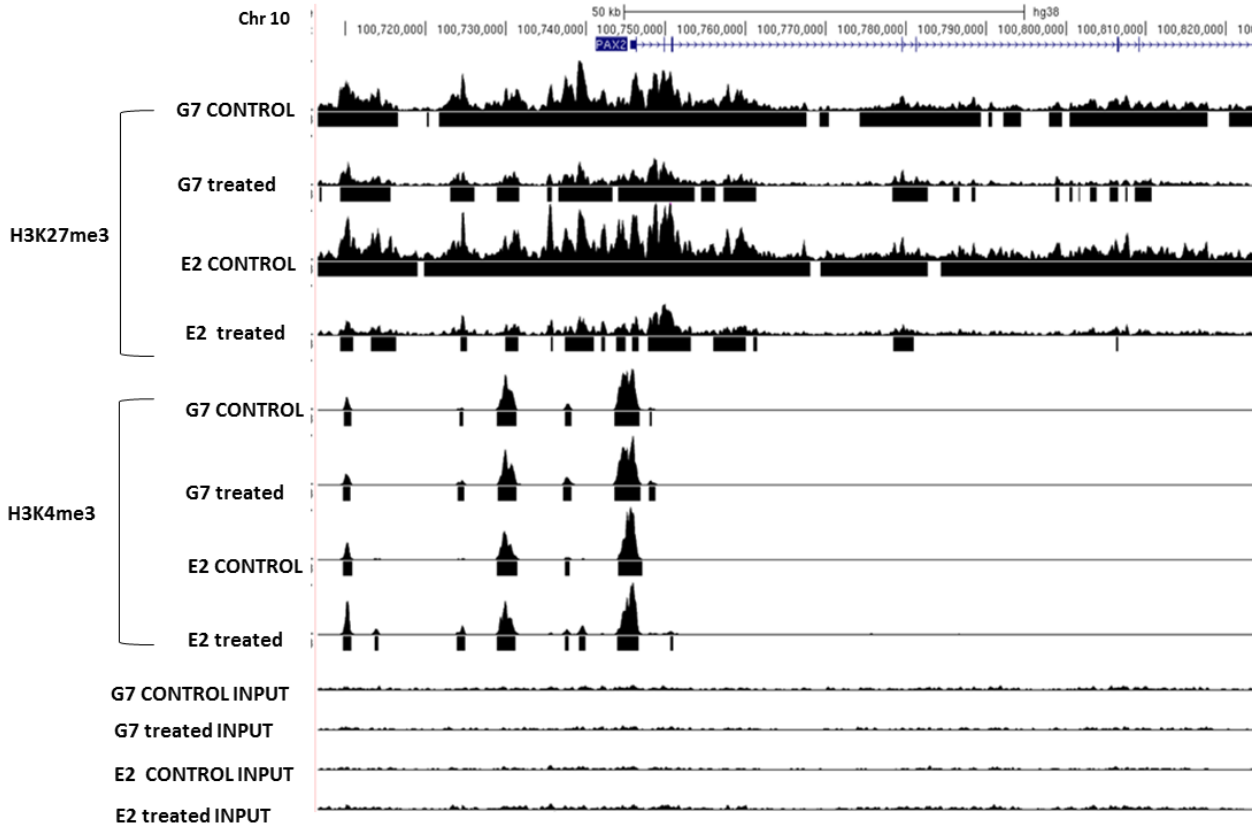

Figure 7-11 ChIP-seq data at the PAX2 gene locus

H3K27me3 and H3K4me3 ChIP-seq data for G7 and E2 cells were converted to BigWig files and displayed on the UCSC genome browser. MACS2 peaks are shown as black boxes underneath their respective BigWig track. The PAX2 gene is shown at the top, and it is transcribed from left to right (indicated by arrows). Deep boxes are exons, thin horizontal lines are introns.

Both MAFB and ZNF467 showed stronger H3K27me3 signal for G7 and E2 control cells compared to treated cells (Figure 7-12 and Figure 7-13). H3K4me3 signal appeared to be relatively unchanged at both MAFB and ZNF467 transcription factors, even though the quantification had indicated an increase in H3K4me3 signal at ZNF467 (Table 7-2). Figure 7-14 shows the ZNF467 locus with the RNA-seq data included. The increase in RNA expression in EPZ6438-treated cells is illustrated by the increased signal in the RNA tracks.

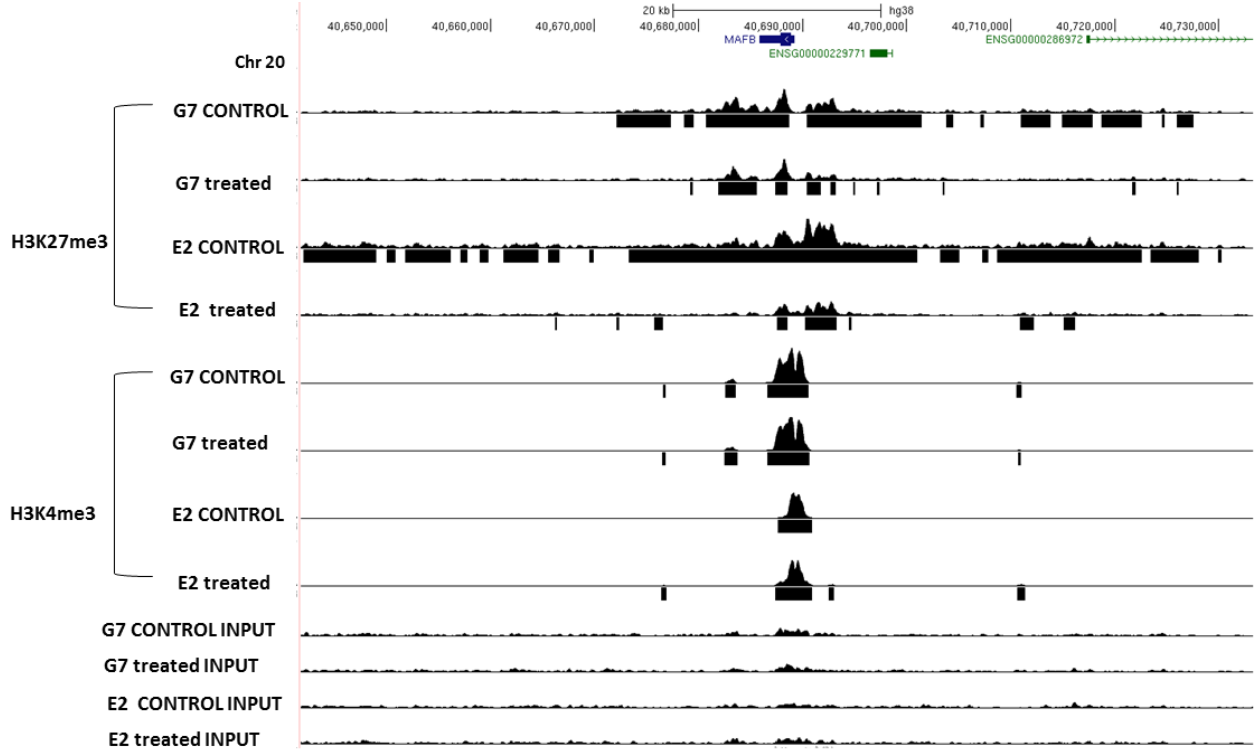

Figure 7-12 ChIP-seq data at the MAFB gene locus

ChIP-seq data of H3K27me3 and H3K4me3 for GBM cell lines were converted to BigWig files and displayed on the UCSC genome browser. Black boxes represents MACS2 peaks underneath their respective BigWig track. Deep boxes are exons, thin horizontal lines are introns. The MAFB gene is shown at the top, and it is transcribed from right to left.

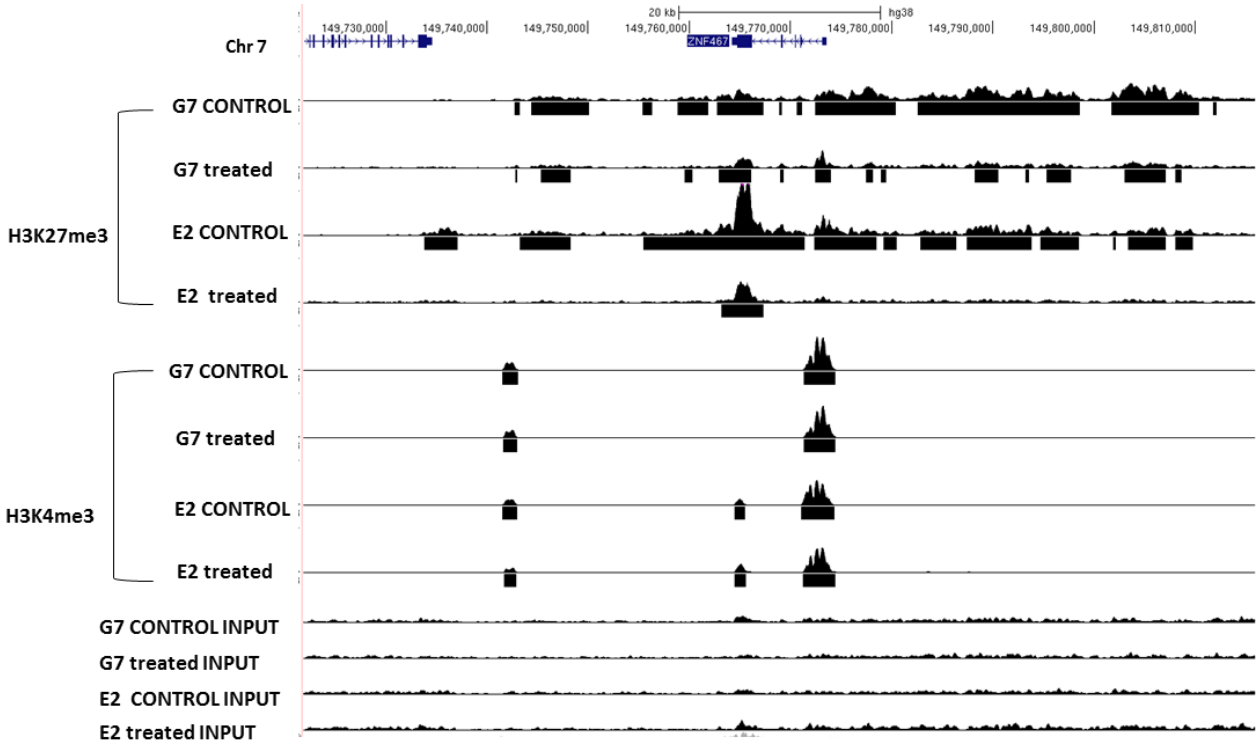

Figure 7-13 ChIP-seq data at the ZNF467 gene locus

ChIP-seq data of H3K27me3 and H3K4me3 for G7 and E2 cell lines were converted to BigWig files and presented on the UCSC genome browser. Deep boxes are exons, thin horizontal lines are introns. Black boxes represents MACS2 peaks underneath their respective BigWig track. The ZNF467 gene is shown at the top, and it is transcribed from right to left.

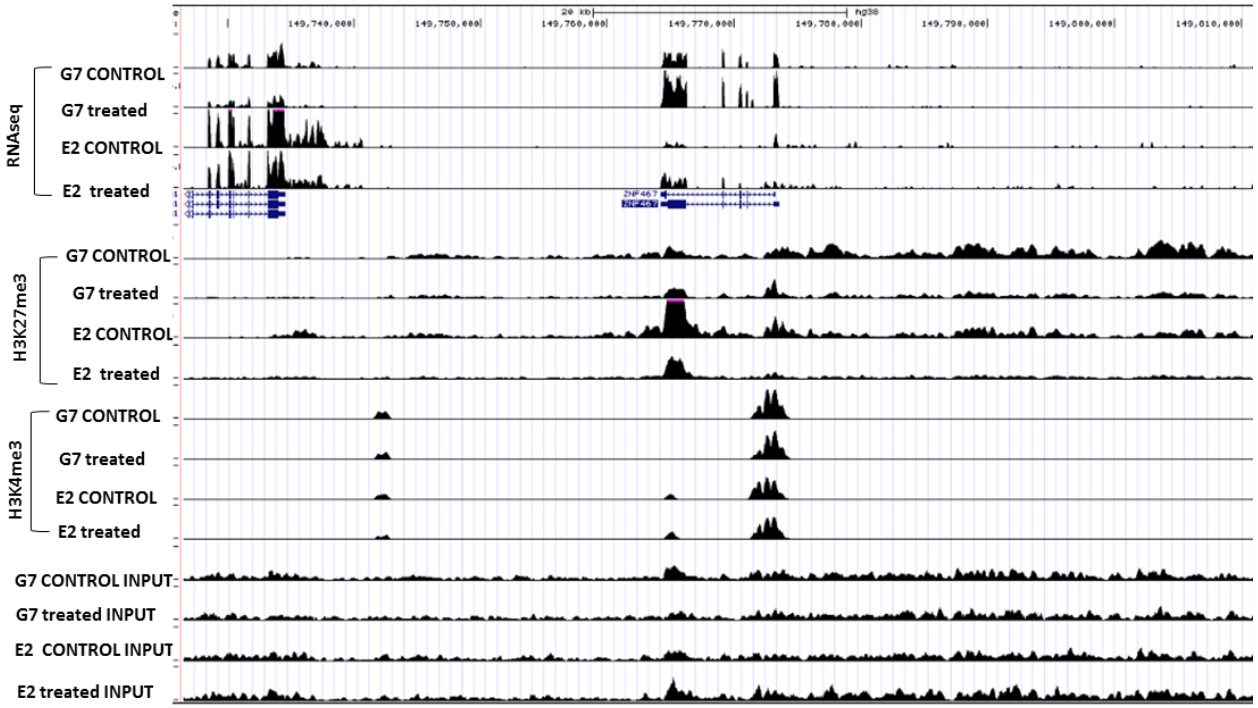

Figure 7-14 RNA-seq and ChIP-seq data at the ZNF467 gene locus

RNA-seq, H3K27me3 and H3K4me3 ChIP-seq data for G7 and E2 cells were converted to BigWig files and displayed on the UCSC genome browser. MACS2 peaks are shown as black boxes underneath their respective BigWig track. The ZNF467 gene is shown and it is transcribed from right to left (indicated by arrows). Deep boxes are exons, thin horizontal lines are introns.

7.5 Discussion

The RNA-seq analyses in previous chapters revealed numerous genes that have changes in expression following EZH2 inhibition. However, it is not possible to distinguish between genes that are direct targets of EZH2, and have thus been directly affected by the inhibition of EZH2 activity, and those genes that are secondary, or indirect targets. The aim of this chapter was to identify potential direct targets of EZH2 through analyses of changes in H3K27me3 across the genome.

The chapter describes ChIP-seq analysis of H3K27me3 and H3K4me3 histone modifications in G7 and E2 cells after treatment with the EZH2 inhibitor EPZ6438. The epigenomic profiles in untreated cells are comparable with publicly available data, confirming successful chromatin immunoprecipitation. ChIP-seq was then integrated with RNA-seq data from chapter 4 in order to

identify potential EZH2 target genes. These are genes that show a decrease in repressive H3K27me3 and an increased in expression following EZH2 inhibition.

In G7 cells, 278 EZH2 targets were identified and this list of genes was enriched in GO terms for neurogenesis and neuron development. The 128 direct targets in E2 cells were also enriched in GO terms for neurogenesis, organ morphogenesis and the response to BMP7 signalling. These results are consistent with the RNA-seq analyses in chapters 4, 5 and 6, which showed that increased expression of genes related to neurogenesis and neuronal function is a common feature of GSCs treated with EPZ6439, UNC1999 and GSK343. The chromatin immunoprecipitation data extends these conclusions, and reveals that genes related to neurogenesis are likely to be direct targets of EZH2.

From this data, it is hypothesise that the upregulation of small number of regulatory factors that control neurogenesis may be driving the changes in expression of large numbers of other genes involved in neuronal development or function. Therefore, the lists of EZH2 target genes were scanned to identify regulatory factors such as growth factors, tyrosine kinase receptors, and transcription factors. Thirty eight regulatory factors were identified from G7 cells, and six from E2 cells. Interestingly, three regulatory factors were common to both G7 and E2 cells: MAFB, PAX2 and ZNF467.

MAFB, PAX2 and ZNF467 are all transcription factors with known roles in regulating differentiation. The PAX2 gene is found to be associated with regulation of neurogenesis in optic nerve of embryo. Overexpression of PAX2 in optic nerve explant promotes glial development and prevents differentiation (Soukkarieh et al., 2007). MAFB was found to be important for the formation of hindbrain (Sturgeon et al., 2011). It also act as a regulator of neuronal linage development (Yu et al., 2013) and synaptogenesis (Pai et al., 2019). ZNF467 is transcription factor belong to ZNF family. Zinc-finger proteins (ZNF) are involved in several molecular mechanisms acting as key role in differentiation of tissue thus play role in cellular processes. ZNF467 is known to regulate differentiation in adipocytes and osteoblasts (Gluscevic *et al.*, 2020), and is expressed in brain cells (Panossian, Seo and Efferth, 2018), although a functional role in the brain has not been investigated.

BMP7 was also highlighted as an EZH2 target in G7 cells, but not in E2 cells. BMP7 is not marked with H3K27me3 in E2 cells, so its expression does not change following EZH2 inhibition. BMP7 is a growth factor that is commonly expressed in the central nervous system. *In vitro* analysis showed the effect of BMP7 on inhibiting proliferation and inducing neuronal like characteristics thus by promoting differentiation in primary GBM. The same study implicated the *in vivo* role of BMP7 in decreasing tumour growth (Tate *et al.*, 2012).

Further work on all of these genes is necessary to investigate whether they do actually have roles in driving the transcriptomic response to EZH2 inhibitors, and how the phenotypic changes relate to the changes in gene expression.

Chapter 8 Conclusion

The aim of this project is to investigate the inhibitory effect of epigenetic drugs on GBM cell lines grown under stem conditions, and to investigate the mechanism action of EZH2 inhibitors on GBM cells.

This study focused on developing GSCs by growing cells on Matrigel in serum-free medium supplemented with growth factors, while bulk differentiated cells were maintained in standard media containing FBS. The heterogeneity of the CSCs population in GBM tumour cell lines was confirmed with qRT-PCR. The data confirmed previous studies showing the lack of a reliable single stem cell marker that can identify the whole CSCs population. The expression levels of stem cell markers in GBM cells cultured under stem cell conditions compared to serum-containing media were evaluated. Although both cell lines showed different gene expression pattern, the analysis revealed that E2 cell lines exhibit more stem like characteristics compared to G7 cells. Genomic variant analysis of transcribed regions was used to identify potential GBM driver mutations, and revealed that both cell lines carry different pathogenic mutations in TP53, and the E2 line has a pathogenic mutation in EGFR. The differing responses of G7 and E2 cell lines throughout this project are likely to be a consequence of the genetic heterogeneity between the two cell lines.

Several epigenetic drugs were tested to determine whether the two GBM cell lines were sensitive to them. Proliferation and survival assays using the BET inhibitor OTX015 showed that the drug did not have an effect on GBM cell lines, not did it increase the sensitivity of the cells to the chemotherapy drug TMZ. In contrast, the BMI1 inhibitor PTC209 inhibited GBM cell proliferation in both short term survival and long term colony forming assays. Furthermore, PTC209 sensitised the cells to radiation treatment, particularly the E2 cell line. This data suggests that the PRC2 complex plays a role in the tumourigenesis of CSCs in GBM cell lines.

Three EZH2 inhibitors were investigated, EPZ6438, UNC1999 and GSK343. All three drugs inhibited colony formation in both cell lines and lead to increased expression of senescence-associated ß-galactosidase, possibly indicating therapy induced senescence. UNC1999 and GSK343 inhibited cell survival

and/proliferation in a short term assay, but there was limited induction of apoptosis.

In order to investigate the mechanistic basis of the phenotypic changes that were observed, changes in gene expression were evaluated using RNA-seq. GO and GSEA analysis revealed similarities between drug treatments in G7 cells. In particular, all three drugs led to increased expression of genes related to neurogenesis. Fewer DEGs were observed in E2 cells, but an increase in neurogenesis-related genes was observed following GSK343 treatment of E2 cells. The profile of H3K27me3 after treatment with EPZ6438 was assayed by ChIP-seq, and genes with reduced levels of H3K27me3 were cross-correlated to the list of upregulated genes from the RNA-seq analysis. Several direct targets of EZH2 were identified that could be driving the neuronal differentiation of the cells, including BMP7, MAFB and PAX2. Overall the data obtained above suggests that cells treated with EZH2 inhibitors shows increased expression of genes related to neurogenesis and neuronal function, indicating the change in cells from undifferentiated, stem cell state to differentiated phenotype.

The effect of the epigenetic inhibitors on the sensitivity of the cells to the standard GBM therapies was also investigated. All three EZH2 inhibitors significantly increased the sensitivity of both cell lines to TMZ, and also increased the sensitivity of the E2 cell line to radiation. This sensitisation may be related to reduced expression of DNA repair genes when EZH2 is inhibited, but further research is required to investigate this further. These data indicate the possibility of combining epigenetic inhibitors with conventional therapies for treatment of GBM. In addition, the BMI1 inhibitor PTC209 could be tested in combination with EZH2 inhibitors to investigate the observations by Jin *et al* (2017) that combining BMI1 and EZH2 inhibitors is a very efficient way of killing GBM cell (Jin *et al.*, 2017). Finally, a key aspect of any cancer drug is its therapeutic index, which refers to how efficiently it targets the cancer cells compared to normal cells. To address this question, drug treatments should be performed on normal NSCs and the data compared to that from the GBM cells.

Further experiments could be carried out to address the data reported in present project, such as spheroid formation assay to test whether GBM cell lines are able to form neurospheres in presence of these drugs (Johnson, Chen and Lo,

2013). To determine if G7 and E2 cell lines treated with EZH2 inhibitors have shifted to neuronal phenotypes, immunohistochemistry experiments could be performed (Pruszak *et al.*, 2007). It is interesting that neither the RNA-seq nor the subsequent ChIP-seq analyses highlighted any further information about the apparent therapy induced senescence indicated by the ß-galactosidase expression. It would be interesting to investigate whether the cells expressing SA-ß galactosidase also show expression of neurogenesis-related genes – are these two separate phenomena or are they occurring in the same cells? Immunofluorescence microscopy and single cell RNA-seq could be useful to disentangle these events.

ChIP-seq provides higher quality of data compared with other ChIP methods (ChIP qPCR and ChiP-ChIP).It is major advantages is high specificity in detection of peaks and transcription factor binding sites. Although ChIP-seq offers superior coverage of genome wide analysis one of the disadvantages of this method that it can be costly. Other disadvantages is that ChIP-seq require high cell number in a sample and sequencing analysis depends on the quality of antibodies used in the experiment (Gilfillan *et al.*, 2012). Input and mock are two most commonly used control sample in ChIP-seq. Mock control uses non specific antibody (IgG). Thus, pulling down targets that are not relevant which makes input more reliable as control sample. Anti-H3 antibody is also used as an alternative control that gives enrichment at the location of Histone. That makes anti-H3 antibody mimics the background in relation to histone modification that is unlike input that skips the immunoprecipitation step (Flensburg *et al.*, 2014).

RNA-seq is wildly used method for identification of DEGs on samples, although the quality of data depends on quality of RNA sample and the depth of sequencing. RNA-seq analysis can provide more insight into transcription factor functional mechanism and their key regulatory network when combined with ChIP-seq analysis. However, this method has its limitation which is lacking specific antibodies for transcription factor.To eliminate this problem CRISPR-Cas9 can be used to create individual maps for transcription factors prior to ChIP-seq (O'Geen *et al.*, 2015).

Alternative methods have been developed to overcome ChIP-seq limitations. CUT & Tag is one of the newest methods that is characterised by its higher resolution of generating signal over background by producing higher quality of data. Other advantages include working with low cell numbers, less sequencing and lower cost (Kaya-Okur *et al.*, 2019). Kinkley *et al.*, suggested using reChIP-seq and normR to look at the bivalency of H3K4me3 and H3K27me3 in human CD4+ central memory T cells (Kinkley *et al.*, 2016) .

References

Abdouh, M., Facchino, S., Chatoo, W., Balasingam, V., Ferreira, J. and Bernier, G. (2009) 'BMI1 sustains human glioblastoma multiforme stem cell renewal', *J Neurosci,* 29(28), pp. 8884-96.

Adhikary, G., Grun, D., Balasubramanian, S., Kerr, C., Huang, J. M. and Eckert, R. L. (2015) 'Survival of skin cancer stem cells requires the Ezh2 polycomb group protein', *Carcinogenesis,* 36(7), pp. 800-10.

Afgan, E., Baker, D., Batut, B., van den Beek, M., Bouvier, D., Cech, M., Chilton, J., Clements, D., Coraor, N., Grüning, B. A., Guerler, A., Hillman-Jackson, J., Hiltemann, S., Jalili, V., Rasche, H., Soranzo, N., Goecks, J., Taylor, J., Nekrutenko, A. and Blankenberg, D. (2018) 'The Galaxy platform for accessible, reproducible and collaborative biomedical analyses: 2018 update', *Nucleic Acids Res,* 46(W1), pp. W537-W544.

Alcantara Llaguno, S. R. and Parada, L. F. (2016) 'Cell of origin of glioma: biological and clinical implications', *Br J Cancer,* 115(12), pp. 1445-1450.

Ali, M. Y., Oliva, C. R., Noman, A. S. M., Allen, B. G., Goswami, P. C., Zakharia, Y., Monga, V., Spitz, D. R., Buatti, J. M. and Griguer, C. E. (2020) 'Radioresistance in Glioblastoma and the Development of Radiosensitizers', *Cancers (Basel),* 12(9).

Alves, A. L. V., Gomes, I. N. F., Carloni, A. C., Rosa, M. N., da Silva, L. S., Evangelista, A. F., Reis, R. M. and Silva, V. A. O. (2021) 'Role of glioblastoma stem cells in cancer therapeutic resistance: a perspective on antineoplastic agents from natural sources and chemical derivatives', *Stem Cell Res Ther,* 12(1), pp. 206.

Auffinger, B., Tobias, A. L., Han, Y., Lee, G., Guo, D., Dey, M., Lesniak, M. S. and Ahmed, A. U. (2014) 'Conversion of differentiated cancer cells into cancer stem-like cells in a glioblastoma model after primary chemotherapy', *Cell Death Differ,* 21(7), pp. 1119-31.

Bachoo, R. M., Maher, E. A., Ligon, K. L., Sharpless, N. E., Chan, S. S., You, M. J., Tang, Y., DeFrances, J., Stover, E., Weissleder, R., Rowitch, D. H., Louis, D. N. and DePinho, R. A. (2002) 'Epidermal growth factor receptor and Ink4a/Arf: convergent mechanisms governing terminal differentiation and transformation along the neural stem cell to astrocyte axis', *Cancer Cell,* 1(3), pp. 269-77.

Bandhavkar, S. (2016) 'Cancer stem cells: a metastasizing menace!', *Cancer Med,* 5(4), pp. 649-55.

Bao, S., Wu, Q., McLendon, R. E., Hao, Y., Shi, Q., Hjelmeland, A. B., Dewhirst, M. W., Bigner, D. D. and Rich, J. N. (2006) 'Glioma stem cells promote radioresistance by preferential activation of the DNA damage response', *Nature,* 444(7120), pp. 756-60.

Batlle, E. and Clevers, H. (2017) 'Cancer stem cells revisited', *Nat Med,* 23(10), pp. 1124-1134.

Bender, S., Tang, Y., Lindroth, A. M., Hovestadt, V., Jones, D. T., Kool, M., Zapatka, M., Northcott, P. A., Sturm, D., Wang, W., Radlwimmer, B., Højfeldt, J. W., Truffaux, N., Castel, D., Schubert, S., Ryzhova, M., Seker-Cin, H., Gronych, J., Johann, P. D., Stark, S., Meyer, J., Milde, T., Schuhmann, M., Ebinger, M., Monoranu, C. M., Ponnuswami, A., Chen, S., Jones, C., Witt, O., Collins, V. P., von Deimling, A., Jabado, N., Puget, S., Grill, J., Helin, K., Korshunov, A., Lichter, P., Monje, M., Plass, C., Cho, Y. J. and Pfister, S. M. (2013) 'Reduced H3K27me3 and DNA hypomethylation are major drivers of gene expression in K27M mutant pediatric high-grade gliomas', *Cancer Cell,* 24(5), pp. 660-72.

Berenguer-Daizé, C., Astorgues-Xerri, L., Odore, E., Cayol, M., Cvitkovic, E., Noel, K., Bekradda, M., MacKenzie, S., Rezai, K., Lokiec, F., Riveiro, M. E. and Ouafik, L. (2016) 'OTX015 (MK-8628), a novel BET inhibitor, displays in vitro and in vivo antitumor effects alone and in combination with conventional therapies in glioblastoma models', *Int J Cancer,* 139(9), pp. 2047-55.

Berezovsky, A. D., Poisson, L. M., Cherba, D., Webb, C. P., Transou, A. D., Lemke, N. W., Hong, X., Hasselbach, L. A., Irtenkauf, S. M., Mikkelsen, T. and deCarvalho, A. C. (2014) 'Sox2 promotes malignancy in glioblastoma by regulating plasticity and astrocytic differentiation', *Neoplasia,* 16(3), pp. 193-206, 206.e19-25.

Bjerke, L., Mackay, A., Nandhabalan, M., Burford, A., Jury, A., Popov, S., Bax, D. A., Carvalho, D., Taylor, K. R., Vinci, M., Bajrami, I., McGonnell, I. M., Lord, C. J., Reis, R. M., Hargrave, D., Ashworth, A., Workman, P. and Jones, C. (2013) 'Histone H3.3. mutations drive pediatric glioblastoma through upregulation of MYCN', *Cancer Discov,* 3(5), pp. 512-9.

Bojko, A., Czarnecka-Herok, J., Charzynska, A., Dabrowski, M. and Sikora, E. (2019) 'Diversity of the Senescence Phenotype of Cancer Cells Treated with Chemotherapeutic Agents', *Cells,* 8(12).
Bonnet, D. and Dick, J. E. (1997) 'Human acute myeloid leukemia is organized as a hierarchy that originates from a primitive hematopoietic cell', *Nat Med,* 3(7), pp. 730-7.
Bownes, L. V., Williams, A. P., Marayati, R., Stafman, L. L., Markert, H., Quinn, C. H., Wadhwani, N., Aye, J. M., Stewart, J. E., Yoon, K. J., Mroczek-Musulman, E. and Beierle, E. A. (2021) 'EZH2 inhibition decreases neuroblastoma proliferation and in vivo tumor growth', *PLoS One,* 16(3), pp. e0246244.
Brescia, P., Ortensi, B., Fornasari, L., Levi, D., Broggi, G. and Pelicci, G. (2013) 'CD133 is essential for glioblastoma stem cell maintenance', *Stem Cells,* 31(5), pp. 857-69.
Brown, D. V., Filiz, G., Daniel, P. M., Hollande, F., Dworkin, S., Amiridis, S., Kountouri, N., Ng, W., Morokoff, A. P. and Mantamadiotis, T. (2017) 'Expression of CD133 and CD44 in glioblastoma stem cells correlates with cell proliferation, phenotype stability and intra-tumor heterogeneity', *PLoS One,* 12(2), pp. e0172791.
Bulstrode, H., Johnstone, E., Marques-Torrejon, M. A., Ferguson, K. M., Bressan, R. B., Blin, C., Grant, V., Gogolok, S., Gangoso, E., Gagrica, S., Ender, C., Fotaki, V., Sproul, D., Bertone, P. and Pollard, S. M. (2017) 'Elevated FOXG1 and SOX2 in glioblastoma enforces neural stem cell identity through transcriptional control of cell cycle and epigenetic regulators', *Genes Dev,* 31(8), pp. 757-773.
Cao, R. and Zhang, Y. (2004) 'SUZ12 is required for both the histone methyltransferase activity and the silencing function of the EED-EZH2 complex', *Mol Cell,* 15(1), pp. 57-67.
Carlsson, S. K., Brothers, S. P. and Wahlestedt, C. (2014) 'Emerging treatment strategies for glioblastoma multiforme', *EMBO Mol Med,* 6(11), pp. 1359-70.
Carén, H., Pollard, S. M. and Beck, S. (2013) 'The good, the bad and the ugly: epigenetic mechanisms in glioblastoma', *Mol Aspects Med,* 34(4), pp. 849-62.
Chambers, I., Colby, D., Robertson, M., Nichols, J., Lee, S., Tweedie, S. and Smith, A. (2003) 'Functional expression cloning of Nanog, a pluripotency sustaining factor in embryonic stem cells', *Cell,* 113(5), pp. 643-55.
Chang, Y. W., Su, Y. J., Hsiao, M., Wei, K. C., Lin, W. H., Liang, C. L., Chen, S. C. and Lee, J. L. (2015) 'Diverse Targets of ß-Catenin during the Epithelial-

Mesenchymal Transition Define Cancer Stem Cells and Predict Disease Relapse', *Cancer Res,* 75(16), pp. 3398-410.
Chen, H., Tu, S. W. and Hsieh, J. T. (2005) 'Down-regulation of human DAB2IP gene expression mediated by polycomb Ezh2 complex and histone deacetylase in prostate cancer', *J Biol Chem,* 280(23), pp. 22437-44.
Chen, J., Li, J., Han, Q., Sun, Z., Wang, J., Wang, S. and Zhao, R. C. (2012a) 'Enhancer of zeste homolog 2 is overexpressed and contributes to epigenetic inactivation of p21 and phosphatase and tensin homolog in B-cell acute lymphoblastic leukemia', *Exp Biol Med (Maywood),* 237(9), pp. 1110-6.
Chen, J., Li, Y., Yu, T. S., McKay, R. M., Burns, D. K., Kernie, S. G. and Parada, L. F. (2012b) 'A restricted cell population propagates glioblastoma growth after chemotherapy', *Nature,* 488(7412), pp. 522-6.
Chen, Q., Zheng, P. S. and Yang, W. T. (2016) 'EZH2-mediated repression of GSK-3β and TP53 promotes Wnt/β-catenin signaling-dependent cell expansion in cervical carcinoma', *Oncotarget,* 7(24), pp. 36115-36129.
Chen, Z., Du, Y., Liu, X., Chen, H., Weng, X., Guo, J., Wang, M., Wang, X. and Wang, L. (2019) 'EZH2 inhibition suppresses bladder cancer cell growth and metastasis via the JAK2/STAT3 signaling pathway', *Oncol Lett,* 18(1), pp. 907-915.
Cheng, L., Huang, Z., Zhou, W., Wu, Q., Donnola, S., Liu, J. K., Fang, X., Sloan, A. E., Mao, Y., Lathia, J. D., Min, W., McLendon, R. E., Rich, J. N. and Bao, S. (2013a) 'Glioblastoma stem cells generate vascular pericytes to support vessel function and tumor growth', *Cell,* 153(1), pp. 139-52.
Cheng, Z., Gong, Y., Ma, Y., Lu, K., Lu, X., Pierce, L. A., Thompson, R. C., Muller, S., Knapp, S. and Wang, J. (2013b) 'Inhibition of BET bromodomain targets genetically diverse glioblastoma', *Clin Cancer Res,* 19(7), pp. 1748-59.
Cheung, L. W., Hennessy, B. T., Li, J., Yu, S., Myers, A. P., Djordjevic, B., Lu, Y., Stemke-Hale, K., Dyer, M. D., Zhang, F., Ju, Z., Cantley, L. C., Scherer, S. E., Liang, H., Lu, K. H., Broaddus, R. R. and Mills, G. B. (2011) 'High frequency of PIK3R1 and PIK3R2 mutations in endometrial cancer elucidates a novel mechanism for regulation of PTEN protein stability', *Cancer Discov,* 1(2), pp. 170-85.
Cheung, T. H. and Rando, T. A. (2013) 'Molecular regulation of stem cell quiescence', *Nat Rev Mol Cell Biol,* 14(6), pp. 329-40.

Chi, P., Allis, C. D. and Wang, G. G. (2010) 'Covalent histone modifications--miswritten, misinterpreted and mis-erased in human cancers', *Nat Rev Cancer,* 10(7), pp. 457-69.
Chittock, E. C., Latwiel, S., Miller, T. C. and Müller, C. W. (2017) 'Molecular architecture of polycomb repressive complexes', *Biochem Soc Trans,* 45(1), pp. 193-205.
Cilibrasi, C., Riva, G., Romano, G., Cadamuro, M., Bazzoni, R., Butta, V., Paoletta, L., Dalprà, L., Strazzabosco, M., Lavitrano, M., Giovannoni, R. and Bentivegna, A. (2017) 'Resveratrol Impairs Glioma Stem Cells Proliferation and Motility by Modulating the Wnt Signaling Pathway', *PLoS One,* 12(1), pp. e0169854.
Clarke, J., Penas, C., Pastori, C., Komotar, R. J., Bregy, A., Shah, A. H., Wahlestedt, C. and Ayad, N. G. (2013) 'Epigenetic pathways and glioblastoma treatment', *Epigenetics,* 8(8), pp. 785-95.
Cole, J. J., Faydaci, B., McGuinness, D., Shaw, R., Maciewicz, R., Robertson, N. and Goodyear, C. S. (2020) 'Searchlight 2: Rapid and comprehensive RNA seq data exploration and visualisation for unlimited differential datasets.', Available: https://github.com/Searchlight2/Searchlight2/
Collins, K., Jacks, T. and Pavletich, N. P. (1997) 'The cell cycle and cancer', *Proc Natl Acad Sci U S A,* 94(7), pp. 2776-8.
Cornago, M., Garcia-Alberich, C., Blasco-Angulo, N., Vall-Llaura, N., Nager, M., Herreros, J., Comella, J. X., Sanchis, D. and Llovera, M. (2014) 'Histone deacetylase inhibitors promote glioma cell death by G2 checkpoint abrogation leading to mitotic catastrophe', *Cell Death Dis,* 5, pp. e1435.
Couturier, C. P., Ayyadhury, S., Le, P. U., Nadaf, J., Monlong, J., Riva, G., Allache, R., Baig, S., Yan, X., Bourgey, M., Lee, C., Wang, Y. C. D., Wee Yong, V., Guiot, M. C., Najafabadi, H., Misic, B., Antel, J., Bourque, G., Ragoussis, J. and Petrecca, K. (2020) 'Single-cell RNA-seq reveals that glioblastoma recapitulates a normal neurodevelopmental hierarchy', *Nat Commun,* 11(1), pp. 3406.
Crea, F., Fornaro, L., Bocci, G., Sun, L., Farrar, W. L., Falcone, A. and Danesi, R. (2012) 'EZH2 inhibition: targeting the crossroad of tumor invasion and angiogenesis', *Cancer Metastasis Rev,* 31(3-4), pp. 753-61.
Dahan, P., Martinez Gala, J., Delmas, C., Monferran, S., Malric, L., Zentkowski, D., Lubrano, V., Toulas, C., Cohen-Jonathan Moyal, E. and Lemarie, A. (2014)

'Ionizing radiations sustain glioblastoma cell dedifferentiation to a stem-like phenotype through survivin: possible involvement in radioresistance', *Cell Death Dis,* 5, pp. e1543.
Dang, C. V. (2012) 'MYC on the path to cancer', *Cell,* 149(1), pp. 22-35.
Dawson, M. A. and Kouzarides, T. (2012) 'Cancer epigenetics: from mechanism to therapy', *Cell,* 150(1), pp. 12-27.
De Vleeschouwer, S. (2017) *Glioblastoma.* Brisbane (AU): Codon Publications.
Deheeger, M., Lesniak, M. S. and Ahmed, A. U. (2014) 'Cellular plasticity regulated cancer stem cell niche: a possible new mechanism of chemoresistance', *Cancer Cell Microenviron,* 1(5).
Denysenko, T., Annovazzi, L., Cassoni, P., Melcarne, A., Mellai, M. and Schiffer, D. (2016) 'WNT/ß-catenin Signaling Pathway and Downstream Modulators in Low- and High-grade Glioma', *Cancer Genomics Proteomics,* 13(1), pp. 31-45.
Denysenko, T., Gennero, L., Juenemann, C., Morra, I., Masperi, P., Ceroni, V., Pragliola, A., Ponzetto, A. and Melcarne, A. (2014) 'Heterogeneous phenotype of human glioblastoma: in vitro study', *Cell Biochem Funct,* 32(2), pp. 164-76.
Du, Z., Jia, D., Liu, S., Wang, F., Li, G., Zhang, Y., Cao, X., Ling, E. A. and Hao, A. (2009) 'Oct4 is expressed in human gliomas and promotes colony formation in glioma cells', *Glia,* 57(7), pp. 724-33.
Easwaran, H., Tsai, H. C. and Baylin, S. B. (2014) 'Cancer epigenetics: tumor heterogeneity, plasticity of stem-like states, and drug resistance', *Mol Cell,* 54(5), pp. 716-27.
Fael Al-Mayhani, T. M., Ball, S. L., Zhao, J. W., Fawcett, J., Ichimura, K., Collins, P. V. and Watts, C. (2009) 'An efficient method for derivation and propagation of glioblastoma cell lines that conserves the molecular profile of their original tumours', *J Neurosci Methods,* 176(2), pp. 192-9.
Fan, T. Y., Wang, H., Xiang, P., Liu, Y. W., Li, H. Z., Lei, B. X., Yu, M. and Qi, S. T. (2014) 'Inhibition of EZH2 reverses chemotherapeutic drug TMZ chemosensitivity in glioblastoma', *Int J Clin Exp Pathol,* 7(10), pp. 6662-70.
Fasano, C. A., Dimos, J. T., Ivanova, N. B., Lowry, N., Lemischka, I. R. and Temple, S. (2007) 'shRNA knockdown of Bmi-1 reveals a critical role for p21-Rb pathway in NSC self-renewal during development', *Cell Stem Cell,* 1(1), pp. 87-99.
Felsberg, J., Thon, N., Eigenbrod, S., Hentschel, B., Sabel, M. C., Westphal, M., Schackert, G., Kreth, F. W., Pietsch, T., Löffler, M., Weller, M., Reifenberger,

G., Tonn, J. C. and Network, G. G. (2011) 'Promoter methylation and expression of MGMT and the DNA mismatch repair genes MLH1, MSH2, MSH6 and PMS2 in paired primary and recurrent glioblastomas', *Int J Cancer,* 129(3), pp. 659-70.
Feng, J., Liu, T., Qin, B., Zhang, Y. and Liu, X. S. (2012) 'Identifying ChIP-seq enrichment using MACS', *Nat Protoc,* 7(9), pp. 1728-40.
Feng, S. and De Carvalho, D. D. (2022) 'Clinical advances in targeting epigenetics for cancer therapy', *FEBS J,* 289(5), pp. 1214-1239.
Fioravanti, R., Stazi, G., Zwergel, C., Valente, S. and Mai, A. (2018) 'Six Years (2012-2018) of Researches on Catalytic EZH2 Inhibitors: The Boom of the 2-Pyridone Compounds', *Chem Rec,* 18(12), pp. 1818-1832.
Flensburg, C., Kinkel, S. A., Keniry, A., Blewitt, M. E. and Oshlack, A. (2014) 'A comparison of control samples for ChIP-seq of histone modifications', *Front Genet,* 5, pp. 329.
Francis, N. J., Kingston, R. E. and Woodcock, C. L. (2004) 'Chromatin compaction by a polycomb group protein complex', *Science,* 306(5701), pp. 1574-7.
Frank, N. Y., Schatton, T. and Frank, M. H. (2010) 'The therapeutic promise of the cancer stem cell concept', *J Clin Invest,* 120(1), pp. 41-50.
Furnari, F. B., Fenton, T., Bachoo, R. M., Mukasa, A., Stommel, J. M., Stegh, A., Hahn, W. C., Ligon, K. L., Louis, D. N., Brennan, C., Chin, L., DePinho, R. A. and Cavenee, W. K. (2007) 'Malignant astrocytic glioma: genetics, biology, and paths to treatment', *Genes Dev,* 21(21), pp. 2683-710.
Gangemi, R. M., Griffero, F., Marubbi, D., Perera, M., Capra, M. C., Malatesta, P., Ravetti, G. L., Zona, G. L., Daga, A. and Corte, G. (2009) 'SOX2 silencing in glioblastoma tumor-initiating cells causes stop of proliferation and loss of tumorigenicity', *Stem Cells,* 27(1), pp. 40-8.
Garrison, E. and Marth, G. (2012) 'Haplotype based variant detection from short read sequencing', 1207-3907, pp. 9, Available: arXiv.
Garros-Regulez, L., Garcia, I., Carrasco-Garcia, E., Lantero, A., Aldaz, P., Moreno-Cugnon, L., Arrizabalaga, O., Undabeitia, J., Torres-Bayona, S., Villanua, J., Ruiz, I., Egaña, L., Sampron, N. and Matheu, A. (2016) 'Targeting SOX2 as a Therapeutic Strategy in Glioblastoma', *Front Oncol,* 6, pp. 222.
Gil, J. and Peters, G. (2006) 'Regulation of the INK4b-ARF-INK4a tumour suppressor locus: all for one or one for all', *Nat Rev Mol Cell Biol,* 7(9), pp. 667-77.

Gilfillan, G. D., Hughes, T., Sheng, Y., Hjorthaug, H. S., Straub, T., Gervin, K., Harris, J. R., Undlien, D. E. and Lyle, R. (2012) 'Limitations and possibilities of low cell number ChIP-seq', *BMC Genomics,* 13, pp. 645.

Ginjala, V., Nacerddine, K., Kulkarni, A., Oza, J., Hill, S. J., Yao, M., Citterio, E., van Lohuizen, M. and Ganesan, S. (2011) 'BMI1 is recruited to DNA breaks and contributes to DNA damage-induced H2A ubiquitination and repair', *Mol Cell Biol,* 31(10), pp. 1972-82.

Glazer, R. I., Hartman, K. D., Knode, M. C., Richard, M. M., Chiang, P. K., Tseng, C. K. and Marquez, V. E. (1986) '3-Deazaneplanocin: a new and potent inhibitor of S-adenosylhomocysteine hydrolase and its effects on human promyelocytic leukemia cell line HL-60', *Biochem Biophys Res Commun,* 135(2), pp. 688-94.

Gluscevic, M., Paradise, C. R., Dudakovic, A., Karperien, M., Dietz, A. B., van Wijnen, A. J. and Deyle, D. R. (2020) 'Functional expression of ZNF467 and PCBP2 supports adipogenic lineage commitment in adipose-derived mesenchymal stem cells', *Gene,* 737, pp. 144437.

Gomez-Roman, N., Stevenson, K., Gilmour, L., Hamilton, G. and Chalmers, A. J. (2017) 'A novel 3D human glioblastoma cell culture system for modeling drug and radiation responses', *Neuro Oncol,* 19(2), pp. 229-241.

Gong, H., Li, Y., Yuan, Y., Li, W., Zhang, H., Zhang, Z., Shi, R., Liu, M., Liu, C., Chen, C., Liu, H. and Chen, J. (2020) 'EZH2 inhibitors reverse resistance to gefitinib in primary EGFR wild-type lung cancer cells', *BMC Cancer,* 20(1), pp. 1189.

Graham, V., Khudyakov, J., Ellis, P. and Pevny, L. (2003) 'SOX2 functions to maintain neural progenitor identity', *Neuron,* 39(5), pp. 749-65.

Gray, F., Cho, H. J., Shukla, S., He, S., Harris, A., Boytsov, B., Jaremko, Ł., Jaremko, M., Demeler, B., Lawlor, E. R., Grembecka, J. and Cierpicki, T. (2016) 'BMI1 regulates PRC1 architecture and activity through homo- and hetero-oligomerization', *Nat Commun,* 7, pp. 13343.

Grinshtein, N., Rioseco, C. C., Marcellus, R., Uehling, D., Aman, A., Lun, X., Muto, O., Podmore, L., Lever, J., Shen, Y., Blough, M. D., Cairncross, G. J., Robbins, S. M., Jones, S. J., Marra, M. A., Al-Awar, R., Senger, D. L. and Kaplan, D. R. (2016) 'Small molecule epigenetic screen identifies novel EZH2 and HDAC inhibitors that target glioblastoma brain tumor-initiating cells', *Oncotarget,* 7(37), pp. 59360-59376.

Gulaia, V., Kumeiko, V., Shved, N., Cicinskas, E., Rybtsov, S., Ruzov, A. and Kagansky, A. (2018) 'Molecular Mechanisms Governing the Stem Cell's Fate in Brain Cancer: Factors of Stemness and Quiescence', *Front Cell Neurosci,* 12, pp. 388.

Gusyatiner, O. and Hegi, M. E. (2018) 'Glioma epigenetics: From subclassification to novel treatment options', *Semin Cancer Biol,* 51, pp. 50-58.

Han Li, C. and Chen, Y. (2015) 'Targeting EZH2 for cancer therapy: progress and perspective', *Curr Protein Pept Sci,* 16(6), pp. 559-70.

Hattermann, K., Flüh, C., Engel, D., Mehdorn, H. M., Synowitz, M., Mentlein, R. and Held-Feindt, J. (2016) 'Stem cell markers in glioma progression and recurrence', *Int J Oncol,* 49(5), pp. 1899-1910.

Heberle, H., Meirelles, G. V., da Silva, F. R., Telles, G. P. and Minghim, R. (2015) 'InteractiVenn: a web-based tool for the analysis of sets through Venn diagrams', *BMC Bioinformatics,* 16, pp. 169.

Hegi, M. E., Diserens, A. C., Gorlia, T., Hamou, M. F., de Tribolet, N., Weller, M., Kros, J. M., Hainfellner, J. A., Mason, W., Mariani, L., Bromberg, J. E., Hau, P., Mirimanoff, R. O., Cairncross, J. G., Janzer, R. C. and Stupp, R. (2005) 'MGMT gene silencing and benefit from temozolomide in glioblastoma', *N Engl J Med,* 352(10), pp. 997-1003.

Helin, K. and Dhanak, D. (2013) 'Chromatin proteins and modifications as drug targets', *Nature,* 502(7472), pp. 480-8.

Herviou, L., Cavalli, G., Cartron, G., Klein, B. and Moreaux, J. (2016) 'EZH2 in normal hematopoiesis and hematological malignancies', *Oncotarget,* 7(3), pp. 2284-96.

Higgins, D. M., Wang, R., Milligan, B., Schroeder, M., Carlson, B., Pokorny, J., Cheshier, S. H., Meyer, F. B., Weissman, I. L., Sarkaria, J. N. and Henley, J. R. (2013) 'Brain tumor stem cell multipotency correlates with nanog expression and extent of passaging in human glioblastoma xenografts', *Oncotarget,* 4(5), pp. 792-801.

Holland, E. C. (2000) 'Glioblastoma multiforme: the terminator', *Proc Natl Acad Sci U S A,* 97(12), pp. 6242-4.

Holmen, S. L. and Williams, B. O. (2005) 'Essential role for Ras signaling in glioblastoma maintenance', *Cancer Res,* 65(18), pp. 8250-5.

Huang, L. E. (2019) 'Friend or foe-IDH1 mutations in glioma 10 years on', *Carcinogenesis,* 40(11), pp. 1299-1307.

Ihira, K., Dong, P., Xiong, Y., Watari, H., Konno, Y., Hanley, S. J., Noguchi, M., Hirata, N., Suizu, F., Yamada, T., Kudo, M. and Sakuragi, N. (2017) 'EZH2 inhibition suppresses endometrial cancer progression via miR-361/Twist axis', *Oncotarget,* 8(8), pp. 13509-13520.
Iwadate, Y. (2016) 'Epithelial-mesenchymal transition in glioblastoma progression', *Oncol Lett,* 11(3), pp. 1615-1620.
Jerabek, S., Merino, F., Schöler, H. R. and Cojocaru, V. (2014) 'OCT4: dynamic DNA binding pioneers stem cell pluripotency', *Biochim Biophys Acta,* 1839(3), pp. 138-54.
Jiang, X., Tan, J., Li, J., Kivimäe, S., Yang, X., Zhuang, L., Lee, P. L., Chan, M. T., Stanton, L. W., Liu, E. T., Cheyette, B. N. and Yu, Q. (2008) 'DACT3 is an epigenetic regulator of Wnt/beta-catenin signaling in colorectal cancer and is a therapeutic target of histone modifications', *Cancer Cell,* 13(6), pp. 529-41.
Jin, X., Jung, J. E., Beck, S. and Kim, H. (2013) 'Cell surface Nestin is a biomarker for glioma stem cells', *Biochem Biophys Res Commun,* 433(4), pp. 496-501.
Jin, X., Kim, L. J. Y., Wu, Q., Wallace, L. C., Prager, B. C., Sanvoranart, T., Gimple, R. C., Wang, X., Mack, S. C., Miller, T. E., Huang, P., Valentim, C. L., Zhou, Q. G., Barnholtz-Sloan, J. S., Bao, S., Sloan, A. E. and Rich, J. N. (2017) 'Targeting glioma stem cells through combined BMI1 and EZH2 inhibition', *Nat Med,* 23(11), pp. 1352-1361.
Johnson, S., Chen, H. and Lo, P. K. (2013) 'Tumorsphere Formation Assays', *Bio Protoc,* 3(3).
Katsushima, K., Shinjo, K., Natsume, A., Ohka, F., Fujii, M., Osada, H., Sekido, Y. and Kondo, Y. (2012) 'Contribution of microRNA-1275 to Claudin11 protein suppression via a polycomb-mediated silencing mechanism in human glioma stem-like cells', *J Biol Chem,* 287(33), pp. 27396-406.
Kaya-Okur, H. S., Wu, S. J., Codomo, C. A., Pledger, E. S., Bryson, T. D., Henikoff, J. G., Ahmad, K. and Henikoff, S. (2019) 'CUT&Tag for efficient epigenomic profiling of small samples and single cells', *Nat Commun,* 10(1), pp. 1930.
Kim, D., Langmead, B. and Salzberg, S. L. (2015) 'HISAT: a fast spliced aligner with low memory requirements', *Nat Methods,* 12(4), pp. 357-60.
Kim, E., Kim, M., Woo, D. H., Shin, Y., Shin, J., Chang, N., Oh, Y. T., Kim, H., Rheey, J., Nakano, I., Lee, C., Joo, K. M., Rich, J. N., Nam, D. H. and Lee, J.

(2013) 'Phosphorylation of EZH2 activates STAT3 signaling via STAT3 methylation and promotes tumorigenicity of glioblastoma stem-like cells', *Cancer Cell,* 23(6), pp. 839-52.
Kim, J. and Orkin, S. H. (2011) 'Embryonic stem cell-specific signatures in cancer: insights into genomic regulatory networks and implications for medicine', *Genome Med,* 3(11), pp. 75.
Kinkley, S., Helmuth, J., Polansky, J. K., Dunkel, I., Gasparoni, G., Fröhler, S., Chen, W., Walter, J., Hamann, A. and Chung, H. R. (2016) 'reChIP-seq reveals widespread bivalency of H3K4me3 and H3K27me3 in CD4(+) memory T cells', *Nat Commun,* 7, pp. 12514.
Knutson, S. K., Kawano, S., Minoshima, Y., Warholic, N. M., Huang, K. C., Xiao, Y., Kadowaki, T., Uesugi, M., Kuznetsov, G., Kumar, N., Wigle, T. J., Klaus, C. R., Allain, C. J., Raimondi, A., Waters, N. J., Smith, J. J., Porter-Scott, M., Chesworth, R., Moyer, M. P., Copeland, R. A., Richon, V. M., Uenaka, T., Pollock, R. M., Kuntz, K. W., Yokoi, A. and Keilhack, H. (2014a) 'Selective inhibition of EZH2 by EPZ-6438 leads to potent antitumor activity in EZH2-mutant non-Hodgkin lymphoma', *Mol Cancer Ther,* 13(4), pp. 842-54.
Knutson, S. K., Warholic, N. M., Johnston, L. D., Klaus, C. R., Wigle, T. J., Iwanowicz, D., Littlefield, B. A., Porter-Scott, M., Smith, J. J., Moyer, M. P., Copeland, R. A., Pollock, R. M., Kuntz, K. W., Raimondi, A. and Keilhack, H. (2014b) 'Synergistic Anti-Tumor Activity of EZH2 Inhibitors and Glucocorticoid Receptor Agonists in Models of Germinal Center Non-Hodgkin Lymphomas', *PLoS One,* 9(12), pp. e111840.
Knutson, S. K., Warholic, N. M., Wigle, T. J., Klaus, C. R., Allain, C. J., Raimondi, A., Porter Scott, M., Chesworth, R., Moyer, M. P., Copeland, R. A., Richon, V. M., Pollock, R. M., Kuntz, K. W. and Keilhack, H. (2013) 'Durable tumor regression in genetically altered malignant rhabdoid tumors by inhibition of methyltransferase EZH2', *Proc Natl Acad Sci U S A,* 110(19), pp. 7922-7.
Koh, C. M., Iwata, T., Zheng, Q., Bethel, C., Yegnasubramanian, S. and De Marzo, A. M. (2011) 'Myc enforces overexpression of EZH2 in early prostatic neoplasia via transcriptional and post-transcriptional mechanisms', *Oncotarget,* 2(9), pp. 669-83.
Kojima, T., Shimazui, T., Hinotsu, S., Joraku, A., Oikawa, T., Kawai, K., Horie, R., Suzuki, H., Nagashima, R., Yoshikawa, K., Michiue, T., Asashima, M., Akaza, H. and Uchida, K. (2009) 'Decreased expression of CXXC4 promotes a malignant

phenotype in renal cell carcinoma by activating Wnt signaling', *Oncogene,* 28(2), pp. 297-305.
Kondo, T., Setoguchi, T. and Taga, T. (2004) 'Persistence of a small subpopulation of cancer stem-like cells in the C6 glioma cell line', *Proc Natl Acad Sci U S A,* 101(3), pp. 781-6.
Kondo, Y., Katsushima, K., Ohka, F., Natsume, A. and Shinjo, K. (2014) 'Epigenetic dysregulation in glioma', *Cancer Sci,* 105(4), pp. 363-9.
Kong, Y., Ai, C., Dong, F., Xia, X., Zhao, X., Yang, C., Kang, C., Zhou, Y., Zhao, Q., Sun, X. and Wu, X. (2018) 'Targeting of BMI-1 with PTC-209 inhibits glioblastoma development', *Cell Cycle,* 17(10), pp. 1199-1211.
Konze, K. D., Ma, A., Li, F., Barsyte-Lovejoy, D., Parton, T., Macnevin, C. J., Liu, F., Gao, C., Huang, X. P., Kuznetsova, E., Rougie, M., Jiang, A., Pattenden, S. G., Norris, J. L., James, L. I., Roth, B. L., Brown, P. J., Frye, S. V., Arrowsmith, C. H., Hahn, K. M., Wang, G. G., Vedadi, M. and Jin, J. (2013) 'An orally bioavailable chemical probe of the Lysine Methyltransferases EZH2 and EZH1', *ACS Chem Biol,* 8(6), pp. 1324-34.
Kosty, J., Lu, F., Kupp, R., Mehta, S. and Lu, Q. R. (2017) 'Harnessing OLIG2 function in tumorigenicity and plasticity to target malignant gliomas', *Cell Cycle,* 16(18), pp. 1654-1660.
Kowalski-Chauvel, A., Modesto, A., Gouaze-Andersson, V., Baricault, L., Gilhodes, J., Delmas, C., Lemarie, A., Toulas, C., Cohen-Jonathan-Moyal, E. and Seva, C. (2018) 'Alpha-6 integrin promotes radioresistance of glioblastoma by modulating DNA damage response and the transcription factor Zeb1', *Cell Death Dis,* 9(9), pp. 872.
Lan, X., Jörg, D. J., Cavalli, F. M. G., Richards, L. M., Nguyen, L. V., Vanner, R. J., Guilhamon, P., Lee, L., Kushida, M. M., Pellacani, D., Park, N. I., Coutinho, F. J., Whetstone, H., Selvadurai, H. J., Che, C., Luu, B., Carles, A., Moksa, M., Rastegar, N., Head, R., Dolma, S., Prinos, P., Cusimano, M. D., Das, S., Bernstein, M., Arrowsmith, C. H., Mungall, A. J., Moore, R. A., Ma, Y., Gallo, M., Lupien, M., Pugh, T. J., Taylor, M. D., Hirst, M., Eaves, C. J., Simons, B. D. and Dirks, P. B. (2017) 'Fate mapping of human glioblastoma reveals an invariant stem cell hierarchy', *Nature,* 549(7671), pp. 227-232.
Langmead, B., Trapnell, C., Pop, M. and Salzberg, S. L. (2009) 'Ultrafast and memory-efficient alignment of short DNA sequences to the human genome', *Genome Biol,* 10(3), pp. R25.

Lathia, J. D., Mack, S. C., Mulkearns-Hubert, E. E., Valentim, C. L. and Rich, J. N. (2015) 'Cancer stem cells in glioblastoma', *Genes Dev,* 29(12), pp. 1203-17.
Ledur, P. F., Onzi, G. R., Zong, H. and Lenz, G. (2017) 'Culture conditions defining glioblastoma cells behavior: what is the impact for novel discoveries?', *Oncotarget,* 8(40), pp. 69185-69197.
Lee, J., Son, M. J., Woolard, K., Donin, N. M., Li, A., Cheng, C. H., Kotliarova, S., Kotliarov, Y., Walling, J., Ahn, S., Kim, M., Totonchy, M., Cusack, T., Ene, C., Ma, H., Su, Q., Zenklusen, J. C., Zhang, W., Maric, D. and Fine, H. A. (2008) 'Epigenetic-mediated dysfunction of the bone morphogenetic protein pathway inhibits differentiation of glioblastoma-initiating cells', *Cancer Cell,* 13(1), pp. 69-80.
Lee, S. Y. (2016) 'Temozolomide resistance in glioblastoma multiforme', *Genes Dis,* 3(3), pp. 198-210.
Lee, T. I., Jenner, R. G., Boyer, L. A., Guenther, M. G., Levine, S. S., Kumar, R. M., Chevalier, B., Johnstone, S. E., Cole, M. F., Isono, K., Koseki, H., Fuchikami, T., Abe, K., Murray, H. L., Zucker, J. P., Yuan, B., Bell, G. W., Herbolsheimer, E., Hannett, N. M., Sun, K., Odom, D. T., Otte, A. P., Volkert, T. L., Bartel, D. P., Melton, D. A., Gifford, D. K., Jaenisch, R. and Young, R. A. (2006) 'Control of developmental regulators by Polycomb in human embryonic stem cells', *Cell,* 125(2), pp. 301-13.
Lee, Y., Kim, K. H., Kim, D. G., Cho, H. J., Kim, Y., Rheey, J., Shin, K., Seo, Y. J., Choi, Y. S., Lee, J. I., Lee, J., Joo, K. M. and Nam, D. H. (2015) 'FoxM1 Promotes Stemness and Radio-Resistance of Glioblastoma by Regulating the Master Stem Cell Regulator Sox2', *PLoS One,* 10(10), pp. e0137703.
Li, J., Vangundy, Z. and Poi, M. (2020) 'PTC209, a Specific Inhibitor of BMI1, Promotes Cell Cycle Arrest and Apoptosis in Cervical Cancer Cell Lines', *Anticancer Res,* 40(1), pp. 133-141.
Liberzon, A., Birger, C., Thorvaldsdóttir, H., Ghandi, M., Mesirov, J. P. and Tamayo, P. (2015) 'The Molecular Signatures Database (MSigDB) hallmark gene set collection', *Cell Syst,* 1(6), pp. 417-425.
Ligon, K. L., Huillard, E., Mehta, S., Kesari, S., Liu, H., Alberta, J. A., Bachoo, R. M., Kane, M., Louis, D. N., Depinho, R. A., Anderson, D. J., Stiles, C. D. and Rowitch, D. H. (2007) 'Olig2-regulated lineage-restricted pathway controls replication competence in neural stem cells and malignant glioma', *Neuron,* 53(4), pp. 503-17.

Lima-Fernandes, E., Murison, A., da Silva Medina, T., Wang, Y., Ma, A., Leung, C., Luciani, G. M., Haynes, J., Pollett, A., Zeller, C., Duan, S., Kreso, A., Barsyte-Lovejoy, D., Wouters, B. G., Jin, J., Carvalho, D. D., Lupien, M., Arrowsmith, C. H. and O'Brien, C. A. (2019) 'Targeting bivalency de-represses Indian Hedgehog and inhibits self-renewal of colorectal cancer-initiating cells', *Nat Commun,* 10(1), pp. 1436.

Liu, G., Yuan, X., Zeng, Z., Tunici, P., Ng, H., Abdulkadir, I. R., Lu, L., Irvin, D., Black, K. L. and Yu, J. S. (2006) 'Analysis of gene expression and chemoresistance of CD133+ cancer stem cells in glioblastoma', *Mol Cancer,* 5, pp. 67.

Liu, L., Jin, G. and Zhou, X. (2015) 'Modeling the relationship of epigenetic modifications to transcription factor binding', *Nucleic Acids Res,* 43(8), pp. 3873-85.

Logan, C. Y. and Nusse, R. (2004) 'The Wnt signaling pathway in development and disease', *Annu Rev Cell Dev Biol,* 20, pp. 781-810.

Lombaerts, M., van Wezel, T., Philippo, K., Dierssen, J. W., Zimmerman, R. M., Oosting, J., van Eijk, R., Eilers, P. H., van de Water, B., Cornelisse, C. J. and Cleton-Jansen, A. M. (2006) 'E-cadherin transcriptional downregulation by promoter methylation but not mutation is related to epithelial-to-mesenchymal transition in breast cancer cell lines', *Br J Cancer,* 94(5), pp. 661-71.

Lopez-Bertoni, H., Lal, B., Li, A., Caplan, M., Guerrero-Cázares, H., Eberhart, C. G., Quiñones-Hinojosa, A., Glas, M., Scheffler, B., Laterra, J. and Li, Y. (2015) 'DNMT-dependent suppression of microRNA regulates the induction of GBM tumor-propagating phenotype by Oct4 and Sox2', *Oncogene,* 34(30), pp. 3994-4004.

Louis, D. N., Ohgaki, H., Wiestler, O. D., Cavenee, W. K., Burger, P. C., Jouvet, A., Scheithauer, B. W. and Kleihues, P. (2007) 'The 2007 WHO classification of tumours of the central nervous system', *Acta Neuropathol,* 114(2), pp. 97-109.

Love, M. I., Huber, W. and Anders, S. (2014) 'Moderated estimation of fold change and dispersion for RNA-seq data with DESeq2', *Genome Biol,* 15(12), pp. 550.

Lu, F., Chen, Y., Zhao, C., Wang, H., He, D., Xu, L., Wang, J., He, X., Deng, Y., Lu, E. E., Liu, X., Verma, R., Bu, H., Drissi, R., Fouladi, M., Stemmer-Rachamimov, A. O., Burns, D., Xin, M., Rubin, J. B., Bahassi, E. M., Canoll, P., Holland, E. C. and Lu, Q. R. (2016) 'Olig2-Dependent Reciprocal Shift in PDGF

and EGF Receptor Signaling Regulates Tumor Phenotype and Mitotic Growth in Malignant Glioma', *Cancer Cell,* 29(5), pp. 669-683.
Lu, H., Sun, J., Wang, F., Feng, L., Ma, Y., Shen, Q., Jiang, Z., Sun, X., Wang, X. and Jin, H. (2013) 'Enhancer of zeste homolog 2 activates wnt signaling through downregulating CXXC finger protein 4', *Cell Death Dis,* 4, pp. e776.
Lu, J., Getz, G., Miska, E. A., Alvarez-Saavedra, E., Lamb, J., Peck, D., Sweet-Cordero, A., Ebert, B. L., Mak, R. H., Ferrando, A. A., Downing, J. R., Jacks, T., Horvitz, H. R. and Golub, T. R. (2005) 'MicroRNA expression profiles classify human cancers', *Nature,* 435(7043), pp. 834-8.
Luo, H., Chen, Z., Wang, S., Zhang, R., Qiu, W., Zhao, L., Peng, C., Xu, R., Chen, W., Wang, H. W., Chen, Y., Yang, J., Zhang, X., Zhang, S., Chen, D., Wu, W., Zhao, C., Cheng, G., Jiang, T., Lu, D., You, Y., Liu, N. and Wang, H. (2015a) 'c-Myc-miR-29c-REV3L signalling pathway drives the acquisition of temozolomide resistance in glioblastoma', *Brain,* 138(Pt 12), pp. 3654-72.
Luo, J. W., Wang, X., Yang, Y. and Mao, Q. (2015b) 'Role of micro-RNA (miRNA) in pathogenesis of glioblastoma', *Eur Rev Med Pharmacol Sci,* 19(9), pp. 1630-9.
López-Arribillaga, E., Rodilla, V., Pellegrinet, L., Guiu, J., Iglesias, M., Roman, A. C., Gutarra, S., González, S., Muñoz-Cánoves, P., Fernández-Salguero, P., Radtke, F., Bigas, A. and Espinosa, L. (2015) 'Bmi1 regulates murine intestinal stem cell proliferation and self-renewal downstream of Notch', *Development,* 142(1), pp. 41-50.
MacDonald, B. T., Tamai, K. and He, X. (2009) 'Wnt/beta-catenin signaling: components, mechanisms, and diseases', *Dev Cell,* 17(1), pp. 9-26.
Mack, S. C., Hubert, C. G., Miller, T. E., Taylor, M. D. and Rich, J. N. (2016) 'An epigenetic gateway to brain tumor cell identity', *Nat Neurosci,* 19(1), pp. 10-9.
Mani, S. A., Guo, W., Liao, M. J., Eaton, E. N., Ayyanan, A., Zhou, A. Y., Brooks, M., Reinhard, F., Zhang, C. C., Shipitsin, M., Campbell, L. L., Polyak, K., Brisken, C., Yang, J. and Weinberg, R. A. (2008) 'The epithelial-mesenchymal transition generates cells with properties of stem cells', *Cell,* 133(4), pp. 704-15.
Mannino, M., Gomez-Roman, N., Hochegger, H. and Chalmers, A. J. (2014) 'Differential sensitivity of Glioma stem cells to Aurora kinase A inhibitors: implications for stem cell mitosis and centrosome dynamics', *Stem Cell Res,* 13(1), pp. 135-43.

Margueron, R., Li, G., Sarma, K., Blais, A., Zavadil, J., Woodcock, C. L., Dynlacht, B. D. and Reinberg, D. (2008) 'Ezh1 and Ezh2 maintain repressive chromatin through different mechanisms', *Mol Cell,* 32(4), pp. 503-18.
Margueron, R. and Reinberg, D. (2011) 'The Polycomb complex PRC2 and its mark in life', *Nature,* 469(7330), pp. 343-9.
Matsuda, Y., Ishiwata, T., Yoshimura, H., Hagio, M. and Arai, T. (2015) 'Inhibition of nestin suppresses stem cell phenotype of glioblastomas through the alteration of post-translational modification of heat shock protein HSPA8/HSC71', *Cancer Lett,* 357(2), pp. 602-11.
Mayr, C., Wagner, A., Loeffelberger, M., Bruckner, D., Jakab, M., Berr, F., Di Fazio, P., Ocker, M., Neureiter, D., Pichler, M. and Kiesslich, T. (2016) 'The BMI1 inhibitor PTC-209 is a potential compound to halt cellular growth in biliary tract cancer cells', *Oncotarget,* 7(1), pp. 745-58.
McKinney, P. A. (2004) 'Brain tumours: incidence, survival, and aetiology', *J Neurol Neurosurg Psychiatry,* 75 Suppl 2, pp. ii12-7.
Mertz, J. A., Conery, A. R., Bryant, B. M., Sandy, P., Balasubramanian, S., Mele, D. A., Bergeron, L. and Sims, R. J. (2011) 'Targeting MYC dependence in cancer by inhibiting BET bromodomains', *Proc Natl Acad Sci U S A,* 108(40), pp. 16669-74.
Meyer, M., Reimand, J., Lan, X., Head, R., Zhu, X., Kushida, M., Bayani, J., Pressey, J. C., Lionel, A. C., Clarke, I. D., Cusimano, M., Squire, J. A., Scherer, S. W., Bernstein, M., Woodin, M. A., Bader, G. D. and Dirks, P. B. (2015) 'Single cell-derived clonal analysis of human glioblastoma links functional and genomic heterogeneity', *Proc Natl Acad Sci U S A,* 112(3), pp. 851-6.
Miller, D. M., Thomas, S. D., Islam, A., Muench, D. and Sedoris, K. (2012) 'c-Myc and cancer metabolism', *Clin Cancer Res,* 18(20), pp. 5546-53.
Miranda, T. B., Cortez, C. C., Yoo, C. B., Liang, G., Abe, M., Kelly, T. K., Marquez, V. E. and Jones, P. A. (2009) 'DZNep is a global histone methylation inhibitor that reactivates developmental genes not silenced by DNA methylation', *Mol Cancer Ther,* 8(6), pp. 1579-88.
Mongiardi, M. P., Savino, M., Falchetti, M. L., Illi, B., Bozzo, F., Valle, C., Helmer-Citterich, M., Ferrè, F., Nasi, S. and Levi, A. (2016) 'c-MYC inhibition impairs hypoxia response in glioblastoma multiforme', *Oncotarget,* 7(22), pp. 33257-71.

Monje, M. (2020) 'Synaptic Communication in Brain Cancer', *Cancer Res,* 80(14), pp. 2979-2982.
Morschhauser, F., Tilly, H., Chaidos, A., McKay, P., Phillips, T., Assouline, S., Batlevi, C. L., Campbell, P., Ribrag, V., Damaj, G. L., Dickinson, M., Jurczak, W., Kazmierczak, M., Opat, S., Radford, J., Schmitt, A., Yang, J., Whalen, J., Agarwal, S., Adib, D. and Salles, G. (2020) 'Tazemetostat for patients with relapsed or refractory follicular lymphoma: an open-label, single-arm, multicentre, phase 2 trial', *Lancet Oncol,* 21(11), pp. 1433-1442.
Nakano, I. (2015) 'Stem cell signature in glioblastoma: therapeutic development for a moving target', *J Neurosurg,* 122(2), pp. 324-30.
Natsume, A., Ito, M., Katsushima, K., Ohka, F., Hatanaka, A., Shinjo, K., Sato, S., Takahashi, S., Ishikawa, Y., Takeuchi, I., Shimogawa, H., Uesugi, M., Okano, H., Kim, S. U., Wakabayashi, T., Issa, J. P., Sekido, Y. and Kondo, Y. (2013) 'Chromatin regulator PRC2 is a key regulator of epigenetic plasticity in glioblastoma', *Cancer Res,* 73(14), pp. 4559-70.
Newell-Price, J., Clark, A. J. and King, P. (2000) 'DNA methylation and silencing of gene expression', *Trends Endocrinol Metab,* 11(4), pp. 142-8.
Nichols, J., Zevnik, B., Anastassiadis, K., Niwa, H., Klewe-Nebenius, D., Chambers, I., Schöler, H. and Smith, A. (1998) 'Formation of pluripotent stem cells in the mammalian embryo depends on the POU transcription factor Oct4', *Cell,* 95(3), pp. 379-91.
Ninova, M., Fejes Tóth, K. and Aravin, A. A. (2019) 'The control of gene expression and cell identity by H3K9 trimethylation', *Development,* 146(19).
O'Geen, H., Henry, I. M., Bhakta, M. S., Meckler, J. F. and Segal, D. J. (2015) 'A genome-wide analysis of Cas9 binding specificity using ChIP-seq and targeted sequence capture', *Nucleic Acids Res,* 43(6), pp. 3389-404.
Orzan, F., Pellegatta, S., Poliani, P. L., Pisati, F., Caldera, V., Menghi, F., Kapetis, D., Marras, C., Schiffer, D. and Finocchiaro, G. (2011) 'Enhancer of Zeste 2 (EZH2) is up-regulated in malignant gliomas and in glioma stem-like cells', *Neuropathol Appl Neurobiol,* 37(4), pp. 381-94.
Otsuka, K., Suzuki, K., Fujimichi, Y., Tomita, M. and Iwasaki, T. (2018) 'Cellular responses and gene expression profiles of colonic Lgr5+ stem cells after low-dose/low-dose-rate radiation exposure', *J Radiat Res,* 59(suppl_2), pp. ii18-ii22.

Pagel, K. A., Kim, R., Moad, K., Busby, B., Zheng, L., Tokheim, C., Ryan, M. and Karchin, R. (2020) 'Integrated Informatics Analysis of Cancer-Related Variants', *JCO Clin Cancer Inform,* 4, pp. 310-317.

Pai, E. L., Vogt, D., Clemente-Perez, A., McKinsey, G. L., Cho, F. S., Hu, J. S., Wimer, M., Paul, A., Fazel Darbandi, S., Pla, R., Nowakowski, T. J., Goodrich, L. V., Paz, J. T. and Rubenstein, J. L. R. (2019) 'Mafb and c-Maf Have Prenatal Compensatory and Postnatal Antagonistic Roles in Cortical Interneuron Fate and Function', *Cell Rep,* 26(5), pp. 1157-1173.e5.

Panossian, A., Seo, E. J. and Efferth, T. (2018) 'Novel molecular mechanisms for the adaptogenic effects of herbal extracts on isolated brain cells using systems biology', *Phytomedicine,* 50, pp. 257-284.

Parsons, D. W., Jones, S., Zhang, X., Lin, J. C., Leary, R. J., Angenendt, P., Mankoo, P., Carter, H., Siu, I. M., Gallia, G. L., Olivi, A., McLendon, R., Rasheed, B. A., Keir, S., Nikolskaya, T., Nikolsky, Y., Busam, D. A., Tekleab, H., Diaz, L. A., Hartigan, J., Smith, D. R., Strausberg, R. L., Marie, S. K., Shinjo, S. M., Yan, H., Riggins, G. J., Bigner, D. D., Karchin, R., Papadopoulos, N., Parmigiani, G., Vogelstein, B., Velculescu, V. E. and Kinzler, K. W. (2008) 'An integrated genomic analysis of human glioblastoma multiforme', *Science,* 321(5897), pp. 1807-12.

Pastori, C., Daniel, M., Penas, C., Volmar, C. H., Johnstone, A. L., Brothers, S. P., Graham, R. M., Allen, B., Sarkaria, J. N., Komotar, R. J., Wahlestedt, C. and Ayad, N. G. (2014) 'BET bromodomain proteins are required for glioblastoma cell proliferation', *Epigenetics,* 9(4), pp. 611-20.

Patel, A. P., Tirosh, I., Trombetta, J. J., Shalek, A. K., Gillespie, S. M., Wakimoto, H., Cahill, D. P., Nahed, B. V., Curry, W. T., Martuza, R. L., Louis, D. N., Rozenblatt-Rosen, O., Suvà, M. L., Regev, A. and Bernstein, B. E. (2014) 'Single-cell RNA-seq highlights intratumoral heterogeneity in primary glioblastoma', *Science,* 344(6190), pp. 1396-401.

Perazzoli, G., Prados, J., Ortiz, R., Caba, O., Cabeza, L., Berdasco, M., Gónzalez, B. and Melguizo, C. (2015) 'Temozolomide Resistance in Glioblastoma Cell Lines: Implication of MGMT, MMR, P-Glycoprotein and CD133 Expression', *PLoS One,* 10(10), pp. e0140131.

Peruzzi, P., Bronisz, A., Nowicki, M. O., Wang, Y., Ogawa, D., Price, R., Nakano, I., Kwon, C. H., Hayes, J., Lawler, S. E., Ostrowski, M. C., Chiocca, E. A. and

Godlewski, J. (2013) 'MicroRNA-128 coordinately targets Polycomb Repressor Complexes in glioma stem cells', *Neuro Oncol,* 15(9), pp. 1212-24.
Prager, B. C., Bhargava, S., Mahadev, V., Hubert, C. G. and Rich, J. N. (2020) 'Glioblastoma Stem Cells: Driving Resilience through Chaos', *Trends Cancer,* 6(3), pp. 223-235.
Pruszak, J., Sonntag, K. C., Aung, M. H., Sanchez-Pernaute, R. and Isacson, O. (2007) 'Markers and methods for cell sorting of human embryonic stem cell-derived neural cell populations', *Stem Cells,* 25(9), pp. 2257-68.
Qazi, M. A., Vora, P., Venugopal, C., McFarlane, N., Subapanditha, M. K., Murty, N. K., Hassell, J. A., Hallett, R. M. and Singh, S. K. (2016) 'A novel stem cell culture model of recurrent glioblastoma', *J Neurooncol,* 126(1), pp. 57-67.
Qin, K., Hou, H., Liang, Y. and Zhang, X. (2020) 'Prognostic value of TP53 concurrent mutations for EGFR- TKIs and ALK-TKIs based targeted therapy in advanced non-small cell lung cancer: a meta-analysis', *BMC Cancer,* 20(1), pp. 328.
Ramírez, F., Ryan, D. P., Grüning, B., Bhardwaj, V., Kilpert, F., Richter, A. S., Heyne, S., Dündar, F. and Manke, T. (2016) 'deepTools2: a next generation web server for deep-sequencing data analysis', *Nucleic Acids Res,* 44(W1), pp. W160-5.
Reya, T., Morrison, S. J., Clarke, M. F. and Weissman, I. L. (2001) 'Stem cells, cancer, and cancer stem cells', *Nature,* 414(6859), pp. 105-11.
Richard, V., Nair, M. G., Santhosh Kumar, T. R. and Pillai, M. R. (2013) 'Side population cells as prototype of chemoresistant, tumor-initiating cells', *Biomed Res Int,* 2013, pp. 517237.
Richly, H., Aloia, L. and Di Croce, L. (2011) 'Roles of the Polycomb group proteins in stem cells and cancer', *Cell Death Dis,* 2, pp. e204.
Ringrose, L. and Paro, R. (2004) 'Epigenetic regulation of cellular memory by the Polycomb and Trithorax group proteins', *Annu Rev Genet,* 38, pp. 413-43.
Rodriguez-Pinilla, S. M., Sarrio, D., Moreno-Bueno, G., Rodriguez-Gil, Y., Martinez, M. A., Hernandez, L., Hardisson, D., Reis-Filho, J. S. and Palacios, J. (2007) 'Sox2: a possible driver of the basal-like phenotype in sporadic breast cancer', *Mod Pathol,* 20(4), pp. 474-81.
Rong, Y., Durden, D. L., Van Meir, E. G. and Brat, D. J. (2006) "Pseudopalisading' necrosis in glioblastoma: a familiar morphologic feature that links vascular

pathology, hypoxia, and angiogenesis', *J Neuropathol Exp Neurol,* 65(6), pp. 529-39.

Rosa, J. d. l., Marta, I., Gallo-Oller, G., Shahi, M. H., Melendez, B., Rey, J. A. and Idoate, M. A. (2016) 'EZH2 as a therapeutic target in Glioblastoma: A cellular and molecular study', 7(6), pp. 8, Available: Journal of Carcinogenesis & Mutagenesis.

Safa, A. R., Saadatzadeh, M. R., Cohen-Gadol, A. A., Pollok, K. E. and Bijangi-Vishehsaraei, K. (2015) 'Glioblastoma stem cells (GSCs) epigenetic plasticity and interconversion between differentiated non-GSCs and GSCs', *Genes Dis,* 2(2), pp. 152-163.

Saleh, T., Bloukh, S., Carpenter, V. J., Alwohoush, E., Bakeer, J., Darwish, S., Azab, B. and Gewirtz, D. A. (2020) 'Therapy-Induced Senescence: An "Old" Friend Becomes the Enemy', *Cancers (Basel),* 12(4).

Sauvageau, M. and Sauvageau, G. (2010) 'Polycomb group proteins: multi-faceted regulators of somatic stem cells and cancer', *Cell Stem Cell,* 7(3), pp. 299-313.

Schiffer, D., Mellai, M., Annovazzi, L., Caldera, V., Piazzi, A., Denysenko, T. and Melcarne, A. (2014) 'Stem cell niches in glioblastoma: a neuropathological view', *Biomed Res Int,* 2014, pp. 725921.

Schwartzentruber, J., Korshunov, A., Liu, X. Y., Jones, D. T., Pfaff, E., Jacob, K., Sturm, D., Fontebasso, A. M., Quang, D. A., Tönjes, M., Hovestadt, V., Albrecht, S., Kool, M., Nantel, A., Konermann, C., Lindroth, A., Jäger, N., Rausch, T., Ryzhova, M., Korbel, J. O., Hielscher, T., Hauser, P., Garami, M., Klekner, A., Bognar, L., Ebinger, M., Schuhmann, M. U., Scheurlen, W., Pekrun, A., Frühwald, M. C., Roggendorf, W., Kramm, C., Dürken, M., Atkinson, J., Lepage, P., Montpetit, A., Zakrzewska, M., Zakrzewski, K., Liberski, P. P., Dong, Z., Siegel, P., Kulozik, A. E., Zapatka, M., Guha, A., Malkin, D., Felsberg, J., Reifenberger, G., von Deimling, A., Ichimura, K., Collins, V. P., Witt, H., Milde, T., Witt, O., Zhang, C., Castelo-Branco, P., Lichter, P., Faury, D., Tabori, U., Plass, C., Majewski, J., Pfister, S. M. and Jabado, N. (2012) 'Driver mutations in histone H3.3 and chromatin remodelling genes in paediatric glioblastoma', *Nature,* 482(7384), pp. 226-31.

Sell, S. (2010) 'On the stem cell origin of cancer', *Am J Pathol,* 176(6), pp. 2584-494.

Sen, R., Dolgalev, I., Bayin, N. S., Heguy, A., Tsirigos, A. and Placantonakis, D. G. (2018) 'Single-Cell RNA Sequencing of Glioblastoma Cells', *Methods Mol Biol,* 1741, pp. 151-170.

Sena, I. F. G., Paiva, A. E., Prazeres, P. H. D. M., Azevedo, P. O., Lousado, L., Bhutia, S. K., Salmina, A. B., Mintz, A. and Birbrair, A. (2018) 'Glioblastoma-activated pericytes support tumor growth via immunosuppression', *Cancer Med,* 7(4), pp. 1232-1239.

Setoguchi, T. and Kondo, T. (2004) 'Nuclear export of OLIG2 in neural stem cells is essential for ciliary neurotrophic factor-induced astrocyte differentiation', *J Cell Biol,* 166(7), pp. 963-8.

Sharma, S., Kelly, T. K. and Jones, P. A. (2010) 'Epigenetics in cancer', *Carcinogenesis,* 31(1), pp. 27-36.

Sharma, V., Purkait, S., Takkar, S., Malgulwar, P. B., Kumar, A., Pathak, P., Suri, V., Sharma, M. C., Suri, A., Kale, S. S., Kulshreshtha, R. and Sarkar, C. (2016) 'Analysis of EZH2: micro-RNA network in low and high grade astrocytic tumors', *Brain Tumor Pathol,* 33(2), pp. 117-28.

Shen, X., Liu, Y., Hsu, Y. J., Fujiwara, Y., Kim, J., Mao, X., Yuan, G. C. and Orkin, S. H. (2008) 'EZH1 mediates methylation on histone H3 lysine 27 and complements EZH2 in maintaining stem cell identity and executing pluripotency', *Mol Cell,* 32(4), pp. 491-502.

Shergalis, A., Bankhead, A., Luesakul, U., Muangsin, N. and Neamati, N. (2018) 'Current Challenges and Opportunities in Treating Glioblastoma', *Pharmacol Rev,* 70(3), pp. 412-445.

Smits, K. M., Melotte, V., Niessen, H. E., Dubois, L., Oberije, C., Troost, E. G., Starmans, M. H., Boutros, P. C., Vooijs, M., van Engeland, M. and Lambin, P. (2014) 'Epigenetics in radiotherapy: where are we heading?', *Radiother Oncol,* 111(2), pp. 168-77.

Smits, M., Nilsson, J., Mir, S. E., van der Stoop, P. M., Hulleman, E., Niers, J. M., de Witt Hamer, P. C., Marquez, V. E., Cloos, J., Krichevsky, A. M., Noske, D. P., Tannous, B. A. and Würdinger, T. (2010) 'miR-101 is down-regulated in glioblastoma resulting in EZH2-induced proliferation, migration, and angiogenesis', *Oncotarget,* 1(8), pp. 710-20.

Soni, P., Qayoom, S., Husain, N., Kumar, P., Chandra, A., Ojha, B. K. and Gupta, R. K. (2017) 'CD24 and Nanog expression in Stem Cells in Glioblastoma:

Correlation with Response to Chemoradiation and Overall Survival', *Asian Pac J Cancer Prev,* 18(8), pp. 2215-2219.
Sottoriva, A., Spiteri, I., Piccirillo, S. G., Touloumis, A., Collins, V. P., Marioni, J. C., Curtis, C., Watts, C. and Tavaré, S. (2013) 'Intratumor heterogeneity in human glioblastoma reflects cancer evolutionary dynamics', *Proc Natl Acad Sci U S A,* 110(10), pp. 4009-14.
Soukkarieh, C., Agius, E., Soula, C. and Cochard, P. (2007) 'Pax2 regulates neuronal-glial cell fate choice in the embryonic optic nerve', *Dev Biol,* 303(2), pp. 800-13.
Stamos, J. L. and Weis, W. I. (2013) 'The ß-catenin destruction complex', *Cold Spring Harb Perspect Biol,* 5(1), pp. a007898.
Stupp, R., Mason, W. P., van den Bent, M. J., Weller, M., Fisher, B., Taphoorn, M. J., Belanger, K., Brandes, A. A., Marosi, C., Bogdahn, U., Curschmann, J., Janzer, R. C., Ludwin, S. K., Gorlia, T., Allgeier, A., Lacombe, D., Cairncross, J. G., Eisenhauer, E., Mirimanoff, R. O., Groups, E. O. f. R. a. T. o. C. B. T. a. R. and Group, N. C. I. o. C. C. T. (2005) 'Radiotherapy plus concomitant and adjuvant temozolomide for glioblastoma', *N Engl J Med,* 352(10), pp. 987-96.
Sturgeon, K., Kaneko, T., Biemann, M., Gauthier, A., Chawengsaksophak, K. and Cordes, S. P. (2011) 'Cdx1 refines positional identity of the vertebrate hindbrain by directly repressing Mafb expression', *Development,* 138(1), pp. 65-74.
Su, I. H., Dobenecker, M. W., Dickinson, E., Oser, M., Basavaraj, A., Marqueron, R., Viale, A., Reinberg, D., Wülfing, C. and Tarakhovsky, A. (2005) 'Polycomb group protein ezh2 controls actin polymerization and cell signaling', *Cell,* 121(3), pp. 425-36.
Subramanian, A., Tamayo, P., Mootha, V. K., Mukherjee, S., Ebert, B. L., Gillette, M. A., Paulovich, A., Pomeroy, S. L., Golub, T. R., Lander, E. S. and Mesirov, J. P. (2005) 'Gene set enrichment analysis: a knowledge-based approach for interpreting genome-wide expression profiles', *Proc Natl Acad Sci U S A,* 102(43), pp. 15545-50.
Suvà, M. L., Rheinbay, E., Gillespie, S. M., Patel, A. P., Wakimoto, H., Rabkin, S. D., Riggi, N., Chi, A. S., Cahill, D. P., Nahed, B. V., Curry, W. T., Martuza, R. L., Rivera, M. N., Rossetti, N., Kasif, S., Beik, S., Kadri, S., Tirosh, I., Wortman, I., Shalek, A. K., Rozenblatt-Rosen, O., Regev, A., Louis, D. N. and Bernstein, B. E. (2014) 'Reconstructing and reprogramming the tumor-propagating potential of glioblastoma stem-like cells', *Cell,* 157(3), pp. 580-94.

Suvà, M. L., Riggi, N., Janiszewska, M., Radovanovic, I., Provero, P., Stehle, J. C., Baumer, K., Le Bitoux, M. A., Marino, D., Cironi, L., Marquez, V. E., Clément, V. and Stamenkovic, I. (2009) 'EZH2 is essential for glioblastoma cancer stem cell maintenance', *Cancer Res,* 69(24), pp. 9211-8.
Sze, C. I., Su, W. P., Chiang, M. F., Lu, C. Y., Chen, Y. A. and Chang, N. S. (2013) 'Assessing current therapeutic approaches to decode potential resistance mechanisms in glioblastomas', *Front Oncol,* 3, pp. 59.
Tate, C. M., Pallini, R., Ricci-Vitiani, L., Dowless, M., Shiyanova, T., D'Alessandris, G. Q., Morgante, L., Giannetti, S., Larocca, L. M., di Martino, S., Rowlinson, S. W., De Maria, R. and Stancato, L. (2012) 'A BMP7 variant inhibits the tumorigenic potential of glioblastoma stem-like cells', *Cell Death Differ,* 19(10), pp. 1644-54.
Thiery, J. P. (2002) 'Epithelial-mesenchymal transitions in tumour progression', *Nat Rev Cancer,* 2(6), pp. 442-54.
Tokheim, C. and Karchin, R. (2019) 'CHASMplus Reveals the Scope of Somatic Missense Mutations Driving Human Cancers', *Cell Syst,* 9(1), pp. 9-23.e8.
Tonini, T., Bagella, L., D'Andrilli, G., Claudio, P. P. and Giordano, A. (2004) 'Ezh2 reduces the ability of HDAC1-dependent pRb2/p130 transcriptional repression of cyclin A', *Oncogene,* 23(28), pp. 4930-7.
Tran, A. N., Lai, A., Li, S., Pope, W. B., Teixeira, S., Harris, R. J., Woodworth, D. C., Nghiemphu, P. L., Cloughesy, T. F. and Ellingson, B. M. (2014) 'Increased sensitivity to radiochemotherapy in IDH1 mutant glioblastoma as demonstrated by serial quantitative MR volumetry', *Neuro Oncol,* 16(3), pp. 414-20.
Tremblay-LeMay, R., Rastgoo, N., Pourabdollah, M. and Chang, H. (2018) 'EZH2 as a therapeutic target for multiple myeloma and other haematological malignancies', *Biomark Res,* 6, pp. 34.
Trépant, A. L., Bouchart, C., Rorive, S., Sauvage, S., Decaestecker, C., Demetter, P. and Salmon, I. (2015) 'Identification of OLIG2 as the most specific glioblastoma stem cell marker starting from comparative analysis of data from similar DNA chip microarray platforms', *Tumour Biol,* 36(3), pp. 1943-53.
Tysnes, B. B. and Mahesparan, R. (2001) 'Biological mechanisms of glioma invasion and potential therapeutic targets', *J Neurooncol,* 53(2), pp. 129-47.
Vasileiou, P. V. S., Evangelou, K., Vlasis, K., Fildisis, G., Panayiotidis, M. I., Chronopoulos, E., Passias, P. G., Kouloukoussa, M., Gorgoulis, V. G. and Havaki, S. (2019) 'Mitochondrial Homeostasis and Cellular Senescence', *Cells,* 8(7).

Veazey, K. J., Muller, D. and Golding, M. C. (2013) 'Prenatal alcohol exposure and cellular differentiation: a role for Polycomb and Trithorax group proteins in FAS phenotypes?', *Alcohol Res,* 35(1), pp. 77-85.

Venneti, S., Garimella, M. T., Sullivan, L. M., Martinez, D., Huse, J. T., Heguy, A., Santi, M., Thompson, C. B. and Judkins, A. R. (2013) 'Evaluation of histone 3 lysine 27 trimethylation (H3K27me3) and enhancer of Zest 2 (EZH2) in pediatric glial and glioneuronal tumors shows decreased H3K27me3 in H3F3A K27M mutant glioblastomas', *Brain Pathol,* 23(5), pp. 558-64.

Verhaak, R. G., Hoadley, K. A., Purdom, E., Wang, V., Qi, Y., Wilkerson, M. D., Miller, C. R., Ding, L., Golub, T., Mesirov, J. P., Alexe, G., Lawrence, M., O'Kelly, M., Tamayo, P., Weir, B. A., Gabriel, S., Winckler, W., Gupta, S., Jakkula, L., Feiler, H. S., Hodgson, J. G., James, C. D., Sarkaria, J. N., Brennan, C., Kahn, A., Spellman, P. T., Wilson, R. K., Speed, T. P., Gray, J. W., Meyerson, M., Getz, G., Perou, C. M., Hayes, D. N. and Network, C. G. A. R. (2010) 'Integrated genomic analysis identifies clinically relevant subtypes of glioblastoma characterized by abnormalities in PDGFRA, IDH1, EGFR, and NF1', *Cancer Cell,* 17(1), pp. 98-110.

Verma, S. K., Tian, X., LaFrance, L. V., Duquenne, C., Suarez, D. P., Newlander, K. A., Romeril, S. P., Burgess, J. L., Grant, S. W., Brackley, J. A., Graves, A. P., Scherzer, D. A., Shu, A., Thompson, C., Ott, H. M., Aller, G. S., Machutta, C. A., Diaz, E., Jiang, Y., Johnson, N. W., Knight, S. D., Kruger, R. G., McCabe, M. T., Dhanak, D., Tummino, P. J., Creasy, C. L. and Miller, W. H. (2012) 'Identification of Potent, Selective, Cell-Active Inhibitors of the Histone Lysine Methyltransferase EZH2', *ACS Med Chem Lett,* 3(12), pp. 1091-6.

Villano, J. L., Seery, T. E. and Bressler, L. R. (2009) 'Temozolomide in malignant gliomas: current use and future targets', *Cancer Chemother Pharmacol,* 64(4), pp. 647-55.

Vogelstein, B., Papadopoulos, N., Velculescu, V. E., Zhou, S., Diaz, L. A. and Kinzler, K. W. (2013) 'Cancer genome landscapes', *Science,* 339(6127), pp. 1546-58.

Wang, D., Lu, P., Zhang, H., Luo, M., Zhang, X., Wei, X., Gao, J., Zhao, Z. and Liu, C. (2014) 'Oct-4 and Nanog promote the epithelial-mesenchymal transition of breast cancer stem cells and are associated with poor prognosis in breast cancer patients', *Oncotarget,* 5(21), pp. 10803-15.

Wang, L. H., Wu, C. F., Rajasekaran, N. and Shin, Y. K. (2018) 'Loss of Tumor Suppressor Gene Function in Human Cancer: An Overview', *Cell Physiol Biochem,* 51(6), pp. 2647-2693.
Wang, R. J., Li, J. W., Bao, B. H., Wu, H. C., Du, Z. H., Su, J. L., Zhang, M. H. and Liang, H. Q. (2015) 'MicroRNA-873 (miRNA-873) inhibits glioblastoma tumorigenesis and metastasis by suppressing the expression of IGF2BP1', *J Biol Chem,* 290(14), pp. 8938-48.
Wang, S. H. and Lin, S. Y. (2013) 'Tumor dormancy: potential therapeutic target in tumor recurrence and metastasis prevention', *Exp Hematol Oncol,* 2(1), pp. 29.
Weber, C. M. and Henikoff, S. (2014) 'Histone variants: dynamic punctuation in transcription', *Genes Dev,* 28(7), pp. 672-82.
Wen, X., Wu, Y., Awadasseid, A., Tanaka, Y. and Zhang, W. (2020) 'New Advances in Canonical Wnt/β-Catenin Signaling in Cancer', *Cancer Manag Res,* 12, pp. 6987-6998.
Wen, Y., Cai, J., Hou, Y., Huang, Z. and Wang, Z. (2017) 'Role of EZH2 in cancer stem cells: from biological insight to a therapeutic target', *Oncotarget,* 8(23), pp. 37974-37990.
Wesolowski, J. R., Rajdev, P. and Mukherji, S. K. (2010) 'Temozolomide (Temodar)', *AJNR Am J Neuroradiol,* 31(8), pp. 1383-4.
Wu, H., Zeng, H., Dong, A., Li, F., He, H., Senisterra, G., Seitova, A., Duan, S., Brown, P. J., Vedadi, M., Arrowsmith, C. H. and Schapira, M. (2013) 'Structure of the catalytic domain of EZH2 reveals conformational plasticity in cofactor and substrate binding sites and explains oncogenic mutations', *PLoS One,* 8(12), pp. e83737.
Xiong, W., Jiao, Y., Huang, W., Ma, M., Yu, M., Cui, Q. and Tan, D. (2012) 'Regulation of the cell cycle via mitochondrial gene expression and energy metabolism in HeLa cells', *Acta Biochim Biophys Sin (Shanghai),* 44(4), pp. 347-58.
Xiong, X., Zhang, J., Li, A., Dai, L., Qin, S., Wang, P., Liu, W., Zhang, Z., Li, X. and Liu, Z. (2020) 'GSK343 induces programmed cell death through the inhibition of EZH2 and FBP1 in osteosarcoma cells', *Cancer Biol Ther,* 21(3), pp. 213-222.
Xu, B., On, D. M., Ma, A., Parton, T., Konze, K. D., Pattenden, S. G., Allison, D. F., Cai, L., Rockowitz, S., Liu, S., Liu, Y., Li, F., Vedadi, M., Frye, S. V., Garcia, B. A., Zheng, D., Jin, J. and Wang, G. G. (2015) 'Selective inhibition of EZH2 and

EZH1 enzymatic activity by a small molecule suppresses MLL-rearranged leukemia', *Blood,* 125(2), pp. 346-57.
Xue, Z., Vis, D. J., Bruna, A., Sustic, T., van Wageningen, S., Batra, A. S., Rueda, O. M., Bosdriesz, E., Caldas, C., Wessels, L. F. A. and Bernards, R. (2018) 'MAP3K1 and MAP2K4 mutations are associated with sensitivity to MEK inhibitors in multiple cancer models', *Cell Res,* 28(7), pp. 719-729.
Yang, H., Ye, D., Guan, K. L. and Xiong, Y. (2012) 'IDH1 and IDH2 mutations in tumorigenesis: mechanistic insights and clinical perspectives', *Clin Cancer Res,* 18(20), pp. 5562-71.
Yu, T., Wang, Y., Hu, Q., Wu, W., Wu, Y., Wei, W., Han, D., You, Y., Lin, N. and Liu, N. (2017) 'The EZH2 inhibitor GSK343 suppresses cancer stem-like phenotypes and reverses mesenchymal transition in glioma cells', *Oncotarget,* 8(58), pp. 98348-98359.
Yu, W. M., Appler, J. M., Kim, Y. H., Nishitani, A. M., Holt, J. R. and Goodrich, L. V. (2013) 'A Gata3-Mafb transcriptional network directs post-synaptic differentiation in synapses specialized for hearing', *Elife,* 2, pp. e01341.
Yu, Z., Pestell, T. G., Lisanti, M. P. and Pestell, R. G. (2012) 'Cancer stem cells', *Int J Biochem Cell Biol,* 44(12), pp. 2144-51.
Yuan, X., Curtin, J., Xiong, Y., Liu, G., Waschsmann-Hogiu, S., Farkas, D. L., Black, K. L. and Yu, J. S. (2004) 'Isolation of cancer stem cells from adult glioblastoma multiforme', *Oncogene,* 23(58), pp. 9392-400.
Zbinden, M., Duquet, A., Lorente-Trigos, A., Ngwabyt, S. N., Borges, I. and Ruiz i Altaba, A. (2010) 'NANOG regulates glioma stem cells and is essential in vivo acting in a cross-functional network with GLI1 and p53', *EMBO J,* 29(15), pp. 2659-74.
Zhang, H., Zhu, D., Zhang, Z., Kaluz, S., Yu, B., Devi, N. S., Olson, J. J. and Van Meir, E. G. (2020) 'EZH2 targeting reduces medulloblastoma growth through epigenetic reactivation of the BAI1/p53 tumor suppressor pathway', *Oncogene,* 39(5), pp. 1041-1048.
Zhang, J., Chen, L., Han, L., Shi, Z., Pu, P. and Kang, C. (2015) 'EZH2 is a negative prognostic factor and exhibits pro-oncogenic activity in glioblastoma', *Cancer Lett,* 356(2 Pt B), pp. 929-36.
Zhang, J. and Jiao, J. (2015) 'Molecular Biomarkers for Embryonic and Adult Neural Stem Cell and Neurogenesis', *Biomed Res Int,* 2015, pp. 727542.

Zhang, Y., Liu, T., Meyer, C. A., Eeckhoute, J., Johnson, D. S., Bernstein, B. E., Nusbaum, C., Myers, R. M., Brown, M., Li, W. and Liu, X. S. (2008) 'Model-based analysis of ChIP-Seq (MACS)', *Genome Biol*, 9(9), pp. R137.
Zhang, Y. F. and Su, B. (2012) 'Peak identification for ChIP-seq data with no controls', *Dongwuxue Yanjiu*, 33(E5-6), pp. E121-8.
Zhou, Q. and Anderson, D. J. (2002) 'The bHLH transcription factors OLIG2 and OLIG1 couple neuronal and glial subtype specification', *Cell*, 109(1), pp. 61-73.
Zong, H., Verhaak, R. G. and Canoll, P. (2012) 'The cellular origin for malignant glioma and prospects for clinical advancements', *Expert Rev Mol Diagn*, 12(4), pp. 383-94.